

The role of the mesenchyme homeobox genes in the
regulation of vascular endothelial cell function

by

Josette M. D. Northcott

A thesis submitted to the Faculty of Graduate Studies of

The University of Manitoba

in partial fulfilment of the requirements for the degree of

DOCTOR OF PHILOSOPHY

Department of Biochemistry and Medical Genetics

University of Manitoba

Winnipeg

Copyright © October 2012

Josette Michelle Douville Northcott

Abstract

The mesenchyme homeobox genes, *MEOX1* and *MEOX2*, encode homeodomain transcription factors. Studies of *Meox1/Meox2* knockout mice established that these proteins are partially redundant during development, suggesting that they may regulate common target genes. In the adult vasculature, *MEOX2* is expressed in vascular smooth muscle and endothelial cells. *MEOX2* has been demonstrated to: i) inhibit proliferation, ii) activate apoptosis and iii) induce senescence. In contrast, the role of *MEOX1* has not been studied in the vasculature. Currently, there are two known target genes of *MEOX2*: cyclin-dependent kinase inhibitor 1A (*CDKN1A/p21^{CIP1/WAF1}*) and cyclin-dependent kinase inhibitor 2A (*CDKN2A/p16^{INK4a}*), which regulate transient (quiescent) and permanent (senescent) cell cycle arrest. Senescence is postulated to contribute to the development of atherosclerotic vascular disease by promoting endothelial dysfunction.

We hypothesized that *MEOX1* and *MEOX2* would activate both *p21^{CIP1/WAF1}* and *p16^{INK4a}* expression, as well as induce apoptosis, cell cycle arrest and senescence in endothelial cells. Furthermore, we postulated that the majority of newly identified *MEOX* target genes in endothelial cells would be regulated by both *MEOX1* and *MEOX2*.

MEOX proteins were expressed in human endothelial cells via adenoviral transduction. Levels of target gene expression were measured by luciferase reporter gene assays, western blot and quantitative real-time PCR. Electrophoretic mobility shift assays were used to demonstrate *MEOX* binding to DNA. Cellular proliferation, senescence, and apoptosis were evaluated. For the identification of novel target genes,

microarrays were used to compare levels of gene expression in endothelial cells transduced with MEOX constructs or control virus.

Both MEOX1 and MEOX2 activated $p21^{CIP1/WAF1}$ and $p16^{INK4a}$ gene transcription, inhibited proliferation and induced apoptosis and senescence in endothelial cells. MEOX activation of $p21^{CIP1/WAF1}$ transcription occurs via a DNA-binding independent mechanism that requires the SP1 transcription factor. In contrast, MEOX activation of $p16^{INK4a}$ transcription is dependent upon DNA-binding. Microarray analysis revealed that both MEOX1 and MEOX2 increased the expression of intercellular adhesion molecule 1 (*ICAM-1*) and decreased the expression of nitric oxide synthase 3 (*NOS3/eNOS*).

Taken together, we conclude that MEOX1 and MEOX2 have similar target genes in endothelial cells including $p21^{CIP1/WAF1}$, $p16^{INK4a}$ and *eNOS*. As increased endothelial senescence and decreased nitric oxide production are hallmarks of endothelial dysfunction, this study proposes a role for the MEOX proteins in the progression of atherosclerotic vascular disease.

Acknowledgements

I would like to recognize and thank the following people for their contributions (be it big, small or abstract) to this thesis.

Dr. Jeffrey Wigle, my super-advisor and mentor - thank you for everything, but especially your honesty, patience, contagious need to learn and teach, and sense of humour! Dr. Michael Czubryt, Dr. James Davie and Dr. Barbara Triggs-Raine, my advisory committee - thank you for your guidance and for always leaving me with more to consider. Dr. Ashok Srivastava, my external examiner – thank you for making time to review my thesis and travel to Winnipeg for my oral examination.

The Canadian Institutes of Health Research, Manitoba Health Research Council, Alzheimer Society of Manitoba, Manitoba Medical Foundation, St. Boniface Hospital Foundation, WRHA Cardiac Sciences Program, University of Manitoba (Institute of Cardiovascular Sciences, Centre on Aging, Division of Neurodegenerative Disorders, Faculty of Graduate Studies), Genome Canada and the American Society for Cell Biology that have provided financial support for me to carry out and present this research – my sincere appreciation.

Dr. Ludger Klews - thank you for teaching me the art of flow cytometry. Dr. Nasrin Mesaeli, Dr. Peter Zahradka and Dr. Ian Dixon, my collaborators - thank you for the opportunities to think outside our lab's paradigm. My colleagues in the Mesaeli lab (esp. Melanie Durston), Czubryt lab, Dixon lab (esp. Dr. Ryan Cunnington), Zahradka lab, Pierce lab, Duhamel lab and Kardami lab – thank you for always sharing (experience, lab reagents, coffee, chocolate, etc.), it has been a pleasure to work alongside you.

My labmates, David Cheung*, Dr. Jijin Lin, Allison Stoddart, Joe Kim, Mona Friesen, Patty Bocangel, Jagan Jangamreddy, Kathy Rawszer, Noha Al-Omari, Shannon Baxter, Teri Moffatt, Krista Herbert*, Ezgi Öğütçen*, Mehdi Eshraghi, Susan Lee, Roien Ahmadie, Marino Novel, Patricia Roche, Sofia M'Seffar, Eman Tomas, Theo Wigle, Julie Gauvin, Jordan Banman, Stone Zhou, Abdellah Bezzahou, Ted and Kevin - thank you for the technical assistance, fun times and life lessons - even those I did not want to learn. *To my dearest buddies – a very grateful thank you for all your help and kindness.

Dr. Klaus Wrogemann and Dr. Patrick Frosk - thank you for starting me off on the right foot and for teaching me about serendipity. Margot Arntfield - thank you for always being there. Nicole Du Guay - thank you for being my personal cheerleader. Sharon and Bill Stiteler (www.disapprovingrabbits.com) and Jorge Cham (www.phdcomics.com) - thank you for making the day a little bit better.

My supportive and loving family, Jean-Claude and Leonette Douville (Dad and Mom), Dr. Renée Douville (sister/best friend/role model/fellow nerd), Derek Foreman, Buster, Nano, Mark and Caryn Northcott, Michael Northcott, Daniel Northcott (♥) and Clover (=:<) - thank you, thank you, thank you, I'm sorry, thank you!

Dedication

This thesis is dedicated to beans, new and old.

Table of contents

Abstract.....	ii
Acknowledgements.....	iv
Dedication.....	v
Table of contents.....	vi
List of tables.....	xiv
List of figures.....	xv
List of appendices.....	xxii
List of abbreviations.....	xxiii
CHAPTER 1: INTRODUCTION.....	1
1.1. The cardiovascular system.....	1
1.1.1. Endothelial cells.....	1
1.1.2. Vascular smooth muscle cells.....	2
1.1.3. Vascular development.....	2
1.1.4. Postnatal angiogenesis.....	6
1.1.5. Endothelial dysfunction and vascular disease.....	6
1.2. Homeobox genes.....	7
1.2.1. The homeodomain.....	8
1.2.2. Classification.....	9
1.2.3. Regulation of angiogenesis by homeodomain proteins.....	10
1.3. Mesenchyme homeobox gene family; MEOX1 and MEOX2.....	11

1.3.1.	Discovery and comparison.....	12
1.3.1.1.	<i>Cloning of the human MEOX genes</i>	12
1.3.1.2.	<i>Domains and percent amino acid identity</i>	12
1.3.2.	Evolution of the <i>MEOX</i> genes	14
1.3.2.1.	<i>MEOX gene homologs</i>	14
1.3.2.2.	<i>MEOX gene ancestry</i>	15
1.3.3.	Embryonic gene expression	16
1.3.3.1.	<i>Human</i>	16
1.3.3.2.	<i>Other vertebrates</i>	16
1.3.3.2.1.	<i>Mouse</i>	16
1.3.3.2.2.	<i>Chick</i>	17
1.3.3.2.3.	<i>Frog</i>	18
1.3.3.3.	<i>Non-vertebrate animals</i>	19
1.3.4.	Role in development	20
1.3.4.1.	<i>Axial skeleton</i>	21
1.3.4.2.	<i>Myogenesis</i>	23
1.3.4.3.	<i>Pharyngeal arch</i>	25
1.3.4.4.	<i>Palate</i>	26
1.3.4.5.	<i>MEOX genes and EMT</i>	26
1.3.5.	Functions of the MEOX proteins in the cardiovascular system	27

1.3.5.1.	<i>Vascular smooth muscle cells</i>	27
1.3.5.2.	<i>Adventitial fibroblasts</i>	30
1.3.5.3.	<i>Endothelial cells</i>	31
1.3.6.	MEOX genes and potential roles in human disease.....	36
1.3.6.1.	<i>Hutchinson-Gilford Progeria Syndrome</i>	37
1.3.6.2.	<i>Alzheimer’s Disease</i>	38
1.3.6.3.	<i>Hepatic portal hypertension</i>	39
1.3.6.4.	<i>Cancer</i>	39
CHAPTER 2: OVERALL RATIONALE, HYPOTHESES AND OBJECTIVES		42
2.1.	Rationale	42
2.2.	Hypothesis.....	43
2.3.	Objectives	43
CHAPTER 3: THE ROLE OF MEOX1 AND MEOX2 IN VASCULAR CELL		
DEATH		44
3.1.	Introduction.....	44
3.1.1.	Apoptosis and necrosis	44
3.2.	Rationale, hypothesis and aims.....	45
3.3.	Materials and methods	47
3.3.1.	Cell culture.....	47
3.3.1.1.	<i>HEK293</i>	47

3.3.1.2.	<i>A7r5</i>	48
3.3.1.3.	<i>VSMCs</i>	48
3.3.1.4.	<i>HUVECs</i>	51
3.3.2.	Expression vectors	51
3.3.3.	Adenovirus production and titering	51
3.3.4.	Immunofluorescence (epifluorescence microscopy)	54
3.3.4.1.	<i>SM α-actin and SM myosin</i>	54
3.3.4.2.	<i>FLAG</i>	54
3.3.4.3.	<i>Acquisition of images</i>	55
3.3.5.	Western blotting.....	55
3.3.6.	TUNEL assays	58
3.3.7.	Cell titer assay.....	59
3.3.8.	LIVE/DEAD assay.....	59
3.3.9.	Flow cytometry (cleaved caspase-3 / 7-AAD).....	60
3.3.10.	Statistical analysis	61
3.4.	Results and discussion	61
3.5.	Conclusions and future directions.....	100
CHAPTER 4:	MEOX1 AND MEOX2 ACTIVATE <i>P21^{CIP1/WAF1}</i> AND <i>P16^{INK4A}</i>	
	EXPRESSION AND INDUCE ENDOTHELIAL CELL SENESCENCE	102
4.1.	Introduction.....	102

4.1.1.	The cell cycle	102
4.1.2.	Senescence	103
4.2.	Rationale, hypothesis and aims.....	104
4.3.	Materials and methods	107
4.3.1.	Cell culture.....	107
4.3.2.	MEOX expression vectors (plasmid and adenovirus)	107
4.3.3.	Immunofluorescence (confocal microscopy).....	107
4.3.4.	Luciferase promoter constructs and LacZ expression vector	108
4.3.5.	Luciferase assays	109
4.3.6.	Quantitative real-time PCR.....	110
4.3.7.	Western blotting and quantification.....	112
4.3.8.	Recombinant MEOX-GST fusion protein production.....	112
4.3.9.	Electrophoretic mobility shift assays	113
4.3.10.	Chromatin immunoprecipitation.....	115
4.3.11.	Senescence-associated β -galactosidase staining	117
4.3.12.	Flow cytometry (cell cycle analysis)	118
4.3.12.1.	<i>Propidium iodide</i>	118
4.3.12.2.	<i>BrdU / 7-AAD</i>	118
4.3.13.	Gene expression knockdown using siRNA.....	119
4.3.14.	Statistical analysis.....	120

4.4.	Results and discussion	121
4.4.1.	Expression of MEOX proteins in HUVECs	121
4.4.2.	MEOX1 and MEOX2 activate $p21^{CIP1/WAF1}$ expression via a DNA-binding independent mechanism	132
4.4.2.1.	<i>MEOX1 and MEOX2 activate transcription from the endogenous $p21^{CIP1/WAF1}$ promoter in endothelial cells.</i>	132
4.4.2.2.	<i>Sequence specific binding of MEOX1 and MEOX2 to DNA is abolished by mutation or deletion of the homeodomain.</i>	146
4.4.2.3.	<i>MEOX1 and MEOX2 activate transcription from the $p21^{CIP1/WAF1}$ promoter via a DNA-binding independent mechanism that requires SP1</i>	151
4.4.3.	MEOX1 and MEOX2 activate $p16^{INK4a}$ expression via a DNA-binding dependent mechanism.....	164
4.4.3.1.	<i>MEOX1 and MEOX2 activate transcription from the endogenous $p16^{INK4a}$ promoter in endothelial cells.</i>	164
4.4.3.2.	<i>MEOX1 and MEOX2 activate transcription from the $p16^{INK4A}$ promoter via a DNA-binding dependent mechanism.</i>	177
4.4.3.3.	<i>MEOX1 and MEOX2 sequence specifically bind to the proximal homeodomain binding site from the $p16^{INK4a}$ promoter.</i>	180
4.4.3.4.	<i>MEOX1 activates transcription of both CDKN2A isoforms in endothelial cells.</i>	186

4.4.4.	MEOX2 is sufficient, but may not be required for <i>p21^{CIP1/WAF1}</i> and <i>p16^{INK4a}</i> expression in ECs	190
4.4.5.	MEOX1 and MEOX2 prevent cellular proliferation and induce senescence	199
4.5.	Conclusions and future directions.....	217
 CHAPTER 5: IDENTIFICATION OF NOVEL MEOX TARGET GENES IN ENDOTHELIAL CELLS		
		220
5.1.	Introduction.....	220
5.2.	Rationale, hypothesis and aims.....	222
5.3.	Materials and methods	224
5.3.1.	Cloning the <i>FOXO4</i> upstream promoter region.....	224
5.3.2.	Luciferase assays	224
5.3.3.	Quantitative real-time PCR.....	225
5.3.4.	Affymetrix expression arrays.....	225
5.3.5.	Data pre-processing and gene set enrichment analysis.....	225
5.3.6.	Western blot	226
5.3.7.	Statistical analysis	226
5.4.	Results and discussion	227
5.4.1.	MEOX2 does not regulate <i>FOXO4</i> gene expression in HUVECs.....	227
5.4.2.	Identification of novel endothelial MEOX target genes.....	232

5.4.2.1.	<i>Preliminary microarray data analysis; quality control and exploratory analysis</i>	235
5.4.2.2.	<i>Discovery of a MEOX2 negative feedback loop</i>	246
5.4.2.3.	<i>Gene set enrichment analysis</i>	252
5.4.2.4.	<i>Validation of putative target genes</i>	257
5.5.	Conclusions and future directions	268
CHAPTER 6: DISCUSSION, CONCLUSIONS AND FUTURE DIRECTIONS...		271
6.1.	Discussion and conclusions	271
6.2.	Future directions	278
REFERENCES		281
APPENDICES		302

List of tables

Table 3-1: List of antibodies and incubation conditions used for western blotting.....	57
Table 4-1: List of primers used for quantitative real-time PCR.	111
Table 4-2: List of EMSA probes.....	114
Table 5-1: Genes that have altered expression levels in response to MEOX over-expression or knockout/knockdown.	221
Table 5-2: Overview of the experimental design classes.....	240
Table 5-3: Novel genes that have altered expression levels in response to MEOX over-expression.	270
Table 6-1: MEOX interacting proteins.	279
Table B-1: List of PCR primers used to create MEOX1 and MEOX2 expression constructs.	309
Table B-2: List of expression vectors and the MEOX1 and MEOX2 proteins that they encode.	310
Table B-3: List of adenoviruses and the MEOX1 and MEOX2 proteins that they encode.	312

List of figures

Figure 1-1: Development of the vascular system.	3
Figure 1-2: The MEOX homeodomain is well conserved.	13
Figure 1-3: Functional roles of MEOX2 in endothelial cells.	32
Figure 3-1: Primary cells isolated from porcine coronary arteries express VSMC markers.	49
Figure 3-2: Difference between the calculated adenoviral titer using the TCID ₅₀ and RapidTiter method for the same viral stocks.	53
Figure 3-3: Expression of MEOX proteins in A7r5 cells does not induce caspase 3 cleavage.....	63
Figure 3-4: Quantification of apoptosis using a fluorescent TUNEL assay.	66
Figure 3-5: Adenoviral over-expression of MEOX proteins in A7r5 cells does not induce apoptosis.	68
Figure 3-6: Expression of MEOX proteins in primary porcine VSMCs.	70
Figure 3-7: Adenoviral over-expression of homeodomain deleted MEOX2 ^{K195_K245del} induces apoptosis in primary VSMCs.....	73
Figure 3-8: Expression of C-terminal FLAG-tagged MEOX proteins in HUVECs.....	76
Figure 3-9: Adenoviral over-expression of C-terminal FLAG-tagged MEOX proteins in HUVECs does not induce apoptosis.	78
Figure 3-10: Adenoviral over-expression of p53 decreases HUVEC viability.	80
Figure 3-11: Adenoviral over-expression of C-terminal FLAG-tagged MEOX proteins in HUVECs does not decrease cell viability.	82
Figure 3-12: Expression of N-terminal FLAG-tagged MEOX proteins in HUVECs.	85

Figure 3-13: Adenoviral over-expression of N-terminal FLAG-tagged MEOX proteins in HUVECs does not induce apoptosis.	87
Figure 3-14: Adenoviral over-expression of N-terminal FLAG-tagged MEOX proteins in HUVECs does not reduce cell viability.	89
Figure 3-15: Hypoxia and nutrient starvation of HUVECs does not potentiate MEOX induction of apoptosis.	92
Figure 3-16: Over-expression of MEOX1 induces caspase-3 cleavage in HUVECs.	95
Figure 3-17: Prolonged over-expression of MEOX1 or MEOX2 does not induce necrotic cell death.	97
Figure 4-1: The cell cycle and the role of MEOX2.	105
Figure 4-2: Schematic representation of the MEOX1 and MEOX2 protein constructs used in this thesis.	122
Figure 4-3: Expression and subcellular localization of MEOX1 and MEOX2 proteins in HEK293 cells.	125
Figure 4-4: Expression and subcellular localization of MEOX1 and MEOX2 proteins in HUVECs.	127
Figure 4-5: Enrichment of MEOX protein expression at the inner nuclear envelope in HUVECs.	130
Figure 4-6: The mRNA expression of <i>MEOX2</i> and <i>p21^{CIP1/WAF1}</i> in HUVECs is affected by serum content.	133
Figure 4-7: MEOX2 dose-dependently up-regulates <i>p21^{CIP1/WAF1}</i> protein expression in HUVECs.	136

Figure 4-8: MEOX2 time-dependently up-regulates $p21^{CIP1/WAF1}$ mRNA and protein expression in HUVECs.	138
Figure 4-9: MEOX2 activates $p21^{CIP1/WAF1}$ mRNA and protein expression via a DNA-binding independent mechanism in endothelial cells.	140
Figure 4-10: MEOX1 and MEOX2 increase total p53 protein expression in HUVECs.	144
Figure 4-11: MEOX1 and MEOX2 sequence specifically bind to DNA probes containing homeodomain binding sites.	147
Figure 4-12: MEOX1 and MEOX2 in transduced HUVEC and transfected HEK293 nuclear extracts bind to a region of the $p21^{CIP1/WAF1}$ promoter.	149
Figure 4-13: MEOX1 and MEOX2 activate transcription from the 2272 bp $p21^{CIP1/WAF1}$ promoter in HEK293 cells.	153
Figure 4-14: MEOX1 and MEOX2 activate transcription from the 232 bp $p21^{CIP1/WAF1}$ promoter independent of DNA-binding.	155
Figure 4-15: Mutant MEOX2 proteins can activate transcription from the 232 bp $p21^{CIP1/WAF1}$ promoter.	159
Figure 4-16: Inhibition of SP1 binding to DNA drastically attenuates MEOX activation from the 232 bp $p21^{CIP1/WAF1}$ promoter.	162
Figure 4-17: MEOX2 seemingly up-regulates p16 ^{INK4a} protein expression in HUVECs.	165
Figure 4-18: Temporal regulation of p16 ^{INK4a} expression by ectopic MEOX2 in HUVECs.	167

Figure 4-19: MEOX1 activates $p16^{INK4a}$ expression in HUVECs 48 hours post-transduction.....	170
Figure 4-20: DNA-binding domain mutated MEOX2 ^{Q235E} does not induce $p16^{INK4a}$ protein expression.	172
Figure 4-21: MEOX2 is present at the $p16^{INK4a}$ promoter in HUVECs.....	175
Figure 4-22: MEOX1 and MEOX2 activate transcription from the 564 bp $p16^{INK4a}$ promoter.....	178
Figure 4-23: MEOX1 and MEOX2 bind to the proximal homeodomain binding site in the $p16^{INK4a}$ promoter.....	182
Figure 4-24: The proximal homeodomain binding site from the $p16^{INK4a}$ promoter is bound by wild-type MEOX proteins in HUVEC nuclear extracts.	184
Figure 4-25: MEOX1, but not MEOX2, activates $p14^{ARF}$ mRNA expression in HUVECs.	187
Figure 4-26: Control non-targeting siRNA pool decreased <i>MEOX2</i> mRNA expression in HUVECs.	191
Figure 4-27: MEOX1 and MEOX2 increase $p21^{CIP1/WAF1}$ and $p16^{INK4a}$ expression in LECs.	194
Figure 4-28: Knockdown of MEOX2 does not decrease $p21^{CIP1/WAF1}$ or $p16^{INK4a}$ mRNA expression in LECs.	196
Figure 4-29: Regulation of HUVEC proliferation by MEOX1 and MEOX2.....	200
Figure 4-30: MEOX1 and MEOX2 increase the proportion of HUVECs in the G ₀ /G ₁ phase of the cell cycle.	202
Figure 4-31: The proliferation rate of HUVECs decreases with increasing passage. ...	205

Figure 4-32: The mRNA and protein expression of <i>p21^{CIP1/WAF1}</i> and <i>p16^{INK4a}</i> increases with passage number in HUVECs.	207
Figure 4-33: Senescence of HUVECs increases with passage number.	209
Figure 4-34: MEOX2 induces endothelial cell senescence.	212
Figure 4-35: DNA-binding dependency of MEOX2 induced endothelial cell senescence.	213
Figure 4-36: MEOX2 mRNA expression is decreased in aged HUVECs.	216
Figure 4-37: Regulation of the endothelial cell cycle by MEOX1 and MEOX2.	218
Figure 5-1: DNA sequence of the putative 2928 bp human <i>FOXO4</i> promoter.	228
Figure 5-2: MEOX2 does not regulate <i>FOXO4</i> transcription in HUVECs.	229
Figure 5-3: Diagrammatic overview of the microarray experiment.	233
Figure 5-4: Microarray quality control.	236
Figure 5-5: Principal component analysis of microarray samples.	238
Figure 5-6: Relative expression of <i>p21^{CIP1/WAF1}</i> and <i>p16^{INK4a}</i> mRNA as measured by microarray hybridization and quantitative real-time PCR.	243
Figure 5-7: Endogenous <i>MEOX2</i> expression in HUVECs is decreased by ectopic <i>MEOX2</i> protein over-expression.	247
Figure 5-8: <i>MEOX2</i> time-dependently down-regulates its own mRNA expression in HUVECs.	250
Figure 5-9: <i>MEOX1</i> and <i>MEOX2</i> decrease the expression of genes involved in angiogenesis, pseudouridine synthesis and cell cycle regulation.	253

Figure 5-10: Heatmap demonstrating selected probe-set expression values from HUVECs over-expressing EGFP, MEOX1, MEOX2 or DNA-binding domain mutated MEOX2 ^{Q235E}	255
Figure 5-11: MEOX protein over-expression does not significantly affect the expression of pseudouridine synthase complex components.....	258
Figure 5-12: MEOX1 and MEOX2 up-regulate <i>ICAM-1</i> mRNA expression in HUVECs.	261
Figure 5-13: MEOX1 and MEOX2 reduce <i>eNOS</i> mRNA and protein expression in HUVECs.	263
Figure 5-14: MEOX1 and MEOX2 repress transcription from the human <i>eNOS</i> promoter.....	266
Figure 6-1: Diagrammatic summary of research findings.	273
Figure A-1: The middle region of MEOX2 is sufficient for interaction with mouse zinc-finger protein 672.....	303
Figure C-1: Expression of N-terminal and C-terminal FLAG-tagged MEOX proteins in HEK293 cells.....	314
Figure C-2: Nuclear localization of N-terminal and C-terminal FLAG-tagged MEOX proteins in HEK293 cells.....	315
Figure C-3: The position or inclusion of the FLAG epitope does not affect MEOX2 transcriptional activation from the 2272 bp <i>p21^{CIP1/WAF1}</i> promoter.	317
Figure C-4: The position of the FLAG-tag does not affect MEOX2 activation of <i>p21^{CIP1/WAF1}</i> expression in endothelial cells.	319

Figure D-1: Test for optimal DNA fragmentation using sonication.....	321
Figure D-2: MEOX2 binds to magnetic beads, but not to polyacrylamide beads.	323
Figure E-1: Summary of MEOX2 bound protein purification using the TAP-TAG system.	326
Figure E-2: Expression of TAP-tagged MEOX proteins in mouse cells transduced with ecotropic retrovirus.	328
Figure E-3: Expression of C-terminal TAP-tagged MEOX proteins in HEK293 cells.	330
Figure E-4: TAP-tagged MEOX proteins bind to a DNA probe containing homeodomain binding sites from the $p21^{CIP1/WAF1}$ promoter.....	332
Figure E-5: TAP-tagged MEOX proteins do not induce $p21^{CIP1/WAF1}$ expression.	334

List of appendices

Appendix A: MEOX2 middle region is sufficient for zinc finger binding.....	302
Appendix B: Description of MEOX construct generation.....	305
Appendix C: The location of the FLAG epitope does not affect MEOX expression or function	313
Appendix D: Chromatin immunoprecipitation optimization and troubleshooting	320
Appendix E: Identification of MEOX binding partners	325

List of abbreviations

AD	Alzheimer's disease
AF	adventitial fibroblast
ANTP	Antennapedia
ARF	alternate reading frame
BAX	BCL2-associated X protein
BCL2	B-cell CLL/lymphoma 2
BrdU	5-bromo-2-deoxyuridine
BSA	bovine serum albumin
CDK	cyclin-dependent kinase
CDKN1A	cyclin-dependent kinase inhibitor 1A
CDKN2A	cyclin-dependent kinase inhibitor 2A
ChIP	chromatin immunoprecipitation
CIP1	CDK-interacting protein 1
DKC1	dyskerin
E	embryonic day
EC	endothelial cell
EGFP	enhanced green fluorescent protein
EMSA	electrophoretic mobility shift assay
EMT	epithelial-mesenchymal transition
eNOS	endothelial nitric oxide synthase
FBS	fetal bovine serum
FOXO4	forkhead box O4

GSEA	gene set enrichment analysis
HEK293	human embryonic kidney 293 cells
HGPS	Hutchinson-Gilford Progeria Syndrome
HOX	homeobox gene
HUVEC	human umbilical vein endothelial cell
ICAM-1	intercellular adhesion molecule 1
INK4a	inhibitor of CDK4
LEC	lymphatic endothelial cell
MEOX	mesenchyme homeobox
miR	microRNA
MOI	multiplicity of infection
NKX3-2	NK3 homeobox 2
NO	nitric oxide
NOS3	nitric oxide synthase 3
PAX	paired box
PBS	phosphate buffered saline
Rb	retinoblastoma protein
ROS	reactive oxygen species
SA- β -gal	senescence-associated beta-galactosidase
siRNA	small interfering RNA
SMP	skim milk powder
TBS	tris-buffered saline
TLS	translation start site

TSS	transcription start site
TUNEL	terminal deoxynucleotidyl transferase dUTP nick end label
UTR	untranslated region
VCAM-1	vascular cell adhesion molecule 1
VEGF	vascular endothelial growth factor
VSMC	vascular smooth muscle cell
WAF1	wild-type p53-activated fragment 1
ZFP672	zinc finger protein 672

CHAPTER 1: INTRODUCTION

1.1. The cardiovascular system

1.1.1. Endothelial cells

Endothelial cells (ECs) are highly specialized squamous epithelial cells that line the lumens of both the cardiovascular and lymphatic systems, including the blood vessels, the heart and the lymph vessels [1]. ECs exist as a continuous monolayer (called the endothelium) that is separated from neighbouring cell types by a specialized sheet of extracellular matrix known as the basement membrane. The endothelium controls many physiological functions such as blood pressure regulation, blood coagulation, inflammation and immune responses [1]. ECs regulate vascular tone by producing and secreting vasoconstrictors (e.g. endothelin-1, angiotensin II) and vasodilators (e.g. nitric oxide (NO), prostacyclin, c-natriuretic peptide) that act upon vascular smooth muscle cells (VSMCs), the contractile force generating cells which encircle the endothelial layer [2]. ECs can also regulate coagulation by expressing either pro- or anti-coagulant molecules that affect platelet adhesion and aggregation [1]. The endothelium regulates inflammation through changes in vascular permeability as well as altered expression of leukocyte adhesion molecules (e.g. intercellular adhesion molecule 1 (ICAM-1), vascular cell adhesion molecule 1 (VCAM-1)) on the luminal surface [1].

EC gene expression profiles are specific to the type (vein, artery or lymphatic), size (macrovascular or microvascular) and tissue origin of the vessel [1,3]. For example, ECs that form the blood-brain barrier express higher levels of tight junction proteins to prevent the diffusion of molecules between the blood and the brain interstitial fluid [4,5].

Therefore, brain ECs also express specific transporters to move essential molecules across this barrier [4,5]. Thus, endothelial cell homeostasis is vital for the proper functioning of the vasculature as well as the health of the organism.

1.1.2. Vascular smooth muscle cells

VSMCs, which make up the medial layer within the blood vessels, provide tone and support to the endothelial cell layer of the arteries and veins. In response to endothelial signals, VSMC contraction is either enhanced or reduced, leading to vasoconstriction or vasodilation, respectively [2]. VSMCs can exist in two phenotypic states; the quiescent (non-proliferative), contractile VSMC phenotype found in stable vessels or the proliferative, synthetic phenotype seen during vascular remodeling and after vascular damage [6]. Proliferative VSMCs are the major contributor to pathologic vascular stenosis (blood vessel narrowing) [7].

1.1.3. Vascular development

The cardiovascular system is the first organ system to develop during embryogenesis. Pluripotent hemangioblast cells within the mesoderm give rise to the blood islands (Figure 1-1). Cells on the periphery of the blood islands differentiate into the ECs that will later form the capillaries [8] (Figure 1-1). During embryogenesis, the process of *de novo* vessel formation by the ECs is termed vasculogenesis [9], which results in the formation of the initial vascular plexus. This process is critically dependent upon vascular endothelial growth factor (VEGF) signalling. Loss of expression of the VEGF ligand, the VEGF receptor (VEGFR)-2 (also known as KDR) or the co-receptors, neuropilin-1 and neuropilin-2, precludes embryonic vasculogenesis [10,11].

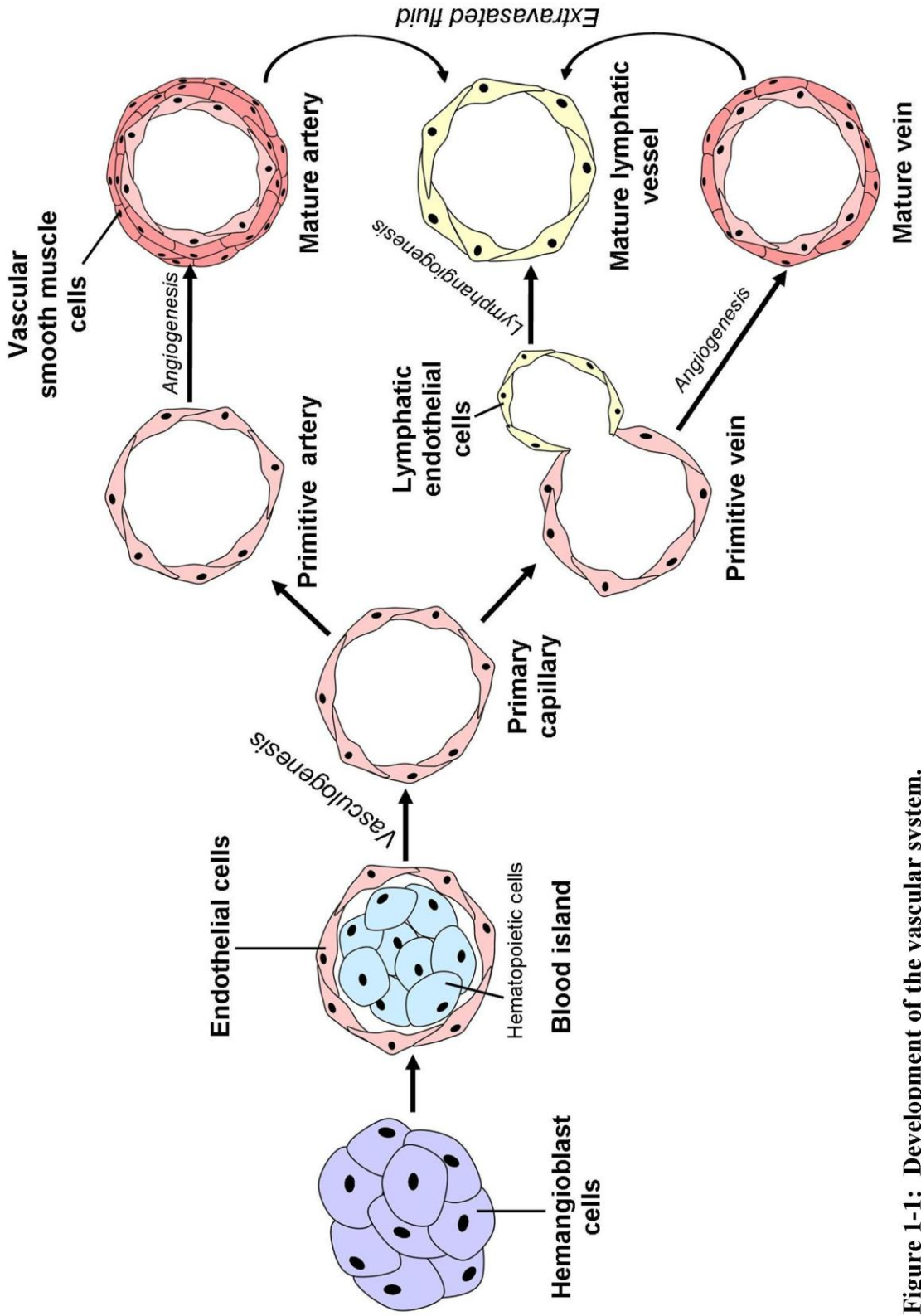


Figure 1-1: Development of the vascular system.

Figure 1-1: Development of the vascular system.

Early in embryogenesis, the hemangioblast gives rise to both endothelial and hematopoietic cells that form the blood islands. After formation of the initial vascular plexus (vasculogenesis), arterial and venous endothelial cells differentiate and then the lymphatic endothelial cells bud off from the developing veins. Finally, during angiogenesis the arteries and veins are refined and vascular smooth muscle cells are recruited to the vessels for stabilization. [17]

Even before the heart begins to beat, the arteries and veins can be distinguished at a molecular level [12]. Ephrin B2 is expressed by arterial ECs while its receptor, ephrin type-B receptor 4, is expressed by venous ECs. Upon establishment of blood flow, the early network of capillaries is remodelled in a process termed angiogenesis [13]. This remodelling includes sprouting and branching, as well as pruning of the initial vascular plexus. Loss of ephrin B2 or ephrin type-B receptor 4 results in defective angiogenic remodelling and embryonic death. During angiogenesis, pericytes and VSMCs are recruited to stabilize the developing vessels in a process that is mediated by angiopoietin-1/endothelial TEK tyrosine kinase (also known as TIE-2) signalling [14]. Pericytes surround the smaller arterioles and venules, while VSMCs are recruited to the larger arteries and veins. Arteries, which have a higher intraluminal pressure than veins, have a much thicker layer of VSMCs surrounding the EC layer (Figure 1-1). Vascular stabilization is essential to prevent excessive vascular permeability and vessel rupture.

A second network of vessels, the lymphatics, are responsible for the uptake of extravasated fluid from the tissues and return this fluid to the cardiovascular system. Lymphatic ECs sprout from the cardinal vein to form lymph sacs that will develop into the lymphatic vessels (Figure 1-1) [15]. Compared to blood vessels, lymphatic vessels are blind-ended, thinner walled and more permeable due to an incomplete basement membrane, fewer inter-EC junctions and much fewer mural support cells (e.g. VSMCs, pericytes) [16]. The processes of vasculogenesis, angiogenesis and lymphangiogenesis require the precise regulation of cellular proliferation, differentiation, and migration to allow the proper formation of the cardiovascular system [12].

1.1.4. Postnatal angiogenesis

Cells of the adult vasculature remain quiescent until a need for new blood supply is encountered, such as in wound healing [18], menstruation [19] and endurance exercise [20]. Induction of postnatal angiogenesis occurs in response to hypoxia and inflammation [13]. The process of angiogenesis must be carefully regulated in order to meet the needs of the organism, but not result in unnecessary growth or remodelling of the blood vessels since excessive angiogenesis and vascular remodelling contributes to the development of diseases such as diabetic retinopathy, atherosclerosis, tumour growth and metastasis [13]. In contrast, insufficient angiogenesis or vascular repair can result in limb ischemia, myocardial infarction, stroke and Alzheimer's disease (AD) [13].

1.1.5. Endothelial dysfunction and vascular disease

A hallmark of vascular disease is endothelial dysfunction [21]. Age, obesity, smoking and diabetes are risk factors that damage ECs and promote the progression of vascular diseases such as atherosclerosis, hypertension and stroke [22]. Acute injury and chronic stress of ECs leads to changes in gene expression, which underlie EC dysfunction [22,23]. Endothelial dysfunction is primarily characterized by the loss of NO bioavailability in the endothelium, which results in decreased vasorelaxation [24]. However, enhanced reactive oxygen species (ROS) production, decreased proliferative capacity and increased expression of pro-thrombotic (e.g. endothelin-1, plasminogen activator inhibitor-1) and pro-inflammatory (e.g. ICAM-1, VCAM-1, E-selectin) mediators are also features of EC dysfunction [24,25].

Indeed, impaired vasodilation is predictive of future adverse cardiovascular events [24,25]. In ECs, the major producer of NO is the endothelial nitric oxide synthase

(eNOS) enzyme, which is encoded by the nitric oxide synthase 3 (*NOS3*) gene. NO production is dependent upon both the level of expression and the activity (regulated by phosphorylation) of eNOS [2,26]. Furthermore, ROS react with NO, producing peroxynitrite, thereby reducing the amount of bioavailable NO [2,26]. Thus, factors that positively/negatively influence eNOS transcription and phosphorylation or ROS production will promote endothelial function/dysfunction.

Moreover, ROS is an inducer of cellular senescence [25,27]. Senescence (permanent cell cycle arrest) is associated with aging and also contributes to atherosclerotic vascular disease [28,29]. Human blood vessels that contain atherosclerotic plaques have a higher proportion of senescent VSMCs and ECs, as compared to non-atherosclerotic vessels [30-32]. Senescent endothelial cells have reduced eNOS expression [33-35], impaired angiogenic capability [36] and altered metabolism, which result in endothelial dysfunction and the progression of vascular diseases, such as atherosclerosis [28,29].

1.2. Homeobox genes

Homeobox genes were discovered by researchers studying the genetic basis of homeotic transformations (replacement of one body segment by another) in the fruit fly, *Drosophila melanogaster*. The classic examples of this phenomenon are the mutation of the Ultrabithorax (*Ubx*) and Antennapedia (*Antp*) genes. Flies with dominant *Ubx* mutations have two sets of wings due to the replacement of the third thoracic segment (T3; haltere and third leg) by a second thoracic segment (T2; wing and second leg) [37]. Mutations in the *Antp* gene give rise to flies that have legs growing in the place of

antennae [37]. *Ubx* and *Antp* gene belong to a cluster of homeobox genes in *Drosophila* that is homologous to the homeobox (*HOX*) gene clusters (A-D) in humans [38]. A fascinating feature of *HOX* homeobox gene clusters is that the expression of the genes along the anterior–posterior axis of the organism matches the order in which the genes are arranged along the chromosome [38,39].

All homeobox genes contain a characteristic sequence motif, termed the homeobox [38]. In the majority of homeobox genes, this motif is 180 bp in length; however some genes (e.g. *HDX*, *HMBOX1*, *IRX1-6*, *MEIS1-3* and *PROX1*) contain extended homeobox sequences [38,40]. The homeobox sequence motif was discovered in 1984 by two independent groups studying *HOX* gene homologs of *Drosophila melanogaster* [41,42]. Since then, many homeobox genes have been identified, distributed throughout the genomes of other animals, plants and fungi [38]. The human genome is estimated to contain 235 functional homeobox genes and 65 homeobox pseudogenes [40]. Homeobox genes encode homeodomain containing transcription factor proteins [38]. Many of the protein products of homeobox genes are involved in regulating cell fate and differentiation as well as controlling the body plan and patterning [38,39].

1.2.1. The homeodomain

The homeodomain, which is encoded by the homeobox, is the DNA-binding domain of homeodomain transcription factors [38]. This domain has been highly conserved throughout evolution. The typical homeodomain is composed of 60 amino acid residues and contains the amino acids WFQNRR at positions 48 – 53 [38]. Structurally, this domain is composed of a flexible amino-terminal arm followed by three

α -helical segments separated by a turn and a fold, respectively [38,43]. Helix I and II are parallel to each other and perpendicular to Helix III [38,43]. These first two α -helices comprise the hydrophobic core of the homeodomain [38,43]. When the homeodomain is bound to DNA, Helix III (also known as the recognition helix) resides within the major groove of the DNA double helix [38,44]. The recognition helix makes essential contacts with DNA bases, establishing the sequence specific binding and stabilization of the protein and DNA interaction [38,45]. Typical homeodomain proteins bind to DNA via an ATTA motif (TAAT, on the complimentary DNA strand) and the glutamine residue at position 50 of the homeodomain is critical for its interaction with this motif [38,45]. In addition to the recognition helix, the flexible amino-terminal arm also interacts with DNA bases within the minor groove [38,44].

1.2.2. Classification

Classification of homeobox genes is achieved through comparative genomics and aims to organize these genes based on evolutionary relationships. The most recent and comprehensive classification scheme for human homeobox genes was published by Holland *et al.* in 2007 [40]. The authors categorized all 300 human homeobox genes and pseudogenes based primarily on the homeodomain sequence, as well as the presence of additional protein domains within these genes [40]. The homeobox gene superclass is split up into 11 classes of genes: ANTP, PRD, LIM, POU, HNF, SINE, TALE, CUT, PROS, ZF and CERS [40]. The ANTP and PRD classes contain the largest number of genes and are further divided into two sub-classes each. The ANTP sub-classes are HOXL (Hox-like) and NKL (Nkx-like), while the PRD class is divided into the PAX and PAXL (Pax-like) subclasses [40]. The HOXL sub-class contains 14 gene families made

up of 52 genes, including the *HOX*, *EVX* and *MEOX* genes [40]. The HOXL homeobox genes are unique in that their chromosomal distribution is primarily clustered. This clustering is thought to have evolved from numerous duplication events of a single *ProtoHOX*-like gene [46].

1.2.3. Regulation of angiogenesis by homeodomain proteins

Numerous homeodomain proteins have been shown to play a role in vascular development and/or post-natal angiogenesis. These include members of the *HOX*, *MEOX* (ANTP class/HOXL subclass), *HHEX*, *NANOG* (ANTP class/NKL subclass), *PRRX* (PRD class), *ISL* (LIM class), and *PROX* (PROS class) gene families.

Homeodomain proteins which have been shown to be essential for proper cardiovascular development in human or mouse include HOXA1 [47], HOXA3 [48,49], HOXA13 [50,51], paired related homeobox 1 (PRRX1) [52] and hematopoietically expressed homeobox (HHEX) [53]. Furthermore the prospero-related homeobox 1 (PROX1) homeodomain protein, although dispensable for the development of the blood vasculature, is essential for the development of the lymphatic vasculature [15,56]. In addition, several homeodomain proteins have been shown to promote post-natal angiogenesis *in vivo* or induce a pro-angiogenic phenotype in ECs *in vitro*. These include HOXA3, HOXA9, HOXB2, HOXB3, HOXB5, HOXB7, HOXD1, HOXD3, ISL LIM homeobox 1 (ISL-1) and Nanog homeobox (NANOG) [54,55,57-69]. These effects are achieved through the up-regulation of target genes that encode pro-angiogenic molecules such as matrix metalloproteinases, collagen, eNOS, ephrins/ephrin receptors, angiopoietin-1/endothelial TEK tyrosine kinase, integrins, urokinase-type plasminogen activator/ urokinase plasminogen activator surface receptor, VEGF/VEGFRs and

cadherin-5 (also known as VE-cadherin). Conversely HOXA5 and HOXD10 have been shown to inhibit angiogenesis by increasing the expression of anti-angiogenic target genes (e.g. thrombospondin 2) and decreasing the expression of pro-angiogenic target genes (e.g. VEGFR-2, ephrin A1) [70-73]. PROX1 is pro-lymphangiogenic and activates the expression of cell cycle and lymphatic specific EC proteins (e.g. cyclin E1, cyclin E2, podoplanin, VEGFR-3 and fibroblast growth factor receptor 3) and decreases the expression of blood specific EC proteins (e.g. laminin, neuropilin-1, ICAM-1) [74-77].

Expression of homeodomain proteins within the vasculature is spatially and temporally regulated. Recently, it was shown that expression of HOXA3 and HOXC11 in the adult mouse is restricted to different blood vessels; HOXA3 was detected in the major arteries of the trunk while HOXC11 was restricted to the hindlimb vasculature [78]. During differentiation of mouse embryonic stem cells into ECs, expression of pro-angiogenic HOXA3 and HOXD5 is increased during the early proliferative/migratory phase, while anti-angiogenic HOXA5 and HOXD10 are expressed during the maturation phase [79]. Similarly, during mesenchymal stem cell differentiation to ECs, expression of HOXA7 and HOXB3 was increased while the expression of HOXA3 and HOXB13 was decreased [80]. Thus, the differential expression of homeobox genes modulates target gene expression and regulates angiogenesis.

1.3. Mesenchyme homeobox gene family; MEOX1 and MEOX2

The *MEOX1* and *MEOX2* genes belong to the ANTP class, HOXL subclass, of homeobox genes and comprise the *Meox* gene family. The *MEOX* genes were named after their restricted expression in the mouse embryo, initially in the mesoderm derived

somites and later in mesenchymal tissues. As discussed in this section, MEOX1 and MEOX2 are involved in the development of muscle and bone and are important regulators of vascular function. Identification of downstream targets of the MEOX proteins has been instrumental in understanding their role in development and in the regulation of cardiovascular cell types.

1.3.1. Discovery and comparison

1.3.1.1. Cloning of the human MEOX genes

The human *MEOX1* and *MEOX2* genes were identified in 1994 [81-83]. The human *MEOX1* gene is located on the long arm of chromosome 17 (q21) [81], whereas the human *MEOX2* gene is located on the short arm of chromosome 7 (p21-p22) [82,83].

1.3.1.2. Domains and percent amino acid identity

We analyzed the degree of conservation between the various functional domains of human MEOX1 and MEOX2 proteins (Figure 1-2) [84]. While the amino acid composition of the MEOX1 and MEOX2 homeodomains is nearly identical (95%), there is a much lower percentage of amino acid identity between MEOX1 and MEOX2 outside of this domain (Figure 1-2) [84]. The homeodomain is the DNA-binding domain of the MEOX proteins. However, the MEOX homeodomains have also been shown to act as protein-protein interaction domains, as in the case of MEOX2 binding to the paired box 3 (PAX3) protein and MEOX1 binding to the sex determining region Y-box 10 (SOX10) protein [85,86].

The N-terminus and middle domain are the next most conserved domains between the MEOX1 and MEOX2 proteins, with 35% and 38% amino acid identity, respectively (Figure 1-2) [84]. There are currently no known functions for the MEOX N-terminal

MEOX protein domains

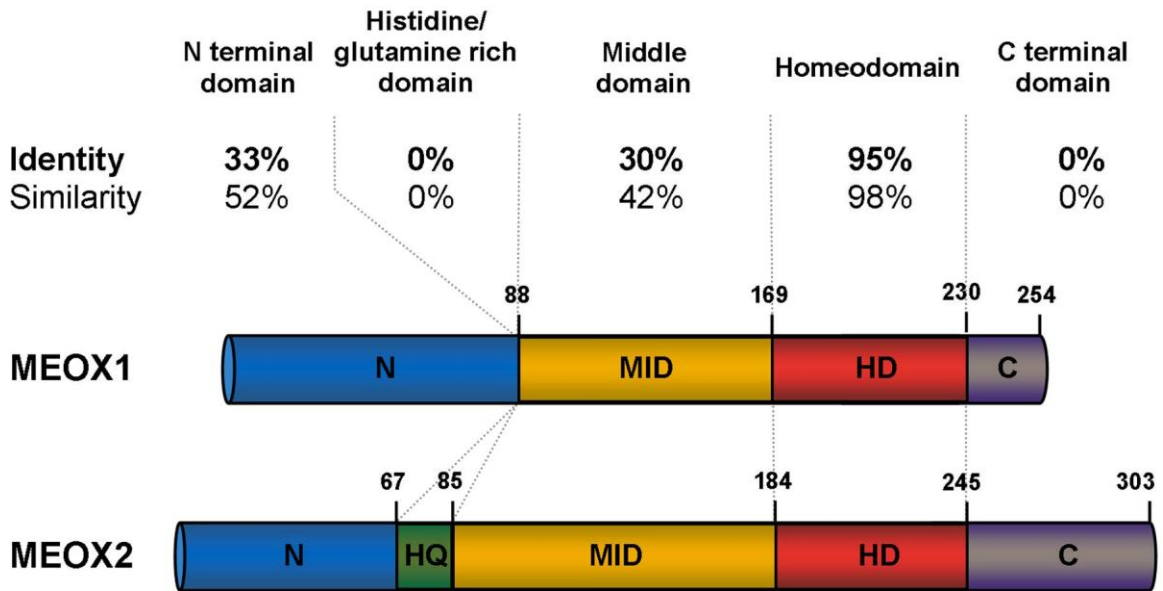


Figure 1-2: The MEOX homeodomain is well conserved.

The amino acid sequence of the corresponding human MEOX1 and MEOX2 protein domains were aligned and compared using the protein Basic Local Alignment Search Tool (BLASTP) program from NCBI (<http://blast.ncbi.nlm.nih.gov>) by enabling the ‘align two or more sequences’ option [92].

domain. However, the middle region, along with the homeodomain, was shown to be important in the regulation of $p16^{INK4a}$ expression [87]. In addition, the middle region of MEOX2 is sufficient for binding to ring finger protein 10 (RNF10) [88] and zinc finger protein 672 (ZFP672) (Appendix A). These results suggest that the middle domain of the MEOX proteins may play a role in mediating protein-protein interactions.

Unlike MEOX2, MEOX1 does not contain a histidine/glutamine rich domain, which is a putative transactivation domain [89]. Previously, the histidine/glutamine rich domain of MEOX2 was shown to be important for the ability of MEOX2 to activate transcription from the $p21^{CIP1/WAF1}$ upstream promoter region, as deletion of this domain dramatically decreased MEOX2 induced reporter gene expression [89]. Similar polyhistidine/polyglutamine rich motifs are found in other human proteins [90], such as the homeodomain transcription factor HOXA1, a known transcriptional activator [91].

1.3.2. Evolution of the *MEOX* genes

1.3.2.1. *MEOX* gene homologs

MEOX genes are found in many species throughout the animal kingdom; however, the number of *MEOX* genes present within the different genomes is varied. Orthologs of human *MEOX1* and *MEOX2* have been cloned from vertebrates such as the mouse (*Mus musculus*) [93], rat (*Rattus rattus*) [94] and chicken (*Gallus gallus*) [95]. In addition, the *Xenopus laevis* (frog) ortholog of *MEOX2* has been described; however the authors were unable to identify a *MEOX1* ortholog in the frog [96]. The single *Xenopus meox* gene is likely a *MEOX2* ortholog as it contains a histidine/glutamine rich domain, which is not present in *MEOX1*. The amino acid sequence of rat *Meox2* is 98% identical to human, 99% identical to mouse, 95% identical to chicken and 86% identical to frog *meox2*

[82,95,96]. The *MEOX2* homeodomain is 100% conserved at the amino acid level between all of these species.

A single *MEOX* gene homolog is also present in the genome of non-vertebrates such as *Branchiostoma floridae* (lancelet) [97], *Ciona intestinalis* (sea squirt) [98], *Saccoglossus kowalevskii* (hemichordate worm) [99], *Drosophila melanogaster* (fruit fly) [100], *Haliothis rufescens* and *Haliothis asinina* (mollusc) [101,102], *Dugesia tigrina* (planarian, non-parasitic flatworm) [103] and *Hydra magnipapillata* [104]. Interestingly, the *Parazoanthus parasiticus* (sponge) genome has two *MEOX* gene homologs [105] and the *Caenorhabditis elegans* (roundworm) genome lacks any identifiable *MEOX* genes [106,107]. *MEOX* gene homologs in lower animals have been identified based on the high degree of nucleic acid sequence conservation within the *MEOX* homeobox and suggests that the *MEOX* genes are very important.

1.3.2.2. *MEOX* gene ancestry

Phylogenetic sequence analysis of homeodomain amino acid sequences identified the *MEOX* genes as being ANTP class homeobox genes [108]. From analysis of the chromosomal location of ANTP class of homeobox genes in human and mouse it was further concluded that the *MEOX* and *EVX* genes belong to the extended *HOX* gene cluster [109]. *MEOX1* and *MEOX2* are found to be loosely linked to the *HOXB* and *HOXA* gene clusters, respectively [107,109]. Based on sequence similarity, it is proposed that *EVX* and *MEOX* gene families arose from a single ancestor gene and that this gene was linked to the *ProtoHOX* gene cluster [107]. Tandem duplication of this homeobox gene cluster created the extended *HOX* cluster and *ParaHOX* cluster [107]. Breakage of the tandem clusters resulted in the *EVX* gene at the posterior end of the *HOX* cluster, the

MEOX gene at the anterior end of the *HOX* cluster and isolation of the *ParaHOX* cluster [107]. Due to the close proximity and sequence similarity of *EVX*, *MEOX* and *HOX* genes, it is postulated that the *MEOX/EVX* gene ancestor and the *ProtoHOX* gene ancestor arose from duplication of a single *HOX*-like gene [46]. Furthermore, as *MEOX1* and *MEOX2* are both found anterior to a *HOX* gene cluster, it is likely that the *MEOX* gene duplication which gave rise to the *MEOX1* and *MEOX2* paralogs occurred as an extension of a *HOX* cluster duplication event [46].

1.3.3. Embryonic gene expression

1.3.3.1. Human

There is very limited knowledge regarding *MEOX* gene expression in humans. *MEOX1* was shown to be expressed in skin during the first and second trimester of development, as well as in neonatal skin [110]. *MEOX1* mRNA was detected in the epidermis, dermis and cells of the hair follicles during the second trimester, while in the third trimester *MEOX1* mRNA expression was restricted to the cells within the inner layer of hair follicles [110]. In contrast, *MEOX1* was not expressed in adult skin [110].

MEOX2 was shown to be expressed in human placenta [111]. *MEOX2* mRNA expression was detected in trophoblast cells in the first trimester, third trimester and term placentas [111,112]. Furthermore, *MEOX2* mRNA expression was also detected in placental macro- and micro-vascular ECs [113].

1.3.3.2. Other vertebrates

1.3.3.2.1. Mouse

Placing the *Cre* recombinase gene under the control of the endogenous mouse *Meox* gene promoters has allowed various researchers to study the initial temporal and spatial

expression of *Meox* genes during embryonic development by screening for reporter gene activation. Using this approach, Tallquist *et al.* [114] demonstrated that *Meox2* is first expressed in epiblast cells of the mouse blastocyst at embryonic day (E) 5.5.

Embryonic *Meox1* expression commences at the onset of somite development, at E7.5 in the presomitic mesoderm [115,116]. *Meox1* mRNA expression remains confined to the presomitic mesoderm and developing somites through to approximately E11.5 when it then also becomes expressed in the pharyngeal arches and the outflow tract of the heart [93,115]. *Meox1* mRNA is not expressed in the mouse limb buds until E11.5, at which time the expression is very low [117,118]. At later stages (E12.5-14.5), *Meox1* mRNA is expressed in the mesenchyme of various developing organs including: gut, body wall, truncus arteriosus and atrioventricular cushions of the heart, kidney, ribs, vertebrae, tongue, jaw and eye muscles [93]. *Meox1* mRNA expression in the developing mouse embryo is highest during somitogenesis (E9.5); however, *Meox1* expression is maintained throughout embryonic development [119].

Meox2 mRNA is not expressed in the presomitic mesoderm, but is expressed in the somites at E8.5 [93]. At E11.5 *Meox2* mRNA expression is detected in the limb buds, mesenchyme of the kidney and palate [115,120,121]. Alluding to its importance in muscle development, MEOX2 protein expression has been found in all three types of muscle during development; myocardium of the heart, smooth muscle of the gut and stomach and skeletal muscles of the head, trunk and limbs [122].

1.3.3.2.2. *Chick*

The embryonic expression of *Meox1* and *Meox2* mRNA in the chick is comparable to that of the mouse. *Meox1* mRNA expression in the developing chick embryo starts in the

pre-somitic mesoderm (stage 6), becomes localized throughout the developing somites (stage 10) and is later restricted to the posterior halves of the somites (stage 20) [118]. At stage 20, *Meox1* mRNA is also detected in the tail bud, first pharyngeal arch and the lateral rectus muscles of the eye [118]. At stage 22, *Meox1* mRNA becomes expressed in the dorsal and ventral regions of limb buds and at stage 25, *Meox1* mRNA is also detected in the fourth and fifth pharyngeal arches, truncus arteriosus of the heart and the oesophagus [118].

Meox2 mRNA expression in the developing chick embryo commences within the formed somites (stage 11), and like *Meox1*, later becomes restricted to the posterior halves of the somites (stage 20) [95,118]. At stage 21, *Meox2* mRNA expression is detected in the myoblasts of the chick limb buds and then in the dorsal and ventral regions (pre-muscle masses) of the limb buds at stage 22 [95,118]. At stage 25, *Meox2* mRNA is detected in the second pharyngeal arch [118]. MEOX2 protein is expressed in the epicardium and myocardium of the chick heart during the late stages of development (stages 35-39) [123].

Thus, the expression patterns of *Meox1* and *Meox2* are similar, but are largely non-overlapping. For example, expression of *Meox1* and *Meox2* mRNA is detected within the dorsal and ventral regions of the developing limb bud, but are only co-expressed in a fraction of these regions [118].

1.3.3.2.3. *Frog*

During *Xenopus* (frog) development, *meox2* mRNA expression begins at the gastrulation stage and increases until the tailbud stage, where it is expressed

predominantly in the trunk and tail [124]. *Xenopus meox2* mRNA expression was detected in undifferentiated mesoderm [124].

1.3.3.3. *Non-vertebrate animals*

As mentioned above, a single *MEOX* gene homolog is found in several non-vertebrate organisms of the animal kingdom and for a few, embryonic expression of these *MEOX* homologs has been studied. For example, during somitogenesis, the *Branchiostoma floridae* (lancelet) *MEOX* gene is expressed in the anterior portion of the presomitic mesoderm and newly formed somites [97]. *MEOX* mRNA expression in the established somite decreases as the subsequent somite is being shaped and is completely lost by the time a new somite is fully formed [97]. During *Ciona intestinalis* (sea squirt) development, *MEOX* gene expression is located in the tail muscles of the embryo [125]. The *Saccoglossus kowalevskii* (hemichordate worm) *MEOX* gene is expressed in the mesoderm along the ventral midline of the developing embryo [99]. Similarly, *MEOX* gene expression in *Haliotis* (mollusc) is limited to the ventral mesoderm that develops into the foot muscle [102]. *MEOX* was not expressed in the early *Haliotis* embryo, but was present during mesodermal differentiation in the larval and post-larval stages [101].

The *MEOX* homolog of *Drosophila melanogaster*, known as *buttonless* (*btn*), is most highly expressed during the early stages of embryonic development of the fruit fly, although very low levels of mRNA transcript were detected in all later stages of development as well as in adult [100]. During the early stages of development, *btn* is highly expressed in the mesoderm-derived dorsal median cells [100]. These cells guide nerve axon extension from the dorsal midline to the muscles of the body wall. In the

absence of *btn*, dorsal median cells are absent and median nerve outgrowth does not occur [100].

1.3.4. Role in development

In order to elucidate the role of MEOX1 and MEOX2 during embryonic development, *Meox* genes were knocked out in the mouse, individually and in combination [126]. Compound heterozygous mice (*Meox1*^{+/-}, *Meox2*^{+/-}) developed normally, while the *Meox1* gene knockout mice (*Meox1*^{-/-}, *Meox2*^{+/-}) had axial skeleton abnormalities and the *Meox2* gene knockout mice (*Meox1*^{+/-}, *Meox2*^{-/-}) had reduced limb musculature [117,126,127]. Skeletal malformations in *Meox1* deficient mice included deformed ribs (missing or bifurcated), hemivertebrae in the lumbar and sacral regions, as well as fused cranial-cervical joints and tail vertebrae, causing these mice to appear smaller and with short kinked tails [126,127]. *Meox1* gene knockout mice do not have musculature defects [126], nor do they have a compensatory increase in *Meox2* expression [127]. *Meox2* deficient mice, in addition to musculature defects, have very mild skeletal defects characterized by fused tail vertebrae [126]. Furthermore, 10%-35% of homozygous *Meox2* gene knockout mice have cleft palates, a phenotype that also occurs in *Meox2* heterozygous mice [117,121].

Double *Meox* gene knockout mice (*Meox1*^{-/-}, *Meox2*^{-/-}) lack an axial skeleton (no ribs, no vertebrae in the lumbar or tail region, malformed vertebrae in the cervical and thoracic region) and have missing or reduced skeletal musculature in the head, neck, trunk and limbs [126]. In addition, double *Meox* gene knockout mice lacked the dorsal brown fat depot [126]. Thus, the developmental defects observed in the double *Meox* knockout mice are more severe than the combined abnormalities observed in each of the single

Meox gene knockout mice. This finding indicates that MEOX1 and MEOX2 have both redundant and distinct roles during development; MEOX1 has a larger role in formation of the skeleton and MEOX2 has a larger role during skeletal muscle formation [126].

Malformations in the double *Meox* gene knockout mice resulted from defects in somite differentiation, including lack of epithelialization and absence of anteroposterior polarity [126]. Indeed, reduced mRNA expression of transcription factor 15 (*Tcf15*; also known as *paraxis*) and delta-like 1 (*Dll1*), which are involved in epithelisation and anteroposterior polarity of the somites, was observed in double *Meox* gene knockout mice [126]. The somites give rise to the dermis of the skin, skeletal muscle and vertebrae, thus accounting for the observed defects in the *Meox* gene knockout mice.

1.3.4.1. Axial skeleton

Akin to the double *Meox* gene knockout mice, *Meox1* deficient mice have defects in somite differentiation; although epithelisation occurs normally, there is a lack of anteroposterior sclerotome polarity [127]. The sclerotome is the portion of the somites that gives rise to the vertebrae and ribs. The sclerotome is composed of loose, lowly proliferative mesenchyme in the anterior compartment and dense, highly proliferative mesenchyme in the posterior compartment [126,127]. The mRNA expression of *Pax1*, *Pax9*, twist homolog 1 (*Twist1*) and forkhead box C2 (*FoxC2*), which are involved in sclerotome differentiation, are decreased in double *Meox* gene knockout mice [126]. Although *Meox1* deficient mice also have skeletal abnormalities, no change in *Pax1*, *Pax9* or *FoxC2* mRNA expression was detected in these mice [127].

However, *Meox1* gene knockout mice have reduced or abolished mRNA expression of UNC homeobox (*Uncx*) and T-box 18 (*Tbx18*), respectively [127]. These factors are

involved in the control of cell proliferation and anteroposterior somite polarity [127]. Moreover, MEOX1 binds to the upstream promoter region of the *Uncx* and *Tbx18* genes *in vivo*, indicating that they are direct transcriptional target genes of MEOX1 during embryonic development [127]. Loss of sclerotome polarity due to reduced *Uncx* and *Tbx18* expression is likely the cause of the vertebral fusions seen in *Meox1* deficient mice.

Furthermore, NK3 homeobox 2 (*Nkx3-2*; also known as *Bapx1*) mRNA expression is reduced in *Meox1* gene knockout mice [127,128], and absent in double *Meox* gene knockout mice [128]. This finding indicates that both MEOX1 and MEOX2 are involved in the maintenance of *Nkx3-2* expression during embryonic development. NKX3-2 is a regulator of cell proliferation and chondrogenic differentiation (cartilage formation) of the sclerotome [127]. *Nkx3-2* was shown to be a direct transcriptional target gene of MEOX1 [128]. MEOX1 binds to the *Nkx3-2* upstream promoter region and can activate transcription from this region via a TAATTA motif (located between -880 bp and -620 bp relative to the transcriptional start site) [128]. MEOX2 was also shown to be able to bind this motif [128]. Furthermore, co-expression of PAX1 or PAX9 increases MEOX1 induced transcription from the *Nkx3-2* upstream promoter region [128]. Inhibition of sclerotome differentiation due to the loss of *Nkx3-2*, *Pax1* and *Pax9* expression in *Meox1*^{-/-}, *Meox2*^{-/-} mice can explain the lack of axial skeleton formation.

Thus, MEOX1 and MEOX2 regulate skeletal development at early stages of embryonic development by up-regulating the expression of genes that are essential for sclerotome polarity and differentiation.

1.3.4.2. *Myogenesis*

Meox2 gene knockout mice lack specific limb muscles and have reduced muscle mass in the remaining muscles [117]. This reduction in muscle mass was shown to be due to a reduction in the number of myofibers [129]. Furthermore, *Meox2* deficient mice have a diminished number of skeletal muscle stem cells ($Pax7^+$, Myogenin⁺) in the developing limb muscles [129]. Consistent with this finding, the mRNA expression of *Pax3*, *Pax7*, myogenic factor 5 (*Myf5*) and myogenin (*Myog*), which are involved in skeletal myogenesis, are decreased in double *Meox* gene knockout mice [126].

Pax3 and *Meox2* mRNA are co-expressed in myoblasts of the developing mouse and chick limb buds [117,118]. *Meox2* mRNA expression is reduced in the mouse limb bud of *Pax3*^{-/-} mice and *Pax3* mRNA expression is reduced in the mouse limb bud of *Meox2*^{-/-} mice [117], suggesting a positive regulatory loop between *Pax3* and *Meox2*. In addition, MEOX2 and PAX3 proteins have been shown to interact [85]. The mRNA expression of the myogenic regulatory factor *Myf5* is also decreased in the limb bud of *Meox2* deficient mice [117]. PAX3 and MEOX2 are capable of binding to the *Myf5* limb enhancer (a homeo/paired binding motif sufficient to drive *Myf5* expression in the limb muscle progenitor cells), but could not activate transcription from the *Myf5* limb enhancer in either 10T1/2 fibroblasts or C2C12 myoblasts [130]. Furthermore, a *Myf5* limb enhancer reporter gene is equally expressed in the limbs of *Meox2*^{+/+} and *Meox2*^{-/-} mice [130]. Thus, the regulation of *Myf5* by MEOX2 functions through a different enhancer region.

Unlike *Meox2*, *Meox1* is not highly expressed in the developing mouse limb bud [117,118]. In the chick limb bud, the region of *Meox1* mRNA expression overlaps with *Pax3*; however, cellular co-expression was not detected [118]. Furthermore, the

expression of *Pax3* was unaffected in *Meox1*^{-/-} mice [127], which is consistent with the lack of limb muscle phenotype in these mice [126]. However, due to the severity of the myogenic defects in the double *Meox* gene knockout mice, it is evident that *Meox1* has a role in muscle development.

The mouse embryonic carcinoma cell line, P19, can be induced to differentiate into cardiac and skeletal muscle cells in the presence of dimethyl sulfoxide (DMSO) and is therefore a frequently utilized model for the study of myogenesis. Addition of DMSO to P19 cells induces *Meox1* mRNA expression [131,132]. MEOX1 over-expression in P19 cells is sufficient to induce cardiomyogenesis in the absence of DMSO and up-regulate the expression of pro-myogenic genes, such as *Nkx2-5*, GATA binding protein 4 (*Gata4*) and myocyte enhancer factor 2C (*Mef2C*) [133]. Combined addition of retinoic acid and DMSO prevents cardiac myogenesis, increases skeletal muscle myogenesis and further increases *Meox1* mRNA expression [131]. Both inhibition (citra treatment) and augmentation (all-trans retinoic acid treatment) of retinoic acid signalling in the developing chick limb bud has been shown to down-regulate the expression of both *Meox1* and *Meox2* mRNA [134]. Indeed, the retinoic acid receptor binds to the *Meox1* upstream promoter region in P19 cells [131], indicating that *Meox1* is a direct target of retinoic acid signalling during myogenesis.

The sonic hedgehog signalling pathway also influences *Meox1* expression and myogenesis. Over-expression of dominant negative GLI-Kruppel family member 2 (GLI2, a mediator of sonic hedgehog signalling) prevents *Meox1* induction in P19 cells and skeletal myogenesis [135,136]. Reciprocal activation exists between MEOX1 and GLI2 in P19 cells [135]. Inhibition of hedgehog signalling, using cyclopamine, delays

the up-regulation of *Meox1* expression in P19 cells undergoing myogenesis [137]. In addition, myogenic differentiation 1 (MYOD1), a protein required for skeletal muscle differentiation, binds to the *Meox1* upstream promoter region and activates *Meox1* mRNA expression in P19 cells [138].

Hence, MEOX proteins are required for the induction and maintenance of pro-myogenic protein expression that is necessary for the specification of muscle cells. However, it was recently shown using C2C12 myoblasts that inhibition of *Meox2* expression by microRNA (miR)-1 and miR-206 is required for terminal differentiation of myoblasts into myotubes [139].

1.3.4.3. Pharyngeal arch

Kirilenko *et al.* [140] demonstrated that *Meox1* expression in the second pharyngeal arch is activated by the homeodomain protein HOXA2. *Meox1* is a direct transcriptional target of HOXA2, which binds to the *Meox1* upstream promoter region *in vivo* and activates *Meox1* transcription through two conserved homeodomain binding sites [140]. *Meox2* is also expressed in the second pharyngeal arch of mice and in tissue of the middle and inner ear of rat [140,141]. Furthermore, both *Meox1* and *Meox2* genes have to be knocked out in mice for morphological defects to arise in the derivatives of this arch (middle ear) [140]. This suggests that *Meox2* is also a target gene of HOXA2 in the second pharyngeal arch. Like *Meox1*, *Nkx3-2* expression is lost in the *HoxA2* gene knockout mice, indicating that HOXA2 may regulate *Nkx3-2* (a MEOX1 target gene) expression in the second pharyngeal arch via increased MEOX1 (and potentially MEOX2) expression [140,142].

1.3.4.4. *Palate*

Meox2, but not *Meox1*, is expressed in the developing mouse palate [121]. *Meox2* mRNA expression is confined to the posterior portion of the palate shelves, which will eventually form the soft palate [121,143,144]. Initially, the *Meox2* domain expression covers >70% of the palate shelf, but as the palate shelves grow to meet one another, the *Meox2* expression domain shrinks to the posterior 25% of the palate shelf [143]. Approximately 10-35% of *Meox2* deficient mice develop cleft palate [117,121]. Clefts were shown to occur after plate shelf fusion, indicating that MEOX2 is required for the maintenance of this seam [121], via unknown mechanisms.

1.3.4.5. *MEOX genes and EMT*

Due to the expression of *MEOX2* in areas where sheets of mesenchymal and epithelial cells contact, several reports have suggested a role for MEOX2 in establishing proper epithelial-mesenchymal interactions during mouse and human development of various embryonic and extra-embryonic structures such as the palate [121,144], teeth [145], kidney [120] and placenta [112]. Over-expression of MEOX2 was shown to block epithelial-mesenchymal transition (EMT) induced by transforming growth factor β 1 (TGF- β 1) in human keratinocytes [146]. Furthermore, silencing of *Meox2* expression enhances induced pluripotent stem cell (iPSC) generation from mouse fibroblasts, a process of cellular reprogramming that is dependent upon mesenchymal-epithelial transition (MET) [147].

In addition, bioinformatic analysis of genes expressed during periods of MET in several mouse tissues at different developmental stages identified MEOX1 as a candidate transcriptional regulator of MET during mouse development [148,149]. Indeed, *Meox1*

was shown to be expressed in mesenchyme of the atrioventricular cushions and truncus arteriosus of the heart, which arise from the EMT of the endocardial layer [93].

1.3.5. Functions of the MEOX proteins in the cardiovascular system

Post-natal MEOX2 expression is principally confined to the cardiovascular system. In the adult rat, high levels of *Meox2* mRNA expression were detected in the heart and aorta [94]. Furthermore, MEOX2 is expressed in VSMCs and ECs of human arteries [150]. Consequently, many studies have focused on the function of MEOX2 within the cells of the vasculature.

In contrast, the expression and function of MEOX1 has been studied much less in the context of the cardiovascular system, although *MEOX1* was shown to be expressed in cardiomyocytes and cardiac fibroblasts [151], as well as in endothelial cells [152].

1.3.5.1. *Vascular smooth muscle cells*

In rat VSMCs, the expression of *Meox2* mRNA is down-regulated *in vitro* in response to serum and growth factors, as well as *in vivo* in response to vascular injury [94,153,154]. The expression of *Meox2* is down-regulated within 1-4 hours of growth factor stimulation or injury and remains low for 24 hours, following which it begins to return to normal levels [94,153]. Hence, *MEOX2* expression is reduced in VSMCs in response to proliferative signals.

Over-expression of MEOX2 in VSMCs inhibits cell proliferation [155-157]. This is due to MEOX2 induced transcriptional up-regulation of the cyclin-dependent kinase (CDK) inhibitor *p21^{CIP1/WAF1}*, decreased CDK2 activity and subsequent cell cycle block in the G₁ phase [156]. Up-regulation of *p21^{CIP1/WAF1}* expression by MEOX2 was shown

to be independent of p53, as MEOX2 was able to increase $p21^{CIP1/WAF1}$ transcription and inhibit cell proliferation in p53 deficient mouse embryonic fibroblasts [156].

Similar to proliferation, MEOX2 over-expression prevents VSMC migration in response to growth factors [158]. Consistent with decreased cell migration, MEOX2 over-expression reduced the cell surface expression of integrin $\alpha v/\beta 3$ and $\alpha v/\beta 5$ (cell surface receptors involved in extracellular matrix attachment), due to the down-regulation of the $\beta 3$ and $\beta 5$ protein subunits [158]. Furthermore, MEOX2 requires $p21^{CIP1/WAF1}$ for the inhibition of integrin $\beta 3$ and $\beta 5$ expression as well as cell migration [158]. MEOX2 over-expression was also shown to decrease integrin $\alpha 2$ mRNA expression in VSMCs [154].

Serum stimulation of MEOX2 over-expressing quiescent VSMCs induced apoptotic cell death [157,159]. Apoptosis induction by MEOX2 is independent of $p21^{CIP1/WAF1}$, p53 and cell cycle inhibition [160]. Rather, MEOX2 induced apoptosis is a result of post-translational changes in the levels of anti-apoptotic B-cell CLL/lymphoma 2 (BCL2) expression (decreased) and pro-apoptotic BCL2-associated X protein (BAX) expression (increased) [160].

In accordance with its roles in preventing proliferation and migration in isolated VSMCs, MEOX2 over-expression has been shown to reduce thickening of the medial VSMC layer and artery occlusion following balloon angioplasty-induced vascular injury *in vivo* [155,156,161]. Furthermore, attenuated integrin $\beta 3$ and $\beta 5$ protein expression as well as increased numbers of apoptotic cells were observed in the medial VSMC layer of injured arteries over-expressing MEOX2 [158,160].

Angiotensin II, a potent vasoconstrictor, also decreases *Meox2* mRNA expression in VSMCs, while the vasodilator c-natriuretic peptide increases *Meox2* mRNA expression in VSMCs [162]. Angiotensin II stimulated decrease of *Meox2* expression in VSMCs was shown to be dependent upon ROS production and the subsequent activation of the mitogen-activated protein kinases 1 and 3 (MAPK1/3; also known as extracellular signal-regulated kinases 1 and 2, ERK1/2) [163]. Another mechanism by which angiotensin II was shown to reduce *Meox2* expression is through miR-130a. Spontaneously hypertensive rats are an animal model of the vascular remodelling that occurs in hypertensive patients. These rats display increased circulating levels of angiotensin II and thickening of the VSMC layer, indicative of enhanced proliferation. Compared to normal rats, spontaneously hypertensive rats were shown to have significantly increased miR-130a expression and reduced *Meox2* mRNA expression in the aorta and superior mesenteric artery [164]. Consistent with this, treatment of isolated VSMCs with angiotensin II was shown to augment miR-130a expression and thereby decrease *Meox2* expression and increase cell proliferation [164].

In addition, down-regulation of *Meox2* expression was observed in the lungs of rats exposed to hypoxia [165]. Similar to the spontaneous hypertensive rat model, hypoxia causes pulmonary hypertension that results in thickening of the pulmonary arterioles due to increased VSMC proliferation, which can be prevented by MEOX2 over-expression [165].

In isolated VSMCs, MEOX2 over-expression prevented hypoxia-induced phosphorylation of MAPK1/3 and cell proliferation. Furthermore, MEOX2 over-expression decreased BCL2 protein expression, increased BAX protein expression and

induced apoptosis in hypoxia treated VSMCs [165,166]. Conversely, knockdown of *Meox2* under normoxic conditions (when expression is high) causes increased VSMC proliferation and BCL2 expression. Treatment of VSMCs with a MAPK kinase inhibitor (U0126) prevented hypoxia-induced repression of *Meox2* expression and induction of cell proliferation [165].

At the level of the *MEOX2* promoter, transcription was shown to be mediated by the SP1 transcription factor and MEF2A in VSMCs [167]. SP1 and MEF2A bound to their respective binding sites in the minimal *MEOX2* upstream promoter region (-125 bp to -75 bp relative to the transcription start site (TSS)) [167].

1.3.5.2. Adventitial fibroblasts

The adventitia is the external connective tissue layer that surrounds the VSMCs. Adventitial fibroblasts (AFs) secrete collagens, the major component of the adventitia. Akin to VSMCs, *MEOX2* inhibits AF proliferation, migration and adhesion, while inducing AF apoptosis [168]. In addition to increasing *p21^{CIP1/WAF1}* expression, *MEOX2* over-expression in AFs was also shown to up-regulate the expression of the CDK inhibitor *p16^{INK4a}* and decrease the expression of *CDK4* [168]. Consistent with decreased migration and adhesion, *MEOX2* over-expression in AFs decreased the expression of integrin β 1, focal adhesion kinase (*Fak*), and their downstream signalling mediators, protein tyrosine kinase 2 β (*Ptk2b*), Kirsten rat sarcoma viral oncogene homolog (*Kras*), mitogen-activated protein kinase kinase 1 (*Map2k1*) and mitogen activated protein kinase 14 (*Mapk14*; also known as *p38*) [168]. Furthermore, *MEOX2* over-expression also blocked TGF- β induced AF proliferation and migration, likely due to the down-regulation of its downstream signalling mediators SMAD family member 2 (*Smad2*),

Smad3 and *Smad4* [168]. In contraposition, knockdown of *Meox2* expression in AFs had the opposite effect to that of MEOX2 over-expression [168].

An *in vivo* study by Liu *et al.* [169] on the effects of MEOX2 over-expression following lipopolysaccharide treatment of the external surface of the aorta showed that MEOX2 inhibits vessel occlusion due to medial and adventitial thickening. Like vascular injury induced by balloon angioplasty and hypertension, which cause damage to the intimal layer of the vessel, *Meox2* expression is decreased in response to adventitial inflammation and over-expression of MEOX2 in the vasculature can inhibit vascular remodeling induced by adventitial inflammation [169]. The decrease in expression of integrin and TGF- β signalling molecules seen in isolated AFs over-expressing MEOX2 was recapitulated in whole vessels over-expressing MEOX2. In addition, decreased expression of many pro-inflammatory proteins (including, but not limited to, interleukins, matrix metalloproteinases, nuclear factor kappa-light-chain-enhancer of activated B cells (NF κ B), VCAM-1 and ICAM-1) was observed in aortic tissue [169]. As whole vessel tissue was used to assess gene expression changes, these results reflect VSMCs, AFs and to a lesser extent ECs; however, many of these changes were confirmed *in vitro* in isolated AFs [169].

1.3.5.3. Endothelial cells

As in VSMCs and AFs, MEOX2 over-expression in ECs increases *p21^{CIP1/WAF1}* expression and decreases cell proliferation and migration [89,150,155,170] (Figure 1-3). Furthermore, MEOX2 modulates EC tube formation *in vitro* and angiogenesis *in vivo*, in a dose dependent manner, where both over-expression and knockdown of *MEOX2* inhibit the formation of new vessel structures by ECs [150,170,171] (Figure 1-3). The inhibitory

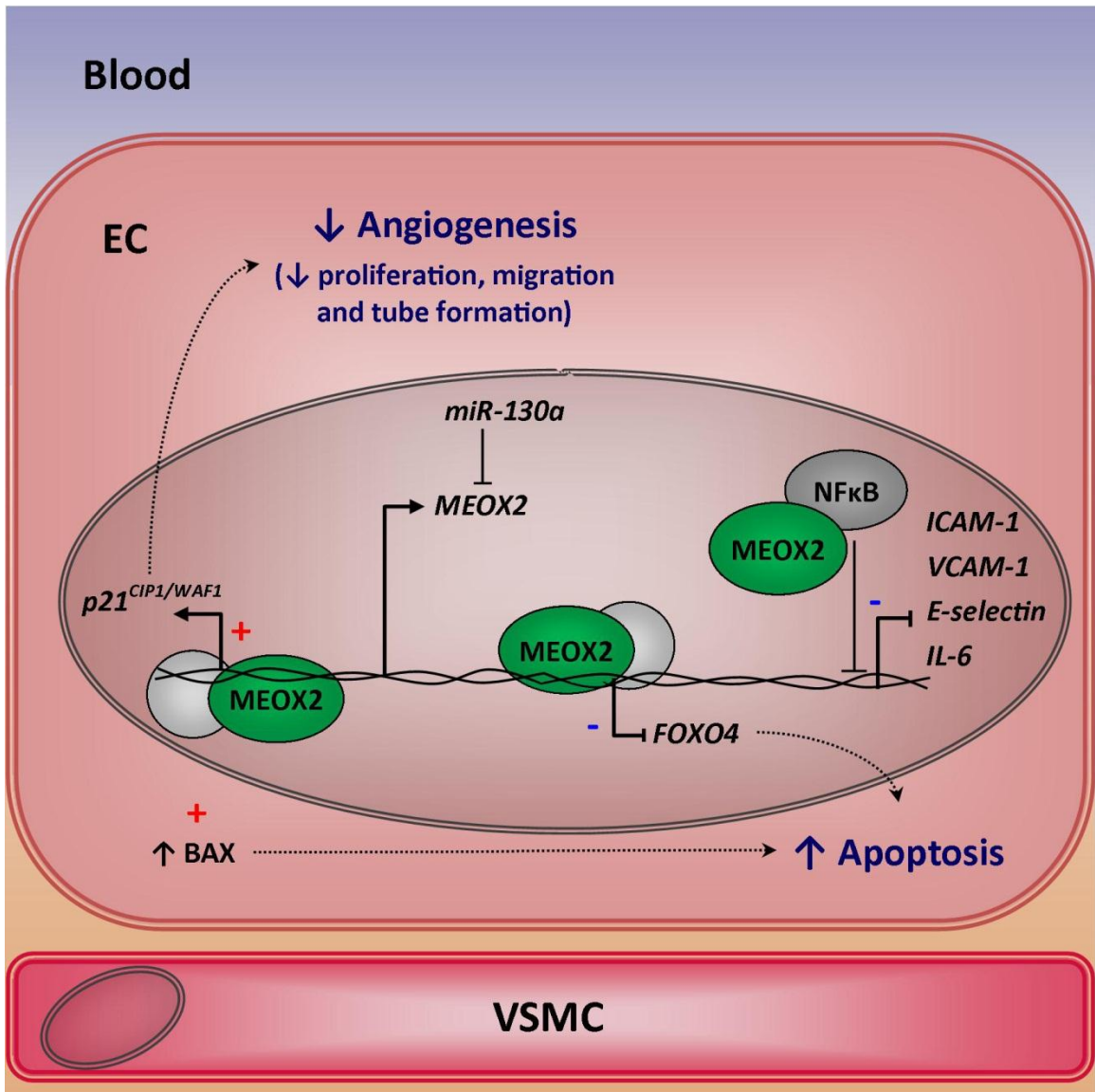


Figure 1-3: Functional roles of MEOX2 in endothelial cells.

Figure 1-3: Functional roles of MEOX2 in endothelial cells. MEOX2 increases *p21^{CIP1/WAF1}* expression and decreases EC proliferation and migration. MEOX2 has also been shown to inhibit tube formation in a dose dependent manner. MEOX2 binds to NFκB and blocks its ability to activate target genes, including *ICAM-1*, *V-CAM-1*, *E-selectin* and *IL-6*. MEOX2 increases the expression of the pro-apoptotic BAX protein by an unknown mechanism. Loss of MEOX2 expression also leads to apoptosis through activation of *FOXO4* expression. In response to growth signals, the expression of *MEOX2* is repressed by *miR-130a*. Blue minus signs indicate a negative effect on gene expression by MEOX2. Red plus signs indicate a positive effect on gene or protein expression by MEOX2. White circles represent the basal transcription machinery.

effect of MEOX2 over-expression on EC tube formation was shown to require the N-terminal region (consisting of the N-terminal, histidine/glutamine rich and middle domains) and the homeodomain [172].

In 2007, Chen *et al.* [89] described the mechanism of MEOX2 mediated $p21^{CIP1/WAF1}$ transcriptional activation in ECs. These authors showed that deletion of either the homeodomain or the histidine/glutamine rich domain of MEOX2 abolishes transcription activation from the $p21^{CIP1/WAF1}$ upstream promoter region, while deletion of the C-terminal domain or the entire N-terminal region, only reduces $p21^{CIP1/WAF1}$ upstream promoter activation by MEOX2 [89]. Similarly, deletion of the homeodomain prevents the inhibition of cell proliferation by MEOX2, while deletion of the N-terminal region only reduces its effect [89], suggesting that cell proliferation is dependent upon $p21^{CIP1/WAF1}$. Furthermore, deletion of the homeodomain binding sites from the $p21^{CIP1/WAF1}$ upstream promoter region abolished MEOX2 activation of transcription from the $p21^{CIP1/WAF1}$ promoter [89]. Chromatin immunoprecipitation (ChIP) and electrophoretic mobility shift assays (EMSAs) showed that MEOX2 binds (via the homeodomain) to ATTA rich motifs located throughout the $p21^{CIP1/WAF1}$ gene locus (from approximately 9.6 kb upstream of the transcriptional start site to within the first intron) [89]. Taken together, these authors concluded that MEOX2 activates $p21^{CIP1/WAF1}$ gene transcription through a homeodomain-DNA-binding dependent mechanism. Furthermore, knockdown of *MEOX2* abolished $p21^{CIP1/WAF1}$ expression, but did not affect the expression of p53 [89].

Over-expression of MEOX2 in ECs was also shown to decrease the expression of NF κ B target genes at the mRNA level, including *E-selectin*, *VCAM-1* and *ICAM-1*,

which are all involved in EC to immune cell adhesion [170] (Figure 1-3). In ECs, MEOX2 bound to the v-rel reticuloendotheliosis viral oncogene homolog A (RELA; also known as p65) subunit of NFκB, as well as to the NFκB inhibitor β (also known as IκB-β) and caused their translocation from the cytosol to the nucleus [172] (Figure 1-3). At low levels of over-expression, MEOX2 activated transcription from the NFκB target gene upstream promoter regions (inhibitor of DNA-binding 1 (*ID1*), *ID3*, interleukin 6 (IL-6) and *ICAM-1*). Whereas at high levels of over-expression, MEOX2 inhibited transcription from these upstream promoter regions [172]. EMSAs were used to demonstrate that MEOX2 prevents NFκB binding to its consensus sequence [170,172]. Deletion of the entire N-terminal region or the homeodomain prevented the interaction of MEOX2 with RELA and transcriptional regulation from the NFκB target gene upstream promoter regions [172].

Treatment of ECs with β-carotene increased *MEOX2* mRNA expression [173]. In contrast, *MEOX2* expression in ECs is decreased by serum and growth factors [71,170]. The *MEOX2* upstream promoter region was shown to be unresponsive to serum or growth factor treatment in ECs [71], indicating that decreased *MEOX2* expression is not a consequence of reduced gene transcription. *In silico* analysis of the 3' untranslated region (UTR) of *MEOX2* mRNA identified many miR binding sites; however, only the expression of miR-130a was positively affected by increased serum concentration [71]. Indeed, the ability of serum treatment to decrease *MEOX2* expression was dependent upon miR-130a targeting the 3'UTR of *MEOX2* mRNA, and subsequently causing its degradation [71] (Figure 1-3). Furthermore, over-expression of miR-130a prevented the inhibitory effects of MEOX2 on EC proliferation, migration and tube formation [71].

The antithesis is true for miR-221. Serum stimulation decreases miR-221 expression [174]. In ECs, miR-221 targets the 3' UTR of the zinc finger E-box binding homeobox 2 (*ZEB2*) mRNA, leading to its degradation [174]. Upon serum stimulation, increased *ZEB2* binding to the *MEOX2* upstream promoter region, via two key binding sites, represses *MEOX2* gene transcription [174]. Accordingly, miR-221 over-expression increases *MEOX2* mRNA levels and inhibits EC migration and tube formation [174].

MEOX2 has also been shown to play a role in EC apoptosis [171]. Both knockdown and over-expression of *MEOX2* leads to increased pro-apoptotic protein expression. Specifically, knockdown of *MEOX2* expression in ECs increased forkhead box O4 (*FOXO4*) expression (pro-apoptotic) and decreased BCL2-like 1 (*BCL2L1*) protein expression (anti-apoptotic), while over expression of *MEOX2* decreased *FOXO4* expression, but increased pro-apoptotic BAX protein expression [171] (Figure 1-3). Thus, maintenance of an optimum level of *MEOX2* expression may be critical for EC viability.

1.3.6. *MEOX* genes and potential roles in human disease

MEOX1 was postulated to be a candidate gene in three human diseases (Naegeli syndrome, Diaphanospondylodysostosis and Hyperostosis corticalis generalisata), but has now been eliminated as the genetic cause of these disorders [175-178]. At the present time, the only association of *MEOX1* and human disease is in cancer. Dermatofibrosarcoma protuberans is a rare form of skin cancer and the region of human chromosome 17 which is commonly amplified in this disease includes the *MEOX1* locus [179]. Consistent with this, *MEOX1* mRNA expression was found to be significantly increased in dermatofibrosarcoma protuberans samples when compared to other soft

tissue tumour samples [179]. However, whether increased *MEOX1* expression contributes to the progression of this type of cancer is unknown. Recently, *MEOX1* was also shown to be highly expressed with pre-B cell leukemia homeobox 1 (*PBX1*) in ovarian cancer tissues [180]. *MEOX1* binds to *PBX1* and is recruited to a subset of *PBX1* target genes in the OVCAR3 ovarian cancer cell line, where it is required for target gene transcription [180]. Furthermore, knockdown of *PBX1* prevents OVCAR3 proliferation, which can be partially overcome by the concomitant over-expression of *MEOX1* [180].

In contrast to *MEOX1*, altered *MEOX2* gene expression has been documented in a number of human diseases, all of which have a vascular component.

1.3.6.1. *Hutchinson-Gilford Progeria Syndrome*

Hutchinson-Gilford Progeria Syndrome (HGPS) is a genetic disorder caused by mutations in the lamin A/C (*LMNA*) gene and is characterized by features of premature aging. Affected individuals generally die around 13 years of age from myocardial infarction or stroke that is caused by accelerated atherosclerosis. Csoka *et al.* [181] compared gene expression profiles of dermal fibroblasts from HGPS individuals that were heterozygous for the *LMNA* GGC>GGT mutation at codon 608 (G>G) to normal age-matched controls using microarray analysis. They found that *MEOX2* mRNA expression was up-regulated 29.1-fold in HGPS cells [181]. Furthermore, homozygous mutation for the *LMNA* AAG>AAC mutation at codon 542 (K>N) also causes HGPS and gene expression analysis of dermal fibroblasts revealed a 5.36-fold increase in *MEOX2* expression in these cells [182].

1.3.6.2. *Alzheimer's Disease*

Hallmarks of AD include decreased cerebral microvasculature and accumulation of neurotoxic Amyloid- β in the brain [183]. *MEOX2* expression is decreased in human brain ECs from AD individuals [171]. These brain ECs have reduced tube formation capability and augmented levels of apoptosis as compared to age matched controls [171]. Knockdown of *MEOX2* in normal human brain ECs recapitulates the defects in tube formation and increased apoptosis observed in the brain ECs from individuals with AD [171]. Furthermore, restoration of *MEOX2* expression in AD brain ECs increases tube formation [171].

Heterozygous *Meox2* gene knockout mice (*Meox2*^{+/-}) were found to have cerebrovascular defects including decreased cerebral blood flow, decreased cerebral capillary density and decreased cerebral angiogenesis in response to hypoxia [171]. Brain ECs from *Meox2*^{+/-} mice have increased pro-apoptotic FOXO4 protein expression, decreased anti-apoptotic BCL2L1 protein expression and decreased tube formation capabilities [171], which is consistent with increased apoptosis and decreased cerebrovasculature. In addition, *Meox2*^{+/-} mice have increased Amyloid- β retention in the brain due to decreased clearance across the blood brain barrier [171]. Expression of the mature form of low density lipoprotein receptor-related protein 1 (LRP1), the major amyloid- β clearance receptor at the blood-brain barrier, is decreased in brain ECs of *Meox2*^{+/-} mice and following knockdown of *MEOX2* in normal brain ECs [171]. This was found to be due to decreased expression of LRP associated protein 1 (LRPAP1), a chaperone required for the proper folding of mature LRP1 [171]. Knockdown of *MEOX2*

in normal human brain ECs decreases *LRPAP1* mRNA and protein expression [171], suggesting that *LRPAP1* is a direct transcriptional target of *MEOX2* transactivation.

More recently, an analysis of copy number variation in autosomal dominant early-onset AD individuals identified a duplication of a genomic region that includes the upstream promoter region and exon 1 of the *MEOX2* gene [184]. Changes in *MEOX2* transcription level were not assessed, but the authors hypothesized that disruption of the regulatory region is likely to reduce *MEOX2* function [184].

1.3.6.3. *Hepatic portal hypertension*

The expression of *MEOX2* mRNA is decreased in the splenic vein of individuals with portal hypertension [185]. Individuals with portal hypertension suffer from high blood pressure in the hepatic portal vein and its associated vessels [18]. This elevated pressure causes atherosclerotic plaques to develop within the splenic vein due to excessive proliferation of VSMCs within the vessel wall [18]. This condition often results in the hemorrhage of associated gastrointestinal vessels [18].

1.3.6.4. *Cancer*

A genome-wide association study by Frullanti *et al.* [186] revealed that the strongest statistical association between a single-nucleotide polymorphism (SNP) and overall survival of individuals with lung adenocarcinoma was a SNP located in the first intron of the *MEOX2* gene. However, the effect of this SNP on *MEOX2* gene expression has not been assessed. Nevertheless, decreased *MEOX2* gene expression has been associated with several forms of cancer. Two major mechanisms have been shown to play a role in *MEOX2* silencing in cancer: microRNAs and DNA methylation.

The 5' UTR of the *MEOX2* gene is 20% methylated in healthy adult lung and 40% methylated in adenocarcinomas and squamous cell lung cancer [187]. This differential level of methylation suggests that *MEOX2* expression is decreased in this form of lung cancer, as methylation of the 5' UTR of the *MEOX2* gene was shown to be inversely correlated with mRNA expression in the lung [187]. Similarly, methylation of the 5' UTR of the *MEOX2* gene was significantly correlated with decreased *MEOX2* expression in wild-type WT1 Wilms' tumour tissue samples and cell lines [188]. However, compared to wild-type WT1 Wilms' tumour tissue samples, mutant WT1 Wilms' tumours have approximately 7-fold higher *MEOX2* expression [189]. Methylation status of the *MEOX2* 5' UTR was not assessed in this latter study; however, this finding indicates that decreased *MEOX2* expression may not be a feature of all cancers.

The expression of miR-130a is augmented in non-small cell lung cancer tissue and is positively correlated with smoking, lymph node metastasis, stage and poor prognosis [190]. As *MEOX2* mRNA is a target of miR-130a mediated degradation [71], its expression is likely decreased in non-small cell lung cancer tissue. In hepatocellular carcinomas, the expression of *MEOX2* mRNA is decreased and the expression of miR-301a is increased, when compared to adjacent non-tumour tissue [191,192]. Furthermore, the expression of miR-301a is positively correlated with tumour stage (early versus late), while the expression of *MEOX2* is negatively correlated with tumour stage and vascular invasion [191,192]. Moreover, a low level of *MEOX2* protein expression in hepatocellular carcinoma tissue is associated with decreased overall patient survival [192]. In the human hepatocellular carcinoma cell line HepG2 and the human lung adenocarcinoma cell line A549, miR-301a targets the 3' UTR of *MEOX2* and thereby

causes *MEOX2* mRNA degradation [191,193]. Inhibition of mir-301a in HepG2 and A549 cells leads to the up-regulation of *MEOX2* mRNA and protein expression [191,193]. Inhibition of miR-301a expression in HepG2 cells decreased cell proliferation and migration, in addition to increasing apoptotic and necrotic cell death [191]. Similarly, in A549 cells, inhibition of miR-301a decreased colony formation ability in soft agar [193]. Conversely, *MEOX2* over-expression in A549 cells decreases proliferation and increases apoptosis [194,195].

Thus, down-regulation of *MEOX2* expression may increase the growth of tumours by directly affecting cancer cell proliferation and migration. Furthermore, as *MEOX2* has been shown to play a role in the regulation of angiogenesis, decreased *MEOX2* may also promote cancer progression by enabling increased tumour neovascularisation, thereby increasing nutrient supply and facilitating metastasis.

CHAPTER 2: OVERALL RATIONALE, HYPOTHESES AND OBJECTIVES

Vascular diseases, including cardiovascular (heart), cerebrovascular (brain) and peripheral vascular (all other vessels) diseases, are the leading cause of death worldwide [196]. In order to effectively prevent and treat vascular diseases, we must first better understand the normal physiology of blood vessels and the changes that occur during disease.

The phenotype of a cell, at any given time, is determined by its gene expression profile. EC dysfunction, the major hallmark of vascular disease, is characterized by numerous gene expression changes that lead to decreased angiogenic potential and nitric oxide production as well as increased expression of pro-inflammatory and pro-thrombotic mediators [21,24,25]. Although many of the signaling pathways that induce these gene expression changes have been identified [197], the direct transcriptional mechanisms that mediate these changes are not well defined.

2.1. Rationale

The mesenchyme homeobox genes, *MEOX1* and *MEOX2*, encode homeodomain transcription factors. In the adult vasculature, *MEOX2* is expressed in vascular smooth muscle and endothelial cells where it inhibits proliferation and induces apoptosis. Furthermore, altered *MEOX2* gene expression has been documented in a number of human diseases (AD, cancer, hepatic portal hypertension and HGPS), all of which have perturbed vascular function [171,181,185]. *MEOX2* may control the transcription of many target genes and thereby modify vascular cell phenotype and function. However, at

present there are only two confirmed direct target genes of MEOX2; the CDK inhibitors *CDKN1A/p21^{CIP1/WAF1}* and *CDKN2A/p16^{INK4a}* [87,89]. MEOX1 is partially redundant to MEOX2 during development, suggesting that that these proteins regulate common target genes. In spite of this, the role of MEOX1 has not been studied in the vasculature.

2.2. Hypothesis

We hypothesised that MEOX1 and MEOX2 would activate *p21^{CIP1/WAF1}* and *p16^{INK4a}* expression, as well as induce apoptosis, cell cycle arrest and senescence in endothelial cells. Furthermore, we postulated that the majority of newly identified MEOX target genes would be regulated by both MEOX1 and MEOX2. As *p21^{CIP1/WAF1}* and *p16^{INK4a}* together are important for mediating permanent cell cycle arrest (senescence), we speculated that MEOX proteins may control endothelial dysfunction.

2.3. Objectives

- I. Compare MEOX induced apoptosis of vascular smooth muscle and endothelial cells.
- II. Elucidate the mechanism and consequences of MEOX mediated transcriptional activation of the CDK inhibitors *p21^{CIP1/WAF1}* and *p16^{INK4a}* in endothelial cells.
- III. Identify and validate novel MEOX target genes in vascular endothelial cells.

CHAPTER 3: THE ROLE OF MEOX1 AND MEOX2 IN VASCULAR CELL DEATH

3.1. Introduction

When the rate of vascular cell death exceeds the rate of vascular cell proliferation, blood vessels become unstable (attributable to VSMC, AF or pericyte cell death) or regress (due to ECs death). While excessive vascular cell death and insufficient reparative angiogenesis contributes to diseases like limb ischemia, stroke and AD, the selective induction of vascular cell apoptosis is currently a therapeutic strategy for the treatment of atherosclerosis, restenosis and solid tumours.

3.1.1. Apoptosis and necrosis

There are various forms of cell death (e.g. apoptosis, autophagy, pyroptosis, necrosis), each of which is characterized by different molecular and phenotypic changes [198,199]. Multiple forms of cell death can take place simultaneously and biochemical assays can distinguish between the types of cell death that are occurring within a population of cells [198,199].

The process of apoptosis is characterized by inter-nucleosomal DNA fragmentation, nuclear and cytosolic condensation and budding-off of membrane enclosed cellular content [200,201]. In response to intrinsic or extrinsic apoptotic stimuli, cells will activate cysteine-dependent aspartate-directed proteases (caspases) through proteolytic cleavage [198,199]. Activation of the effector caspase-3 is central to the apoptotic process as it is responsible for the subsequent cleavage and activation of other proteins which directly mediate the apoptotic process [199]. Loss of mitochondrial

outer membrane integrity is also a feature of apoptosis and is a result of increased pro-apoptotic protein (e.g. BAX) expression in proportion to the level of anti-apoptotic protein (e.g. BCL2, BCL2L1) expression [202]. Mitochondrial outer membrane permeability results in the release of mitochondrial proteins (e.g. cytochrome c) into the cytosol, which potentiates caspase activation [202]. Apoptosis is a controlled process that does not result in a loss of plasma membrane integrity, and therefore does not induce an inflammatory response [200].

In contrast, necrosis does not involve caspase activation or outer mitochondrial membrane permeability. Necrosis is characterized by adenosine triphosphate (ATP) depletion and cellular swelling (oncosis) that ultimately culminates in plasma membrane rupture [199]. Therefore, unlike apoptosis, necrosis results in the loss of plasma membrane integrity and the release of cellular constituents into the intercellular space, which elicits a pro-inflammatory response [199].

3.2. Rationale, hypothesis and aims

MEOX2 over-expression was first shown to induce apoptosis in serum stimulated, but not quiescent, primary rat aortic VSMCs [159]. MEOX2 induced apoptosis correlated with increased protein expression of BAX and decreased protein expression of BCL2 [159]. However, MEOX2 over-expression did not alter the mRNA expression of *BAX* or *BCL2*, indicating that they are not target genes of MEOX2 transcriptional regulation [159]. BAX expression was necessary for MEOX2-induced apoptosis, while over-expression of BCL2 was sufficient to prevent the induction of apoptosis by MEOX2 [159]. Although apoptosis was dependent upon serum stimulation, MEOX2 induced

apoptosis was demonstrated to be independent of p53, p21^{CIP1/WAF1}, and cell cycle inhibition [159]. More recently, MEOX2 over-expression was shown to induce apoptosis in adventitial fibroblasts and A549 cells [168,195].

Furthermore, MEOX2 has also been shown to play a role in EC apoptosis [171]. Both knockdown and over-expression of MEOX2 leads to increased pro-apoptotic protein expression. Specifically, knockdown of MEOX2 expression in ECs decreased anti-apoptotic BCL2L1 protein expression, while over-expression of MEOX2 increased pro-apoptotic BAX protein expression [171]. Decreased BCL2L1 expression in ECs was proposed to occur via MEOX2-induced transcriptional down-regulation of the transcription factor FOXO4 [171]. FOXO4 induces the expression of another transcription factor, BCL6, which directly represses *BCL2L1* gene expression [203].

In order to better understand the mechanism of MEOX2 induced apoptosis, we wanted to identify the protein domains of MEOX2 that were required for this ability. The homeodomain is both capable of DNA-binding as well as mediating protein-protein interactions [85,89], and is therefore likely to be required for MEOX2 induced apoptosis. In addition, we have shown that the middle domain of MEOX2 is sufficient to bind zinc finger proteins (Appendix A) and therefore postulate that this domain may mediate protein interactions with other transcriptional co-factors. The homeodomain and middle domain are the most highly conserved protein domains between human MEOX1 and MEOX2 (Figure 1-2)[84]. To the best of our knowledge, the ability of MEOX1 to induce apoptosis has not been assessed.

We hypothesised that analogous to MEOX2, MEOX1 would induce apoptosis and that the induction of apoptosis by the MEOX proteins would be dependent upon the presence of the homeodomain.

To address this hypothesis, our aims were to:

- i) Determine if MEOX1 over-expression results in apoptotic induction.
- ii) Identify the MEOX protein domains that are required for MEOX induced apoptosis by over-expressing mutant MEOX proteins.

3.3. Materials and methods

3.3.1. Cell culture

All cells were maintained in a standard cell culture incubator at 37°C with 5% CO₂, except when stated otherwise. Cells exposed to hypoxic treatment were placed in a custom made Plexiglas chamber that was kept within a standard cell culture incubator (maintained at 37°C) and was connected via a PROOX oxygen controller (Reming Bioinstruments Company) to a gas tank containing 5% CO₂ and 95% N₂.

3.3.1.1. HEK293

The human embryonic kidney cell line, HEK293A (ATCC), was cultured in HyQ Dulbecco's Modified Eagle's Medium/High Glucose with 4.0 mM L-glutamine and sodium pyruvate (HyQ DMEM/High Glucose) (HyClone) containing 5% Fetal Bovine Serum (FBS) (HyClone) and 1% Penicillin/Streptomycin (Pen/Strep) (Gibco).

3.3.1.2. A7r5

The A7r5 (ATCC) embryonic rat thoracic aorta smooth muscle cell line [204], was cultured in HyQ DMEM/High Glucose (HyClone) containing 10% FBS (HyClone) and 1% Pen/Strep (Gibco).

3.3.1.3. VSMCs

Primary coronary artery VSMCs were isolated from porcine hearts as described by Saward and Zahradka [205]. Hearts were obtained from an abattoir and quickly placed on ice. The left coronary artery was flushed with phosphate buffered saline (PBS; 137 mM NaCl, 2.68 mM KCl, 4.29 mM Na₂HPO₄, 1.47 mM KH₂PO₄) containing 10% Pen/Strep/Fungizone (Gibco) and then dissected from the heart. Next, the isolated vessel was rinsed in PBS containing 10% Pen/Strep/Fungizone (Gibco), cut into 2-5 mm thick rings and then placed in HyQ DMEM/High Glucose (HyClone) containing 20% FBS (HyClone) and 10% Pen/Strep/Fungizone (Gibco). Coronary artery rings were incubated at 37°C with 5% CO₂ for 2-4 days, after which the media was changed to HyQ DMEM/High Glucose (HyClone) containing 20% FBS (HyClone) and 1% Pen/Strep/Fungizone (Gibco). After 5-10 days in culture, cells began to migrate from the coronary artery rings. Seven days after the start of cell migration from the explants, the coronary artery rings were transferred to new dishes. VSMCs, which migrated from the explants between days 7-14 after the start of cell migration, were subsequently cultured in HyQ DMEM/High Glucose (HyClone) containing 5% FBS (HyClone) and 1% Pen/Strep (Gibco) for experimental use. The purity of the VSMC population was verified by fluorescent immunocytochemistry (described in section 3.3.4.1) using smooth muscle (SM) α -actin and SM myosin as VSMC markers (Figure 3-1).

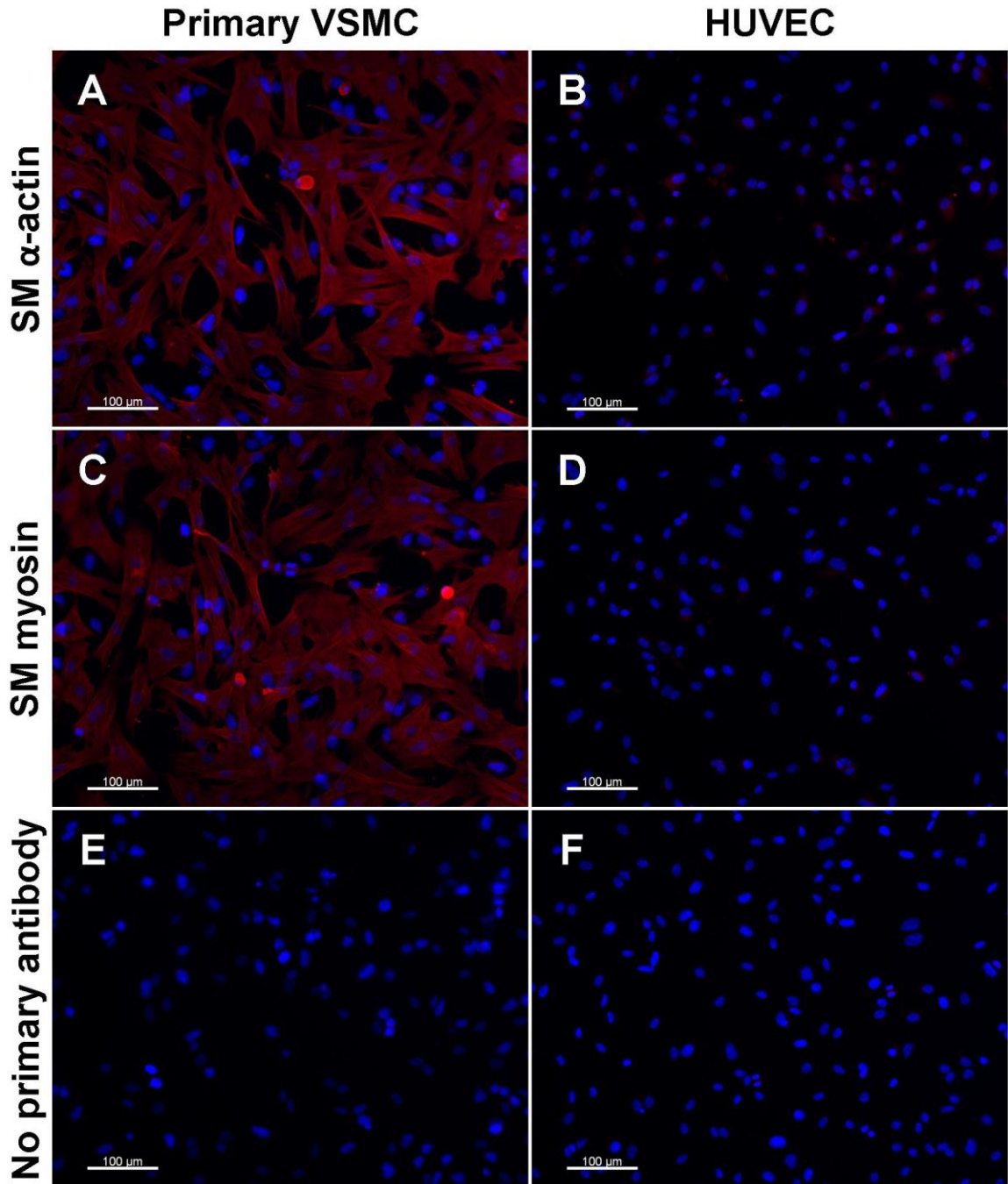


Figure 3-1: Primary cells isolated from porcine coronary arteries express VSMC markers.

Figure 3-1: Primary cells isolated from porcine coronary arteries express VSMC markers.

Porcine vascular smooth muscle cells were immunostained using antibodies against smooth muscle (SM) α -actin (panels **A** and **B**) and SM myosin (panels **C** and **D**). Cells incubated without primary antibody (panels **E** and **F**) served as controls for non-specific binding by the secondary antibody. Primary porcine VSMCs were positive for both SM α -actin and SM myosin expression (red in panels **A** and **C**). Human umbilical vein endothelial cells (HUVECs) were used as a negative control for the expression of VSMC markers (panels **B** and **D**). Nuclei are stained with DAPI (blue). Scale bars represent 100 μ m.

3.3.1.4. HUVECs

Human umbilical vein endothelial cells (HUVECs) (Clonetics) were cultured in Endothelial Cell Growth Medium (EGM-2) (Clonetics) which contains 2% FBS, epidermal growth factor (rhEGF), basic fibroblast growth factor (rhFGF-B), insulin-like growth factor 1 (R³-IGF-1), VEGF, hydrocortisone, heparin, ascorbic acid and gentamicin/amphotericin-B (GA-1000). Cells exposed to nutrient starvation were placed in Endothelial cell Basal Medium (EBM-2) (Clonetics) containing 0.2% FBS.

3.3.2. Expression vectors

Details regarding the cloning of the C-terminal EGFP and FLAG-tagged MEOX1, MEOX1^{K180_K230del}, MEOX2, MEOX2^{K195_245del} and MEOX2^{T89_V182del} expression constructs are described in Appendix B.

3.3.3. Adenovirus production and titering

Ad-EGFP was a gift from Dr. G. Pierce (University of Manitoba), Ad-LacZ was a gift from Dr. M. Czubryt (University of Manitoba) and Ad-p53-EGFP was a gift from Dr. N. Mesaeli (Weill Cornell Medical College in Qatar). Cloning of the MEOX1, MEOX2, MEOX2^{Q235E} and MEOX2^{K195_K245del} constructs into the pShuttle vector is described in Appendix B. Production and amplification of the adenoviral stocks was achieved using the AdEasy vector system (Qbiogene). Briefly, the pShuttle vector containing a MEOX cDNA and the pAdEasy vector were linearized using the *PmeI* restriction enzyme and then co-transformed into the recombination competent *Escherichia coli* (*E.coli*) BJ5183 strain. Next, colonies were screened by *PacI* restriction enzyme digestion for homologous recombination events between the pShuttle and pAdEasy vectors. The recombinant pAd vector was linearized using the *PacI* restriction enzyme and then

transfected into the packaging cell line HEK293A, in which virus is produced. Virus from the initial plaques was amplified by three rounds of infection of HEK293A cells. All adenoviral titres were determined using the RapidTiter kit (Clontech), as we determined that this method is faster, more sensitive (Figure 3-2) and less subjective (lower inter-operator variance, data not shown) than the standard TCID₅₀ method.

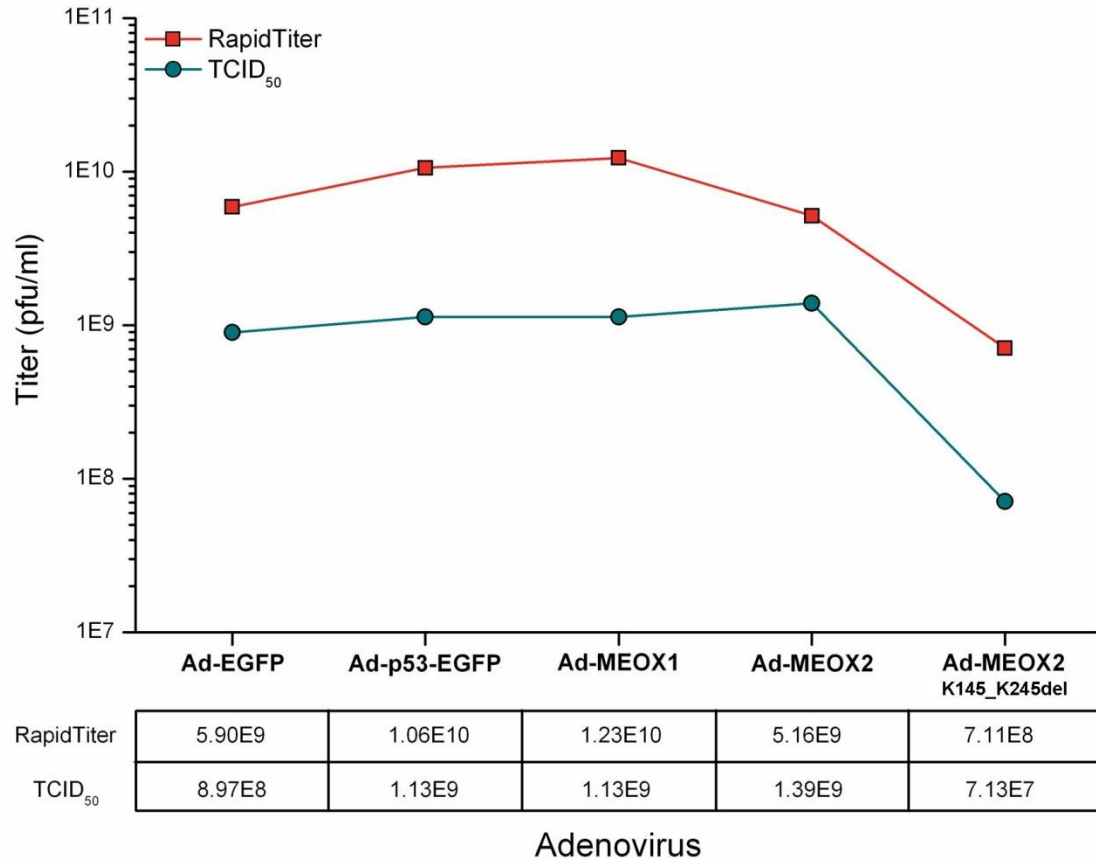


Figure 3-2: Difference between the calculated adenoviral titer using the TCID₅₀ and RapidTiter method for the same viral stocks.

The titer of each adenoviral stock was measured using the TCID₅₀ method (visual identification of cytopathic effect within a population of cells) and the RapidTiter method (antibody detection of viral coat protein production by cells). Using the RapidTiter method, the calculated titer was a median 9-fold higher than the calculated titer obtained using the TCID₅₀ method, indicating that the RapidTiter method is a more sensitive technique.

3.3.4. Immunofluorescence (epifluorescence microscopy)

3.3.4.1. *SM α -actin and SM myosin*

Cells plated onto glass coverslips were washed once with PBS and then fixed with 100% methanol (Fisher) at -20°C for 10 minutes. Subsequently, the methanol was removed and the cells on coverslips were allowed to dry in a fume hood for 5 minutes at room temperature. Cells on coverslips were blocked overnight at 4°C in PBS containing 0.1% bovine serum albumin (BSA). Primary mouse anti-SM α -actin antibody [1A4] (Sigma) and primary mouse anti-SM myosin [HSM-V] (Sigma) were diluted 1:500 and 1:100 in blocking buffer, respectively. Primary antibodies were incubated with cells on coverslips overnight at 4°C. Coverslips were then washed three times with PBS. Texas Red conjugated goat anti-mouse IgG secondary antibody (Invitrogen) was diluted 1:400 in blocking buffer and then incubated with cells on coverslips for 1 hour at room temperature. Coverslips were then washed 3 times with PBS and mounted onto slides using SlowFade Gold antifade reagent with DAPI (Invitrogen).

3.3.4.2. *FLAG*

VSMCs and HUVECs (1×10^5 cells/well) were transduced with adenovirus at 100-500 MOI and then plated onto glass coverslips (for HUVECs, coverslips were coated with collagen I (BD Biosciences)) in 6-well tissue culture plates. At 48 hours post-transduction, cells were washed once with PBS and then fixed in 4% paraformaldehyde (EMD Chemicals) for 30 minutes at room temperature. Cells on coverslips were washed three times with PBS then blocked with 5% v/v goat serum (Sigma) in PBS containing 0.3% v/v Triton-X-100 (PBS-T) overnight at 4°C. Primary mouse anti-FLAG antibody [M2] (Sigma) was diluted 1:1000 in blocking buffer and incubated with cells on

coverslips for 2 hours at room temperature. Coverslips were then washed three times with PBS-T. Alexa Fluor 488 conjugated goat anti-mouse IgG secondary antibody (Invitrogen) was diluted 1:400 in blocking buffer and incubated with cells on coverslips for 1 hour at room temperature. Coverslips were then washed three times with PBS-T and once with PBS prior to mounting onto slides using SlowFade Gold antifade reagent with DAPI (Invitrogen).

3.3.4.3. Acquisition of images

Images were acquired with a ZeissAxioskop 2 mot plus microscope equipped with an AxioCam digital camera and AxioVision 4.6 software (Zeiss).

3.3.5. Western blotting

A7r5 cells (8×10^4 cells/well) were plated into 6-well tissue culture plates and then 48 hours later, the media was changed to Opti-MEM I (Gibco) containing 10% Calf Serum (Gibco). Each well of cells was then transfected with 4 μ g MEOX expression vector DNA using 10 μ L Lipofectamine 2000 Reagent (Invitrogen). Media was changed back to growth medium after 4 hours. HUVECs (2.5×10^5 cells/plate) were transduced at 500 MOI and then plated onto 6 cm tissue culture plates. Prior to harvest, one well of mock transfected A7r5 cells or one plate of untransduced HUVECs was treated with staurosporine (Fisher) at a final concentration of 2.5 mM for 4 hours.

At 24 (A7r5) or 48 (HUVEC) hours post-transfection, cells were washed once with PBS and then cells were harvested using RIPA buffer (50 mM Tris pH 7.4, 150 mM NaCl, 1 mM EDTA, 1 mM EGTA, 0.5% Na-deoxycholate, 1% Triton-X 100 and 0.1% SDS) containing Complete Mini Protease Inhibitor Cocktail (Roche). Whole cell lysates were centrifuged for 15 seconds to pellet cell debris. To assure equal loading between

samples, protein assays were performed prior to sample preparation using the DC Protein Assay Kit (Bio-Rad) and an Ultrospec 2000 (Pharmacia Biotech) or MRX-TC revelation spectrophotometer (Dynex Technologies) set to 540 nm. Samples were prepared with 3× loading buffer (166.4 mM Tris pH 7.4, 33.3% glycerol, 6.6% SDS, 0.3% bromophenol blue and 100 mM DTT) and then boiled for 5 minutes to denature the proteins prior to loading. Proteins were separated by SDS-PAGE and then transferred to nitrocellulose membranes (Bio-Rad) by electrophoretic tank transfer. Membranes were stained with Ponceau S solution (0.1% w/v Ponceau S (Fisher), 5% v/v acetic acid) to visually ensure equal protein loading.

Primary antibodies used for western blotting were: rabbit anti-cleaved caspase-3 (Asp175) [5A1E] (Cell Signaling), mouse anti-FLAG [M2] (Sigma) and rabbit anti-actin (pan) (Sigma). Antibodies were diluted in blocking buffer composed of 5% skim milk powder (SMP) dissolved in Tris-buffered saline (TBS; 50 mM Tris pH 8.0, 138 mM NaCl and 2.68 mM KCl), unless otherwise stated. Primary antibody dilutions and incubation conditions are listed in Table 3-1. Horseradish peroxidase conjugated goat anti-mouse IgG and goat anti-rabbit IgG secondary antibodies (Molecular Probes) were diluted 1:5000 and incubated for 1 hour at room temperature. Antibodies were detected using Western Blotting Luminol Reagent (Santa Cruz Biotechnology) and images were acquired using a Fluor-S MAX MultiImager (Bio-Rad) equipped with Quantity One software (Bio-Rad) or CL-Xposure blue X-ray film.

Table 3–1: List of antibodies and the dilution conditions used for western blotting.

Company	Clone	Antibody name	Host	Dilution	Buffer
Sigma	-	Actin (pan)	rabbit	1:2000	5% SMP/TBS
Cell Signaling	5A1E	Cleaved caspase-3 (Asp175)	rabbit	1:1000	5% SMP/ 0.1% Tween-20/TBS
Santa Cruz	H-300	Dyskerin	rabbit	1:1000	5% SMP/TBS
Cell Signaling	-	eNOS	rabbit	1:1000	5% BSA/TBS
Sigma	M2	FLAG	mouse	1:5000	5% SMP/TBS
Millipore	JOL2	Lamin A+C	mouse	1:200	5% BSA/TBS
Santa Cruz	DCS-50	p16	mouse	1:50	5% BSA/TBS
Sigma	CP74	p21	mouse	1:2000	5% SMP/TBS
Santa Cruz	FL-393	p53	rabbit	1:200	5% BSA/TBS
Cell Signaling	-	Phospho-eNOS (Thr495)	rabbit	1:1000	5% BSA/TBS
AbCam	DM1A	α -Tubulin	mouse	1:1000	5% SMP/TBS

SMP; skim milk powder
 BSA; bovine serum albumin
 TBS; Tris-buffered saline

3.3.6. TUNEL assays

HEK293 (1.6×10^5 cells/well) were plated onto glass coverslips in 6-well tissue culture plates and then 48 hours later, the media was changed to Opti-MEM I (Gibco) containing 10% Calf Serum (Gibco). The cells on each coverslip were then transfected with 4 μ g MEOX expression vector DNA using 10 μ L Lipofectamine 2000 Reagent (Invitrogen). Media was changed back to growth medium after 4 hours. Alternatively, A7r5, VSMCs and HUVECs (1×10^5 cells/well) were transduced with adenovirus at 100-500 MOI and then plated onto glass coverslips (for HUVECs, coverslips were coated with collagen I (BD Biosciences)) in 6-well tissue culture plates. Prior to fixation, one well of mock transfected or untransduced cells was treated with staurosporine (Fisher) at a final concentration of 2.5 mM for 4 hours. At 24 hours post-transfection or 24-72 hours post-transduction, cells were washed once with PBS and then fixed for 30 minutes at room temperature with 4% paraformaldehyde (EMD Chemicals). The coverslips were washed three times with PBS-T and then terminal deoxynucleotidyl transferase dUTP nick end labelled (TUNEL) using the In Situ Cell Death Detection Kit with TMR red (Roche). Briefly, the washed coverslips were incubated with the TUNEL reaction mixture for 60 minutes at room temperature, rinsed three times with PBS and then mounted onto glass slides using SlowFade Gold antifade reagent with DAPI (Invitrogen). Fluorescence images of 16 random fields (200 \times) per coverslip were acquired using a Zeiss Axioskop 2 mot plus microscope. The number of TUNEL positive nuclei was counted by an observer that was blinded to the identity of the slides and then expressed as a percentage of the total number of nuclei counted.

3.3.7. Cell titer assay

HUVECs (5×10^3 cells/well) were transduced with adenovirus at 250 or 500 MOI and then plated into 8 replicate wells of a 96-well tissue culture plate. At 48 hours post-transduction the media was replaced with 100 μ L fresh growth media and 20 μ L CellTiter 96 AQueous One Solution Reagent (Promega). The absorbance at 500 nm was read every hour, from 0-4 hours, after the addition of the CellTiter Reagent using a MRX-TC revelation spectrophotometer (Dynex Technologies).

3.3.8. LIVE/DEAD assay

HUVECs (5×10^4 cells/plate) were transduced with adenovirus at 250 MOI and then plated onto 3.5 cm tissue culture plates. At 72 hours post-transduction, the media was collected and then the cells were washed once with PBS, lifted using 0.5% Trypsin-EDTA (Gibco) and then collected using the initial media and PBS wash. Cells were pelleted by centrifugation at $225 \times g$ for 5 minutes at room temperature, following which the media was discarded and the cells were resuspended in PBS containing 2 μ M calcein AM and 2 μ M ethidium homodimer-1 (components of the LIVE/DEAD Viability/Cytotoxicity Assay Kit; Invitrogen). After incubation at room temperature for 15 minutes, cells were gently mixed and an aliquot was placed on a slide with a coverslip on top. Immediately, fluorescence images of 16 random fields (200 \times) per coverslip were acquired using a Zeiss Axioskop 2 mot plus microscope. The number of calcein AM positive cells (live) and ethidium homodimer-1 positive cells (dead) were counted by an observer that was blinded to the identity of the slides and then expressed as a percentage of the total number of cells counted. Saponin (Sigma) was used as a positive control for

cell death and was added at a final concentration of 1 mg/mL to one plate of untransduced cells 10 minutes prior to collection.

3.3.9. Flow cytometry (cleaved caspase-3 / 7-AAD)

HUVECs (3×10^5 cells/plate) were transduced with adenovirus at 250 MOI and then plated onto 10 cm tissue culture plates. Prior to harvest, one well of untransduced HUVECs was treated with staurosporine (Fisher) at a final concentration of 2.5 mM for 4 hours. At 72 hours post-transduction, the media was collected and then the cells were washed once with PBS, lifted using 0.5% Trypsin-EDTA (Gibco) and then collected using the initial media and PBS wash. Cells were pelleted by centrifugation, following which the media was discarded and the cells were resuspended in PBS. Subsequently, 4% formaldehyde solution (4% paraformaldehyde, 1.1 M NaCl, 21.4 mM KCl, 34.3 mM Na₂HPO₄, 11.8 mM KH₂PO₄), was added to a final concentration of 2% and the cells were fixed at 37°C for 10 minutes, then cooled at 4°C for 1 minute. Ice-cold 100% methanol (Fisher) was added to a final concentration of 90% and the cells were incubated at 4°C for 30 minutes and then placed at -20°C overnight. Cells were pelleted by centrifugation, following which the supernatant was discarded and the cells were resuspended in PBS containing 0.5% BSA. This step was repeated twice and then the cells were incubated at room temperature for 10 minutes in the PBS/0.5% BSA solution. Primary rabbit anti-cleaved caspase-3 (Asp175) [5A1E] (Cell Signaling) was added at 1:100 dilution and then incubated with the cells at room temperature for 1 hour. Cells were diluted 30-fold with PBS containing 0.5% BSA, pelleted by centrifugation and then the supernatant was discarded. Cells were resuspended in PBS/0.5% BSA solution containing 1:100 diluted Alexa Fluor 488 conjugated goat anti-mouse IgG secondary

antibody (Invitrogen) and then incubated at room temperature for 1 hour. Cells were diluted 30-fold with PBS containing 0.5% BSA, pelleted by centrifugation and then the supernatant was discarded. Cells were resuspended in PBS/0.5% BSA solution containing 1:50 diluted 0.2 mg/mL 7-aminoactinomycin D (7-AAD, Invitrogen) solution (0.2 mg 7-AAD, 2% acetone, 98% PBS) and then incubated at room temperature for 15 minutes. All centrifugation steps were carried out at $350 \times g$ for 5 minutes at room temperature. In duplicate, 1×10^4 gated cells per sample were counted using a BD FACSCalibur flow cytometer. The results were analyzed using FlowJo software (Tree Star, Inc.).

3.3.10. Statistical analysis

Analysis of variance (ANOVA) followed by Tukey post-hoc tests, were used to evaluate the changes between untreated and drug treated cells, MEOX proteins and the EGFP or LacZ control, MEOX1 and MEOX2, as well as wild-type versus mutant MEOX2. Changes were considered significant if the p-value was less than 0.05. Statistical analysis was performed using Origin 8.5 software.

3.4. Results and discussion

MEOX2 over-expression was shown to induce apoptosis in proliferating cells [159,160]. In order to determine the domains required for MEOX induced apoptosis, we transfected HEK293 cells with MEOX-EGFP fusion protein constructs and then assayed for apoptosis. We chose the HEK293 cell line as it is readily transfected with high efficiency. Fluorescent microscopy was used to detect cells that were positive for cleaved caspase-3 or DNA fragmentation (as assessed by TUNEL), both markers of

apoptosis. As a positive control, we used staurosporine, a cell-permeable non-specific protein kinase inhibitor, to induce apoptosis [206,207]. Expression of either wild-type or mutant MEOX proteins in HEK293 cells did not induce apoptosis (data not shown). The majority of cells that were either caspase-3 or TUNEL positive did not express the MEOX-EGFP fusion proteins, and the relative amount of apoptosis observed was not increased compared to the mock transfected control (data not shown).

Thus, we hypothesized that MEOX-induced apoptosis may be a phenomena that is not ubiquitous to all cell types. As MEOX2 induced apoptosis was first observed in VSMCs [159], we switched to the A7r5 vascular smooth muscle cell line to test the effects of the various MEOX constructs. Transfection of A7r5 cells with either MEOX-EGFP or MEOX-FLAG fusion protein constructs did not induce caspase-3 cleavage, as assessed by western blot (Figure 3-3). Staurosporine treatment was used as a positive control for induction of caspase-3 cleavage (Figure 3-3).

We then hypothesized that the level of MEOX over-expression achieved using lipid-mediated transfection was insufficient to cause apoptosis. To achieve greater levels of MEOX protein over-expression, we transduced A7r5 cells at a high multiplicity of infection (MOI) with adenoviral vectors encoding C-terminal FLAG-tagged MEOX fusion proteins. Adenovirus encoding enhanced green fluorescent protein (EGFP) was used as a control for the effects of adenoviral transduction, and an adenovirus encoding a C-terminal EGFP-tagged p53 protein was used as a positive control for apoptosis. TUNEL assays were used to detect apoptosis in the various adenoviral transduced samples. TUNEL assays detect DNA fragmentation, a characteristic marker of apoptosis that occurs during the late phase of the apoptotic process. The amount of apoptosis in

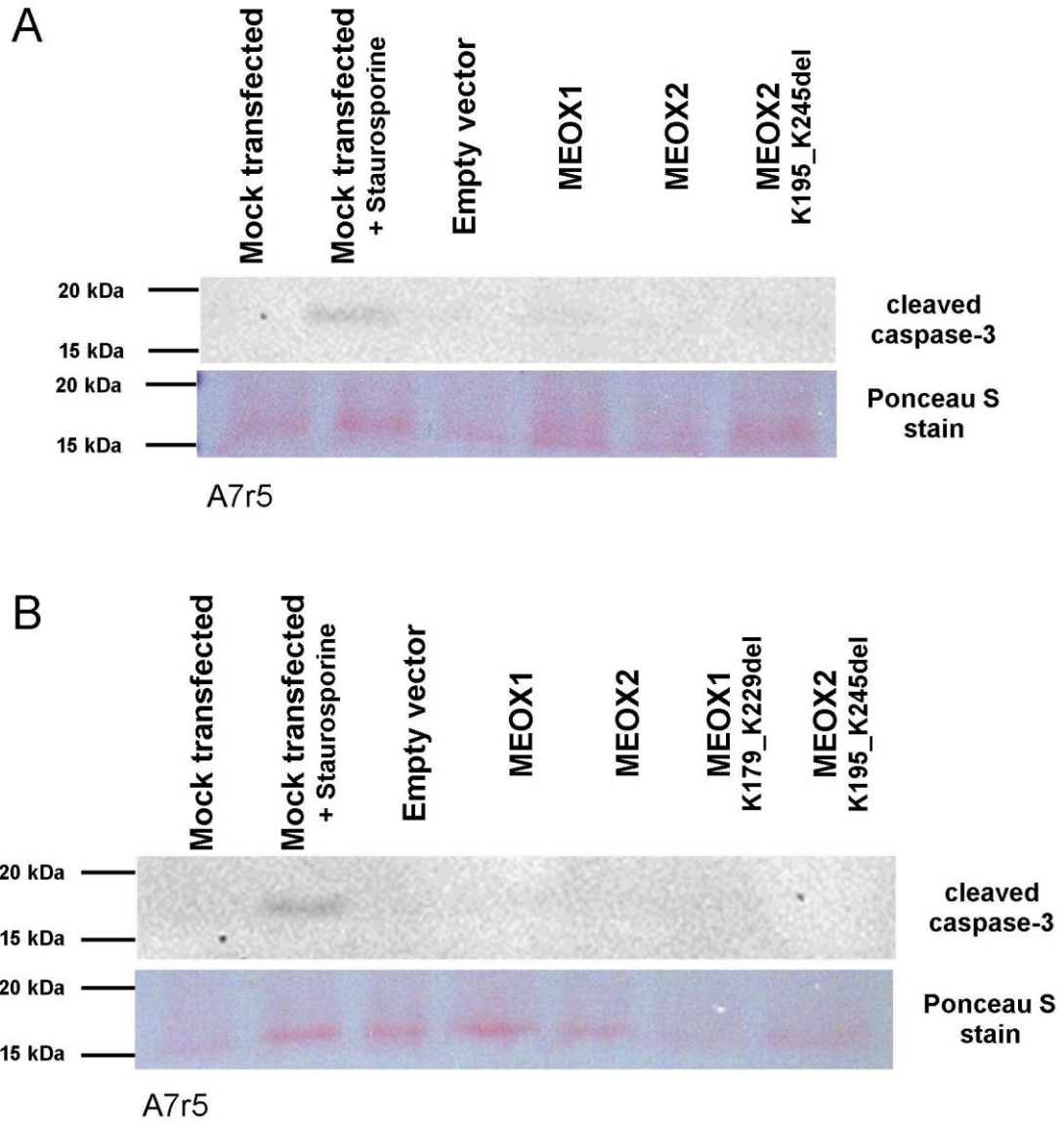


Figure 3-3: Expression of MEOX proteins in A7r5 cells does not induce caspase 3 cleavage.

Figure 3-3: Expression of MEOX proteins in A7r5 cells does not induce caspase 3 cleavage.

Representative western blots showing cleaved caspase-3 in A7r5 cells at 24 hours post-transfection with MEOX-FLAG (**A**) or MEOX-EGFP (**B**) fusion protein constructs. Neither MEOX1, MEOX2, homeodomain deleted MEOX1 (MEOX1^{K180_K230del}), nor homeodomain deleted MEOX2 (MEOX2^{K195_K245del}) induced caspase-3 cleavage in A7r5 cells. Mock transfected cells and empty vector transfected cells were used as negative controls. Staurosporine treatment of mock transfected cells served as a positive control for induction of caspase-3 cleavage. Ponceau S stain was used as a loading control. The protein molecular mass, indicated in kDa, is shown on the left hand side of each image.

each sample was quantified by dividing the number of TUNEL positive nuclei by the total number of nuclei to obtain the percentage of apoptotic cells (Figure 3-4). There was no difference in the percentage of apoptotic cells observed in untransduced A7r5 cells when compared to cells transduced with the EGFP expressing adenoviral control (Figure 3-5, panel A). Over-expression of MEOX proteins was verified by western blot (Figure 3-5, panel B). Neither MEOX1, MEOX2, nor homeodomain deleted MEOX2^{K195_K245del} induced apoptosis in A7r5 cells (Figure 3-5, panel A). Furthermore, over-expression of p53 did not induce apoptosis in this cell type (Figure 3-5, panel A).

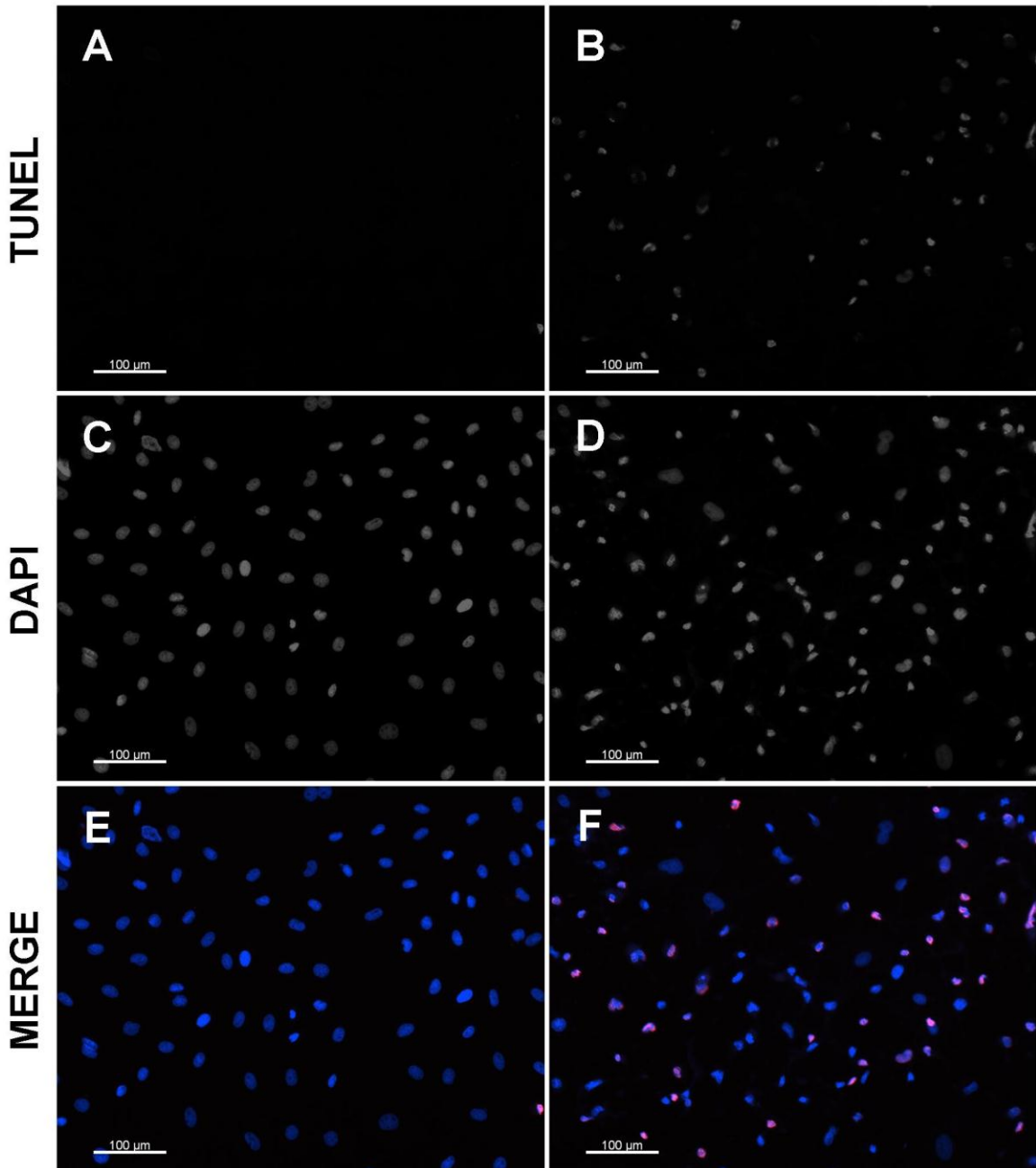
Although the A7r5 VSMC cell line was derived from the thoracic aorta of embryonic rats, these cells have been shown to have adult-like characteristics, slow growth rates and low serum induced early gene expression [208]. The A7r5 cell line is polyploid with many chromosomal aberrations [208], which may explain why these cells do not display increased apoptosis in response to p53 over-expression (Figure 3-5, panel A).

Next, we wanted to confirm our findings in primary VSMCs. We isolated VSMCs from porcine coronary arteries and then used these cells for TUNEL assays, as described for A7r5 cells. To assess the efficiency of adenoviral transduction of primary VSMCs and the level of MEOX protein expression, we used an anti-FLAG antibody to detect MEOX-FLAG fusion protein expression by immunofluorescence and western blot (Figure 3-6). A dose dependent increase in EGFP, p53, MEOX1 and MEOX2 expression was observed in primary VSMCs (Figure 3-6). Furthermore, the majority of primary VSMCs expressed the adenoviral encoded proteins, indicating that these cells can be efficiently transduced (Figure 3-6, panel A). In contrast, we could only detect a few cells expressing the homeodomain deleted MEOX2^{K195_K245del} by immunofluorescence (data

A7r5

Untreated

Staurosporine



G

$$\text{Percent apoptosis} = \frac{\# \text{ TUNEL}^+ \text{ nuclei}}{\text{Total} \# \text{ nuclei (DAPI}^+)} \times 100$$

Figure 3-4: Quantification of apoptosis using a fluorescent TUNEL assay.

Figure 3-4: Quantification of apoptosis using a fluorescent TUNEL assay.

Representative fluorescent microscopy showing TUNEL labelling (white in panels **A** and **B**; red in panels **E** and **F**) in A7r5 cells which were either untreated or treated with 2.5 μ M staurosporine for 4 hours. Nuclei are stained with DAPI (white in panels **C** and **D**; blue in panels **E** and **F**). Scale bars represent 100 μ m. (**G**) Equation used to calculate the percent apoptosis in a population of TUNEL stained cells.

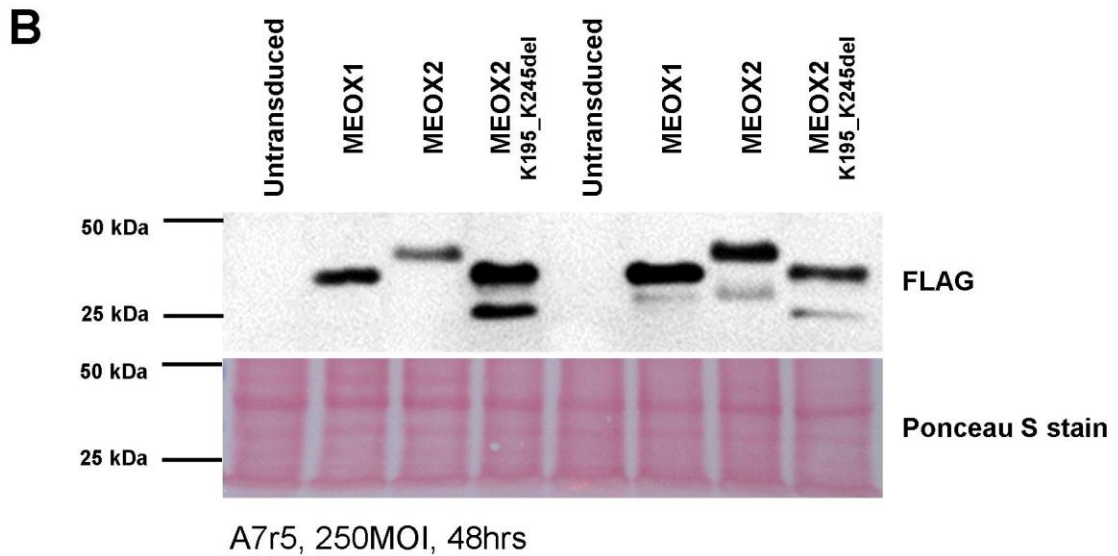
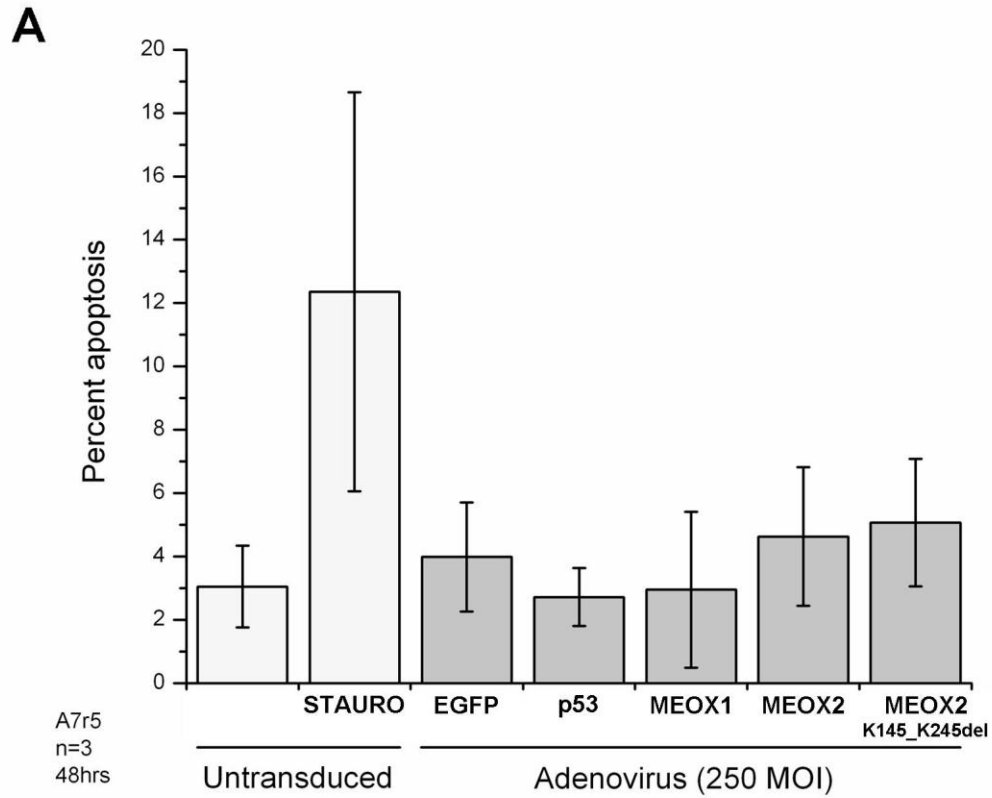


Figure 3-5: Adenoviral over-expression of MEOX proteins in A7r5 cells does not induce apoptosis.

Figure 3-5: Adenoviral over-expression of MEOX proteins in A7r5 cells does not induce apoptosis.

(A) Percent apoptosis in A7r5 cells 48 hours after adenoviral transduction at 250 MOI. Staurosporine (STAURO) was used as a positive control for increased TUNEL incorporation. Error bars represent the standard error of the mean (n=3). (B) Representative western blot showing the expression of C-terminal FLAG-tagged MEOX proteins in A7r5 cells 48 hours after adenoviral transduction at 250 MOI. In addition to the full length proteins (top bands), degradation products (lower bands) were also observed. Replicate samples are from two different sets of transductions. Ponceau S stain was used as a loading control. The protein molecular mass, indicated in kDa, is shown on the left hand side of each image.

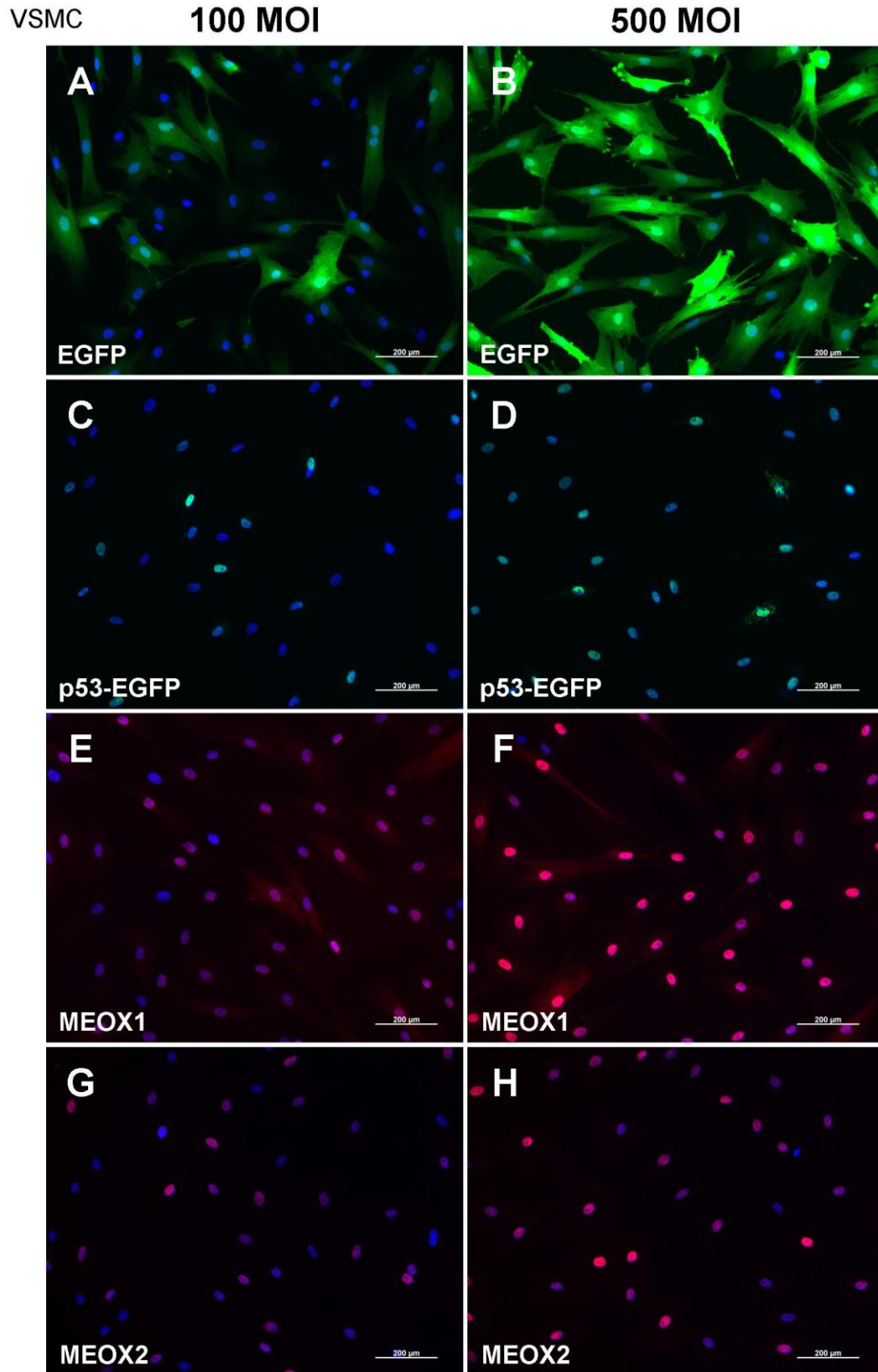


Figure 3-6: Expression of MEOX proteins in primary porcine VSMCs.

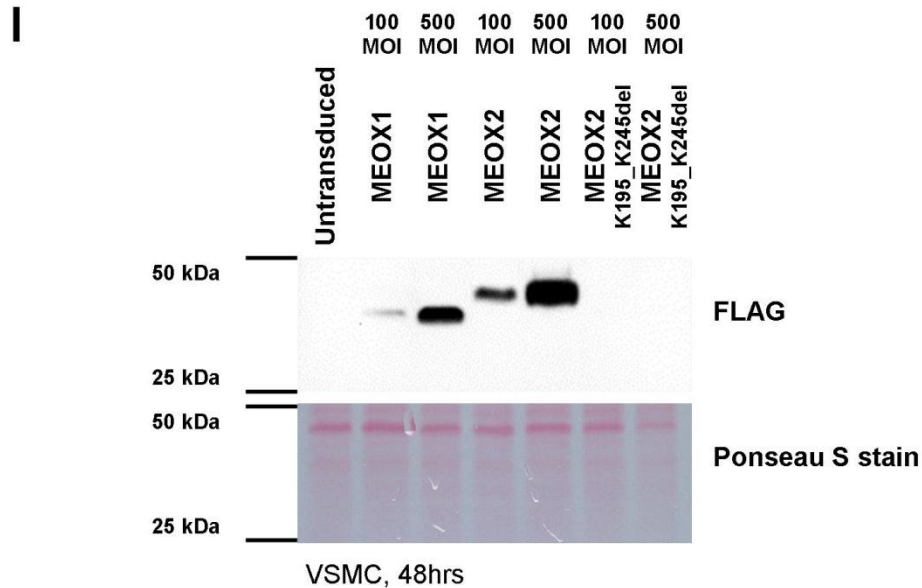


Figure 3-6: Expression of MEOX proteins in primary porcine VSMCs.

Representative immunofluorescence images showing the expression of EGFP (green in panels **A** and **B**) and p53-EGFP (green in panels **C** and **D**), as well as the C-terminal FLAG-tagged MEOX1 (red in panels **E** and **F**) and MEOX2 (red in panels **G** and **H**) proteins in primary VSMCs 48 hours after adenoviral transduction at 100 and 500 MOI. Nuclei are stained with DAPI (blue). Scale bars represent 200 μ m. **(I)** Representative western blot showing the expression of C-terminal FLAG-tagged MEOX proteins in primary VSMCs 48 hours after adenoviral transduction at 100 and 500 MOI. Ponceau S stain was used as a loading control. The protein molecular mass, indicated in kDa, is shown on the left hand side of each image.

not shown) and were unable to detect its expression by western blot (Figure 3-6, panel B). Quantification of the number of TUNEL positive cells in primary VSMCs transduced at 100 MOI with the various adenoviral constructs showed no changes in the number of apoptotic cells (Figure 3-7, panel A). However, in primary VSMCs transduced at 500 MOI, we observed increased apoptosis in cells over-expressing homeodomain deleted MEOX2^{K195_K245del}, but no difference in the amount of apoptosis was observed in cells over-expressing wild-type MEOX1 or MEOX2 as compared to the EGFP control (Figure 3-7, panel B). This suggests that MEOX1 and MEOX2 do not induce apoptosis in VSMCs under these conditions.

The significant increase in the level of apoptosis induced by homeodomain deleted MEOX2^{K195_K245del} is not detected in cells transduced at the same MOI with the EGFP adenoviral control or wild-type MEOX2, indicating that this cytotoxic effect is not due to viral load. Intriguingly, we were unable to detect the expression of MEOX2^{K195_K245del} by western blot under the same transduction conditions (Figure 3-6, panel B). A potential explanation of these observations is that MEOX2^{K195_K245del} may be misfolded or unstable, leading to its rapid degradation, cellular stress and induction of apoptosis. In support of this idea, MEOX2^{K195_K245del} appeared to be more stably expressed in A7r5 cells and over-expression of MEOX2^{K195_K245del} did not increase apoptosis in A7r5 cells (Figure 3-5).

Subsequently, we wanted to compare our findings in VSMCs to that of ECs, therefore we repeated the TUNEL assays using HUVECs. We observed efficient adenoviral transduction of HUVECs and high levels of C-terminal FLAG-tagged MEOX1 and MEOX2 fusion proteins by immunofluorescence and western blot

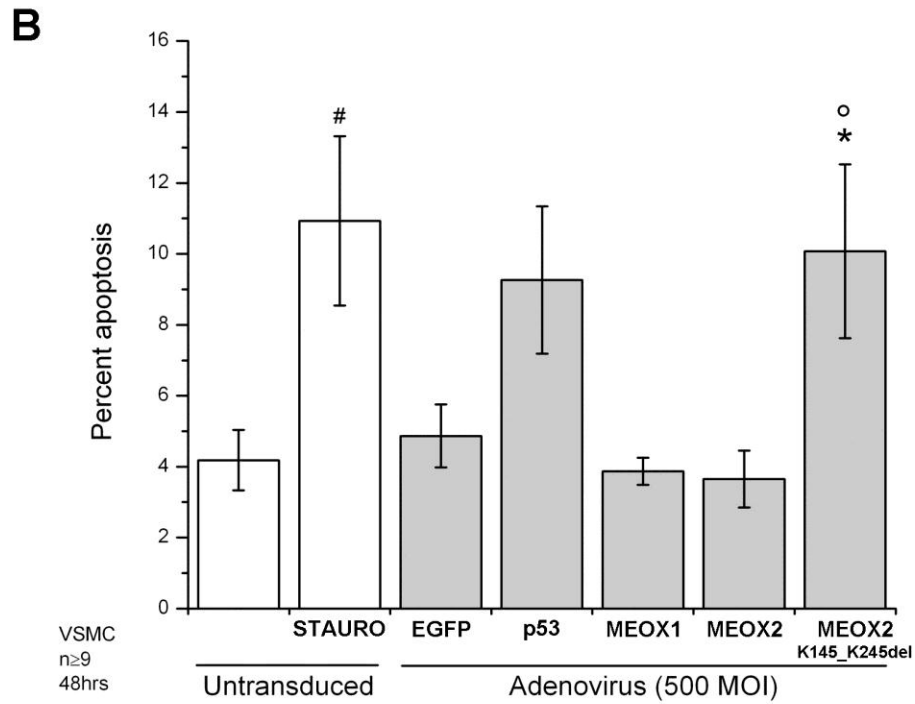
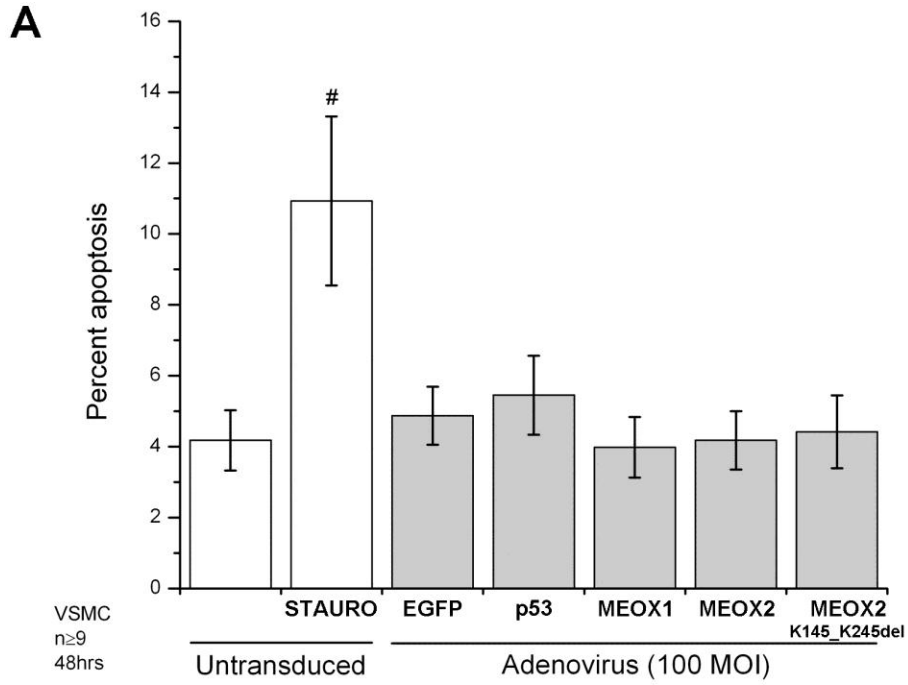


Figure 3-7: Adenoviral over-expression of homeodomain deleted MEOX2^{K195_K245del} induces apoptosis in primary VSMCs.

Figure 3-7: Adenoviral over-expression of homeodomain deleted MEOX2^{K195_K245del} induces apoptosis in primary VSMCs.

Percent apoptosis in primary VSMCs 48 hours after adenoviral transduction at 100 MOI (A) and 500 MOI (B). Staurosporine (STAURO) was used as a positive control for increased TUNEL incorporation. # Indicates a statistically significant change ($p < 0.05$) between untreated and staurosporine treated untransduced cells. * Indicates a statistically significant change ($p < 0.05$) when compared to the EGFP control. ○ Indicates a statistically significant difference ($p < 0.05$) between wild-type and mutant MEOX2. Error bars represent the standard error of the mean ($n \geq 9$ (A), $n \geq 9$ (B)).

(Figure 3-8). As was observed in primary VSMCs, homeodomain deleted MEOX2^{K195_K245del} expression was seen in fewer cells by immunofluorescence and was less abundant in HUVEC lysates, as shown by western blot (Figure 3-8). Quantification of the number of TUNEL positive cells in each population of transduced HUVECs showed no change in the number of apoptotic cells (Figure 3-9). In contrast to what was observed in VSMCs (Figure 3-7, panel B), homeodomain deleted MEOX2^{K195_K245del} did not induce apoptosis in HUVECs (Figure 3-9).

In order to assess whether MEOX1 and MEOX2 over-expression may decrease the overall viability of ECs we performed CellTiter assays. This assay is based on the production of a formazan dye from the bioreduction of the MTS tetrazolium compound by metabolically active cells. The optical density (OD) of the cell culture medium at 490nm is directly proportional to the amount of formazan dye produced. A reduction in formazan production is indicative of reduced cell number either due to decreased proliferation or increased apoptosis. Changes in cell viability were assessed 48 hours post-transduction of HUVECs with the recombinant adenovirus constructs. When compared to untransduced HUVECs, there was no change in the viability of cells transduced with either 250 or 500 MOI adenovirus encoding EGFP, indicating that viral transduction did not affect cell viability (Figure 3-10). In contrast, over-expression of p53 significantly decreased the number of viable cells, as indicated by the slower production of formazan over time (Figure 3-10). When MEOX1, MEOX2 or homeodomain deleted MEOX2^{K195_K245del} was over-expressed in HUVECs for 48 hours, the viability of the cells was unchanged (Figure 3-11).

HUVEC

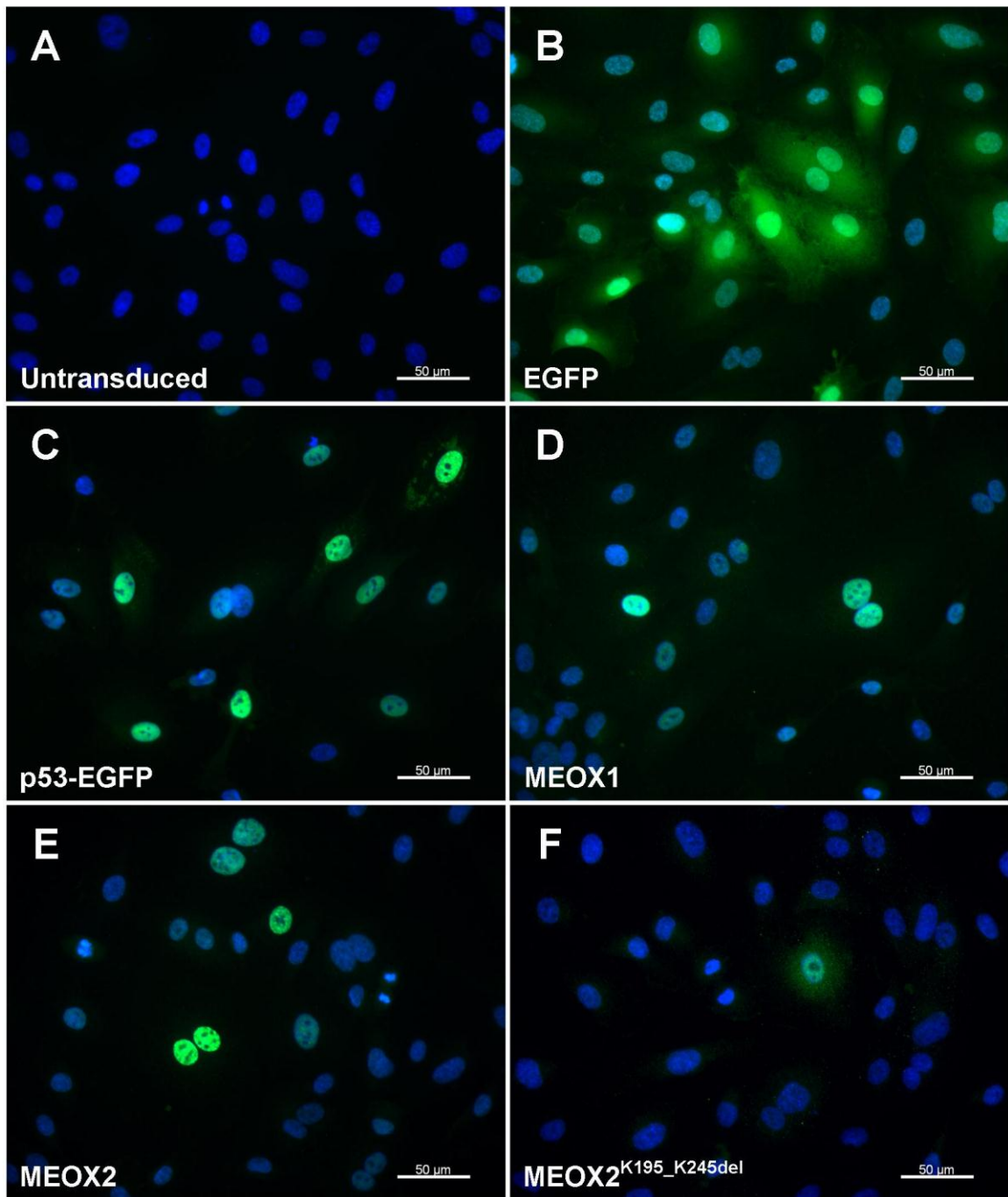


Figure 3-8: Expression of C-terminal FLAG-tagged MEOX proteins in HUVECs.

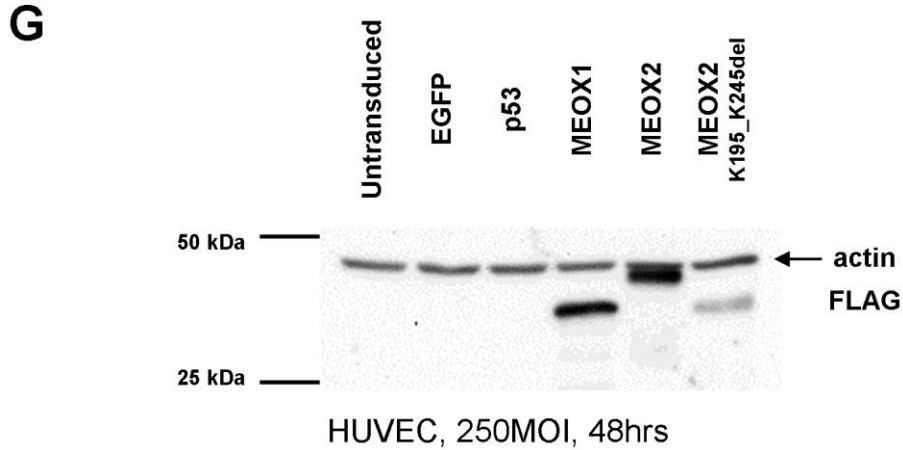


Figure 3-8: Expression of C-terminal FLAG-tagged MEOX proteins in HUVECs.

Representative immunofluorescence images showing the expression of EGFP (green in panel **B**), p53-EGFP (green in panel **C**) and C-terminal FLAG-tagged MEOX proteins (green in panels **D-F**) in HUVECs 48 hours after adenoviral transduction at 250 MOI. Untransduced HUVECs were used as a negative control (panel **A**). Nuclei are stained with DAPI (blue). Scale bars represent 50 μ m. (**G**) Representative western blot showing the expression of C-terminal FLAG-tagged MEOX proteins in HUVECs 48 hours after adenoviral transduction at 250 MOI. Actin was used as a loading control. The protein molecular mass, indicated in kDa, is shown on the left hand side of the image.

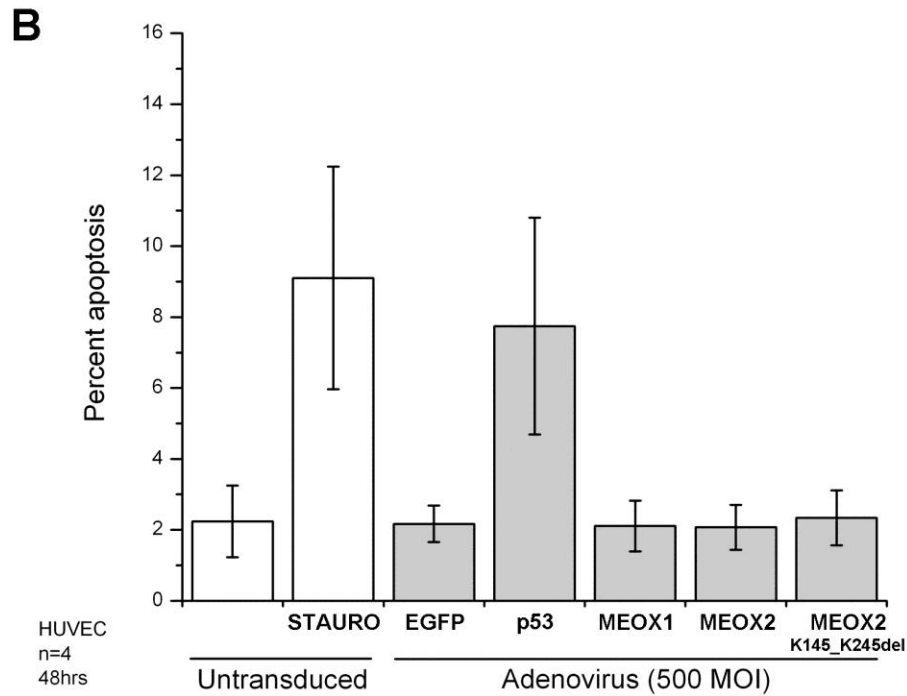
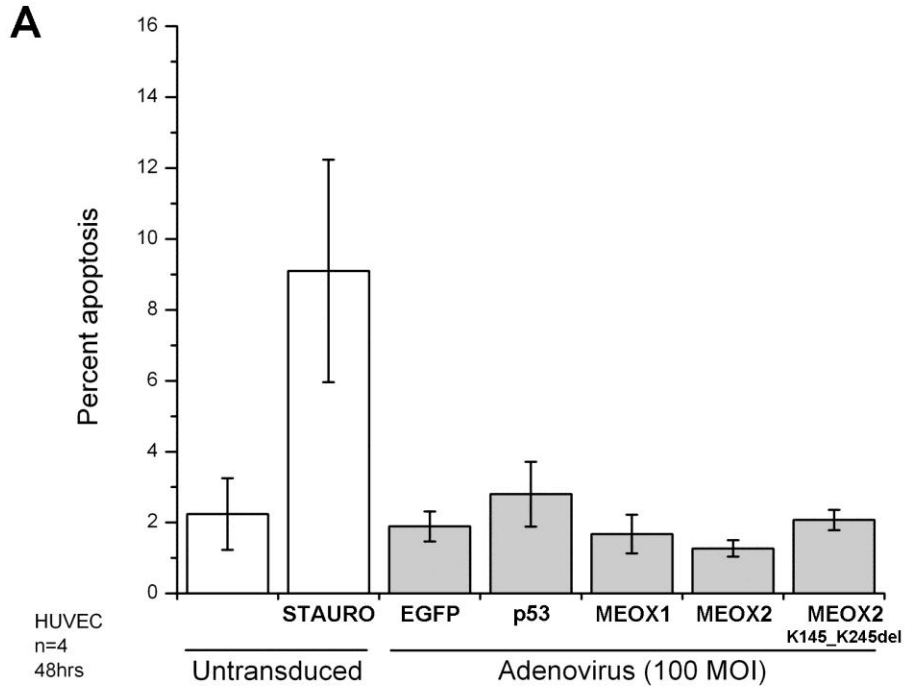


Figure 3-9: Adenoviral over-expression of C-terminal FLAG-tagged MEOX proteins in HUVECs does not induce apoptosis.

Figure 3-9: Adenoviral over-expression of C-terminal FLAG-tagged MEOX proteins in HUVECs does not induce apoptosis.

Percent apoptosis in HUVECs 48 hours after adenoviral transduction at 100 MOI (**A**) and 500 MOI (**B**). Staurosporine (STAURO) was used as a positive control for increased apoptosis. Error bars represent the standard error of the mean (n=4 (A), n=4 (B)).

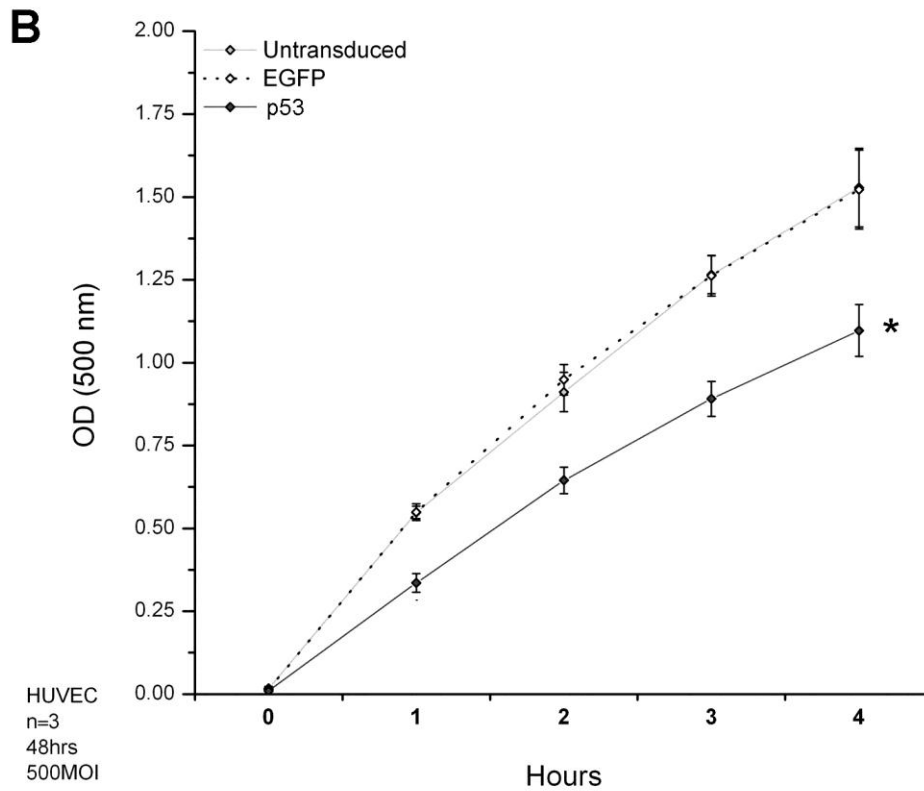
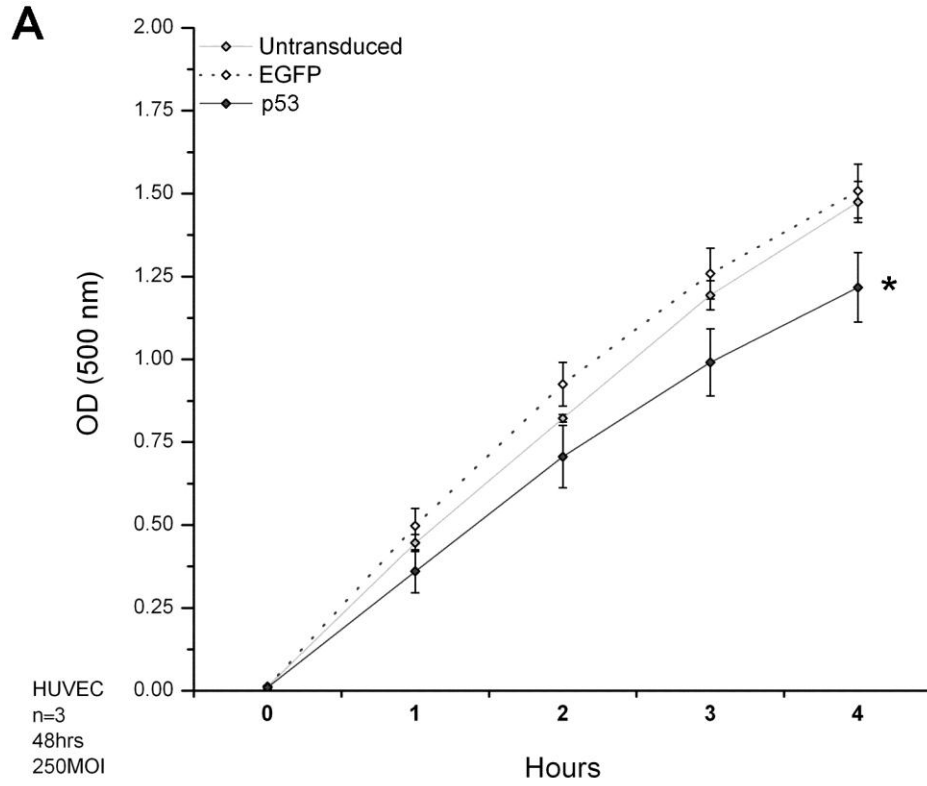


Figure 3-10: Adenoviral over-expression of p53 decreases HUVEC viability.

Figure 3-10: Adenoviral over-expression of p53 decreases HUVEC viability.

Differences in HUVEC viability were measured using the CellTiter assay 48 hours after adenoviral transduction at 250 MOI (A) and 500 MOI (B). The optical density (OD) at 500 nm is proportional to the amount of formazan dye produced by viable cells. Compared to untransduced HUVECs, over-expression of EGFP did not affect the production of formazan dye over time, indicating that adenoviral transduction does not cause a change in cell viability. Over-expression of p53 significantly decreased cell viability, as indicated by the slower production of formazan dye over time. * Indicates a statistically significant change ($p < 0.05$) when compared to the EGFP control for the same time point. Error bars represent the standard error of the mean ($n=3$ (A), $n=3$ (B)).

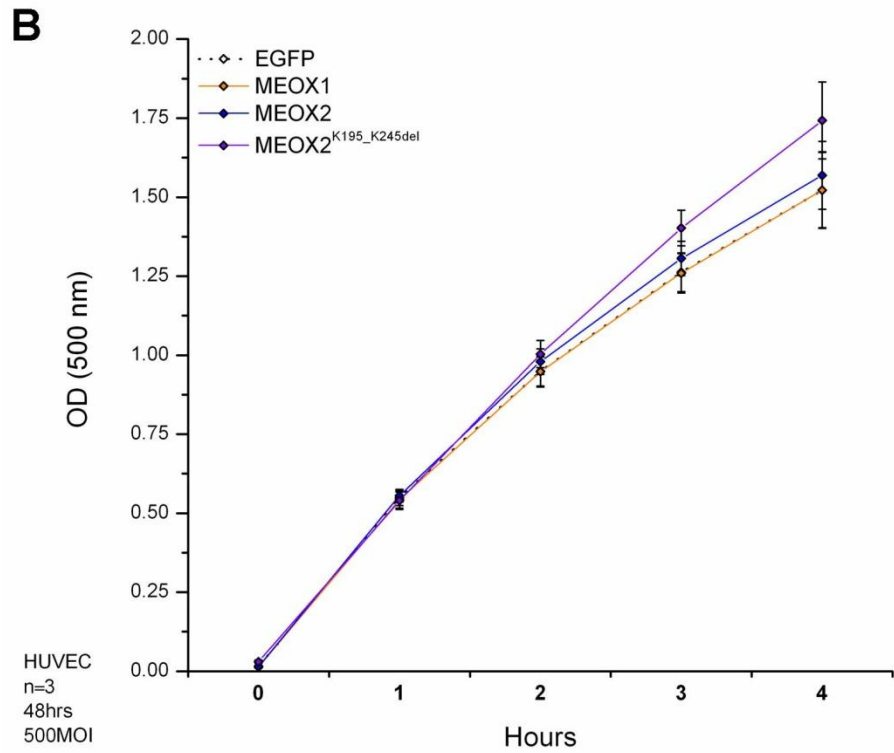
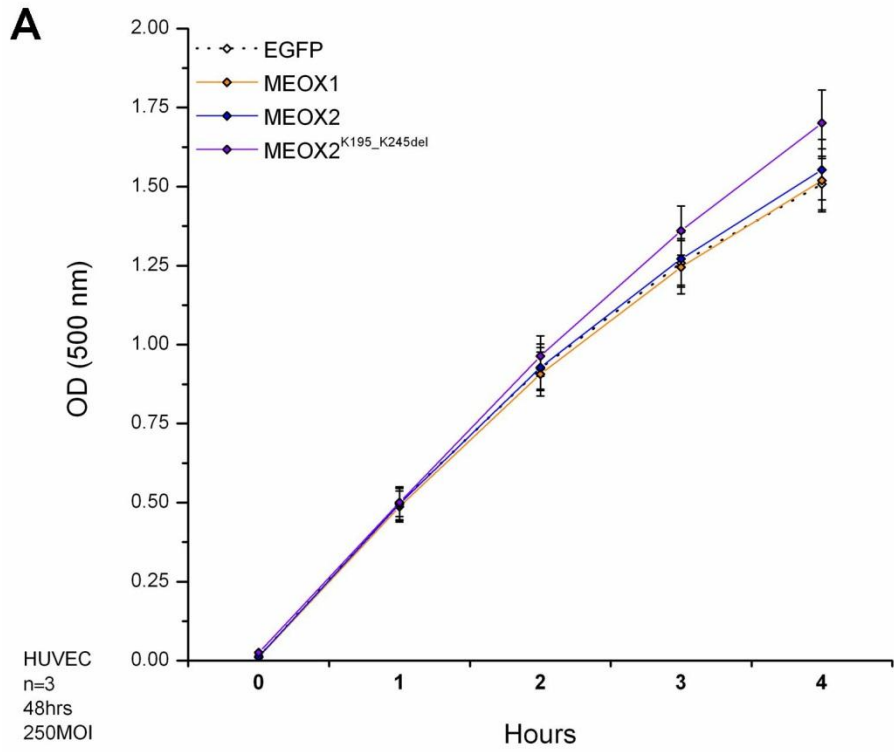


Figure 3-11: Adenoviral over-expression of C-terminal FLAG-tagged MEOX proteins in HUVECs does not decrease cell viability.

Figure 3-11: Adenoviral over-expression of C-terminal FLAG-tagged MEOX proteins in HUVECs does not decrease cell viability.

Differences in HUVEC viability were measured using the CellTiter assay 48 hours after adenoviral transduction at 250 MOI (**A**) and 500 MOI (**B**). The optical density (OD) at 500 nm is proportional to the amount of formazan dye produced by viable cells. Compared to the EGFP adenoviral control, MEOX1, MEOX2 and MEOX2^{K195_K245del} over-expression did not affect the production of formazan dye over time, indicating no change in cell viability. Error bars represent the standard error of the mean (n=3 (A), n=3 (B)).

Although there was no apparent effect of the location of the FLAG-tag on the expression or function of MEOX1 or MEOX2 (Appendix C), we sought to verify that the C-terminal FLAG epitope was not affecting the ability of MEOX1 and MEOX2 to induce apoptosis. To this end, we transduced HUVECs with N-terminal FLAG-tagged MEOX adenoviral constructs and then performed TUNEL and CellTiter assays as described above. HUVECs were efficiently transduced as indicated by robust expression, by both immunofluorescence and western blot, of N-terminal FLAG-tagged MEOX1, MEOX2, DNA-binding domain mutated MEOX2^{Q235E} and to a lesser extent, homeodomain deleted MEOX2^{K195_K245del} (Figure 3-12). Quantification of TUNEL assays showed that neither MEOX1 nor MEOX2 induced apoptosis in HUVECs (Figure 3-13). Similarly, the DNA-binding domain mutated MEOX2^{Q235E} and homeodomain deleted MEOX2^{K195_K245del} were also unable to induce apoptosis (Figure 3-13). CellTiter assays were also performed to assess whether N-terminal FLAG-tagged MEOX1 and MEOX2 expression leads to decreased overall viability of ECs. Wild-type MEOX1 and MEOX2, as well as DNA-binding domain mutated MEOX2^{Q235E} and homeodomain deleted MEOX2^{K195_K245del} did not affect cell viability as compared to the EGFP control (Figure 3-14).

It was documented by Xia *et al.* [166] that MEOX2 over-expression alone was not sufficient to induce apoptosis in pulmonary artery VSMCs; however, in combination with hypoxia treatment a marked increase in apoptosis was observed. Thus, we sought to determine whether hypoxic treatment of HUVECs could potentiate the ability of MEOX2 to induce EC apoptosis. In addition, the effect of nutrient starvation was also tested. The combination of hypoxia and nutrient starvation was used to simulate ischemia. Transduced HUVECs were cultured in growth media for 24 hours, following which the

HUVEC

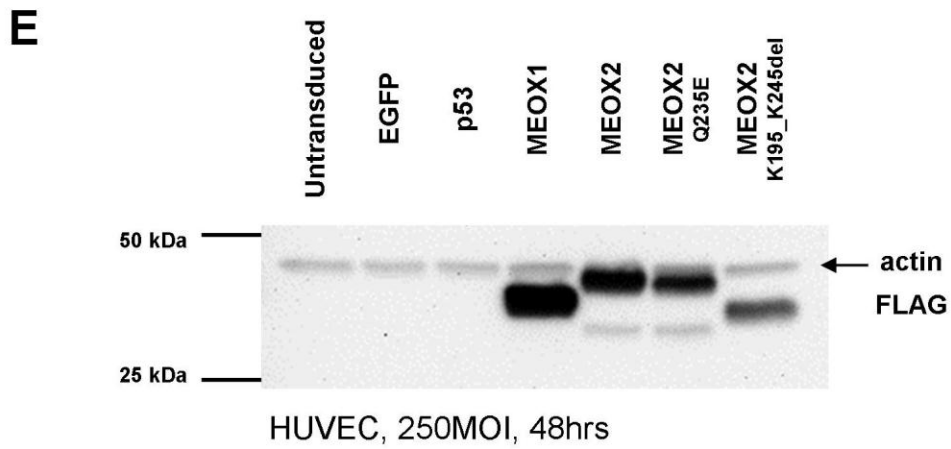
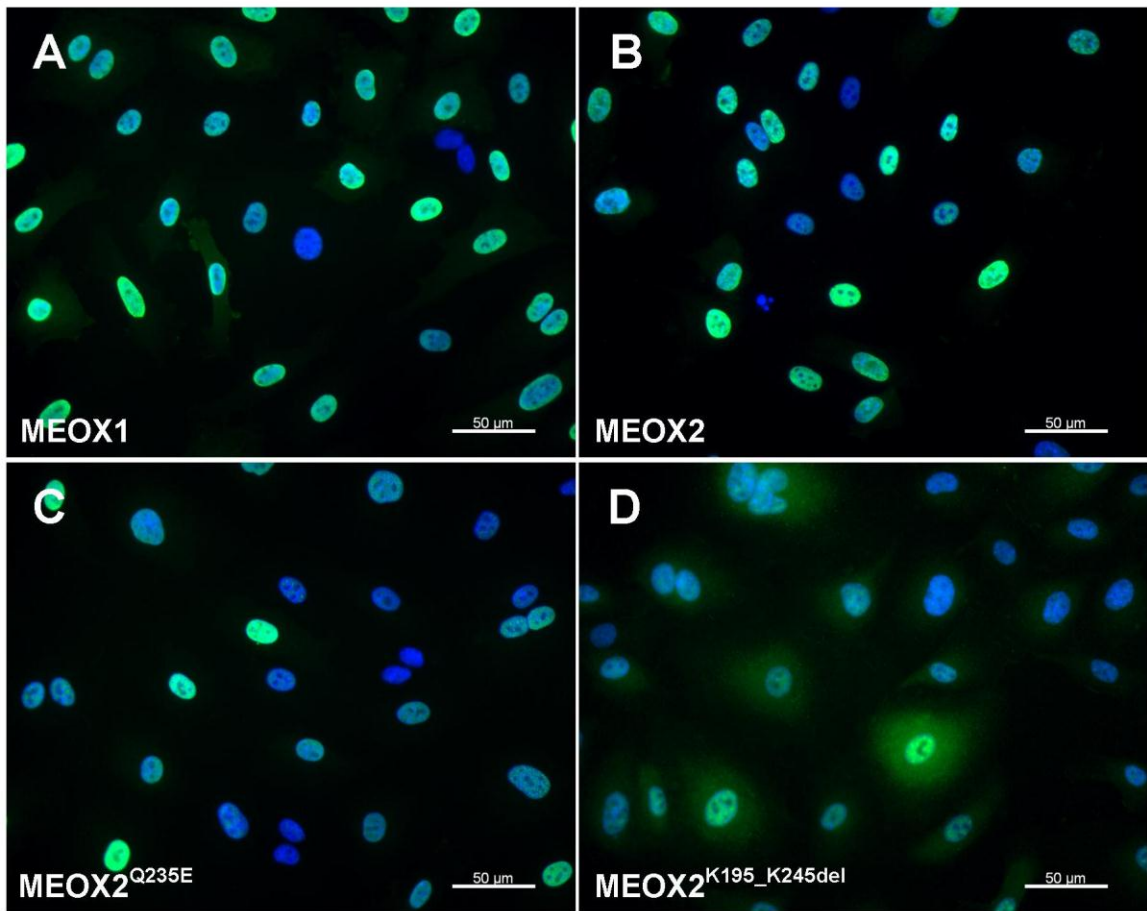


Figure 3-12: Expression of N-terminal FLAG-tagged MEOX proteins in HUVECs.

Figure 3-12: Expression of N-terminal FLAG-tagged MEOX proteins in HUVECs.

Representative immunofluorescence showing the expression of N-terminal FLAG-tagged MEOX proteins (green in panels **A-D**) in HUVECs 48 hours after adenoviral transduction at 250 MOI. Nuclei are stained with DAPI (blue). Scale bars represent 50 μm . (**E**) Representative western blot showing the expression of N-terminal FLAG-tagged MEOX proteins in HUVECs 48 hours after adenoviral transduction at 250 MOI. Actin was used as a loading control. The protein molecular mass, indicated in kDa, is shown on the left hand side of the image.

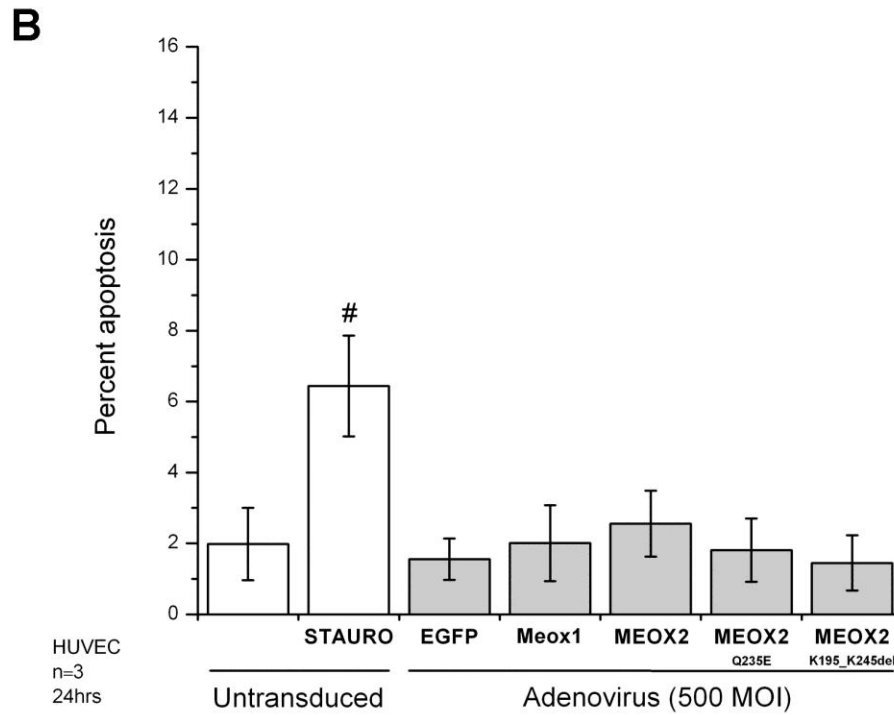
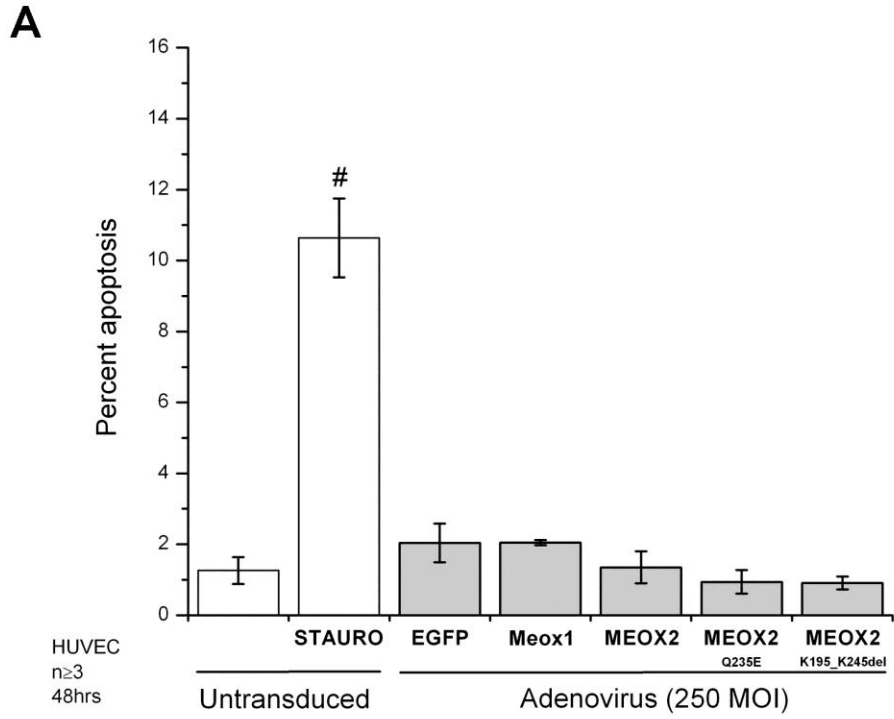


Figure 3-13: Adenoviral over-expression of N-terminal FLAG-tagged MEOX proteins in HUVECs does not induce apoptosis.

Figure 3-13: Adenoviral over-expression of N-terminal FLAG-tagged MEOX proteins in HUVECs does not induce apoptosis.

Percent apoptosis in HUVECs after adenoviral transduction at 250 MOI for 48 hours (**A**) and 500 MOI for 24 hours (**B**). Staurosporine (STAURO) was used as a positive control for increased TUNEL incorporation. # Indicates a statistically significant change ($p < 0.05$) between untreated and staurosporine treated untransduced cells. Error bars represent the standard error of the mean ($n \geq 3$ (A), $n = 3$, (B)).

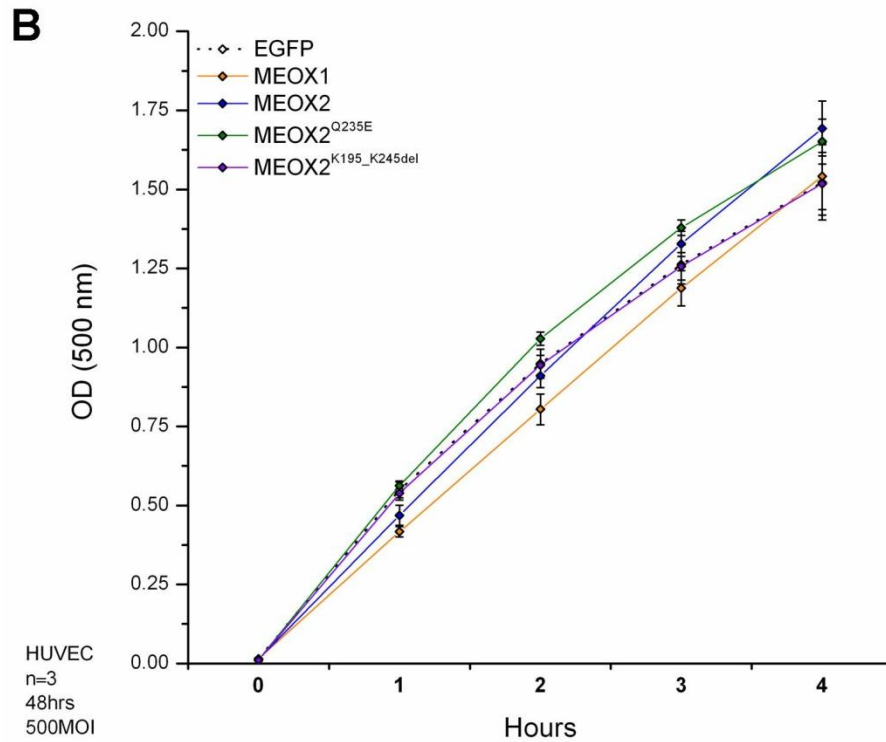
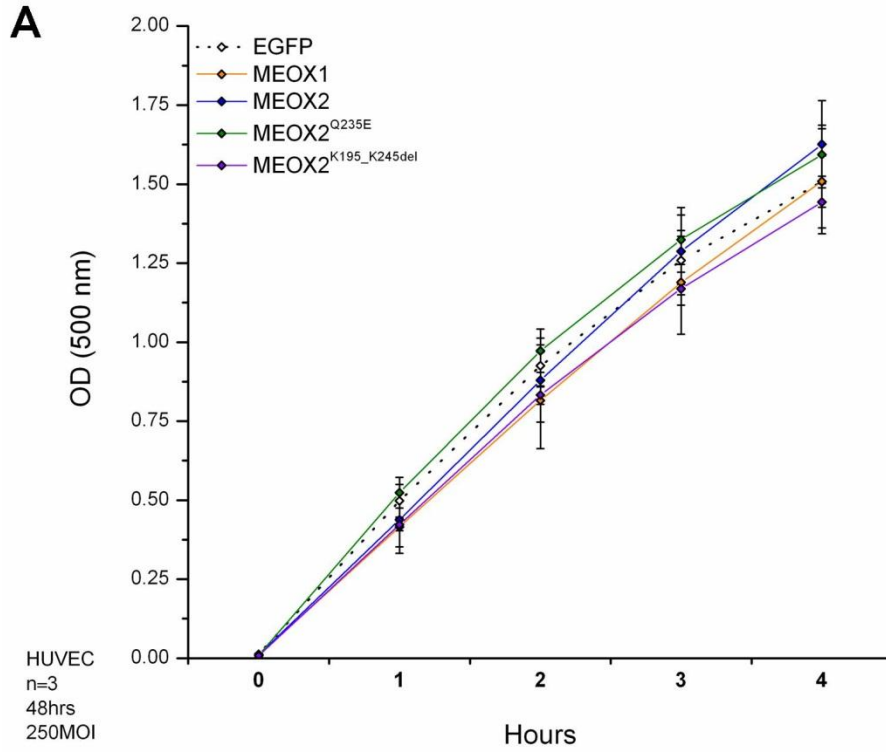


Figure 3-14: Adenoviral over-expression of N-terminal FLAG-tagged MEOX proteins in HUVECs does not reduce cell viability.

Figure 3-14: Adenoviral over-expression of N-terminal FLAG-tagged MEOX proteins in HUVECs does not reduce cell viability.

Differences in HUVEC viability were measured using the CellTiter assay 48 hours after adenoviral transduction at 250 MOI (**A**) and 500 MOI (**B**). The optical density (OD) at 500 nm is proportional to the amount of formazan dye produced by viable cells. Compared to the EGFP adenoviral control, MEOX1, MEOX2, MEOX2^{Q235E} and MEOX2^{K195_K245del} over-expression did not affect the production of formazan dye over time, indicating no change in cell viability. Error bars represent the standard error of the mean (n=3(A), n=3 (B)).

cells were exposed to one of four conditions; standard (growth media/normoxia), hypoxic (growth media/hypoxia), nutrient starved (basal media + 0.2% FBS/normoxia) and ischemic (basal media + 0.2% FBS/hypoxia). TUNEL assays were performed 48 and 72 hours post-transduction. Quantification of the number of TUNEL positive cells revealed that hypoxic treatment of HUVECs did not induce apoptosis in untransduced or adenoviral transduced cells at either time point (Figure 3-15). In contrast, 48 hours of nutrient starvation under normoxic conditions induced significant apoptosis in untransduced cells (Figure 3-15). There was no difference in the amount of apoptosis observed between nutrient starved cells transduced with adenovirus encoding either MEOX2 or the EGFP control (Figure 3-15). Cell proliferation is induced by serum and growth factors, and their removal often leads to apoptosis. We observed that adenoviral transduction was protective against nutrient starvation-induced apoptosis of ECs under normoxic conditions. Adenoviral transduction inhibits cell cycle progression and slows ECs proliferation (Figure 4-29). It is possible that this decreased rate of proliferation protects cells from undergoing nutrient starvation-induced apoptosis.

Although no change in apoptosis was observed in ECs over-expressing MEOX2 for 48 hours, we observed that MEOX2 over-expression for 72 hours significantly increased the level of apoptosis in HUVECs cultured in growth media, irrespective of hypoxia treatment (Figure 3-15). Thus, prolonged over-expression of MEOX2 is sufficient to induce apoptosis in ECs.

Subsequently, we wanted to confirm that prolonged over-expression of MEOX2 can induce EC apoptosis. To do so, we chose to assess caspase-3 cleavage which occurs earlier in the apoptotic process than DNA fragmentation (detected by TUNEL). We

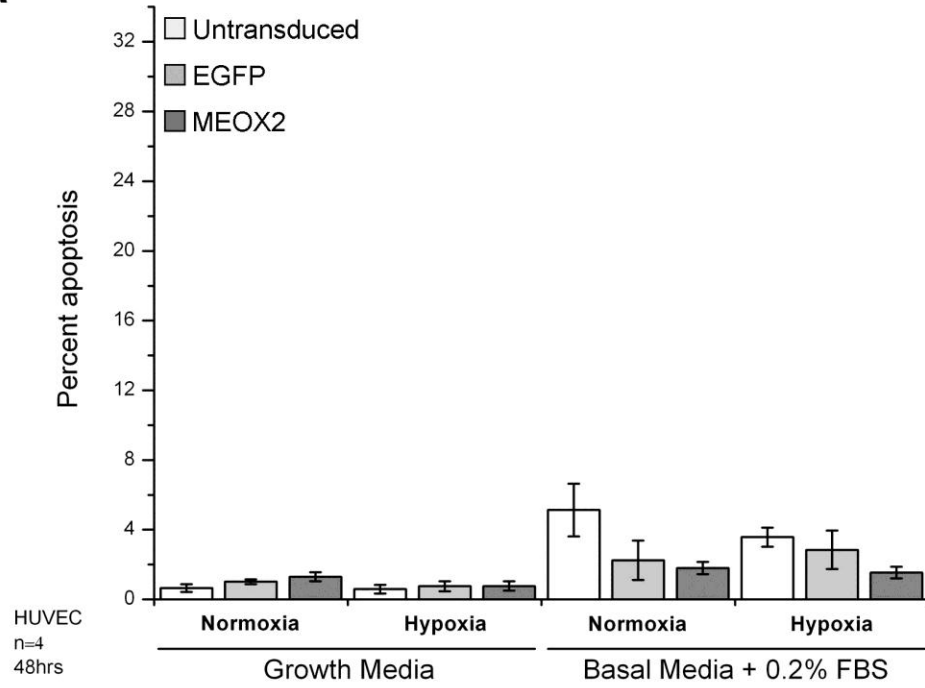
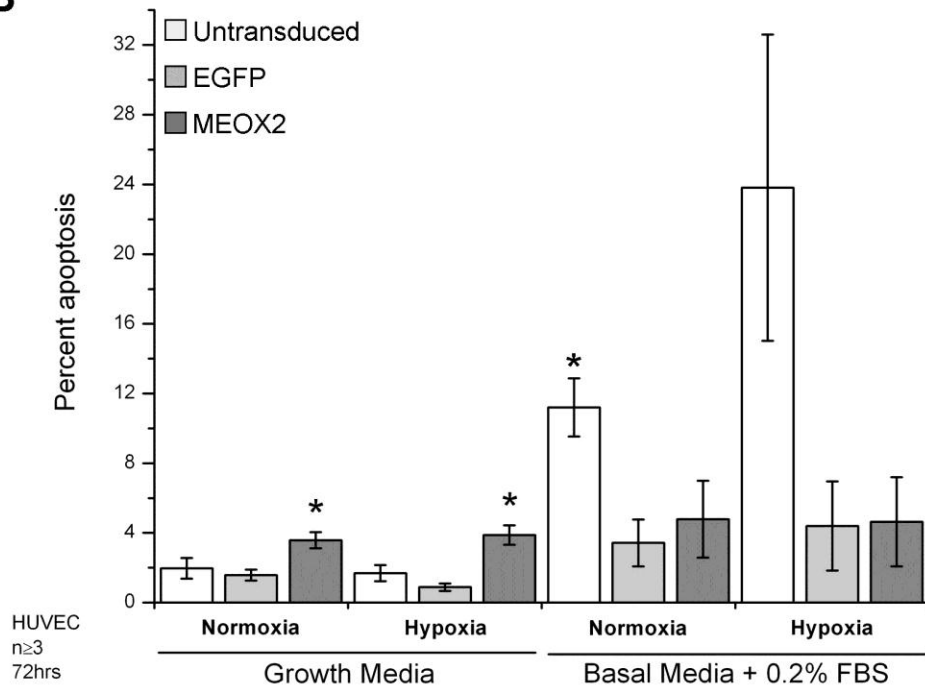
A**B**

Figure 3-15: Hypoxia and nutrient starvation of HUVECs does not potentiate MEOX induction of apoptosis.

Figure 3-15: Hypoxia and nutrient starvation of HUVECs does not potentiate MEOX induction of apoptosis.

Percent apoptosis, as measured by TUNEL incorporation, in HUVECs transduced at 250 MOI with adenovirus for 24 hours and then subjected to one of four treatments (\pm hypoxia, \pm basal media containing 0.2% FBS) for 24 hours (**A**) or 48 hours (**B**). Hypoxic treatment of HUVECs had no effect on the amount of apoptosis observed. Nutrient starvation (basal media containing 0.2% FBS) significantly increased the level of apoptosis in untransduced HUVECs, but not transduced HUVECs. MEOX2 over-expression induced apoptosis in HUVECs cultured in growth media for 72 hours, irrespective of hypoxic treatment. * Indicates a statistically significant change ($p < 0.05$) compared to EGFP over-expressing cells under the same treatment conditions. Error bars represent the standard error of the mean ($n=4$ (A), $n \geq 3$ (B)).

measured caspase-3 cleavage in HUVECs over-expressing N-terminal FLAG-tagged MEOX fusion proteins by western blot (data not shown) and flow cytometry. There was no change in the amount of cleaved caspase-3 in cells transduced with the LacZ adenoviral control, as compared to untransduced cells (Figure 3-16). In contrast, compared to the LacZ control, over-expression of MEOX1 significantly increased the amount of cleaved caspase-3 in HUVECs (Figure 3-16). Wild-type MEOX2 and DNA-binding domain mutated MEOX2^{Q235E} did not increase the amount of cleaved caspase-3 in HUVECs (Figure 3-16). The observation that MEOX2 did not induce significant caspase-3 cleavage at 48 hours post-transduction was not entirely surprising given that MEOX2 did not increase TUNEL staining until 72 hours post-transduction (Figure 3-15). Thus, both MEOX1 and MEOX2 can induce EC apoptosis; as indicated by increased DNA fragmentation (MEOX2: Figure 3-15) or caspase-3 cleavage (MEOX1: Figure 3-16).

To assess whether MEOX1 and MEOX2 also affect necrotic cell death, we used the LIVE/DEAD assay. This assay relies on the integrity of the plasma membrane to differentially stain live and dead cells. Live cells, having intact plasma membranes, contain cytosolic esterases that cleave the calcein-AM ester bond and thereby trap the fluorescent calcein molecule within the cell. Dead cells, having ruptured plasma membranes, allow ethidium homodimer-1 to enter the cell, bind to DNA and thereby become highly fluorescent. The percent cell death can be calculated by dividing the number of ethidium homodimer-1 positive cells by the total number of cells counted (Figure 3-17, panel A). HUVECs were transduced with N-terminal FLAG-tagged MEOX constructs for 72 hours prior to performing the LIVE/DEAD assays. Treatment

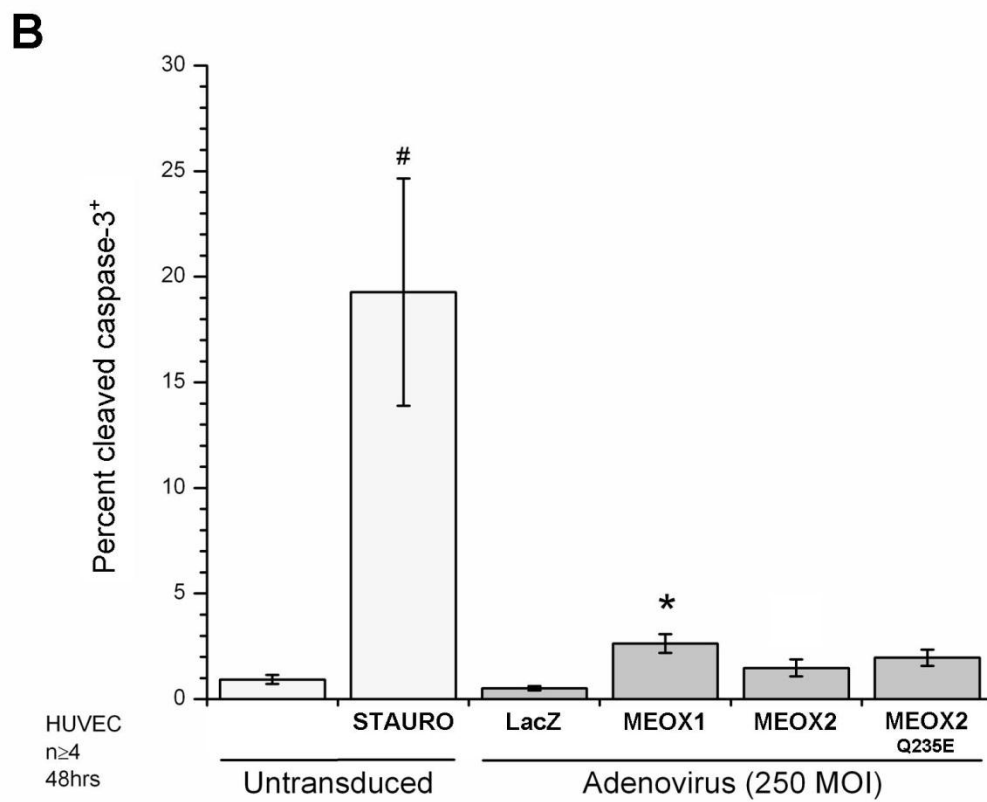
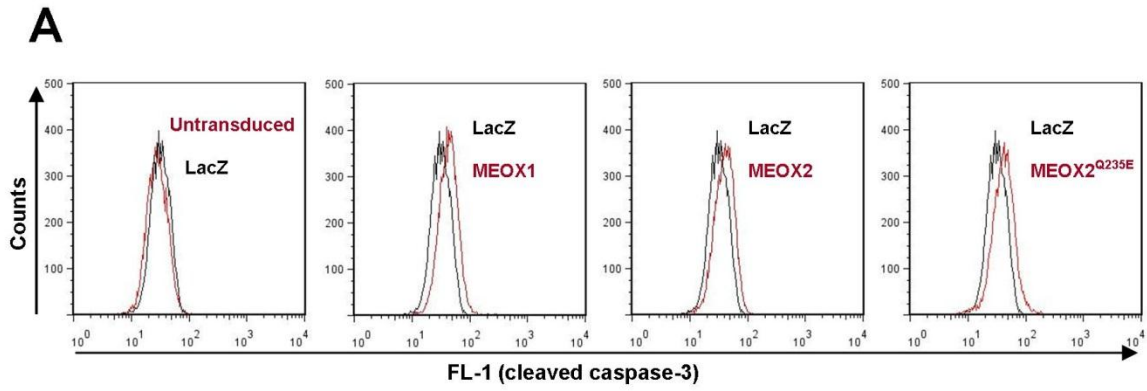


Figure 3-16: Over-expression of MEOX1 induces caspase-3 cleavage in HUVECs.

Figure 3-16: Over-expression of MEOX1 induces caspase-3 cleavage in HUVECs.

(A) Representative flow cytometry plots showing the fluorescence intensity histograms for cleaved caspase-3 staining (fluorescence intensity versus number of cells). HUVECs were transduced at 250 MOI for 48 hours, following which cells were fixed and stained for cleaved caspase-3. (B) Percent cleaved caspase-3 in HUVECs transduced at 250 MOI for 48 hours, as assessed by flow cytometry. There is no difference between untransduced and cells transduced with LacZ encoding adenovirus. Compared to the LacZ control, over-expression of MEOX1 induces caspase-3 cleavage in HUVECs; however, there is no increase in cleaved caspase-3 staining in cells over-expressing MEOX2 or DNA-binding domain mutated MEOX2^{Q235E}. Staurosporine was used as a positive control for increased caspase-3 cleavage. # Indicates a statistically significant change ($p < 0.05$) between untreated and staurosporine treated untransduced cells. * Indicates a statistically significant change ($p < 0.05$) when compared to the LacZ control. Error bars represent the standard error of the mean ($n \geq 4$).

A

$$\text{Percent cell death} = \left(\frac{\# \text{ Ethidium homodimer-1}^+ \text{ cells}}{\text{Total \# cells (Calcein AM}^+ + \text{Ethidium homodimer-1}^+)} \right) \times 100$$

B

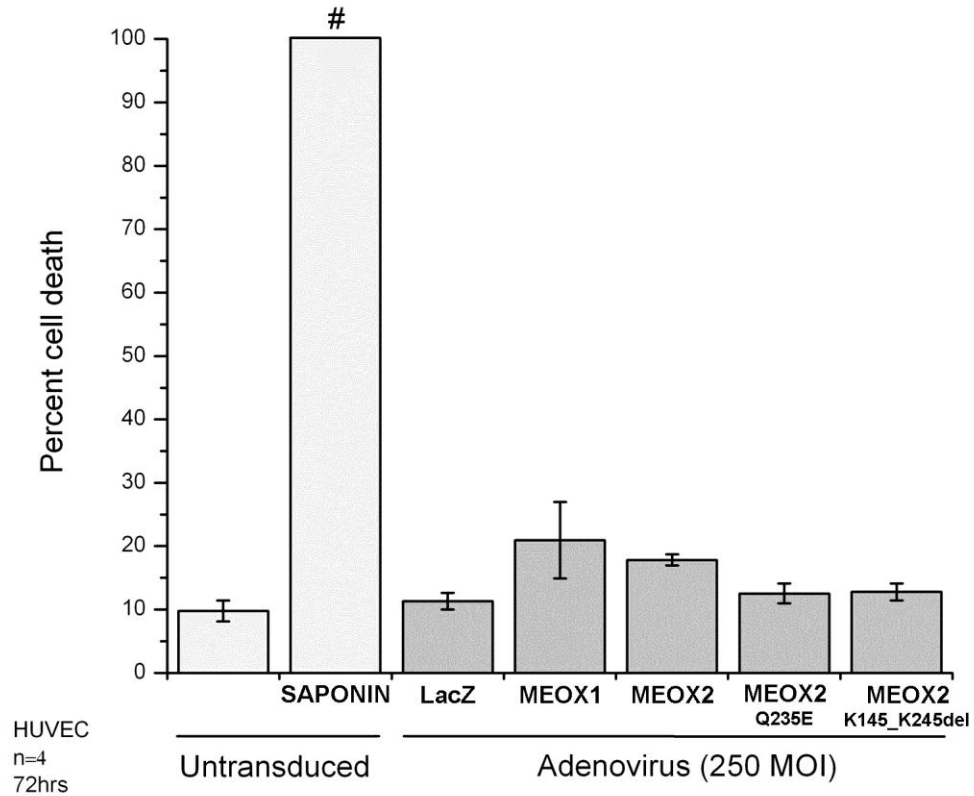


Figure 3-17: Prolonged over-expression of MEOX1 or MEOX2 does not induce necrotic cell death.

Figure 3-17: Prolonged over-expression of MEOX1 or MEOX2 does not induce necrotic cell death.

(A) The equation used to calculate the percent cell death using the LIVE/DEAD assay. Live cells (intact plasma membrane) are stained by the vital dye calcein AM, while dead cells (perforated plasma membrane) are stained by ethidium homodimer-1. (B) Percent cell death in HUVECs transduced at 250 MOI with adenovirus for 72 hours, as measured using the LIVE/DEAD assay. The percent cell death in untransduced HUVECs and cells transduced with the LacZ viral control was the same, indicating that adenoviral transduction does not cause cell death. Compared to the LacZ control, over-expression of MEOX1, MEOX2 or the DNA-binding deficient versions of MEOX2 (MEOX2^{Q235E} and MEOX2^{K195_K245del}) did not result in increased necrotic cell death. Saponin was used as a positive control for death due to loss of plasma membrane integrity. # Indicates a statistically significant change ($p < 0.05$) between untreated and saponin treated untransduced cells. Error bars represent the standard error of the mean (n=4).

of cells with saponin, a compound capable of forming pores in the cell membrane [209], was used as a positive control for cell death. There was no difference in the percent cell death observed in untransduced cells and those transduced with the LacZ adenoviral control (Figure 3-17, panel B), indicating that prolonged exposure to adenovirus does not induce necrotic cell death. Furthermore, prolonged over-expression of MEOX1, MEOX2, DNA-binding domain mutated MEOX2^{Q235E} or the homeodomain deleted MEOX2^{K195_K245del} did not induce necrotic cell death in HUVECs (Figure 3-17, panel B).

3.5. Conclusions and future directions

We established that prolonged over-expression of MEOX1 or MEOX2 in endothelial cells is sufficient to induce apoptotic cell death. By 48 hours post-transduction, MEOX1 increased the level of apoptosis by 5.2 fold (Figure 3-16), as assessed by caspase-3 cleavage. However, MEOX2 did not cause a significant increase in apoptosis until 72 hours post-transduction, when a 2.3 fold increase was observed by TUNEL (Figure 3-15). These findings suggest that in ECs MEOX1 may be a stronger inducer of apoptotic cell death than MEOX2. In contrast, neither MEOX1 nor MEOX2 was able to induce necrotic cell death in HUVECs by 72 hours post-transduction (Figure 3-17). It was shown *in vivo* that a minimum of 22% endothelial cell death is required to cause significant microvascular regression [210]. Maintained over-expression of MEOX1 and MEOX2 in ECs during physiological or pathological conditions (e.g. MEOX2 expression in HGPS) may result in exacerbated levels of apoptosis that could destabilize blood vessels due to vascular cell death.

We did not observe MEOX1 or MEOX2 (wild-type) induced apoptosis in VSMCs by 48 hours post-transduction. However, given the results in ECs, we need to repeat the TUNEL experiments at a later timepoint (no sooner than 72 hours post-transduction) in order to draw conclusions about the ability of the MEOX proteins to induce apoptosis in this cell type. We hypothesize that if the VSMC experiments were repeated at 72 hours post-transduction instead of 48 hours, we would observe a significant increase in apoptosis occurring in MEOX over-expressing cells.

Future directions of this study are to repeat the cleaved caspase-3 and TUNEL experiments in HUVECs and primary VSMCs at 72 hours post-transduction with the

DNA-binding domain mutated MEOX1^{Q219E} and MEOX2^{Q235E}. These experiments will allow us to determine conclusively whether MEOX1 and MEOX2 induced apoptosis is dependent upon their ability to bind to DNA. Furthermore, we will generate adenoviral constructs encoding middle domain and histidine/glutamine rich domain deleted versions of MEOX2 and assess their ability to induce apoptosis upon over-expression in HUVECs and primary VSMCs. We will use electron microscopy to verify necrotic and apoptotic cell death of ECs and VSMCs over-expressing MEOX1 and MEOX2. As well, we will identify the intermediate factors involved in MEOX mediated vascular cell death.

CHAPTER 4: MEOX1 AND MEOX2 ACTIVATE *P21^{CIP1/WAF1}* AND *P16^{INK4A}* EXPRESSION AND INDUCE ENDOTHELIAL CELL SENESENCE

4.1. Introduction

Cells of the adult vasculature are typically quiescent, existing in a state of long-term arrest, only re-entering the cell cycle when there is a need for new blood vessel formation [28,211]. Physiological angiogenesis in the adult occurs during wound healing, endurance exercise and menstruation in women [18-20]. Vascular injury, due to environmental factors (e.g. smoking) or physical damage (e.g. angioplasty) will also initiate cell cycle re-entry and proliferation of vascular cells in order to repair the injured vessel. However, aged blood vessels have impaired angiogenic capabilities [212]. It has been proposed that the increase in senescent cells in aged blood vessels is the cause of this decreased angiogenic potential. Indeed, populations of senescent ECs were shown to have impaired angiogenic capabilities *in vitro* [36].

4.1.1. The cell cycle

Cellular proliferation is dependent upon cell cycle progression from G₀/G₁ through mitosis. The cell cycle is controlled by the sequential association of cyclin proteins with CDKs. While CDKs are constitutively expressed throughout the cell cycle, specific cyclin proteins are only produced during certain phases of the cell cycle [213,214]. Formation of cyclin/CDK complexes enables CDK phosphorylation and produces active kinases that subsequently phosphorylate target proteins [213]. Cyclin/CDK complexes thereby act as switches to control which cellular processes occur during the various phases of the cell cycle.

CDK inhibitors block cellular proliferation and govern cell cycle checkpoints. CDK inhibitors bind to CDKs, impeding their association with cyclin proteins and hence, prevent active cyclin/CDK complex formation [213]. In the absence of active cyclin/CDKs, the subsequent phosphorylation of downstream targets does not occur and the cell cycle is halted.

The CDK inhibitors p21^{CIP1/WAF1} and p16^{INK4a} are encoded by the *CDKN1A* and *CDKN2A* genes, respectively. While p21^{CIP1/WAF1} prevents Cyclin E/CDK2 association, p16^{INK4a} inhibits Cyclin D/CDK4 interaction [213,214]. Both of these cyclin/CDK complexes phosphorylate the retinoblastoma protein (pRb) [214]. Phosphorylation of pRb is required for cell cycle progression from G₁ to S phase [214]. Thus, both p21^{CIP1/WAF1} and p16^{INK4a} inhibit cell cycle progression at the G₁/S cell cycle checkpoint by preventing phosphorylation of pRb. Interestingly, the *CDKN2A* gene also encodes p14^{ARF}, another protein involved in cell cycle regulation [215]. By preventing the p53 E3 ubiquitin protein ligase homolog of transformed mouse 3T3 cell double minute 2 (MDM2) inhibition of p53, p14^{ARF} causes the activation of p53, up-regulation of p21^{CIP1/WAF1} and cell cycle inhibition [215].

The G₁/S cell cycle checkpoint is critical for determining whether a cell will enter into S phase and replicate its genome, or enter into an arrested state [213]. This state of G₁ arrest can be either temporary (quiescence) or it can be permanent (senescence) [213].

4.1.2. Senescence

Cellular senescence was first described in the 1960s by Leonard Hayflick to explain the limited proliferation capacity of normal diploid human fibroblasts in culture [216,217]. Senescence can be induced by many different stimuli that can be divided into

two broad categories; replicative senescence and stress-induced premature senescence [218]. Replicative senescence is associated with telomere shortening [219,220], whereas stress-induced premature senescence is independent of telomere shortening. Examples of cellular stress that can induce premature senescence include DNA damage, oxidative stress and oncogene activation (e.g. Harvey rat sarcoma viral oncogene homolog (HRAS) over-expression) [221-223]. There are only a few well accepted markers of cellular senescence including increased p21^{CIP1/WAF1} expression, p16^{INK4a} expression [224], heterochromatic foci formation [225], nuclear promyelocytic leukemia (PML) protein aggregation [226] and senescence-associated β -galactosidase (SA- β -gal) expression [227]. However, none of these markers are entirely specific to senescence and none are a feature of all forms of senescence [223]. EC senescence causes endothelial cell dysfunction and is thought to promote atherosclerotic vascular disease [218].

4.2. Rationale, hypothesis and aims

MEOX2, is also known as the growth arrest specific homeobox (GAX) [94] due to its ability to prevent cell cycle progression via transcriptional up-regulation of the CDK inhibitor p21^{CIP1/WAF1} [89,156]. MEOX2 over-expression has been shown to induce p21^{CIP1/WAF1} expression and inhibits cell proliferation in VSMCs [156], fibroblasts [87,168], keratinocytes [146] as well as in ECs [89,150] (Figure 4-1). Furthermore, MEOX2 over-expression has also been shown to induce the expression of the CDK inhibitor p16^{INK4a} in fibroblasts [87,168] (Figure 4-1). Consistent with increased levels of p21^{CIP1/WAF1} and p16^{INK4a} protein, MEOX2 over-expression in primary human fibroblasts arrested cells in the G₁ phase and induced premature senescence [87].

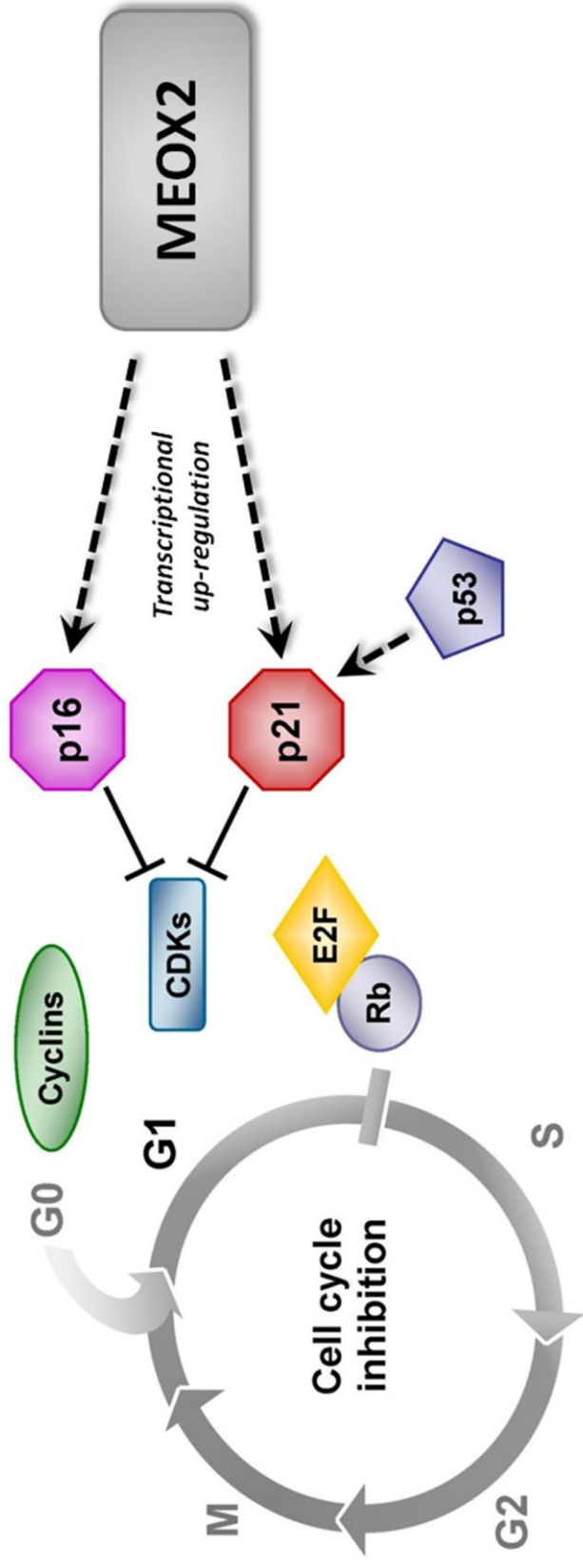


Figure 4-1: The cell cycle and the role of MEOX2.

MEOX2 increases the expression of the cyclin dependent kinase (CDK) inhibitors p21^{CIP1/WAF1} and p16^{INK4a} and thereby inhibits cell cycle progression from G₁ to S phase [156, 87]. Activation of p21^{CIP1/WAF1} by MEOX2 is independent of p53 [156]. In the absence of active cyclin/CDK complexes, hypophosphorylated retinoblastoma (Rb) remains bound to the E2F transcription factor, preventing it from activating the genes that are necessary for S phase entry [213].

Currently, $p21^{CIP1/WAF1}$ and $p16^{INK4a}$ are the only confirmed transcriptional targets of MEOX2 [87,89] and it is unknown whether MEOX1 is also able to transactivate these targets. MEOX gene knockout studies in mice have suggested that MEOX1 and MEOX2 have partially redundant functions during development [126]. This suggests that the MEOX transcription factors may regulate the expression of similar sets of target genes. In support of this hypothesis, the amino acid composition of the MEOX1 and MEOX2 homeodomains is nearly identical [84]. Canonically, control of target gene transcription by homeodomain proteins is achieved through direct binding of DNA via the homeodomain. However, the homeodomain has also been shown to act as a protein-protein interaction module in several homeodomain proteins, including MEOX1 and MEOX2 [85,86], thereby permitting homeodomain transcription factors to modify target gene transcription without binding DNA directly.

We hypothesised that MEOX1 would be capable of up-regulating the MEOX2 target genes $p21^{CIP1/WAF1}$ and $p16^{INK4a}$ in ECs. Furthermore, we theorised that increased $p21^{CIP1/WAF1}$ and $p16^{INK4a}$ expression by MEOX proteins in ECs would be correlated with permanent cell cycle arrest and EC senescence.

To address these hypotheses our aims were to:

- i) Assess the ability of MEOX1 to induce $p21^{CIP1/WAF1}$ and $p16^{INK4a}$ expression in ECs.
- ii) Test if DNA-binding by the MEOX proteins is required for $p21^{CIP1/WAF1}$ and $p16^{INK4a}$ transactivation.
- iii) Determine if the MEOX proteins are required for $p21^{CIP1/WAF1}$ and $p16^{INK4a}$ expression in ECs.
- iv) Determine if MEOX1 and MEOX2 over-expression induces EC senescence.

4.3. Materials and methods

4.3.1. Cell culture

All cells were maintained in a standard cell culture incubator at 37°C with 5% CO₂. HEK293 cells and HUVECs were cultured as described in sections 3.3.1.1 and 3.3.1.4, respectively. Neonatal human dermal lymphatic microvascular endothelial cells (LECs) (Clonetics) were cultured in Microvascular Endothelial Cell Growth Medium (EGM-2-MV) (Clonetics) which contains 5% FBS, rhEGF, rhFGF-B, R³-IGF-1, VEGF, hydrocortisone, ascorbic acid and GA-1000.

4.3.2. MEOX expression vectors (plasmid and adenovirus)

Cloning of all MEOX1 and MEOX2 constructs is described in Appendix B, while adenovirus production and titering is described in section 3.3.3.

4.3.3. Immunofluorescence (confocal microscopy)

HUVECs (1×10^5 cells/well) were transduced at a MOI of 250 with adenovirus and then plated onto collagen I (BD Biosciences) coated glass coverslips in 6-well tissue culture plates. At 48 hours post-transduction, cells were washed with PBS, fixed with 4% paraformaldehyde (EMD Chemicals) and then blocked with 5% goat serum in PBS at room temperature for 30 minutes.

Cells on coverslips were then incubated with primary mouse anti-FLAG [M2] (Sigma) antibody followed by Alexa Fluor 488 conjugated goat anti-mouse IgG (Invitrogen) secondary antibody as described in section 3.3.4.2. Subsequently, coverslips were washed three times with PBS-T. Cells on coverslips were incubated for 3 hours at room temperature with 1 mg/mL propidium iodide (Invitrogen) diluted 1:100 in blocking

buffer prior to being mounted onto slides. Coverslips were washed three times with PBS-T, once with PBS and then mounted onto slides using FluorSave Reagent (CalBiochem).

Alternatively, after blocking, cells on coverslips were incubated overnight at 4°C with primary mouse anti-Lamin A+C antibody [JOL2] (Millipore) diluted 1:50 in blocking buffer. Subsequently, coverslips were washed three times with PBS-T and then incubated at room temperature for 1 hour with Texas Red conjugated goat anti-mouse IgG (Invitrogen) secondary antibody diluted 1:200 in blocking buffer. Coverslips were washed three times with PBS-T. Cells on coverslips were then incubated with primary mouse anti-FLAG [M2] (Sigma) antibody followed by Alexa Fluor 488 conjugated goat anti-mouse IgG (Invitrogen) secondary antibody as described in section 3.3.4.2. Coverslips were washed three times with PBS-T, once with PBS and then mounted onto slides using SlowFade Gold antifade reagent with DAPI (Invitrogen).

All images were acquired with an Olympus IX70 confocal laser microscope using FluoView 2.0 software.

4.3.4. Luciferase promoter constructs and LacZ expression vector

The WWP-LUC vector containing the $p21^{CIP1/WAF1}$ upstream promoter region, a gift from Dr. B. Vogelstein (Johns Hopkins University) [228], was digested with *SstI/HindIII* and the resulting 2272 bp human $p21^{CIP1/WAF1}$ promoter was cloned into the pGL3-basic vector (Promega). The 232 bp $p21^{CIP1/WAF1}$ promoter was amplified by polymerase chain reaction (PCR) from the 2272 bp $p21^{CIP1/WAF1}$ promoter, digested with *XhoI/HindIII* and then ligated into the pGL3-basic vector. The 232 bp $p21^{CIP1/WAF1}$ promoter was then verified by DNA sequencing at the University of Calgary. The pGL3 vector containing the 564 bp $p16^{INK4A}$ upstream promoter region (pGL3-INK4a) was a

gift from Dr. S. Chanda (Burnham Institute for Medical Research) [87]. The pGL3-basic and pcDNA3-LacZ vectors were a gift from Dr. N. Mesaeli (Weill Cornell Medical College in Qatar).

4.3.5. Luciferase assays

HEK293 cells and HUVECs (1.5×10^5 cells/well) were plated into 6-well tissue culture plates (for HUVECs, plates were coated with collagen I (BD Biosciences)) containing growth media. Media was changed to Opti-MEM I (Gibco) containing 10% Calf Serum (Gibco) 48 hours after plating. Each well of HEK293 cells was transfected using 15 μ L Lipofectamine 2000 Reagent (Invitrogen), 3 μ g transcription factor vector DNA, 2 μ g promoter vector DNA and 1 μ g β -galactosidase vector DNA. For the *p21^{CIP1/WAF1}* promoter luciferase assays in HUVECs, cells were transfected with a total of 1 μ g transcription factor vector DNA, 1 μ g promoter vector DNA and 0.5 μ g β -galactosidase vector DNA using 6.25 μ L Lipofectamine LTX and 2.5 μ L Plus Reagent (Invitrogen). For *p16^{INK4a}* promoter luciferase assays in HUVECs, cells were transfected with a total of 1 μ g transcription factor vector DNA, 0.5 μ g promoter vector DNA and 0.5 μ g β -galactosidase vector DNA using 5 μ L Lipofectamine 2000 (Invitrogen). In all experiments, media was changed back to growth medium 4 hours post-transfection. Mithramycin A (200 ng/mL final concentration [229,230]), or the same volume of methanol (vehicle), was diluted in growth medium and added to the cells 4 hours post-transfection.

Luciferase assays were performed 24 hours after transfection or mithramycin A treatment using a Lumat LB 9507 luminometer and luciferase buffer containing 20 mM Tricine, 1.07 mM MgCO₃, 2.67 mM MgSO₄, 0.1 mM EDTA, 33.3 mM DTT, 270 μ M

coenzyme A, 470 μ M luciferin, and 530 μ M ATP. β -galactosidase assays were performed using a solution containing 0.8 μ g/ μ L ONPG and a MRX-TC revelation spectrophotometer (Dynex Technologies) set to 415 nm. To control for transfection efficiency, luciferase assay values were normalized to the β -galactosidase assay values for each sample. Empty expression vectors were used to control for basal promoter activity. Fold activation was calculated by dividing the relative luciferase unit value of each sample by the value obtained for the empty vector control.

4.3.6. Quantitative real-time PCR

HUVECs (2.5×10^5 cells/plate) were transduced with adenovirus and then plated onto 6 cm tissue culture plates. RNA was isolated using the RNeasy Plus kit (Qiagen) following the manufacturer's instructions. One step real-time PCR was performed using an iQ5 thermocycler (BioRad) and the iScript One-Step PCR kit with SybrGreen (BioRad) or the BR 1-Step SYBR Green qRT-PCR Kit (Quanta). Relative gene quantification ($2^{-\Delta\Delta CT}$ method) was performed where the mRNA expression of *p21^{CIP1/WAF1}*, *p16^{INK4a}* or *p14^{ARF}* were compared to the mRNA expression of the *β -actin* control. PCR products were resolved on 2% agarose gels and cloned using the TOPO TA cloning kit (Invitrogen). The resulting constructs were verified by sequencing. Primer sequences are listed in Table 4-1.

Table 4–1: List of primers used for quantitative real-time PCR.

Primer	Direction	Sequence	Reference
P21	Forward	5'-GGAGACTCTCAGGGTCGAAAAC-3'	
P21	Reverse	5'-GGGCTTCCTCTTGGAGAAGATC-3'	
P16	Forward	5'-ATGGAGCCTTCGGCTGACT-3'	
P16	Reverse	5'-CGTAACTATTCCGGTCCGTTG-3'	
P14	Forward	5'-GTTTTTCGTGGTTCACATC-3'	
P14	Reverse	5'-CCTCAGTAGCATCAGCAC-3'	
MEOX2	Forward	5'-TTCAACCTCTCCCACCTTTGAC-3'	
MEOX2	Reverse	5'-CAGCGGCCAGTCTCCTTTAC-3'	
FOXO4	Forward	proprietary QuantiTect primer sequence	Qiagen
FOXO4	Reverse	proprietary QuantiTect primer sequence	Qiagen
DKC1	Forward	5'-GGACTATATCAGGACAGGTTTCATT-3'	RTPrimerDB # 4484
DKC1	Reverse	5'-CGTCGAAATCCAGGCTACCA-3'	RTPrimerDB #4484
NOP10	Forward	5'-GTCCCTTAAACTGATGTC-3'	
NOP10	Reverse	5'-CCTCACACAAGCATAATC-3'	
ICAM-1	Forward	5'-GTATGAACTGAGCAATGTG-3'	
ICAM-1	Reverse	5'-CGTAGGGTAAGGTTCTTG-3'	
eNOS	Forward	5'-TGGTACATGAGCACTGAGATCG-3'	PrimerBank# 10835161a3
eNOS	Reverse	5'-CCACGTTGATTTCCACTGCTG-3'	PrimerBank# 10835161a3
β -ACT	Forward	5'-AGGCCAACCCGGGAGAAGATG-3'	
β -ACT	Reverse	5'-CAGAGGGGTACAGGGATAGCAC-3'	

4.3.7. Western blotting and quantification

HUVECs (2.5×10^5 cells/plate) were transduced with adenovirus and then plated onto 6 cm tissue culture plates. Cells were harvested and protein samples were prepared, then separated by SDS-PAGE as described in section 3.3.4.4. For p16^{INK4a}/α-tubulin blots, proteins were transferred from the acrylamide gels to nitrocellulose membranes with a pore size of 0.2 μm (Bio-Rad) by electrophoretic semi-dry transfer. For all other western blots, proteins were transferred from acrylamide gels to nitrocellulose membranes with a 0.45 μm pore size (Bio-Rad) using electrophoretic tank transfer. Primary antibodies used for western blotting were: mouse anti-p21^{CIP1/WAF1} [CP74] (Sigma), mouse anti-p16^{INK4a} [DCS-50] (Santa Cruz), rabbit anti-p53 [FL-393] (Santa Cruz), mouse anti-FLAG [M2] (Sigma), rabbit anti-actin (pan) (Sigma), mouse anti-α-tubulin [DMA1] (AbCam) and mouse anti-Lamin A+C [JOL2] (Millipore). Primary antibody dilutions and incubation conditions are listed in Table 3-1. Horseradish peroxidase conjugated secondary antibodies were incubated and detected as described in section 3.3.4.4. Protein band intensities were quantified using the adjusted volume measurement (Adj.Vol.; CNT*mm²) in the Quantity One software (Bio-Rad).

4.3.8. Recombinant MEOX-GST fusion protein production

Cloning of MEOX1 and MEOX2 glutathione S-transferase (GST) constructs is described in Appendix B. Briefly, pET-41a(+)-MEOX constructs were transformed into Rosetta-gami 2(DE3)pLysS competent cells (Novagen) for the production of recombinant C-terminal GST-tagged proteins. Proteins were isolated using the BugBuster GST Bind Purification Kit (Novagen) as per the manufacturer's recommendations with the addition of 0.5 mM PMSF and protease inhibitor cocktail (0.1 mg/mL aprotinin, 0.1 mg/mL

phosphoramidone, 0.1 mg/mL TLCK, 0.2 mg/mL TPCK, 0.1 mg/mL APMSF, 0.1 mg/mL E-64, 0.05 mg/mL leupeptin, 0.01 mg/mL I pepstatin) to all buffers.

4.3.9. Electrophoretic mobility shift assays

Two hundred nanograms of recombinant GST-fusion protein was used per EMSA binding reaction. Alternatively, HUVECs (7.5×10^5 cells/plate) were transduced at a MOI of 50 with adenovirus then plated onto 10 cm tissue culture plates. Nuclear proteins were isolated using the NE-PER nuclear and cytoplasmic extraction kit (Pierce) at 72 hours post-transduction and 5 μ L nuclear extract was used per binding reaction.

EMSAs were carried out using the LightShift Chemiluminescent EMSA Kit (Pierce). The sequence of all EMSA probes are listed in the Table 4-2. Binding reactions (20 μ L) were incubated for 30 minutes at room temperature in a buffer containing 10 mM Tris pH 7.5, 50 mM KCl, 1 mM DTT, 50 ng/ μ L Poly(dI•dC), 5% glycerol, 0.05% NP-40, 3.5mM MgCl₂, 0.5 mM EDTA, 0.25 mg/ml BSA and 30 – 90 fmol biotin end-labelled probe. For cold competition reactions, 8 – 18 pmol unlabelled probe was added (200 molar excess) and then incubated for 15 minutes at room temperature prior to the addition of the biotin labelled probe. Super-shift reactions containing 1 – 1.5 μ g normal mouse IgG (Millipore), anti-FLAG [M2] antibody (Sigma) or anti-MEOX2 [6A5] antibody (Millipore) were incubated overnight at 4°C, prior to the addition of biotin labelled probe. Luminescence was detected using CL-Xposure blue X-ray film (Thermo Scientific).

Table 4-2: List of EMSA probes.

Probe	Gene promoter	Binding sites	Sequence	Reference [#]
A6	p21 ^{CIP1/WAF1}	Wild-type homeodomain	5'-CCCCGATGGCATTACAATTACAGATGACACT-3'	Chen 2007 [89]
MT11	p21 ^{CIP1/WAF1}	Mutant homeodomain	5'-CCCCGATGGCAGTACAAGTACAGATGACACT-3'	Chen 2007 [89]
SP1	p21 ^{CIP1/WAF1}	Wild-type SP1	5'-GAGCGGGGTCCC GCCCTCCTTGAGGGGGCC-3'	
D16WT	p16 ^{INK4a}	Wild-type homeodomain (Distal)	5'-CTCCCCCGTCCGTATTAAATAAACCTCATC-3'	
D16MT	p16 ^{INK4a}	Mutant homeodomain (Distal)	5'-CTCCCCCGTCCGTAGGAAATAAACCTCATC-3'	
P16WT	p16 ^{INK4a}	Wild-type homeodomain (Proximal)	5'-GCTTTTCTTATGATTAAAAGAAGAAAGCCA-3'	
P16MT	p16 ^{INK4a}	Mutant homeodomain (Proximal)	5'-GCTTTTCTTATGAGGAAAAGAAGAAAGCCA-3'	

4.3.10. Chromatin immunoprecipitation

ChIP was carried out using the solutions from the EZ-ChIP kit (Millipore), except where stated otherwise. HUVECs (7.5×10^5 cells/plate) were transduced with adenovirus at 25 MOI and then plated onto 10 cm tissue culture plates containing 10 mL growth media (one 10 cm plate per ChIP). Forty-eight hours post-transduction, cells were cross-linked using 37% formaldehyde solution (VWR) added to the growth medium at a final concentration of 1% v/v formaldehyde. Cells were incubated at room temperature for 10 minutes, after which 10X glycine solution was added to a final concentration of 1X and then incubated at room temperature for 5 minutes to quench the cross-linking reaction. The cells were then washed twice with ice cold PBS containing protease inhibitors (Roche). Cells were collected and then pelleted by centrifugation at $1000 \times g$ for 5 minutes at 4°C.

Cell pellets were resuspended in SDS Lysis Buffer containing Protease Inhibitor Cocktail II and then incubated on ice for 10 minutes, after which the cell suspension was passed through a 27 ½ gauge syringe 3 times to break up the cells. The cell solution was then sonicated on ice 10 times for 10 seconds (with 30 seconds of rest in between) using a Misonix XL-2000 series sonicator (Qsonica) set to “2” (optimization of sonication conditions is discussed in Appendix D). The sonicated cell lysate was centrifuged at $15,000 \times g$ for 10 minutes at 4°C to remove insoluble material.

At this point, an aliquot of sonicated cell lysate was removed and the crosslinking was reversed by the addition of 8% v/v 5M NaCl solution and incubation overnight at 65°C. The DNA fragments were subsequently purified by phenol:chloroform extraction followed by ethanol precipitation and then analyzed by agarose gel electrophoresis.

The remaining sonicated cell lysate was diluted 1:9 with ChIP Dilution Buffer containing Protease Inhibitor Cocktail II and pre-cleared for 3 hours at 4°C by rotating incubation with Protein A/G Ultralink Resin (Pierce) (the choice of beads used for pre-clearing and chromatin/antibody collection is discussed in Appendix D). The resin was pelleted by centrifugation at 4000 × g for 1 minute at 4°C and the pre-cleared sonicated cell lysate was moved to a new tube. At this point, 1% was removed as Input and stored at 4°C and the remaining pre-cleared sonicated cell lysate was used for ChIP. To each ChIP, 2.5% v/v 2% BSA, 2% v/v 25 mg/mL yeast tRNA (Invitrogen) and 10 µg antibody was added. Antibodies used for ChIP were normal mouse IgG (Millipore), anti-RNA polymerase II [CTD4H8] (phospho- and non-phospho-RNAP) (Millipore) and anti-FLAG [M2] (Sigma). ChIPs were incubated overnight at 4°C with rotation.

Chromatin/antibody complexes were collected by rotating incubation with Protein G Agarose for 2 hours at 4°C. The agarose was pelleted by centrifugation at 5000 × g for 1 minute at 4°C. The supernatant was removed and the agarose was washed by rotating incubation with ice cold buffers at 4°C as follows: one 10 minute wash with Low Salt Immune Complex Wash Buffer, one 30 minute wash with High Salt Immune Complex Wash Buffer, one 30 minute wash with LiCl Immune Complex Wash Buffer and two 10 minute washes with TE Buffer. The immunoprecipitated chromatin was eluted from the agarose by incubation with freshly prepared Elution buffer (5% v/v 20% SDS, 10% v/v 1 M NaHCO₃) for 15 minutes at room temperature. Elution buffer was also added to the Input samples. Crosslinking was reversed by the addition of 8% v/v 5M NaCl solution and incubation overnight at 65°C. RNA and protein were degraded by sequential RNase A (10 mg/mL) and Proteinase K (10 mg/mL) digestion. The chromatin was then purified

using the QIAquick PCR purification Kit (Qiagen) as per the manufacturer's recommendations. Subsequently, the purified chromatin in nuclease-free water was analyzed by standard PCR. Chromatin from the *p16^{INK4a}* upstream promoter region was detected using the p16 forward 5'-TACGACTAGAAAGTGTCCCCCTAC-3' and p16 reverse 5'-TAGAACACTGAGCACTTTTTCTGG-3' primers [87]. Chromatin from the glyceraldehyde 3-phosphate dehydrogenase (*GAPDH*) core promoter was detected using the control primers from the EZ-ChIP kit (Millipore).

4.3.11. Senescence-associated β -galactosidase staining

HUVECs (1×10^5 cells/well) were transduced with adenovirus at 250 MOI and then plated onto collagen I (BD Biosciences) coated glass coverslips in 6-well tissue culture plates. Forty-eight hours post-transduction, cells were washed twice with PBS and then fixed for 5 minutes at room temperature with 2% paraformaldehyde (EMD Chemicals) diluted in PBS. Coverslips were washed twice with PBS and then freshly prepared SA- β -gal staining solution (40 mM citric acid/sodium phosphate, pH 6.0, 150 mM NaCl, 2 mM MgCl₂, 5mM potassium ferricyanide, 5 mM potassium ferrocyanide, 1 mg/mL X-gal) was added and incubated overnight at 37°C [227]. The following day, coverslips were rinsed three times with double distilled water. Nuclei were stained with Mayer's hematoxylin solution (Sigma) at room temperature for 2 minutes and then rinsed three times with double distilled water. Coverslips were mounted onto glass slides using FluorSave Reagent (CalBiochem). Phase contrast images of 16 random fields (20 \times) per coverslip were acquired using a Zeiss Axioskop 2 mot plus microscope equipped with an AxioCam digital camera and AxioVision 4.6 software (Zeiss). The number of SA- β -gal

positive cells was counted by an observer that was blinded to the identity of the slides and then expressed as a percentage of the total number of counted cells.

4.3.12. Flow cytometry (cell cycle analysis)

For all experiments, HUVECs (3×10^5 cells/plate) were transduced with adenovirus at 100 MOI and then plated onto 10 cm tissue culture plates containing growth media. Centrifugation steps were carried out at $350 \times g$ for 5 minutes at room temperature. 1×10^4 gated cells per sample were counted using a BD FACSCalibur flow cytometer. The results were analyzed using FlowJo software (Tree Star, Inc.).

4.3.12.1. *Propidium iodide*

Forty eight hours post-transduction, the media was collected and the cells were washed once with PBS, lifted using 0.5% Trypsin-EDTA (Gibco) and then collected using the initial media and PBS wash. Cells were pelleted by centrifugation, following which the media was discarded and the cells were resuspended in 0.5 mL PBS. Cells were fixed by adding 4 mL 70% ethanol and incubating the cells for 2 hours at 4°C. The fixed cells were pelleted by centrifugation, washed once with PBS, and then resuspended in freshly prepared propidium iodide staining solution (PBS containing 0.5 mg/mL RNaseA (Invitrogen), 0.02 mg/mL propidium iodide (Invitrogen) and 0.1% Triton-X-100 (Sigma)). Cells were incubated at room temperature for 30 minutes prior to analysis by flow cytometry.

4.3.12.2. *BrdU / 7-AAD*

Forty-eight hours post-transduction cells were treated with 5'-bromo-2'-deoxyuridine (BrdU) (Fisher) at a final concentration of 10 μ M for 1 hour at 37°C with 5% CO₂. Cells were washed three times with PBS, trypsinized and then pelleted by

centrifugation. The cell pellets were resuspended in 0.5 mL PBS, following which 2 mL cold 70% ethanol was added and the cells were fixed overnight at 4°C. Cells were pelleted by centrifugation and then resuspended in 1 mL freshly prepared 2N HCl and incubated at room temperature for 25 minutes. Subsequently, 2 mL PBS containing 3% FBS (PBS/FBS) was added to the cells, which were then pelleted by centrifugation. The cell pellet was resuspended in 1 mL 0.1 M sodium borate pH 8.5 and incubated at room temperature for 2 minutes. PBS/FBS (2 mL) was added to the cells, which were then pelleted by centrifugation. This step was repeated, following which cells were resuspended in 0.1 mL PBS/FBS containing 5 µL Alexa Fluor 488 conjugated mouse anti-BrdU [MoBU-1] antibody and then incubated for 2 hours at room temperature. Subsequently, 2 mL PBS/FBS was added to the cells, which were then pelleted by centrifugation. Lastly, the cell pellet was then resuspended in 0.5 mL PBS/FBS containing 10 µL 0.2 mg/mL 7-aminoactinomycin D (7-AAD) (Invitrogen) and incubated for 15 minutes at room temperature prior to analysis by flow cytometry.

4.3.13. Gene expression knockdown using siRNA

HUVECs and LECs (2×10^5 cells/plate) were plated onto 3.5 cm tissue culture plates containing growth media. Media was changed to fresh growth media 24 hours after the cells were plated. Subsequently, each plate of cells was transfected using 4 µL DharmaFECT1 (Dharmacon) and 0.2 picomoles ON-TARGETplus siRNA (Dharmacon) or siGLO green transfection indicator siRNA (Dharmacon). Media was changed to fresh growth media 24 hours after transfection. The human MEOX2 ON-TARGETplus SMARTpool (Dharmacon), that contains 4 siRNA specific to MEOX2 mRNA, was used

to knockdown MEOX2 expression. The ON-TARGETplus non-targeting pool (Dharmacon) was used as a negative control.

4.3.14. Statistical analysis

For luciferase assay data, ANOVA followed by Tukey post-hoc tests were used to evaluate the changes between MEOX proteins and the empty vector control, MEOX1 and MEOX2, as well as wild-type and mutant MEOX proteins. For all other experiments, ANOVA followed by Tukey post-hoc tests were used to evaluate the changes between MEOX proteins and the EGFP control, MEOX1 and MEOX2, as well as wild-type versus mutant MEOX proteins. Changes were considered significant if the p-value was less than 0.05. Statistical analysis was performed using Origin 8.5 software.

4.4. Results and discussion

4.4.1. Expression of MEOX proteins in HUVECs

To study the effects of MEOX1 and MEOX2 expression in endothelial cells we generated MEOX1 and MEOX2 expression constructs (Figure 4-2) that contain a FLAG epitope at either the N-terminus or the C-terminus of the protein. In addition to wild-type MEOX1 and MEOX2, we created full length constructs in which their homeodomains were mutated so that we could study the DNA-binding requirement of MEOX protein function. The MEOX1^{Q219E} and the MEOX2^{Q235E} constructs contain the entire MEOX homeodomain, but include a glutamine to glutamate substitution at position 50 of the homeodomain (Figure 4-2). This mutation has previously been shown to result in DNA-binding defective homeodomain proteins [231,232]. As well, two homeodomain deletion versions of MEOX2 were generated; MEOX2^{K195_K245del} which lacks the entire homeodomain except for the flexible amino-terminal arm, and MEOX2^{K188_K245del} in which the entire homeodomain has been removed (Figure 4-2). Furthermore, we created MEOX2 mutant constructs, MEOX2^{H68_Q85del} and MEOX2^{T89_V182del}, in which the histidine/glutamine rich domain or the middle domain was deleted, respectively.

The level of expression and subcellular localization of the various FLAG-tagged MEOX proteins were first verified by western blot in HEK293 cells, due to their ease of transfection. As the transfection of primary endothelial cells is very inefficient, we used adenoviral transduction to over-express the various MEOX proteins in HUVECs. To achieve close to 100% transduction of HUVECs, we delivered an adenoviral dose greater than 100 MOI (data not shown). As shown in Chapter 3, these doses of adenovirus were not cytotoxic. Subsequently, we evaluated the level of expression and subcellular

MEOX protein constructs

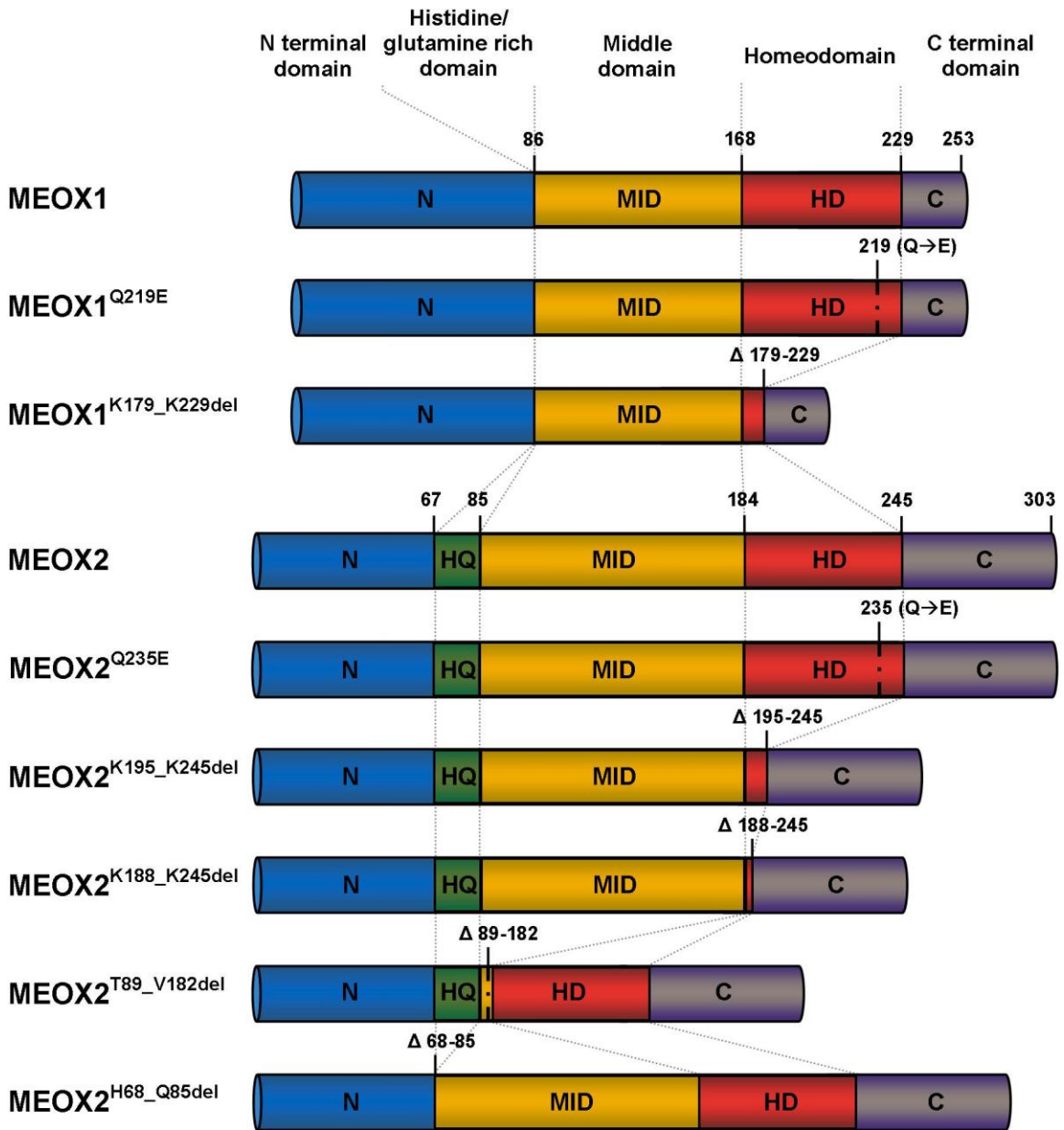


Figure 4-2: Schematic representation of the MEOX1 and MEOX2 protein constructs used in this thesis.

Figure 4-2: Schematic representation of the MEOX1 and MEOX2 protein constructs used in this thesis.

Three mouse MEOX1 constructs were generated: wild-type, homeodomain mutated (Q219E) and homeodomain deleted (K179_K229del). Five human MEOX2 constructs were generated: wild-type, homeodomain mutated (Q235E), homeodomain deleted (K195_K245del and K188_K245del), middle domain deleted (T89_V182del) and histidine/glutamine rich domain deleted (H68_Q85del). N: N-terminal domain, HQ: histidine/glutamine rich domain, MID: middle domain, HD: homeodomain, C: C-terminal domain.

localization of the FLAG-tagged MEOX proteins in HUVECs using fluorescent immunocytochemistry.

Comparable levels of protein expression were observed for all MEOX constructs in HEK293 cells by western blot (Figure 4-3, panel A; Figure C-1), however the subcellular localization of the MEOX proteins was quite different (Figure 4-3, panel B). Similar subcellular localization of MEOX proteins was observed in HEK293 cells (Figure 4-3, panel B) and HUVECs (Figure 4-4). MEOX1 and MEOX2 differed slightly in subcellular localization. Although both MEOX1 and MEOX2 were localized predominantly to the nucleus, MEOX1 was also consistently detected in the cytoplasm (Figure 4-3, panel B; Figure 4-4). Although the reason for this difference in localization is not known, we speculate that unique protein binding partners may explain the cytosolic localization of MEOX1. DNA-binding domain mutated MEOX1^{Q219E} and MEOX2^{Q235E} were both localized to the nucleus; however, an increased amount of cytosolic protein was detected for both mutants as compared to their wild-type counterparts (Figure 4-3, panel B). In contrast, homeodomain deleted MEOX2^{K195_K245del} differed dramatically in localization from that of either the wild-type MEOX2 or the DNA-binding domain mutated MEOX2^{Q235E} proteins, as it was detected predominantly in both the cytoplasm and as punctate nuclear aggregates (Figure 4-3, panel B; Figure 4-4). The cytoplasmic localization of the MEOX2^{K195_K245del} protein occurred despite the predicted nuclear localization signal being left intact. Furthermore, homeodomain deleted MEOX2^{K188_K245del}, which lacks the predicted nuclear localization signal, was identical to MEOX2^{K195_K245del} with respect to both the level of expression and cytosolic localization (data not shown). The punctate nuclear aggregates of homeodomain deleted

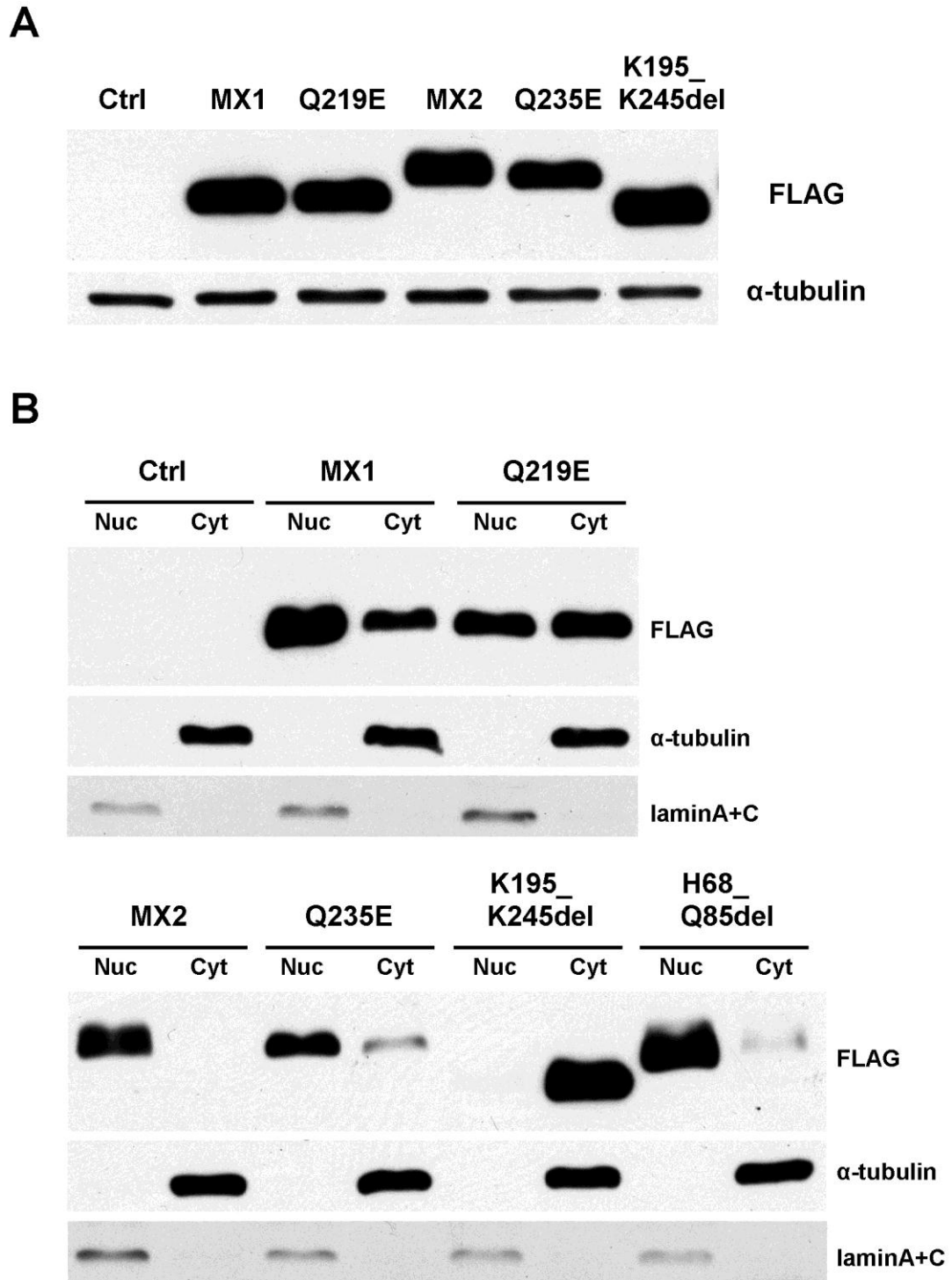


Figure 4-3: Expression and subcellular localization of MEOX1 and MEOX2 proteins in HEK293 cells.

Figure 4-3: Expression and subcellular localization of MEOX1 and MEOX2 proteins in HEK293 cells.

Representative western blots showing the relative level of expression (A) and subcellular localization (B) of MEOX proteins in HEK293 cells 48 hours after transfection. (A) All constructs were expressed at approximately the same level. (B) Wild-type MEOX1 (MX1) and DNA-binding domain mutated MEOX1^{Q219E} (Q219E) was expressed in both the nucleus and the cytosol. The expression of wild-type MEOX2 (MX2), DNA-binding domain mutated MEOX2^{Q235E} (Q235E) and histidine/glutamine rich domain deleted MEOX2^{H68-Q85del} (H68_Q85del) was primarily nuclear, while the expression of homeodomain deleted MEOX2^{K195-K245del} (K195_K245del) was exclusively cytosolic. Notably, there was an increased amount of MEOX1^{Q219E}, MEOX2^{Q235E} and MEOX2^{H68-Q85del} located in the cytosol, as compared to their wild-type counterpart. The N-terminally tagged MEOX proteins were detected using an anti-FLAG antibody. The empty expression vector was used as a negative control (Ctrl). Lamin A+C was used as nuclear (Nuc) marker and α -tubulin was used as a cytoplasmic (Cyt) marker.

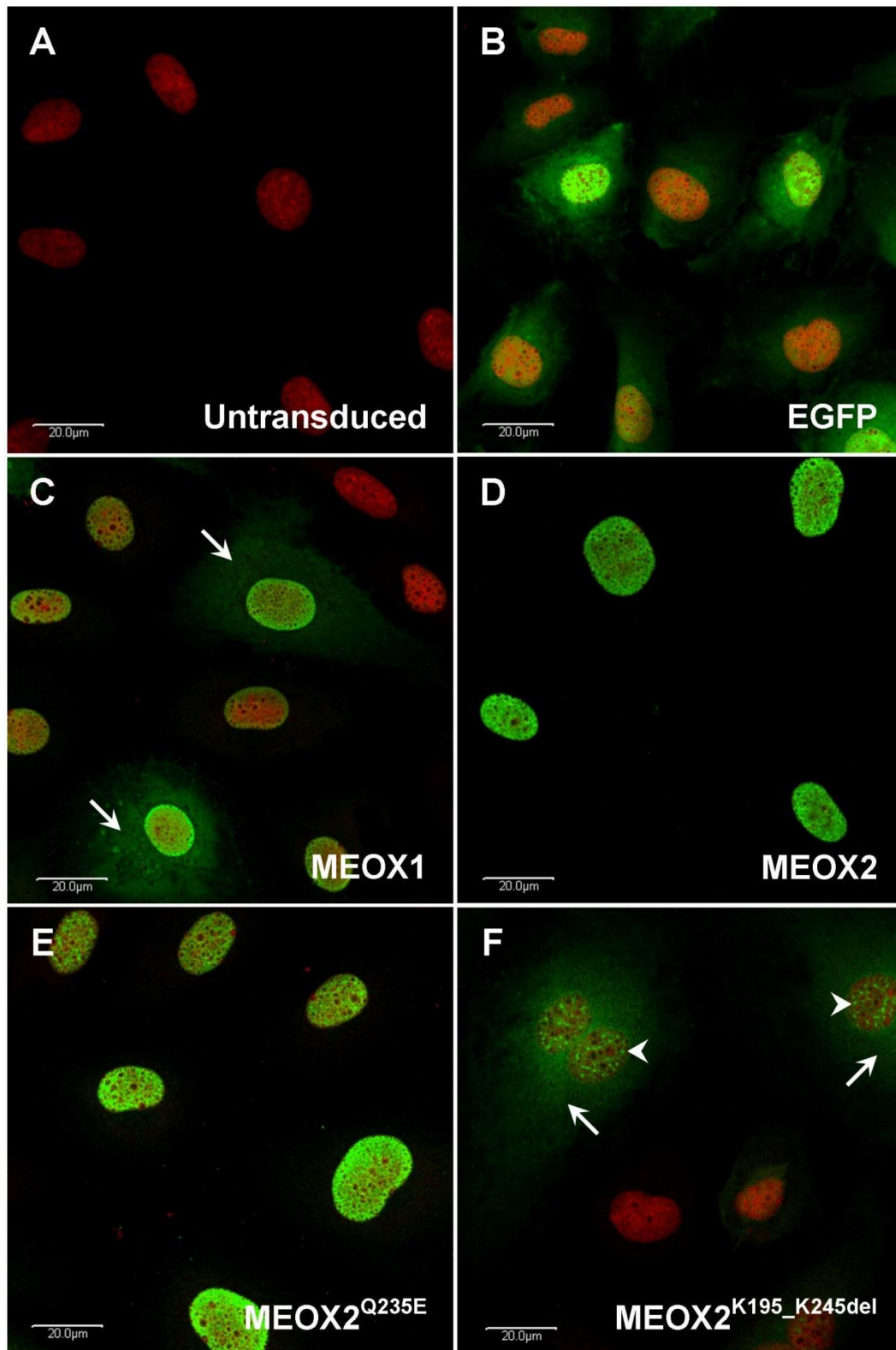


Figure 4-4: Expression and subcellular localization of MEOX1 and MEOX2 proteins in HUVECs.

Figure 4-4: Expression and subcellular localization of MEOX1 and MEOX2 proteins in HUVECs.

Representative fluorescent immunocytochemistry showing the localization and level of expression of the MEOX proteins in HUVECs 48 hours after adenoviral transduction at a multiplicity of infection of 250. The N-terminally tagged MEOX proteins (MEOX1, MEOX2, DNA-binding domain mutated MEOX2^{Q235E} and homeodomain deleted MEOX2^{K195_K245del}) (panels **C-F**) were detected using an anti-FLAG antibody (green) and nuclei were stained with propidium iodide (red). Untransduced HUVECs were used as a negative control (panel **A**) and enhanced green fluorescent protein (EGFP) was used as a control for adenoviral transduction (panel **B**). Arrows indicate cytoplasmic staining and arrowheads indicate punctate nuclear aggregates. Scale bar represents 20 μm .

MEOX2^{K195_K245del} have been shown to co-localize with splicing factor SC35, a component of the nuclear speckles [233]. Thus, deletion of the MEOX2 homeodomain altered its subcellular localization and will also likely affect its function. For this reason, we limited our use of the homeodomain deleted constructs. Histidine/glutamine rich domain deleted MEOX2^{H68_Q85del}, which lacks the putative transactivation domain, is expressed at a similar level and has the same subcellular localization as wild-type MEOX2 in HEK293 cells (Figure 4-3).

An interesting feature of MEOX1 nuclear localization was that MEOX1 appeared to be consistently enriched at the periphery of the nucleus. This enrichment was also noted with MEOX2, but to a much lesser extent. To better visualize this effect, we repeated the fluorescent immunocytochemistry using an anti-Lamin A+C antibody to demarcate the nuclear envelope. Indeed, it appeared that the density of MEOX1 and MEOX2 protein expression was increased at the inner nuclear envelope (Figure 4-5). Furthermore, this enrichment at the nuclear envelope was not seen with the DNA-binding domain mutated MEOX2^{Q235E} (Figure 4-5). Thus, it is intriguing to speculate that transcriptional regulation by MEOX1 and MEOX2 may be directed, via interaction with the nuclear lamina or nuclear envelope proteins, to genes that are located at the nuclear periphery.

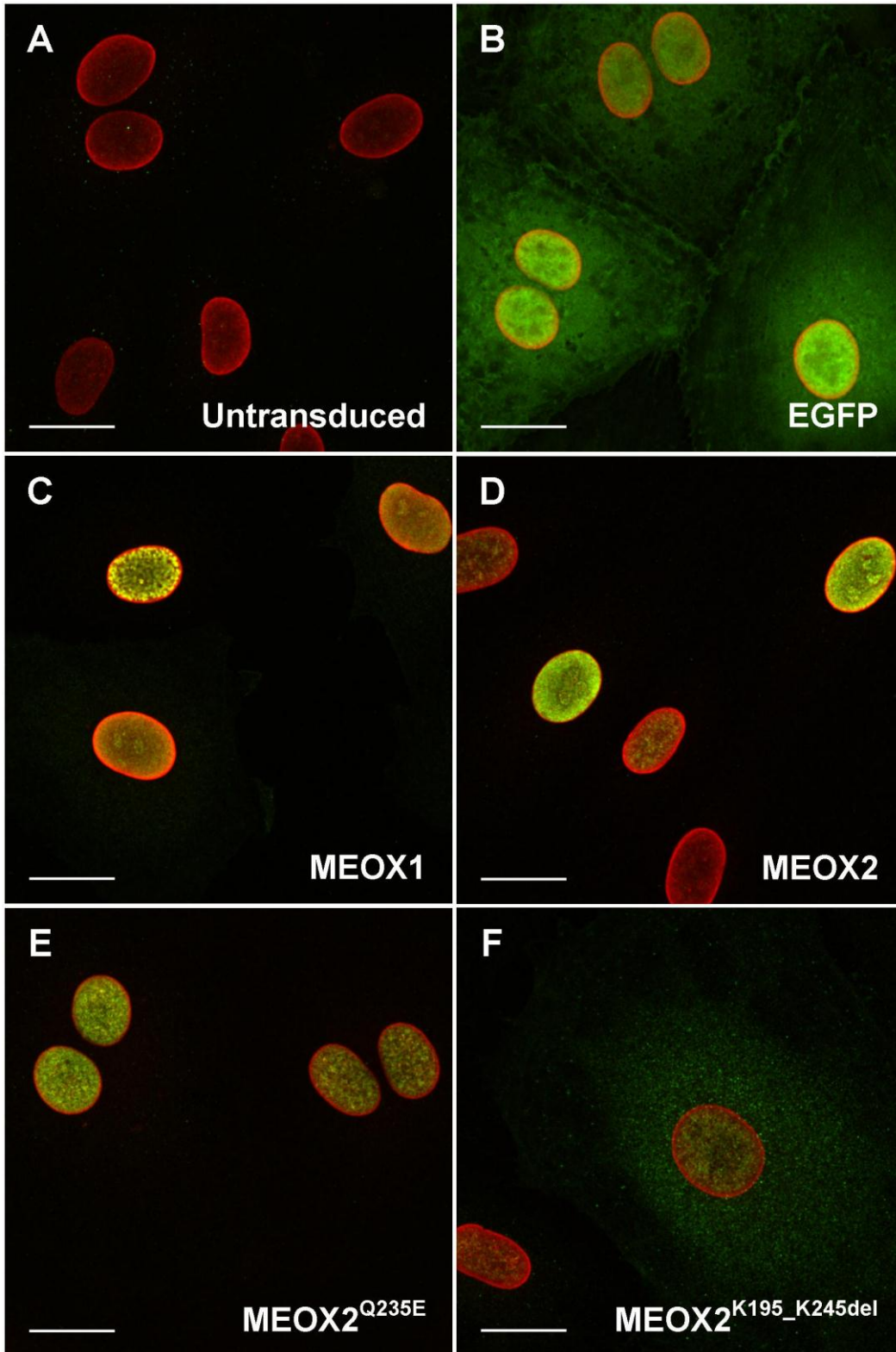


Figure 4-5: Enrichment of MEOX protein expression at the inner nuclear envelope in HUVECs.

Figure 4-5: Enrichment of MEOX protein expression at the inner nuclear envelope in HUVECs.

Representative fluorescent immunocytochemistry showing localization of the MEOX proteins in HUVECs 48 hours after adenoviral transduction at a multiplicity of infection of 250. N-terminal tagged MEOX proteins (MEOX1, MEOX2, DNA-binding domain mutated MEOX2^{Q235E} and homeodomain deleted MEOX2^{K195_K245del}) (panels C-F) were detected using an anti-FLAG antibody (green) and the nuclear envelope was detected using an anti-Lamin A+C antibody (red). Untransduced HUVECs were used as a negative control (panel A) and enhanced green fluorescent protein (EGFP) was used as a control for adenoviral transduction (panel B). Scale bar represents 20 μ m.

4.4.2. MEOX1 and MEOX2 activate $p21^{CIP1/WAF1}$ expression via a DNA-binding independent mechanism

4.4.2.1. *MEOX1 and MEOX2 activate transcription from the endogenous $p21^{CIP1/WAF1}$ promoter in endothelial cells.*

The CDK inhibitor, $p21^{CIP1/WAF1}$, was the first direct transcriptional target identified for MEOX2 [89,156]. MEOX2 expression in VSMCs is decreased by mitogen stimulation, which leads to decreased $p21^{CIP1/WAF1}$ expression and cell cycle progression [94,156].

We first wanted to determine whether the same phenomenon occurs in primary ECs. HUVECs were cultured in either growth media (which contains 2% FBS and defined growth factors) or basal media containing 0.2% FBS for 18 hours, following which the media was changed to either fresh growth media, basal media containing 0.2% FBS, basal media containing 2.0% FBS or basal media containing 10% FBS for 12 hours. Quantitative real-time PCR was used to measure the relative mRNA expression of *MEOX2* and $p21^{CIP1/WAF1}$. With the removal of defined growth factors and serum from the growth media (Figure 4-6, panel A, compare EGM to EBM + 0.2% FBS) there was a trend toward increased *MEOX2* expression. Conversely, increasing the serum content from 0.2% to 10% decreased *MEOX2* expression (Figure 4-6, panel A). As anticipated, the levels of $p21^{CIP1/WAF1}$ mRNA in response to serum mirrored the trend in *MEOX2* mRNA expression (Figure 4-6, panel B).

In order to study the dynamics of MEOX2 regulation of $p21^{CIP1/WAF1}$ gene transcription in endothelial cells, we over-expressed MEOX2 in HUVECs and measured the changes in $p21^{CIP1/WAF1}$ expression. MEOX2 dose dependently increased $p21^{CIP1/WAF1}$

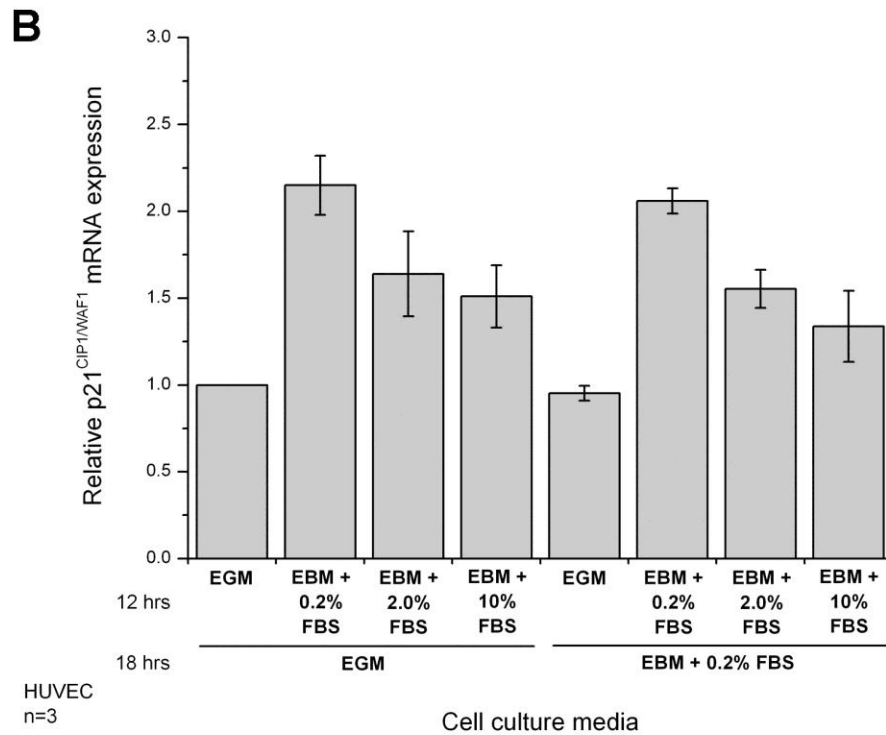
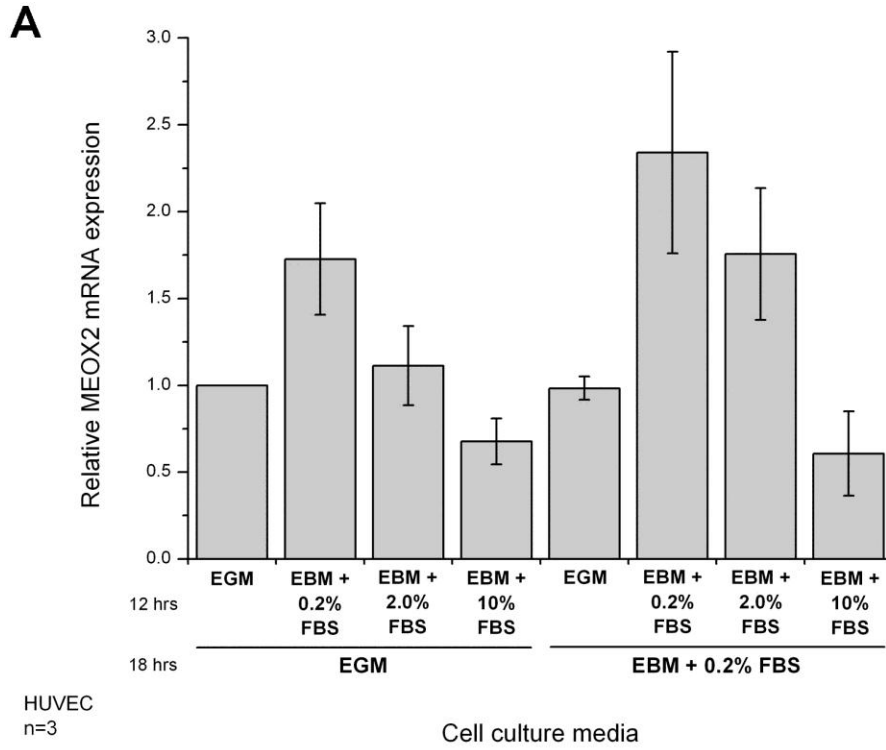


Figure 4-6: The mRNA expression of *MEOX2* and *p21^{CIP1/WAF1}* in HUVECs is affected by serum content.

Figure 4-6: The mRNA expression of *MEOX2* and *p21^{CIP1/WAF1}* in HUVECs is affected by serum content.

HUVECs were cultured in growth media or basal media containing 0.2% FBS for 18 hours after which the media was changed to one of four treatments (growth media, basal media containing 0.2% FBS, basal media containing 2.0% FBS or basal media containing 10% FBS) for 12 hours prior to RNA isolation. **(A)** The mRNA expression of *MEOX2* trends towards an increase with the removal of defined growth factors from the media and decreases with increasing serum content. ° Indicates a statistically significant change ($p < 0.05$) from cells cultured in basal media containing 0.2% FBS. Error bars represent the standard error of the mean ($n=3$). **(B)** The mRNA expression of *p21^{CIP1/WAF1}* mirrors the expression of *MEOX2*. * Indicates a statistically significant change ($p < 0.05$) from cells cultured in growth media. Error bars represent the standard error of the mean ($n=3$).

protein expression in HUVECs 48 hours after adenoviral transduction (Figure 4-7). Based on this experiment, we chose to use a viral dose of 250 MOI for future studies because there was clear up-regulation of $p21^{CIP1/WAF1}$ by MEOX2 at this dose and no increase in $p21^{CIP1/WAF1}$ expression due to the effects of control adenovirus transduction. Subsequently, time course experiments were performed to study the level of $p21^{CIP1/WAF1}$ induction by MEOX2 at various times post-transduction. We did not detect MEOX2 expression until 24 hours post-transduction (Figure 4-8, panel B). MEOX2 significantly increased $p21^{CIP1/WAF1}$ mRNA expression at 48 and 72 hours, while $p21^{CIP1/WAF1}$ protein expression was significantly increased at 36, 48 and 72 hours post-transduction (Figure 4-8). Furthermore, we saw a modest, but significant increase in $p21^{CIP1/WAF1}$ mRNA expression in response to control viral transduction at 72 hours (Figure 4-8, panel A). Thus, we chose to continue our experiments using 250 MOI of adenovirus and assessing changes in $p21^{CIP1/WAF1}$ expression 48 hours post-transduction.

To compare the ability of MEOX1, MEOX2 and mutant MEOX2 proteins to induce the expression of endogenous $p21^{CIP1/WAF1}$ in endothelial cells, we transduced HUVECs using adenoviral vectors, following which we performed quantitative real-time PCR and western blot analysis to measure the changes in $p21^{CIP1/WAF1}$ expression at the mRNA and protein level, respectively. Ectopic expression of p53 was used as an alternate positive control for the induction of $p21^{CIP1/WAF1}$, since p53 is a well characterized transcriptional activator of the $p21^{CIP1/WAF1}$ gene [228,234]. Compared to the EGFP control, we observed a three-fold increase in $p21^{CIP1/WAF1}$ mRNA levels and more than a two-fold increase in $p21^{CIP1/WAF1}$ protein levels 48 hours after adenoviral delivery of p53 (Figure 4-9). Likewise, expression of MEOX1 or MEOX2 resulted in

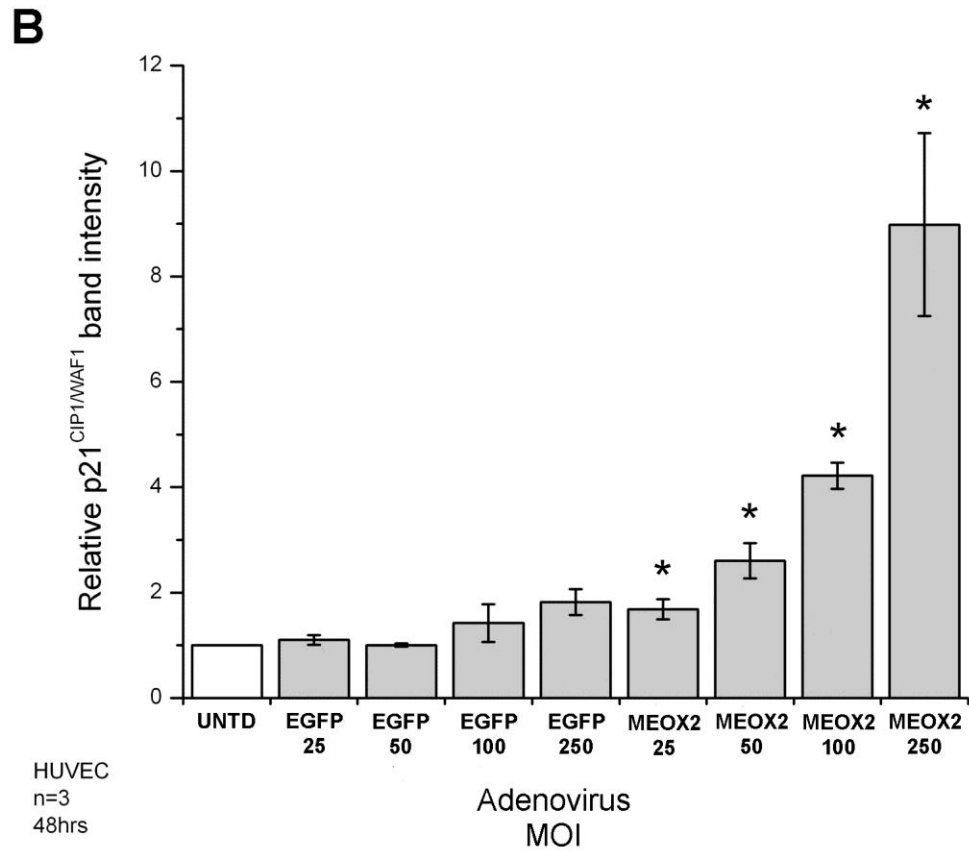
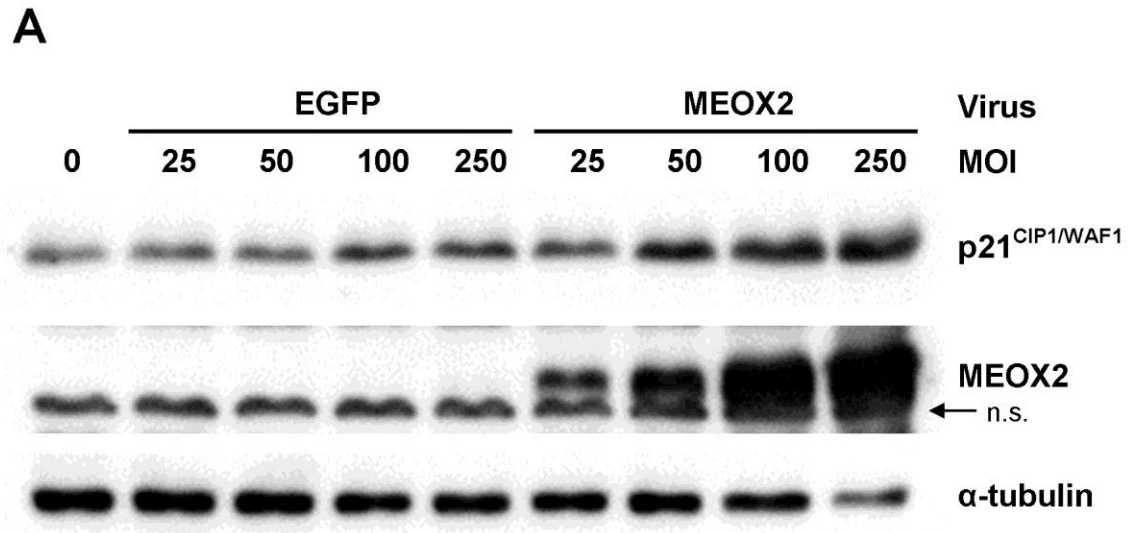


Figure 4-7: MEOX2 dose-dependently up-regulates p21^{CIP1/WAF1} protein expression in HUVECs.

Figure 4-7: MEOX2 dose-dependently up-regulates p21^{CIP1/WAF1} protein expression in HUVECs.

(A) Representative western blot showing increased p21^{CIP1/WAF1} protein in HUVECs transduced with MEOX2 expressing adenovirus. n.s. denotes a non-specific band. (B) Quantification of the relative amount of p21^{CIP1/WAF1} protein 48 hours after transduction with 25, 50, 100 or 250 MOI of adenovirus encoding EGFP or N-terminal FLAG-tagged MEOX2. Untransduced HUVECs (UNTD) were used as the control. The intensity of the p21^{CIP1/WAF1} band was normalized to the α -tubulin loading control. * Indicates a statistically significant change ($p < 0.05$) between MEOX2 and EGFP over-expressing cells at the same MOI. Error bars represent the standard error of the mean (n=3).

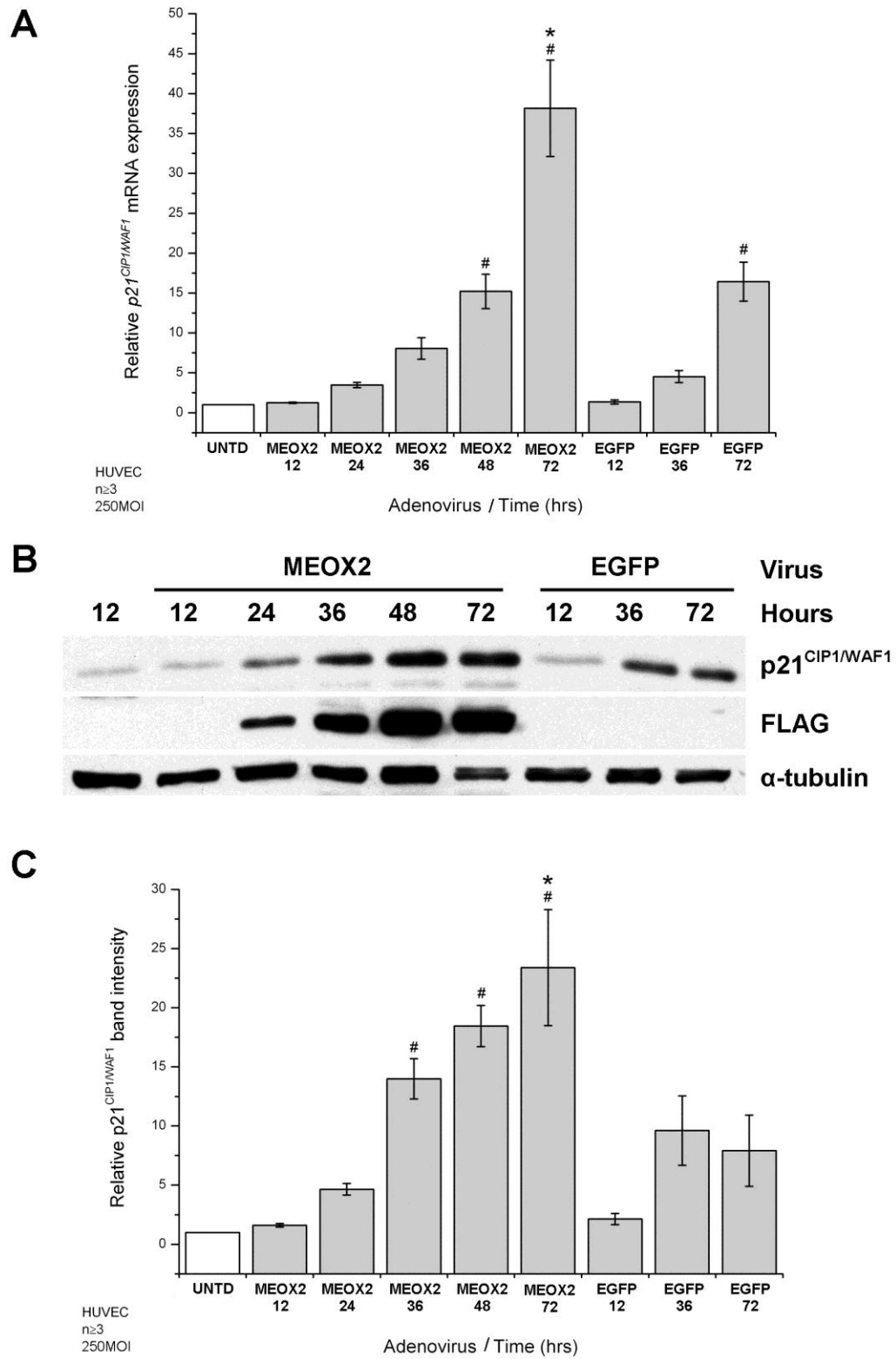


Figure 4-8: MEOX2 time-dependently up-regulates $p21^{CIP1/WAF1}$ mRNA and protein expression in HUVECs.

Figure 4-8: MEOX2 time-dependently up-regulates $p21^{CIP1/WAF1}$ mRNA and protein expression in HUVECs.

(A) Level of $p21^{CIP1/WAF1}$ mRNA relative to untransduced HUVECs (UNTD). Total RNA was isolated from HUVECs at 12, 24, 36, 48 and 72 hours after adenoviral transduction at 250 MOI and the relative amount of mRNA was measured by quantitative real-time PCR. β -actin mRNA expression was used for inter-sample normalisation. (B) Representative western blot showing increased $p21^{CIP1/WAF1}$ protein in HUVECs over-expressing MEOX2. N-terminal FLAG-tagged MEOX2 was detected using an anti-FLAG antibody. (C) Quantification of the relative amount of $p21^{CIP1/WAF1}$ protein at 12, 24, 36, 48 and 72 hours after transduction with 250 MOI of adenovirus encoding EGFP or N-terminal FLAG-tagged MEOX2. The intensity of the $p21^{CIP1/WAF1}$ band was normalized to the α -tubulin loading control. # Indicates a statistically significant change ($p < 0.05$) from untransduced HUVECs. * Indicates a statistically significant difference ($p < 0.05$) between MEOX2 and EGFP over-expressing cells at the same time point. Error bars represent the standard error of the mean ($n \geq 3$ (A), $n \geq 3$ (C)).

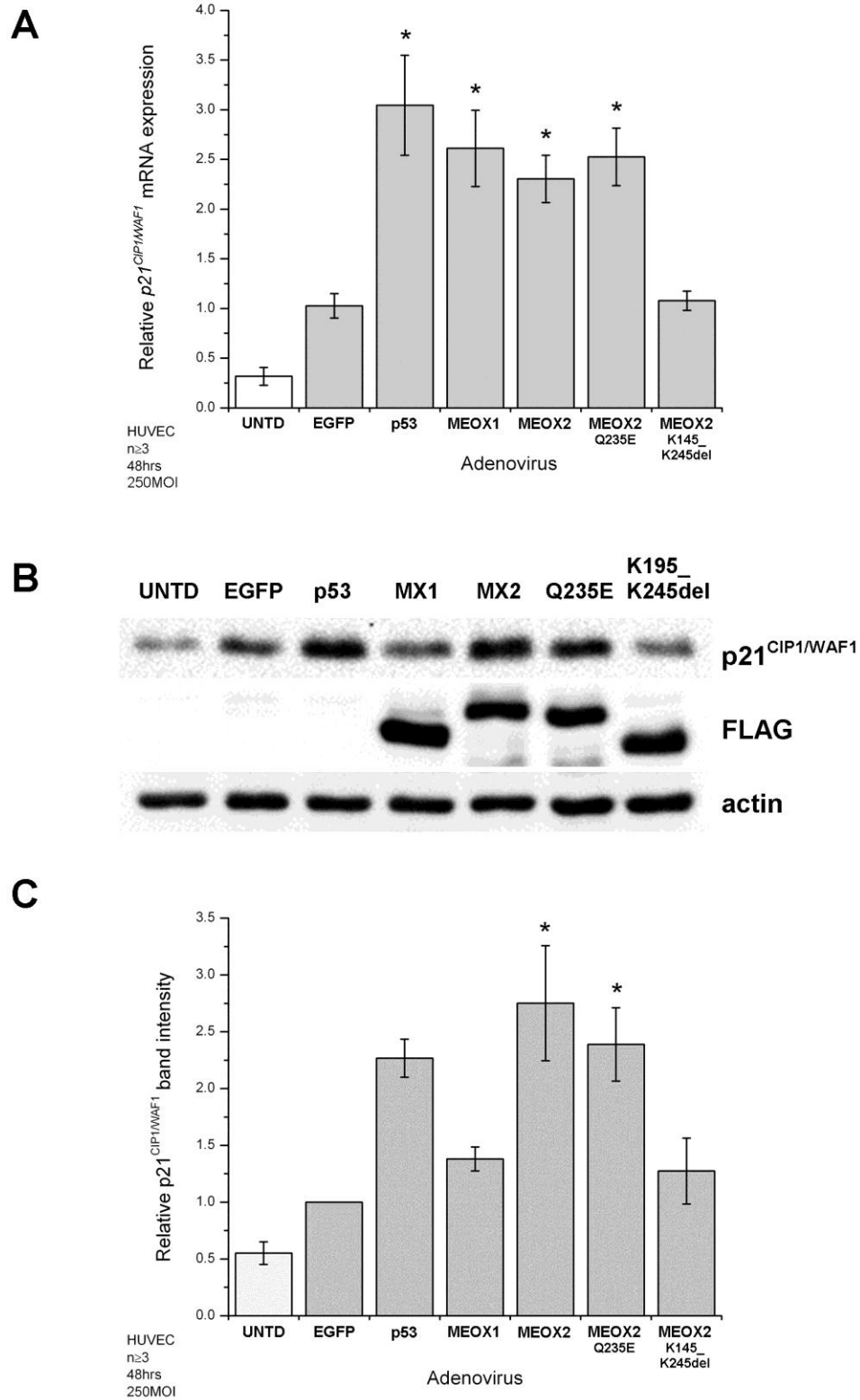


Figure 4-9: MEOX2 activates $p21^{CIP1/WAF1}$ mRNA and protein expression via a DNA-binding independent mechanism in endothelial cells.

Figure 4-9: MEOX2 activates $p21^{CIP1/WAF1}$ mRNA and protein expression via a DNA-binding independent mechanism in endothelial cells.

(A) Relative level of $p21^{CIP1/WAF1}$ mRNA compared to EGFP transduced HUVECs. Total RNA was isolated from HUVECs 48 hours after adenoviral transduction at 250 MOI and the amount mRNA was measured by quantitative real-time PCR. β -actin mRNA expression was used for inter-sample normalisation. (B) A representative western blot showing increased $p21^{CIP1/WAF1}$ protein in HUVECs expressing ectopic MEOX2 (MX2) or DNA-binding domain mutated MEOX2^{Q235E} (Q235E) but not MEOX1 (MX1) or homeodomain deleted MEOX2^{K195_K245del} (K195_K245del). (C) Quantification of the relative amount of $p21^{CIP1/WAF1}$ protein compared to EGFP transduced HUVECs. Total protein was isolated from HUVECs 48 hours after adenoviral transduction at 250 MOI. The intensity of the $p21^{CIP1/WAF1}$ band was normalized to the actin loading control. * Indicates a statistically significant change ($p < 0.05$) from EGFP over-expressing cells. Error bars represent the standard error of the mean ($n \geq 3$ (A), $n \geq 3$ (C)).

significantly increased $p21^{CIP1/WAF1}$ mRNA expression. Interestingly, although MEOX1 was as effective as MEOX2 at inducing $p21^{CIP1/WAF1}$ mRNA expression (Figure 4-9, panel A), this potency did not correlate with a similar induction of $p21^{CIP1/WAF1}$ protein expression (Figure 4-9, panels B and C). MEOX2 increased $p21^{CIP1/WAF1}$ protein expression comparable to p53 (Figure 4-9, panels B and C). In contrast, MEOX1 did not significantly induce $p21^{CIP1/WAF1}$ protein expression (Figure 4-9, panels B and C). We observed similar changes in the level of $p21^{CIP1/WAF1}$ protein expression after C-terminal FLAG-tagged MEOX protein over-expression (Appendix C). Thus, it appears that $p21^{CIP1/WAF1}$ is a transcriptional target of MEOX1, however the disconnect between the levels of mRNA and protein suggest that the $p21^{CIP1/WAF1}$ protein stability or translation efficiency of the $p21^{CIP1/WAF1}$ mRNA is decreased in the presence of MEOX1.

Notably, the DNA-binding domain mutated MEOX2^{Q235E} was able to activate endogenous $p21^{CIP1/WAF1}$ expression at the mRNA and protein levels equivalent to wild-type MEOX2 (Figure 4-9). This result suggests that activation of the $p21^{CIP1/WAF1}$ gene by MEOX2 is DNA-binding independent. In contrast to DNA-binding domain mutated MEOX2^{Q235E}, the homeodomain deleted MEOX2^{K195_K245del} was not able to activate transcription of $p21^{CIP1/WAF1}$. MEOX2 activation of the $p21^{CIP1/WAF1}$ gene was previously reported to be dependent upon DNA-binding, as a similar homeodomain deleted version of MEOX2 (MEOX2^{K188_245del}) could not activate transcription from a 2.4 kb $p21^{CIP1/WAF1}$ upstream promoter region [89,156]. However, we hypothesize that homeodomain deleted MEOX2^{K195_K245del} and MEOX2^{K188_K245del} are unable to activate transcription from the $p21^{CIP1/WAF1}$ promoter because of aberrant subcellular localization (predominantly cytoplasmic; Figure 4-3, panel B; Figure 4-4; Figure 4-5 and data not

shown). This altered localization may prevent their association with either the $p21^{CIP1/WAF1}$ upstream promoter region or requisite transcriptional co-factors.

Transcriptional activation of $p21^{CIP1/WAF1}$ by MEOX2 was shown to be independent from p53, as MEOX2 was able to induce $p21^{CIP1/WAF1}$ expression in p53 deficient cells [156]. Therefore, we wanted to confirm that p53 was not contributing to the activation of $p21^{CIP1/WAF1}$ by the MEOX proteins in HUVECs. To our surprise, both MEOX1 and MEOX2, increased p53 protein levels in HUVECs, as compared to the EGFP control (Figure 4-10). Augmented p53 protein may not be due to MEOX induced transcription of p53 mRNA, as we did not detect any changes in the amount of p53 transcript by microarray (data not shown). Thus, MEOX1 and MEOX2, via an unknown mechanism, increase p53 protein synthesis or decrease p53 protein degradation. Although there is increased p53 protein in MEOX1 and MEOX2 over-expressing HUVECs, it is unclear whether p53 is contributing to MEOX induced $p21^{CIP1/WAF1}$ expression for the following reason: DNA-binding domain mutated MEOX2^{Q235E} does not increase p53 expression to the same level as wild-type MEOX2 (Figure 4-10), but the induction of $p21^{CIP1/WAF1}$ in response to MEOX2^{Q235E} or wild-type MEOX2 is comparable (Figure 4-10, panel A). Furthermore, it should be noted that the stability and transcriptional capability of p53 are regulated by a number of post-transcriptional modifications [235] and the antibody that we have used for western blot analysis detects p53 irrespective of the post-translational modification status of the protein. Thus, although the total levels of p53 are increased by MEOX1 and MEOX2, we have yet to assess whether there is an increase in transcriptionally active p53 protein.

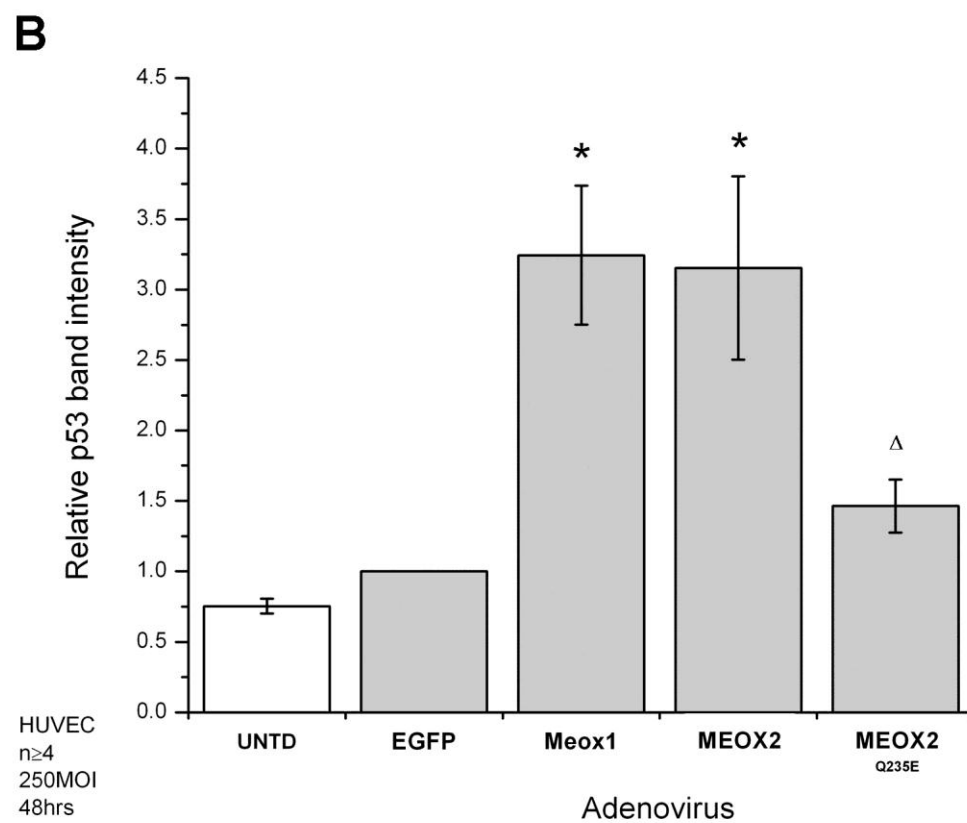
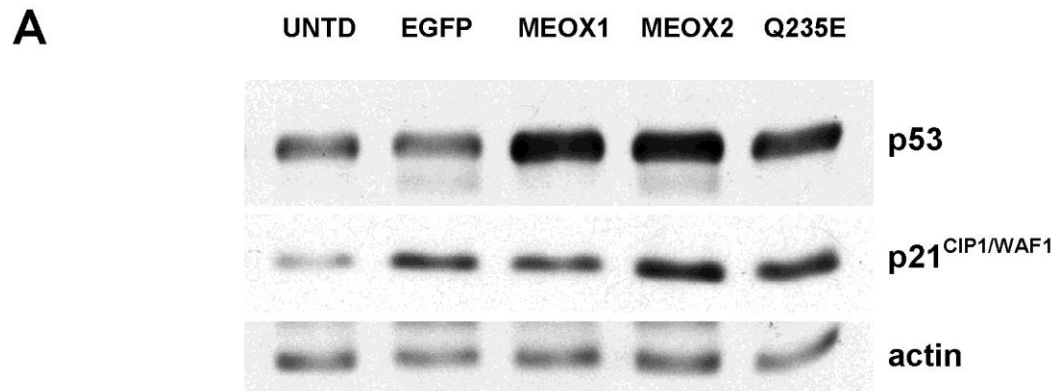


Figure 4-10: MEOX1 and MEOX2 increase total p53 protein expression in HUVECs.

Figure 4-10: MEOX1 and MEOX2 increase total p53 protein expression in HUVECs.

(A) Representative western blot showing increased p53 and p21^{CIP1/WAF1} protein in HUVECs over-expressing MEOX2. MEOX1 increases p53 expression, but not p21^{CIP1/WAF1} protein expression. DNA-binding domain mutated MEOX2^{Q235E} (Q235E) increases p21^{CIP1/WAF1} protein expression to the same level as wild-type MEOX2, but does not significantly increase p53 protein expression. (B) Quantification of the relative amount of p53 protein compared to EGFP transduced HUVECs. Total protein was isolated from HUVECs 48 hours after adenoviral transduction at 250 MOI. Untransduced HUVECs (UNTD) were used as a control. The intensity of the p53 band was normalized to the actin loading control. * Indicates a statistically significant change (p<0.05) from EGFP over-expressing cells. Δ Indicates a statistically significant difference (p<0.05) between wild-type MEOX2 and DNA-binding domain mutated MEOX2^{Q235E}. Error bars represent the standard error of the mean (n≥4).

4.4.2.2. Sequence specific binding of MEOX1 and MEOX2 to DNA is abolished by mutation or deletion of the homeodomain.

In order to verify that wild-type MEOX1 and MEOX2 are capable of sequence specific binding to DNA and that DNA-binding domain mutated MEOX1^{Q219E}, MEOX2^{Q235E} and homeodomain deleted MEOX2^{K195_K245del} are unable to bind to DNA, we performed EMSAs. We used two different probe sequences previously shown to contain MEOX DNA-binding sites; the first sequence originated from the *Nkx3-2* upstream promoter region [128] and the other from the *p21^{CIP1/WAF1}* upstream promoter region [89]. These sequences are located approximately 0.8 kb and 9.5 kb upstream of the transcription start sites of these genes, respectively. As demonstrated using recombinant GST-tagged proteins, both MEOX1 and MEOX2 were able to bind these probes (Figure 4-11, panels A and B). Unlike wild-type MEOX proteins, no shift was observed with DNA-binding domain mutated MEOX2^{Q235E} or homeodomain deleted MEOX2^{K195_K245del} fusion proteins (Figure 4-11, panels A and B), indicating that these proteins were indeed unable to bind DNA. The same results were obtained when nuclear extracts from HUVECs and HEK293 cells expressing FLAG-tagged MEOX proteins were incubated with the *p21^{CIP1/WAF1}* probe (Figure 4-12, panels A and B). Wild type MEOX1 and MEOX2 were able to bind to the DNA probe, but the DNA-binding domain mutated MEOX1^{Q219E} (Figure 4-12, panel B), MEOX2^{Q235E} (Figure 4-12, panels A and B) and homeodomain deleted MEOX2^{K195_K245del} could not (Figure 4-12, panel A). In addition, the histidine/glutamine rich domain deleted MEOX2^{H68_Q85del} bound to the *p21^{CIP1/WAF1}* probe, demonstrating that deletion of this domain does not affect the ability of MEOX2 to bind DNA (Figure 4-12, panel B).

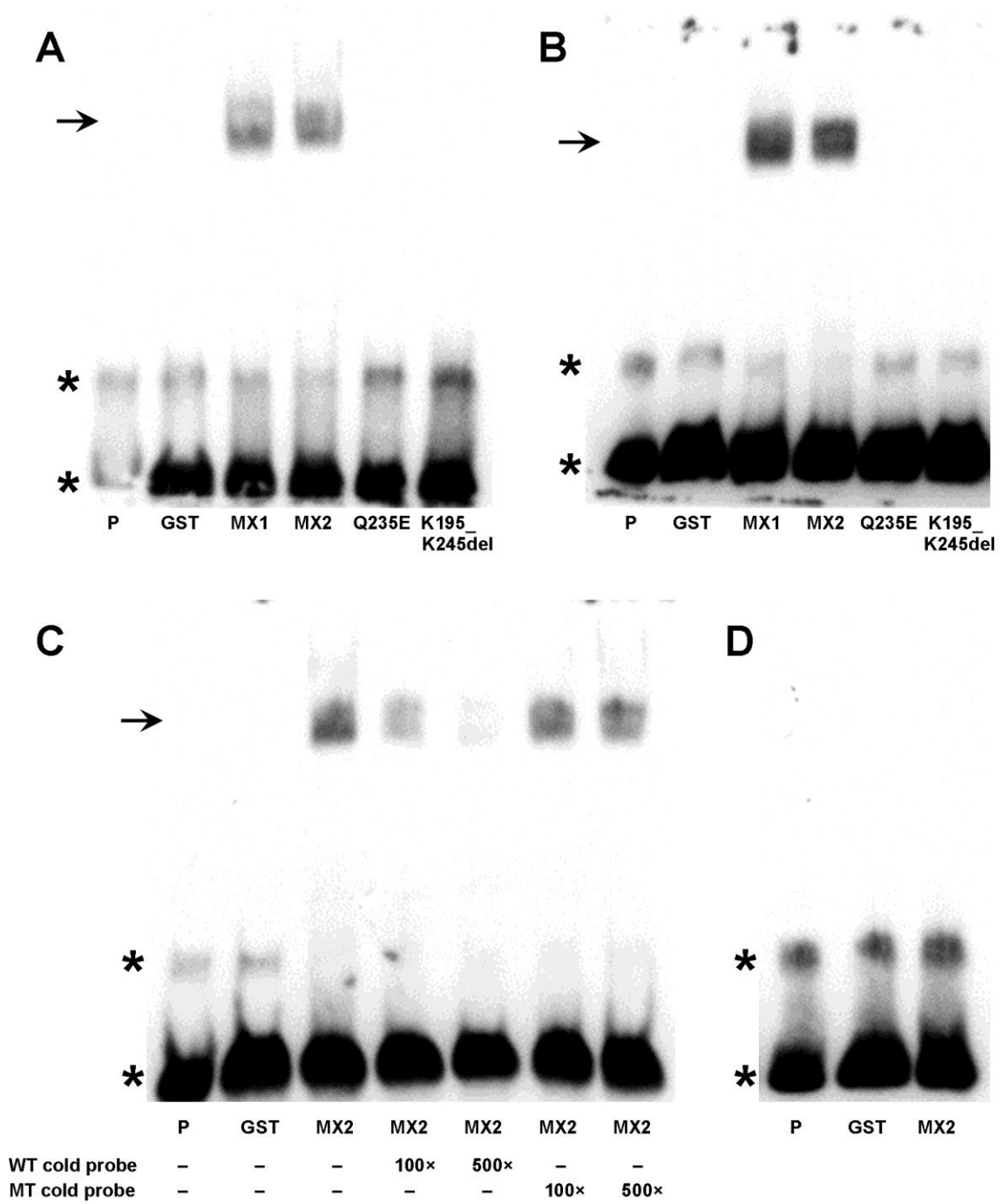


Figure 4-11: MEOX1 and MEOX2 sequence specifically bind to DNA probes containing homeodomain binding sites.

Figure 4-11: MEOX1 and MEOX2 sequence specifically bind to DNA probes containing homeodomain binding sites.

EMSA were used to assess the DNA-binding capabilities of the various MEOX proteins. The DNA probes contained two MEOX2 binding sites originating from either the *Nkx3-2* gene upstream promoter region [128] (A) or a sequence -9519 bp to -9489 bp upstream of the *p21^{CIP1/WAF1}* transcription start site [89] (B). Recombinant GST-tagged MEOX1 (MX1) and MEOX2 (MX2) bound to the probes (arrow) whereas the DNA-binding domain mutated MEOX2^{Q235E} (Q235E), homeodomain deleted MEOX2^{K195_K245del} (K195_K245del) and GST alone did not. (C) Binding of MEOX2 to the *p21^{CIP1/WAF1}* DNA probe (arrow) could be competed with excess wild type *p21^{CIP1/WAF1}* (WT), but not with excess mutant *p21^{CIP1/WAF1}* (MT) cold probe, in which the homeodomain binding sites were mutated. (D) Neither MEOX2 nor GST bind to a probe that contains only SP1 binding sites originating from approximately -80 bp upstream of the *p21^{CIP1/WAF1}* transcription start site. In all EMSAs, the first lane contains the biotinylated probe (P) alone and the unbound probe is indicated by asterisks (*).

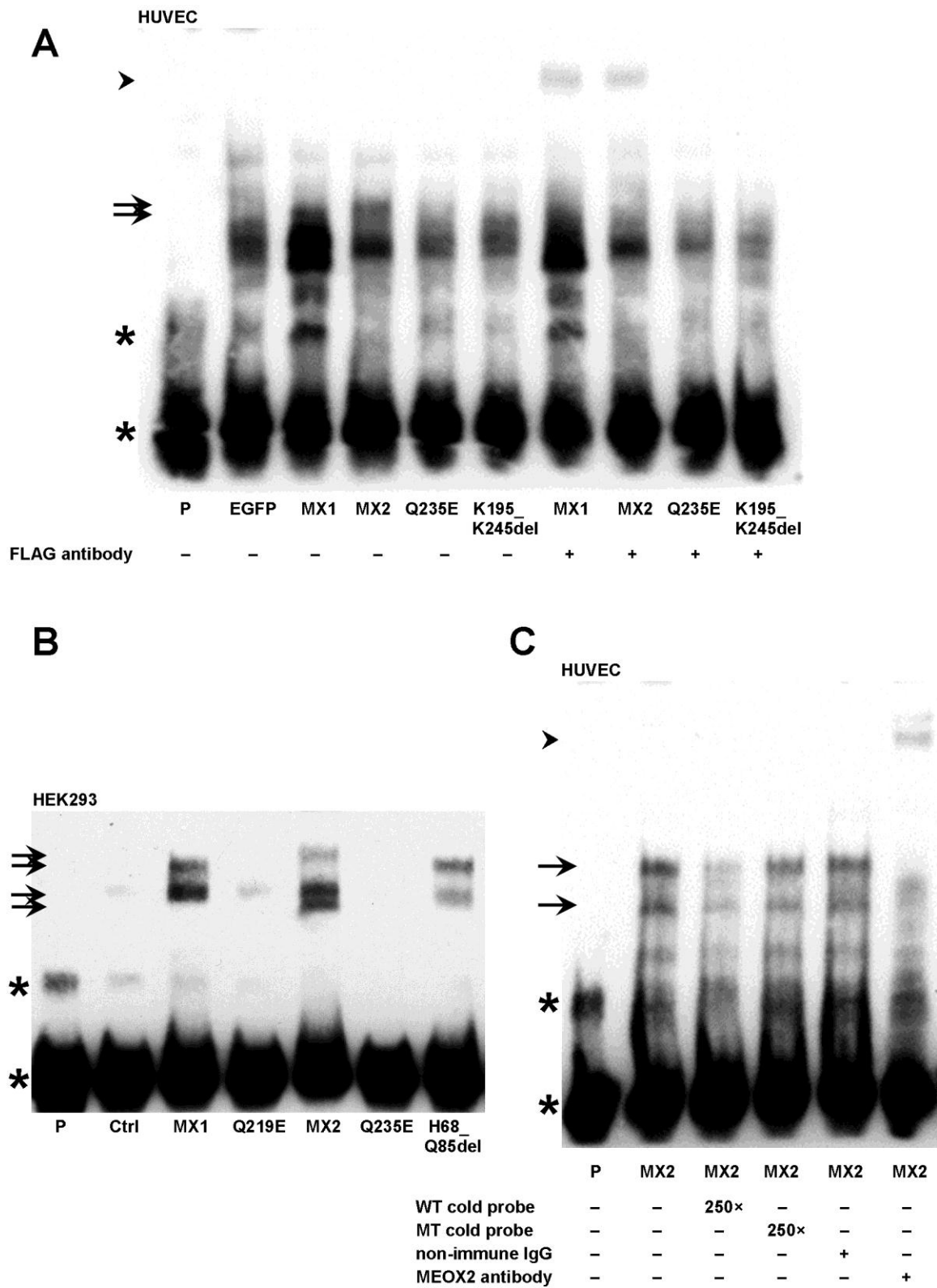


Figure 4-12: MEOX1 and MEOX2 in transduced HUVEC and transfected HEK293 nuclear extracts bind to a region of the $p21^{CIP1/WAF1}$ promoter.

Figure 4-12: MEOX1 and MEOX2 in transduced HUVEC and transfected HEK293 nuclear extracts bind to a region of the $p21^{CIP1/WAF1}$ promoter.

A DNA probe containing the sequence from -9519 bp to -9489 bp upstream of the $p21^{CIP1/WAF1}$ transcription start site [89] was used to test the DNA-binding ability of wild-type and mutant MEOX proteins in cell extracts. (A) Nuclear extracts from HUVECs expressing N-terminally FLAG-tagged MEOX1 (MX1) and MEOX2 (MX2) resulted in distinct shifted complexes (arrows), that were not seen with the EGFP, DNA-binding domain mutated MEOX2^{Q235E} (Q235E) or homeodomain deleted MEOX2^{K195_K245del} (K195_K245del) nuclear extracts. Addition of an anti-FLAG antibody to nuclear extracts from MEOX1 and MEOX2 infected cells, but not EGFP, MEOX2^{Q235E} or MEOX2^{K195_K245del} infected cells, resulted in the formation of a super-shift complex (arrowhead). (B) MEOX1, MEOX2 and histidine/glutamine rich domain deleted MEOX2^{H68_Q85del} (H68_Q85del) in HEK293 nuclear extracts bind to the $p21^{CIP1/WAF1}$ probe (arrows), while DNA-binding domain mutated MEOX1^{Q219E} (Q219E) and MEOX2^{Q235E} do not. Nuclear extracts from HEK293 cells transfected with empty vector were used as a negative control (Ctrl). (C) Binding of the DNA probe by MEOX2 in endothelial cell nuclear extracts (arrows) was competed with excess wild type (WT), but not mutant (MT) cold probe. Addition of MEOX2 antibody, but not non-immune IgG, caused the formation of a super-shift complex (arrowhead). In all EMSAs, the first lane only contains the biotinylated probe (P) and the unbound probe is indicated by asterisks (*).

Binding of MEOX2 to the biotinylated $p21^{CIP1/WAF1}$ DNA probe could be competed with excess wild type (WT), but not with excess mutant (MT) cold probe, in which the homeodomain binding sites were mutated (Figure 4-11, panel C; Figure 4-12, panel C). This demonstrated that MEOX2 binding to this DNA fragment was dependent upon the canonical homeodomain binding site sequence ATTA. Furthermore, we showed that the shifted complexes (arrows) that formed when the $p21^{CIP1/WAF1}$ DNA probe was incubated with nuclear extracts from HUVECs expressing MEOX1 and MEOX2 could be super-shifted (arrowhead) using an antibody specific to the FLAG epitope (Figure 4-12, panel A); or in the case of MEOX2, an antibody specific to MEOX2 but not a non-immune antibody (Figure 4-12, panel C). This confirms that the MEOX proteins are contained within the shifted complexes that are formed by DNA probe-protein interaction.

In contrast to the $Nkx3-2$ and $p21^{CIP1/WAF1}$ DNA probes that contain homeodomain binding sites, MEOX2 did not bind to a DNA probe whose sequence originated from the $p21^{CIP1/WAF1}$ upstream promoter region, located approximately -80 bp upstream of the transcription start site, and only contained SP1 binding sites (Figure 4-11, panel D). GST alone (Figure 4-11), nuclear extracts from HEK293 cells transfected with empty vector (Figure 4-12, panel B) or nuclear extracts from EGFP expressing HUVECs (Figure 4-12, panel A) were used as negative controls for these DNA-binding experiments.

4.4.2.3. *MEOX1 and MEOX2 activate transcription from the $p21^{CIP1/WAF1}$ promoter via a DNA-binding independent mechanism that requires SP1*

In order to further dissect the mechanism of $p21^{CIP1/WAF1}$ transcription regulation by MEOX1 and MEOX2, we subsequently tested the ability of the MEOX proteins to

activate transcription of a luciferase reporter gene that was placed under the control of the $p21^{CIP1/WAF1}$ upstream promoter region. A 2.4 kb $p21^{CIP1/WAF1}$ luciferase promoter was previously shown to be activated by MEOX2 [156]. In HUVECs, we saw that MEOX2 could activate transcription from the 2272 bp $p21^{CIP1/WAF1}$ promoter (Figure 4-13, panel A). However, MEOX1 did not significantly activate transcription from the 2272 bp $p21^{CIP1/WAF1}$ promoter in HUVECs (Figure 4-13, panel A).

As the transfection efficiency of HUVECs is very low, we used HEK293 cells for our further luciferase experiments. In HEK293 cells, we observed that both MEOX1 and MEOX2 activated the expression of the luciferase reporter from the 2272 bp $p21^{CIP1/WAF1}$ promoter (Figure 4-13, panel B). Specifically, the MEOX proteins induced greater than a two-fold activation of the luciferase reporter, when compared to the empty vector control (Figure 4-13, panel B). Furthermore, both DNA-binding domain mutated MEOX1^{Q219E} and MEOX2^{Q235E} were able to activate the 2272 bp $p21^{CIP1/WAF1}$ promoter to a level comparable to wild-type proteins (Figure 4-13, panel B), indicating their ability to bind DNA is not required. Notably, this finding is consistent with the observation that MEOX2^{Q235E} was able to activate endogenous $p21^{CIP1/WAF1}$ expression at the mRNA and protein levels to equivalent degrees as observed for wild-type MEOX2 (Figure 4-9).

The 2272 bp $p21^{CIP1/WAF1}$ promoter contains several transcription factor binding sites, including one p53 binding site, seven putative homeodomain binding sites and six SP1 binding sites (Figure 4-14, panel A). Progressive truncation of the 2272 bp $p21^{CIP1/WAF1}$ promoter was performed in order to determine the minimal upstream promoter region that is sufficient for MEOX induced transcription activation. Equivalent activation of the luciferase reporter by MEOX1 and MEOX2 was still seen with a

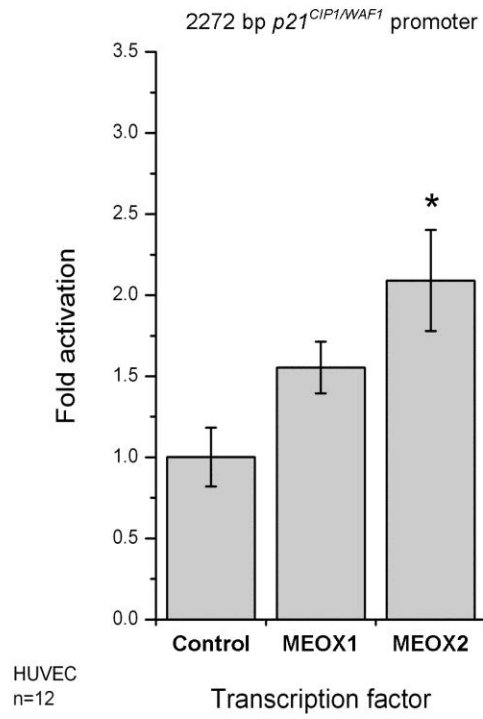
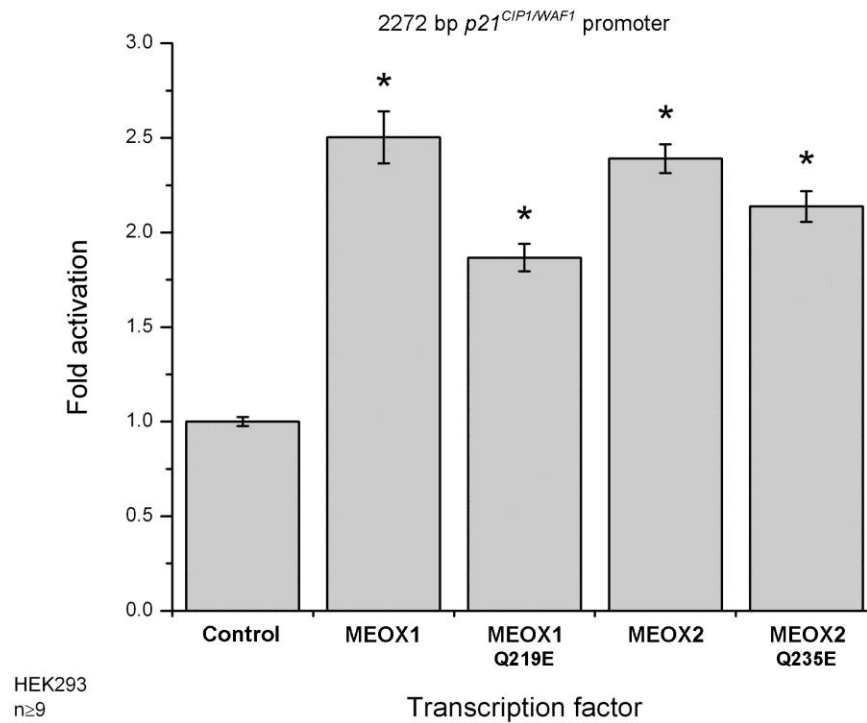
A**B**

Figure 4-13: MEOX1 and MEOX2 activate transcription from the 2272 bp *p21^{CIP1/WAF1}* promoter in HEK293 cells.

Figure 4-13: MEOX1 and MEOX2 activate transcription from the 2272 bp $p21^{CIP1/WAF1}$ promoter in HEK293 cells.

(A) Activation of the 2272 bp $p21^{CIP1/WAF1}$ promoter driven luciferase reporter gene by MEOX2 in HUVECs. (B) Activation of the luciferase reporter gene from the 2272 bp $p21^{CIP1/WAF1}$ promoter by wild type MEOX1, MEOX2 and their respective DNA-binding mutant versions MEOX1^{Q219E} and MEOX2^{Q235E} in HEK293 cells. * Indicates a statistically significant change ($p < 0.05$) when compared to the empty vector control. Error bars represent the standard error of the mean ($n=12$ (A), $n \geq 9$ (B)).

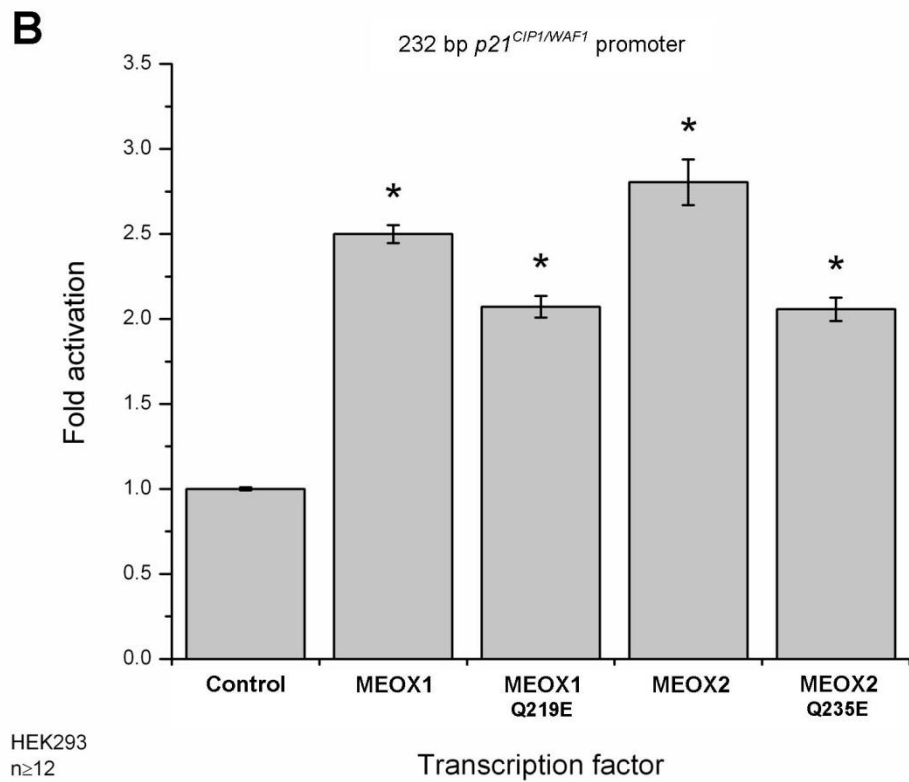
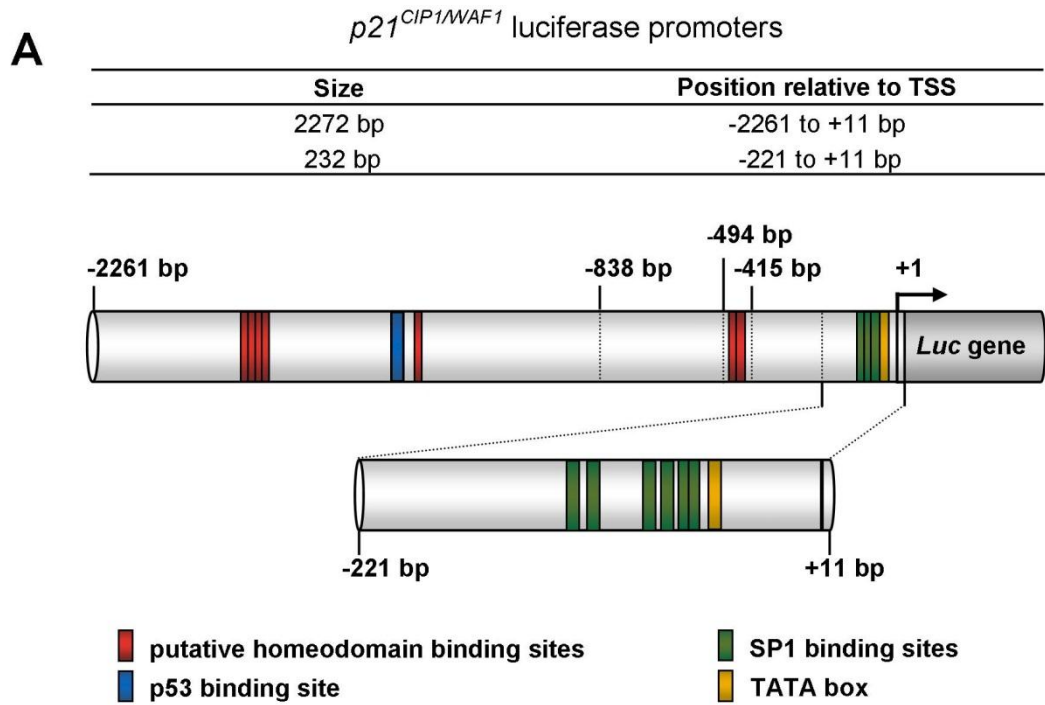


Figure 4-14: MEOX1 and MEOX2 activate transcription from the 232 bp $p21^{CIP1/WAF1}$ promoter independent of DNA-binding.

Figure 4-14: MEOX1 and MEOX2 activate transcription from the 232 bp $p21^{CIP1/WAF1}$ promoter independent of DNA-binding.

(A) Schematic diagram of the human 2272 bp and 232 bp $p21^{CIP1/WAF1}$ promoter luciferase constructs. The 5' termini are indicated relative to the transcriptional start site (TSS) (arrow). Relevant transcription factor binding sites (p53, homeodomain, SP1 and TATA) are also shown. (B) Activation of the 232 bp $p21^{CIP1/WAF1}$ promoter driven luciferase reporter gene by MEOX1 and MEOX2 in HEK293 cells. MEOX1^{Q219E} and MEOX2^{Q235E} activate transcription from the 232 bp $p21^{CIP1/WAF1}$ promoter, which contains no homeodomain binding sites, indicating that MEOX1 and MEOX2 activation of $p21^{CIP1/WAF1}$ gene transcription is DNA-binding independent. * Indicates a statistically significant change ($p < 0.05$) when compared to the empty vector control. Error bars represent the standard error of the mean ($n \geq 12$).

minimal upstream promoter region that contained only the most proximal 232 bp of the $p21^{CIP1/WAF1}$ promoter (Figure 4-14, panel B). It was previously shown that MEOX2 activation of the $p21^{CIP1/WAF1}$ upstream promoter region is independent of p53 activity [156]. Indeed, MEOX2 significantly activated the 232 bp $p21^{CIP1/WAF1}$ promoter, which lacks the p53 binding site (Figure 4-14, panel B). Furthermore, deletion of the putative homeodomain binding sites did not affect MEOX2 induced transcription from the $p21^{CIP1/WAF1}$ upstream promoter region. The 232 bp promoter contains multiple SP1 binding sites, but no homeodomain binding sites. DNA-binding domain mutated MEOX1^{Q219E} and MEOX2^{Q235E} were both able to activate transcription from the 232 bp $p21^{CIP1/WAF1}$ promoter (Figure 4-14, panel B), further demonstrating that MEOX1 and MEOX2 do not need to bind DNA in order to induce $p21^{CIP1/WAF1}$ transcription.

DNA-binding independent activation of the $p21^{CIP1/WAF1}$ upstream promoter region by MEOX proteins indicates that these transcription factors are acting as transcriptional co-activators through protein-protein interactions with other transcription factors. In order to determine whether specific protein domains are involved in MEOX2 mediated activation of $p21^{CIP1/WAF1}$, we repeated the luciferase experiments with various MEOX2 deletion mutant constructs. The histidine/glutamine rich domain of MEOX2 was previously shown to be important for the ability of MEOX2 to activate transcription from a 2.4 kb $p21^{CIP1/WAF1}$ upstream promoter region, as deletion of this domain dramatically decreased MEOX2 induced reporter gene expression [89]. Interestingly, MEOX1 does not contain a histidine/glutamine rich domain, but is still able to activate transcription of $p21^{CIP1/WAF1}$. Furthermore, in our hands, histidine/glutamine rich domain deleted MEOX2^{H68_Q85del} was able to activate transcription from the 232 bp $p21^{CIP1/WAF1}$

promoter to the same level as wild-type MEOX2 (Figure 4-15, panel A). Unexpectedly, the homeodomain deleted MEOX2^{K195_K245del} and MEOX2^{K188_K245del} mutants were also able to activate transcription of the luciferase reporter gene from the 232 bp *p21*^{CIP1/WAF1} promoter (Figure 4-15, panel B), albeit to a lesser level than wild-type MEOX2. This finding opposes our observation that homeodomain deleted MEOX2^{K195_K245del} cannot activate *p21*^{CIP1/WAF1} transcription from the endogenous promoter in HUVECs. This discrepancy in the results may be due to the difference in cell type (HEK293 cell line versus primary endothelial cells) or the nature of the promoter DNA (plasmid DNA versus chromatin). However, this result demonstrates that DNA-binding is not required for MEOX2 activation of *p21*^{CIP1/WAF1} expression. Furthermore, MEOX2^{T89_V182del} which lacks the middle domain (a putative protein-protein interaction domain sufficient for binding to zinc-finger proteins) was also able to activate transcription from the 232 bp *p21*^{CIP1/WAF1} promoter (Figure 4-15, panel C). Comparable to the homeodomain deleted MEOX2 proteins, middle domain deleted MEOX2^{T89_V182del} was significantly less potent than wild-type MEOX2 (Figure 4-15, panel C). The middle domain, along with the homeodomain, was shown to be important in the regulation of *p16*^{INK4a} expression [87]. Similarly, our luciferase results using mutant MEOX2 proteins suggest that the middle domain and homeodomain may play a role in mediating protein-protein interactions with other transcription factors to enhance activation of *p21*^{CIP1/WAF1} by MEOX2.

Thus, our luciferase data identifies the MEOX responsive segment of the *p21*^{WAF1/CIP1} upstream promoter region as residing within the most proximal 232 bp, through which MEOX1 and MEOX2 activate transcription independent of DNA-binding. This region does not contain homeodomain binding sites but does contain several SP1

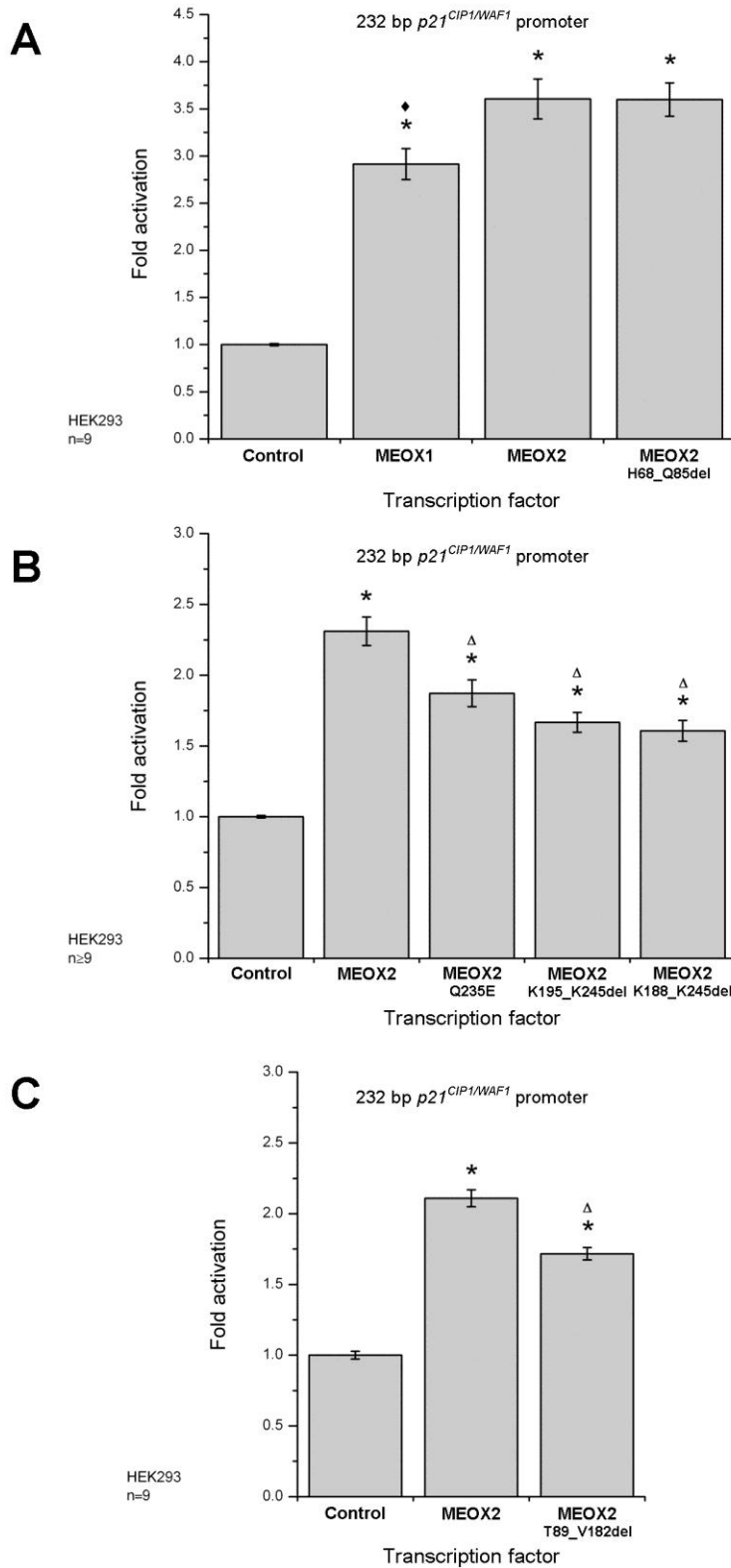


Figure 4-15: Mutant MEOX2 proteins can activate transcription from the 232 bp *p21^{CIP1/WAF1}* promoter.

Figure 4-15: Mutant MEOX2 proteins can activate transcription from the 232 bp *p21^{CIP1/WAF1}* promoter.

(A) Histidine/glutamine rich domain mutated MEOX2^{H68_Q85del} activates transcription from the 232 bp *p21^{CIP1/WAF1}* promoter in HEK293 cells to the same level as wild-type MEOX2. (B) DNA-binding domain mutated MEOX2^{Q235E}, as well as homeodomain deleted MEOX2^{K195_K245del} and MEOX2^{K188_K245del} activate transcription from the 232 bp *p21^{CIP1/WAF1}* promoter in HEK293 cells, but are less potent activators than wild-type MEOX2. (C) Middle domain deleted MEOX2^{T89_V182del} can also activate transcription from the 232 bp *p21^{CIP1/WAF1}* promoter in HEK293 cells, but is less potent than wild-type MEOX2. * Indicates a statistically significant change ($p < 0.05$) when compared to the empty vector control. ♦ Indicates a statistically significant difference ($p < 0.05$) between MEOX1 and MEOX2. Δ Indicates a statistically significant difference ($p < 0.05$) between wild-type and mutant versions of MEOX2. Error bars represent the standard error of the mean (n=9 (A), n≥9 (B), n=9 (C)).

binding sites. SP1 belongs to the specificity protein/krüppel-like factor (SP/KLF) protein family, which consists of triple zinc finger containing transcription factors [236,237]. As such, it is conceivable that the SP/KLF family members may be capable of interacting with MEOX1 and MEOX2 via the MEOX middle domain, which was shown to be sufficient for zinc finger protein interaction (Appendix A). To interrogate the role of SP1 in mediating MEOX activation of the $p21^{CIP1/WAF1}$ upstream promoter region, we inhibited SP1 binding by treating cells, which were transfected with the 232 bp $p21^{CIP1/WAF1}$ promoter and MEOX expression plasmids, with mithramycin A. Mithramycin A binds GC-rich regions of DNA and thereby inhibits SP1 interaction with its binding sites [229,230]. This treatment drastically attenuated both MEOX1 and MEOX2 mediated activation of the 232 bp $p21^{CIP1/WAF1}$ promoter (Figure 4-16).

Thus, our results demonstrate that the $p21^{CIP1/WAF1}$ gene is a transcriptional target of both MEOX1 and MEOX2 and that activation of $p21^{CIP1/WAF1}$ expression by the MEOX proteins occurs via a DNA-binding independent mechanism. Furthermore, we show that the MEOX proteins are transcriptional co-activators of $p21^{CIP1/WAF1}$ gene transcription and assert their function via DNA-bound SP1 (potentially through protein-protein interaction). Although MEOX2 was shown by chromatin immunoprecipitation [89] and EMSA (Figure 4-11, panel B and [89]) to bind to ATTA sequences approximately 9.6 kb upstream of the $p21^{CIP1/WAF1}$ transcription start site, our results demonstrate that this DNA-binding is not required for MEOX2 activated $p21^{CIP1/WAF1}$ gene expression. One possible scenario that could account for the observed binding of MEOX2 to the upstream ATTA sequences is that MEOX2 binding to this site may induce looping of the DNA, bringing an unknown enhancer element within close proximity to

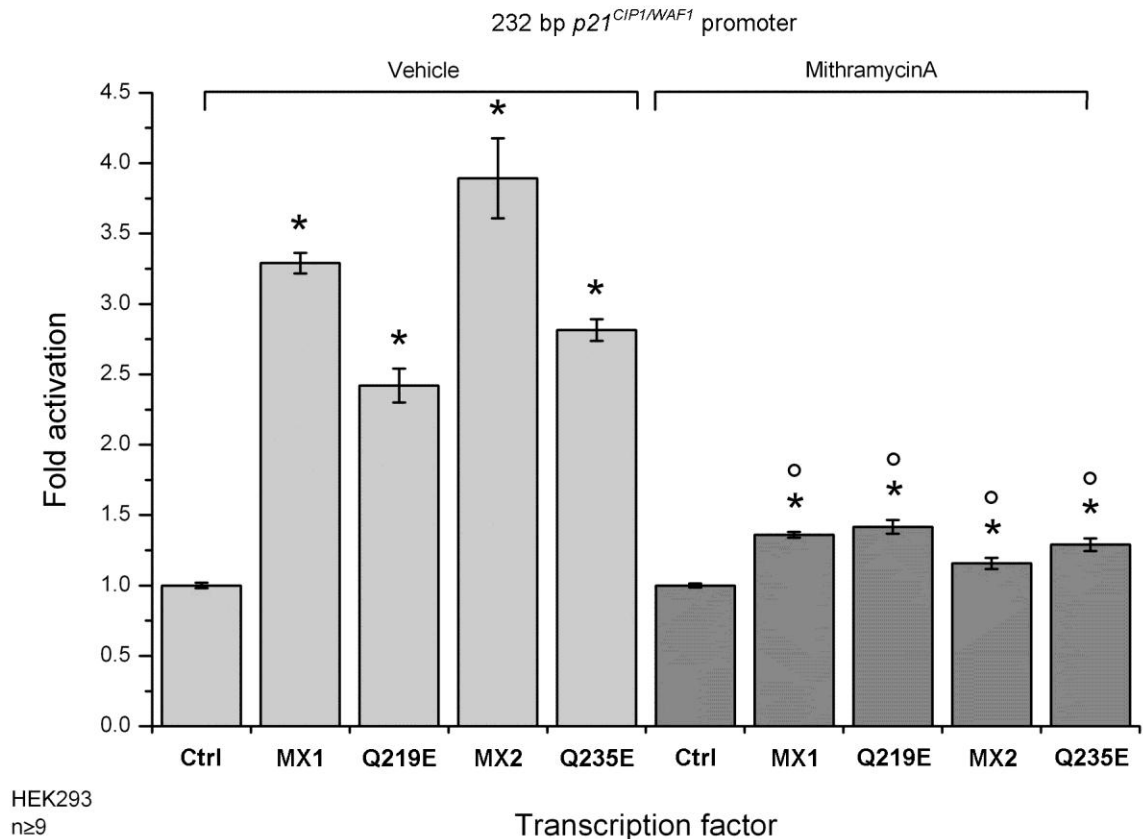


Figure 4-16: Inhibition of SP1 binding to DNA drastically attenuates MEOX activation from the 232 bp $p21^{CIP1/WAF1}$ promoter.

Treatment of HEK293 cells with mithramycin A but not vehicle (methanol) for 24 hours blocked wild-type MEOX1 (MX1), DNA-binding domain mutated MEOX1^{Q219E} (Q219E), wild-type MEOX2 (MX2) and DNA-binding domain mutated MEOX2^{Q235E} (Q235E) mediated activation of the luciferase reporter gene from the 232 bp $p21^{CIP1/WAF1}$ promoter. * Indicates a statistically significant change ($p < 0.05$) when compared to the empty vector control. ○ Indicates a statistically significant difference ($p < 0.05$) between vehicle and mithramycin A treatment. Error bars represent the standard error of the mean ($n \geq 9$).

the basal transcription machinery and ultimately enhancing $p21^{CIP1/WAF1}$ gene transcription. However, there is no evidence to support this model at this time. Future experiments based on the chromatin conformation capture (3C) technique, which allows the detection of interactions between selected genomic regions, are required to address this question.

4.4.3. MEOX1 and MEOX2 activate $p16^{INK4a}$ expression via a DNA-binding dependent mechanism

The CDK inhibitor $p16^{INK4a}$ has been shown to be a direct transcriptional target of MEOX2 [87]. Therefore, we wanted to compare the activation of $p21^{CIP1/WAF1}$ and $p16^{INK4a}$ by MEOX2 and also examine whether $p16^{INK4a}$ is also a transcriptional target of MEOX1 in endothelial cells.

4.4.3.1. MEOX1 and MEOX2 activate transcription from the endogenous $p16^{INK4a}$ promoter in endothelial cells.

First, we transduced HUVECs at increasing MOI with EGFP or MEOX2 encoding adenovirus and then used western blot analysis to compare the effects of viral dose and MEOX2 expression on endogenous $p16^{INK4a}$ expression at the protein level. Compared to the EGFP control, over-expression of MEOX2 in HUVECs seemingly increased $p16^{INK4a}$ protein expression (Figure 4-17). We observed the greatest effect with 250 MOI; therefore, we continued our studies using this dose of adenovirus. Subsequently, time course experiments were performed to study the level of $p16^{INK4a}$ induction by MEOX2 at various times post-transduction. HUVECs were transduced, following which we performed quantitative real-time PCR and western blot analysis to measure the changes in $p16^{INK4a}$ expression at the mRNA and protein level, respectively. We noticed that viral transduction did not significantly induce $p16^{INK4a}$ mRNA and protein expression in HUVECs (Figure 4-18). In addition, MEOX2 did not significantly increase $p16^{INK4a}$ mRNA and protein expression until 72 hours post-transduction (Figure 4-18). In contrast, MEOX2 significantly increased $p21^{CIP1/WAF1}$ mRNA and protein expression by 48 hours (Figure 4-9). This finding suggests that MEOX2 may not be as

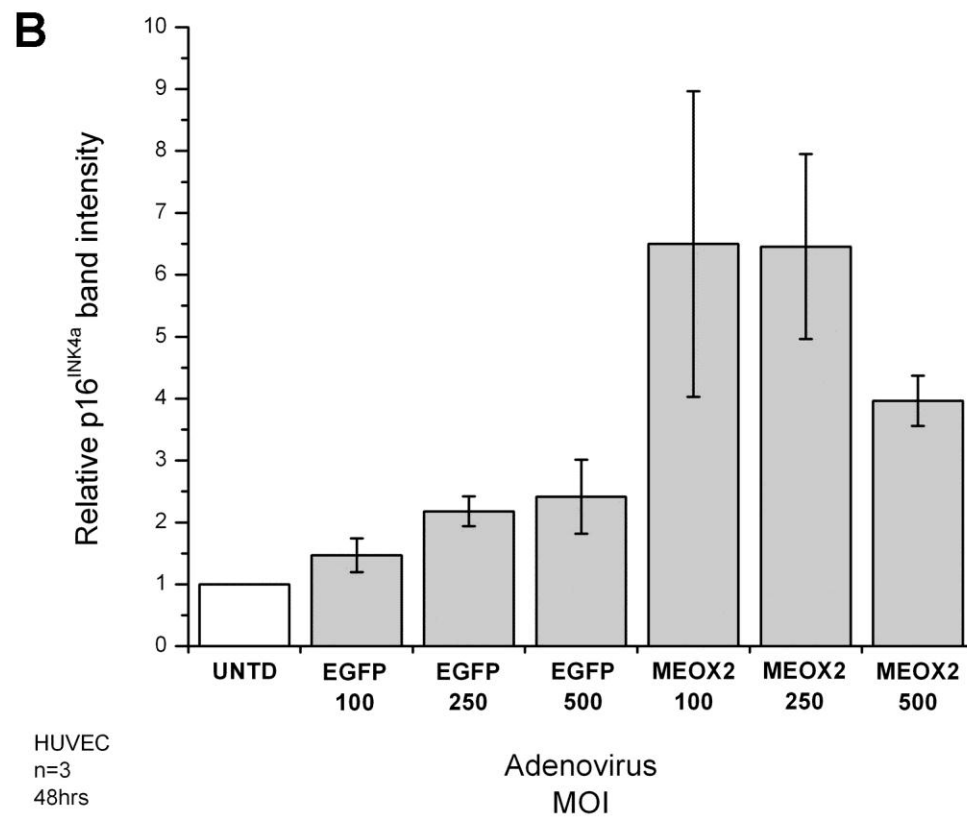
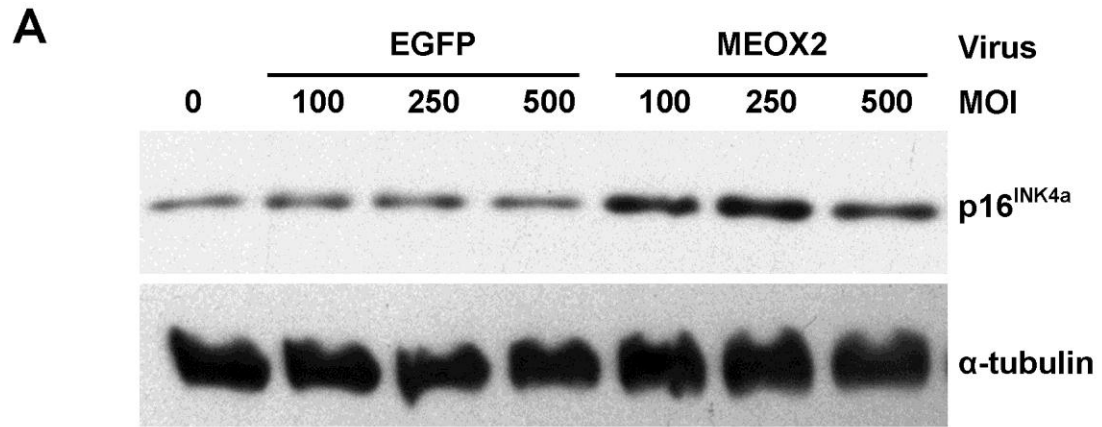


Figure 4-17: MEOX2 seemingly up-regulates p16^{INK4a} protein expression in HUVECs.

Figure 4-17: MEOX2 seemingly up-regulates p16^{INK4a} protein expression in HUVECs.

(A) Representative western blot showing p16^{INK4a} protein in HUVECs over-expressing MEOX2. (B) Quantification of the relative amount of p16^{INK4a} protein 48 hours after transduction with 100, 250 or 500 MOI of adenovirus encoding EGFP or N-terminal FLAG-tagged MEOX2. Untransduced HUVECs (UNTD) were used as a control. The intensity of the p16^{INK4a} band was normalized to the α -tubulin loading control. Error bars represent the standard error of the mean (n=3).

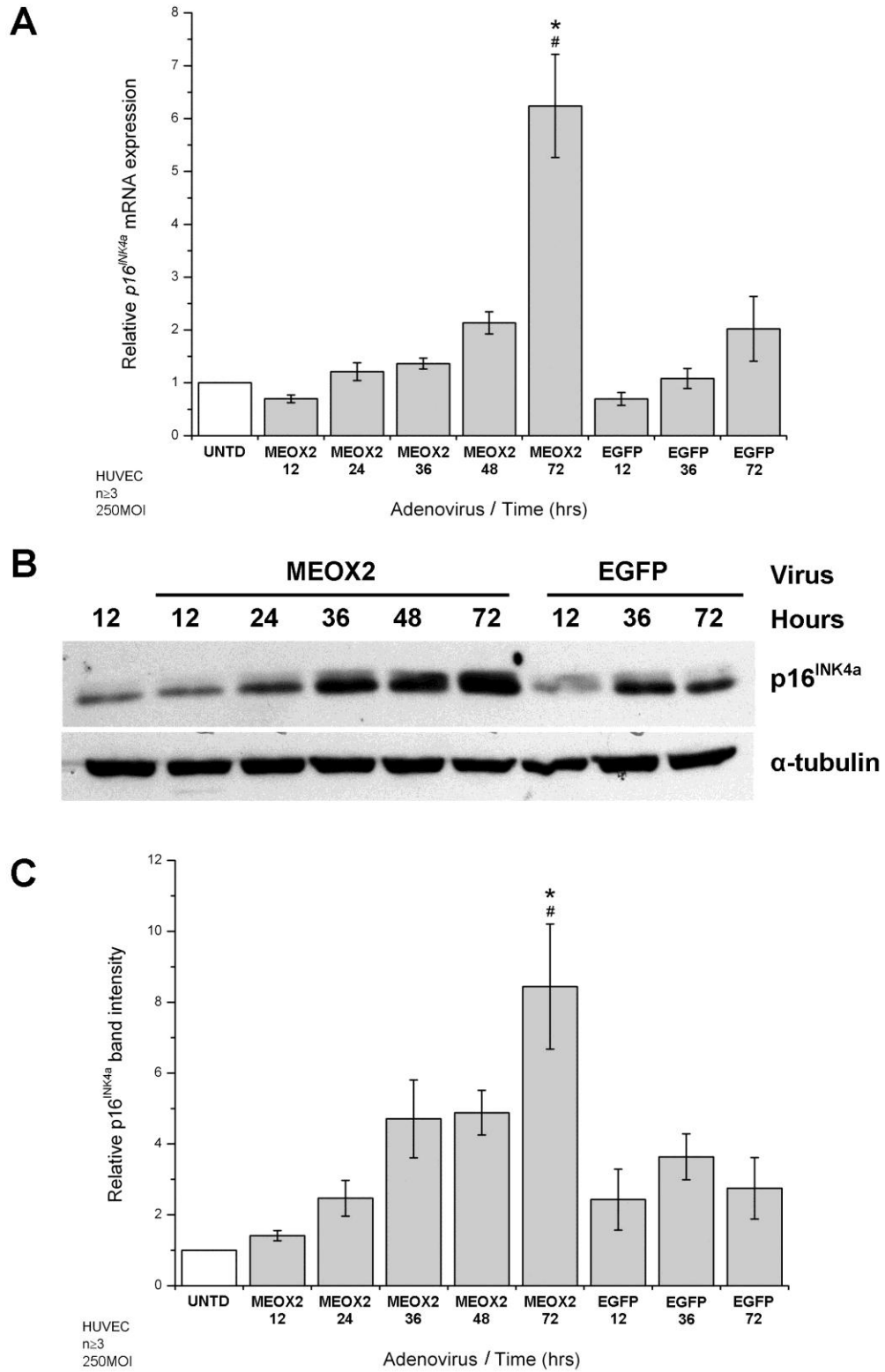


Figure 4-18: Temporal regulation of $p16^{INK4a}$ expression by ectopic MEOX2 in HUVECs.

Figure 4-18: Temporal regulation of $p16^{INK4a}$ expression by ectopic MEOX2 in HUVECs.

(A) Level of $p16^{INK4a}$ mRNA relative to untransduced HUVECs. Total RNA was isolated from HUVECs at 12, 24, 36, 48 and 72 hours after adenoviral transduction at 250 MOI and the relative amount of mRNA was measured by quantitative real-time PCR. β -actin mRNA expression was used for inter-sample normalisation. (B) Representative western blot showing increased $p16^{INK4a}$ protein in HUVECs over-expressing MEOX2. (C) Quantification of the relative amount of $p16^{INK4a}$ protein at 12, 24, 36, 48 and 72 hours after transduction with 250 MOI of adenovirus encoding EGFP or N-terminal FLAG-tagged MEOX2. The intensity of the $p16^{INK4a}$ band was normalized to the α -tubulin loading control. # Indicates a statistically significant change ($p < 0.05$) from untransduced HUVECs (UNTD). * Indicates a statistically significant difference ($p < 0.05$) between MEOX2 and EGFP over-expressing cells at the same time point. Error bars represent the standard error of the mean ($n \geq 3$ (A), $n \geq 3$ (C)).

potent of an activator of $p16^{INK4a}$ transcription in ECs. Differential transcriptional co-factor interaction or competition with other proteins at the upstream promoter region of the $p21^{CIP1/WAF1}$ and $p16^{INK4a}$ genes may influence the temporal association of MEOX2 with these promoters. Prolonged association of a transcription factor with a gene promoter has been shown to augment the levels of mRNA transcription [238,239].

To confirm these observations, we chose to continue our experiments using 250 MOI of adenovirus and measure changes in $p16^{INK4a}$ expression at 48 and 72 hours post-transduction. We compared the ability of MEOX1, MEOX2 and DNA-binding domain mutated MEOX2^{Q235E} to induce the expression of endogenous $p16^{INK4a}$ in endothelial cells. At 48 hours post-transduction we saw a dramatic increase in $p16^{INK4a}$ expression at both the mRNA and protein level in HUVECs over-expressing MEOX1 (Figure 4-19). In contrast, MEOX2 did not induce $p16^{INK4a}$ mRNA or protein expression 48 hours after transduction (Figure 4-19). At 72 hours post-transduction, however, we observed that MEOX2 significantly increased $p16^{INK4a}$ mRNA and protein expression (Figure 4-20). An even greater induction of $p16^{INK4a}$ mRNA and protein expression was seen at this time point when MEOX1 was over-expressed (Figure 4-20). Specifically, from these results it appears that MEOX1 is approximately three-fold more potent than MEOX2 at activating $p16^{INK4a}$ expression. Thus, while $p16^{INK4a}$ was identified as a MEOX2 target gene, MEOX1 is a much stronger activator of $p16^{INK4a}$ transcription. Differences in MEOX1 versus MEOX2 activation of common target genes, as well as their activation of unique target genes, are likely to be due to: i) the presence of unique transactivation motifs within these proteins, or ii) the ability of these proteins to interact with distinct transcriptional co-factors via protein-protein interaction domains.

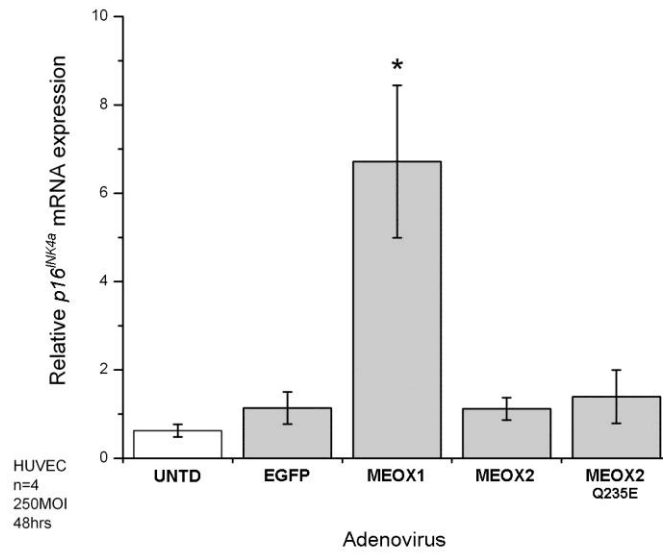
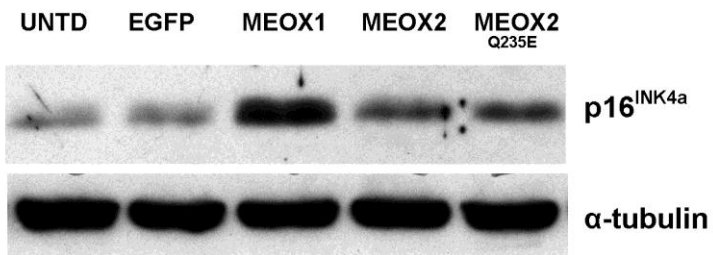
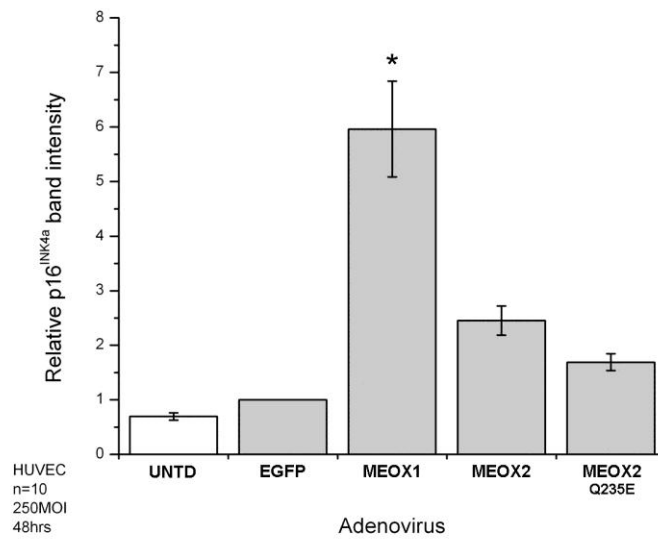
A**B****C**

Figure 4-19: MEOX1 activates $p16^{INK4a}$ expression in HUVECs 48 hours post-transduction.

Figure 4-19: MEOX1 activates $p16^{INK4a}$ expression in HUVECs 48 hours post-transduction.

(A) Relative level of $p16^{INK4a}$ mRNA compared to EGFP transduced HUVECs. Total RNA was isolated from HUVECs 48 hours after adenoviral transduction at 250 MOI and the relative amount of mRNA was measured by quantitative real-time PCR. β -actin mRNA expression was used for inter-sample normalisation. (B) A representative western blot showing increased $p16^{INK4a}$ protein in HUVECs over-expressing MEOX1. (C) Quantification of the relative amount of $p16^{INK4a}$ protein compared to EGFP transduced HUVECs. Total protein was isolated from HUVECs 48 hours after adenoviral transduction at 250 MOI with N-terminal FLAG-tagged constructs. The intensity of the $p16^{INK4a}$ band was normalized to the α -tubulin loading control. UNTD signifies untransduced HUVECs. * Indicates a statistically significant change ($p < 0.05$) between MEOX1 and EGFP over-expressing cells. Error bars represent the standard error of the mean (n=4 (A), n=10 (C)).

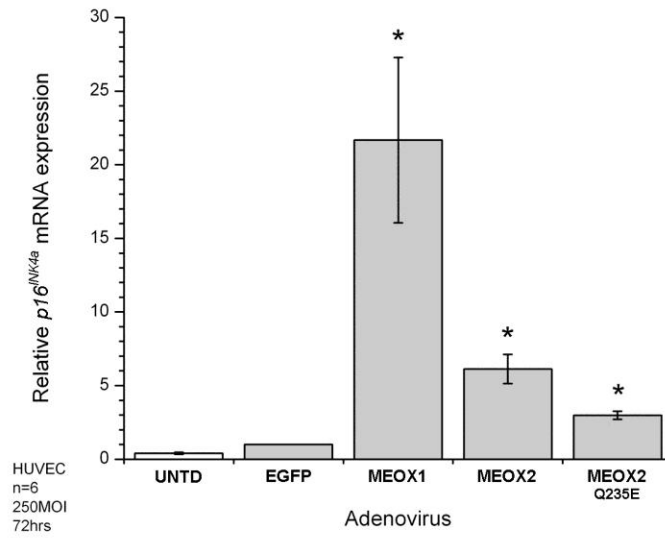
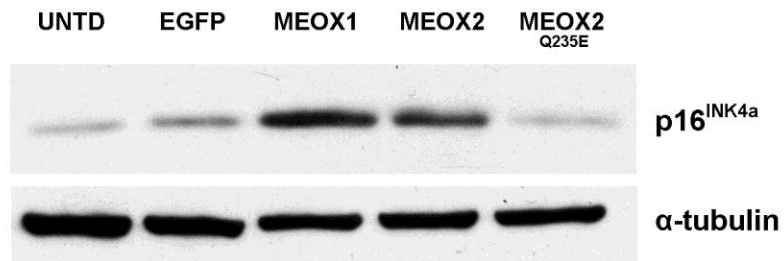
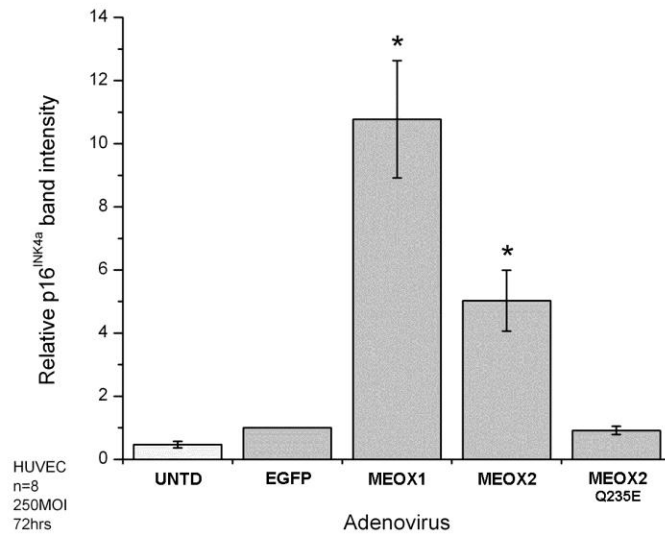
A**B****C**

Figure 4-20: DNA-binding domain mutated MEOX2^{Q235E} does not induce p16^{INK4a} protein expression.

Figure 4-20: DNA-binding domain mutated MEOX2^{Q235E} does not induce p16^{INK4a} protein expression.

(A) Relative level of *p16^{INK4a}* mRNA compared to EGFP transduced HUVECs. Total RNA was isolated from HUVECs 72 hours after adenoviral transduction at 250 MOI and the relative amount of mRNA was measured by quantitative real-time PCR. *β-actin* mRNA expression was used for inter-sample normalisation. (B) A representative western blot showing increased p16^{INK4a} protein in HUVECs over-expressing MEOX1 and MEOX2 but not DNA-binding domain mutated MEOX2^{Q235E}. (C) Quantification of the relative amount of p16^{INK4a} protein compared to EGFP transduced HUVECs. Total protein was isolated from HUVECs 72 hours after adenoviral transduction at 250 MOI with N-terminal FLAG-tagged constructs. The intensity of the p16^{INK4a} band was normalized to the actin loading control. UNTD signifies untransduced HUVECs. * Indicates a statistically significant change (p<0.05) between MEOX and EGFP over-expressing cells. Error bars represent the standard error of the mean (n=6 (A), n=8 (C)).

Although we observed a small but significant increase in $p16^{INK4a}$ mRNA expression with DNA-binding domain mutated MEOX2^{Q235E} at 72 hours post-transduction, this activation did not correlate with increased $p16^{INK4a}$ protein expression (Figure 4-20), indicating that the ability of MEOX2 to bind DNA is essential for its activation of $p16^{INK4a}$ expression.

Subsequently, we performed chromatin immunoprecipitation experiments to confirm the presence of MEOX2 at the $p16^{INK4a}$ upstream promoter region. To ensure that we achieved the desired shearing of genomic DNA, we reverse cross-linked the sonicated chromatin, purified the DNA fragments and separated them by agarose gel electrophoresis. Figure 4-21, panel A shows the sonicated chromatin DNA fragment size. The majority of DNA fragments were between 100 and 700 bp in length, with an enrichment of ~300 bp fragments (Figure 4-21, panel A). Chromatin fragments associated with MEOX2 were immunoprecipitated using an anti-FLAG antibody. Non-immune IgG, as well as the omission of antibody, were used as controls for non-specific immunoprecipitation. We used PCR to test for the presence of a 349 bp segment of the $p16^{INK4a}$ upstream promoter region (from -968 to -620 bp, relative to the translation start site; [87]) in the immunoprecipitated chromatin samples. In HUVECs over-expressing MEOX2, but not EGFP, we immunoprecipitated chromatin that contained the $p16^{INK4a}$ upstream promoter sequence (Figure 4-21, panel B), indicating that MEOX2 is present at the $p16^{INK4a}$ promoter in HUVECs. From the same immunoprecipitated samples, we repeated the PCR using primers that amplify a 166 bp DNA segment which encompasses the area surrounding the *GAPDH* transcription start site. In both EGFP and MEOX2 over-expressing HUVECs, we showed that chromatin originating from the area

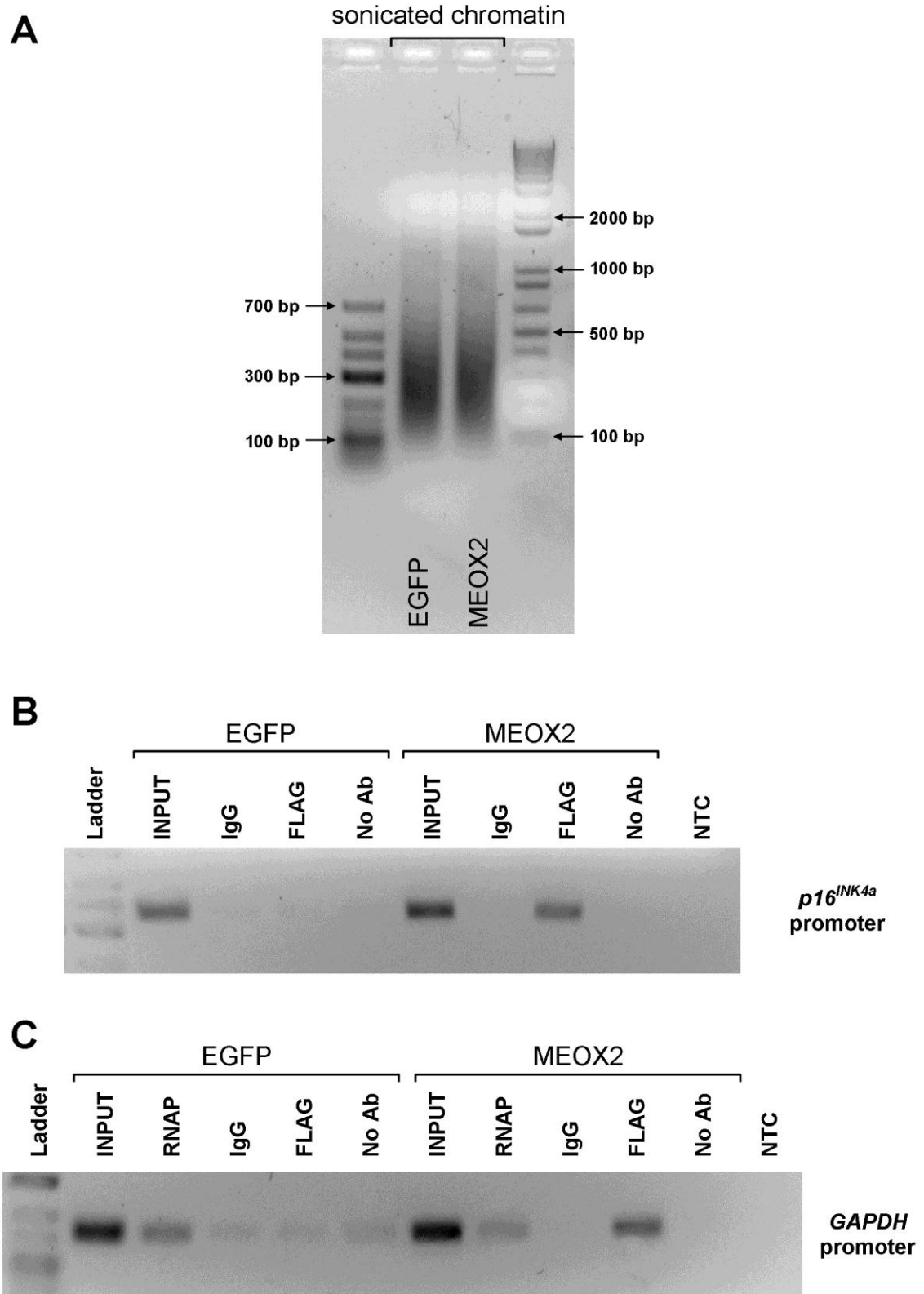


Figure 4-21: MEOX2 is present at the *p16^{INK4a}* promoter in HUVECs.

Figure 4-21: MEOX2 is present at the $p16^{INK4a}$ promoter in HUVECs.

(A) DNA fragment sizes of sonicated, reverse cross-linked and RNase treated input chromatin from HUVECs over-expressing EGFP or N-terminal FLAG-tagged MEOX2.

(B) The $p16^{INK4a}$ upstream promoter region can be immunoprecipitated with an anti-FLAG antibody in HUVECs over-expressing N-terminal FLAG-tagged MEOX2 but not EGFP. Non-immune IgG and no antibody (No Ab) were used as controls for non-specific immunoprecipitation. The no template control (NTC) was used to detect PCR

contamination. (C) The *GAPDH* core promoter region was immunoprecipitated with an anti-RNA polymerase II antibody (RNAP) in HUVECs over-expressing EGFP or MEOX2, while the anti-FLAG antibody only immunoprecipitated the *GAPDH* promoter in HUVECs over-expressing N-terminal FLAG-tagged MEOX2. Non-immune IgG and no antibody (No Ab) were used as controls for non-specific immunoprecipitation. The no template control (NTC) was used to detect PCR contamination.

surrounding the *GAPDH* transcription start site was immunoprecipitated using an anti-RNA polymerase II antibody (Figure 4-21, panel B). This finding was expected as *GAPDH* is a constitutively transcribed gene. Surprisingly, in HUVECs over-expressing MEOX2 (but not EGFP), we immunoprecipitated chromatin that contained the area surrounding the *GAPDH* transcription start site when using the anti-FLAG antibody (Figure 4-21, panel B). This finding indicates that MEOX2 is also present at the *GAPDH* promoter in HUVECs. There are no MEOX binding sites in the region surrounding the *GAPDH* start site. Furthermore, we did not detect any change in the levels of *GAPDH* mRNA in our microarray analysis of HUVECs over-expressing MEOX2 (data not shown). Hence, it is unlikely that the presence of MEOX2 at the *GAPDH* promoter indicates a functional role for MEOX2 in *GAPDH* gene transcription. The functional relevance of MEOX2 association with the regulatory region of this gene remains to be determined.

4.4.3.2. *MEOX1 and MEOX2 activate transcription from the $p16^{INK4A}$ promoter via a DNA-binding dependent mechanism.*

To elucidate the mechanism of $p16^{INK4a}$ transcription regulation by MEOX1 and MEOX2, we used a luciferase reporter gene under the control of a 564 bp $p16^{INK4a}$ upstream promoter region. This 564 bp $p16^{INK4a}$ promoter construct was previously shown to be responsive to MEOX2 in human U2OS osteosarcoma cells [87]. Two putative homeodomain binding sites are contained within the 564 bp $p16^{INK4a}$ promoter construct (Figure 4-22, panel A). In luciferase reporter gene assays, both MEOX1 and MEOX2 activated transcription from the 564 bp $p16^{INK4a}$ promoter in HUVECs, when compared to the empty vector control (Figure 4-22, panel B). Furthermore, similar to

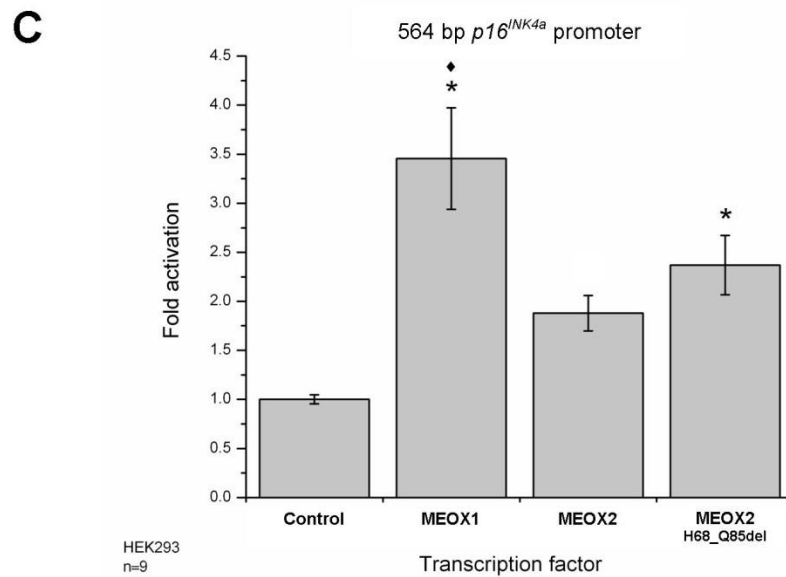
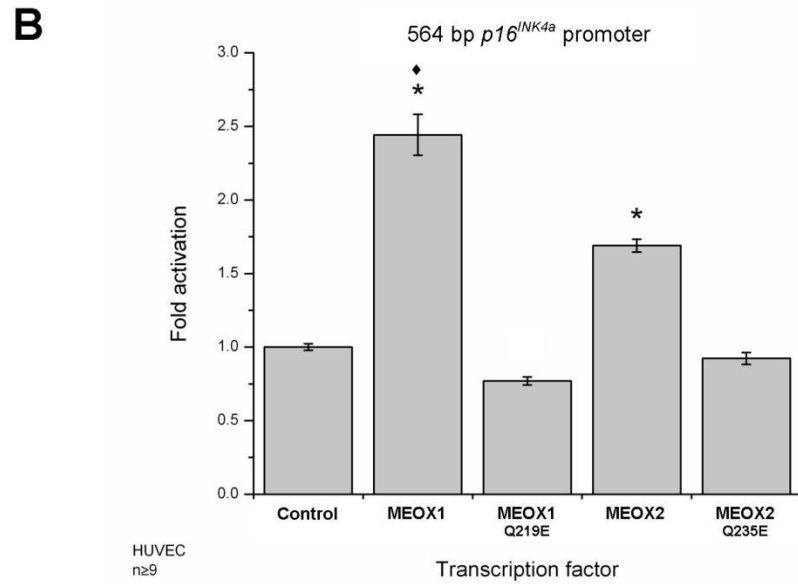
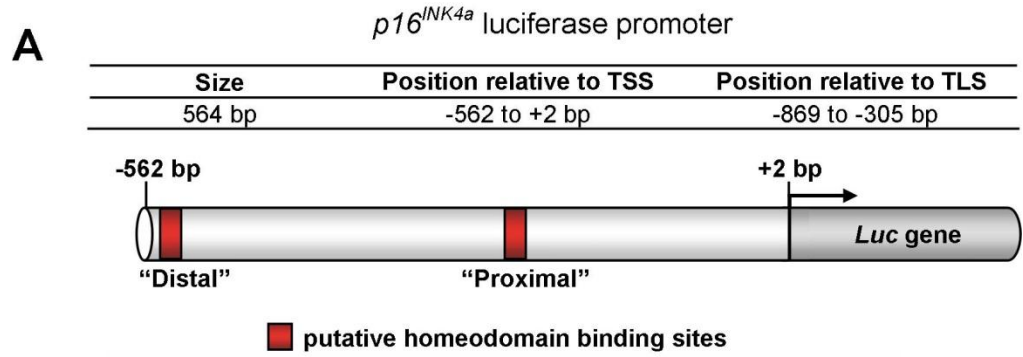


Figure 4-22: MEOX1 and MEOX2 activate transcription from the 564 bp *p16^{INK4a}* promoter.

Figure 4-22: MEOX1 and MEOX2 activate transcription from the 564 bp $p16^{INK4a}$ promoter.

(A) Schematic representation of the human 564 bp $p16^{INK4a}$ promoter luciferase construct. The base pair positions are indicated relative to the transcriptional start site (TSS). The position relative to the translational start site (TLS) is listed in the table. (B) Activation of the luciferase reporter gene from the 564 bp $p16^{INK4a}$ promoter by wild type MEOX1 and MEOX2 but not by the DNA-binding domain mutant versions of MEOX1 (MEOX1^{Q219E}) or MEOX2 (MEOX2^{Q235E}). Luciferase assays were performed in HUVECs. (C) MEOX2^{H68-Q85del} activation of the luciferase reporter gene from the 564 bp $p16^{INK4a}$ promoter is comparable to wild type MEOX2. * Indicates a statistically significant change ($p < 0.05$) when compared to the empty vector control. ♦ Indicates a statistically significant difference ($p < 0.05$) between MEOX1 and MEOX2. Error bars represent the standard error of the mean ($n \geq 9$ (B), $n = 9$ (C)).

what we observed from the endogenous $p16^{INK4a}$ locus (Figure 4-20), MEOX1 was a significantly more potent inducer of transcription from the $p16^{INK4a}$ upstream promoter region than MEOX2 (Figure 4-22, panel B). DNA-binding domain mutated MEOX1^{Q219E} and MEOX2^{Q235E} did not activate transcription from this $p16^{INK4a}$ upstream promoter region in HUVECs (Figure 4-22, panel B), suggesting that the ability of MEOX1 and MEOX2 to bind DNA, via the homeodomain, is required to activate $p16^{INK4a}$ expression.

Analogous to our findings using the $p21^{CIP1/WAF1}$ luciferase promoter construct (Figure 4-15, panel A), there was no difference in the ability of wild-type MEOX2 and histidine/glutamine rich domain deleted MEOX2^{T89-V182del} to activate transcription from the $p16^{INK4a}$ luciferase promoter in HUVECs (Figure 4-22, panel C). Thus, our results do not support the hypothesis that the histidine/glutamine rich domain functions as a transactivation domain within MEOX2.

4.4.3.3. *MEOX1 and MEOX2 sequence specifically bind to the proximal homeodomain binding site from the $p16^{INK4a}$ promoter.*

We sought to determine which of the two putative homeodomain binding sites (proximal or distal) in the 564 bp $p16^{INK4a}$ promoter were bound by MEOX1 and MEOX2. Since MEOX1^{Q219E} and MEOX2^{Q235E} did not activate $p16^{INK4a}$ expression, we hypothesized that MEOX activation of $p16^{INK4a}$ requires DNA-binding and therefore the MEOX proteins would bind to one, or both, of the homeodomain binding sites within this upstream promoter region. To address this question, we designed EMSA probes that contained either the distal or proximal homeodomain binding sites.

With recombinant proteins we observed that wild-type MEOX1 and MEOX2 bound to a DNA probe which contains the proximal, but not the distal homeodomain binding site (Figure 4-23, panels A and B). When the Distal probe was incubated with recombinant GST-tagged MEOX proteins, no specific protein-DNA complexes were formed (Figure 4-23, panel A). As predicted, the DNA-binding domain mutated MEOX2^{Q235E} did not bind to either of the *p16^{INK4a}* probes (Figure 4-23, panels A and B). To confirm that MEOX1 and MEOX2 protein/Proximal probe interaction was dependent upon the homeodomain binding site within the probe, the ATTA motif was mutated to AGGA. Competition reactions show that the wild-type Proximal probe, but not the mutant Proximal probe, successfully competed for binding to MEOX1 and MEOX2 (Figure 4-23, panels C and D).

Similar results were observed when the EMSAs were repeated using nuclear extracts of HUVECs transduced with different adenoviruses. Incubation of the Distal probe with HUVEC nuclear extracts produced three different sized complexes; however, none of these complexes were dependent on MEOX protein expression (Figure 4-24, panel A). In contrast, incubation of the Proximal probe with nuclear lysates derived from either MEOX1 or MEOX2 transduced cells resulted in the formation of specific protein-DNA complexes (Figure 4-24, panel B). Intriguingly, as was seen with recombinant GST-tagged proteins, two different sized probe/protein complexes were consistently observed in the presence of MEOX1, but only one complex was seen in the presence of MEOX2 (arrows) (Figure 4-23, panels B, C and D; Figure 4-24, panel B). The complexes observed when the Proximal probe was incubated with nuclear lysates derived from DNA-binding domain mutated MEOX2^{Q235E} transduced cells were not specific, as

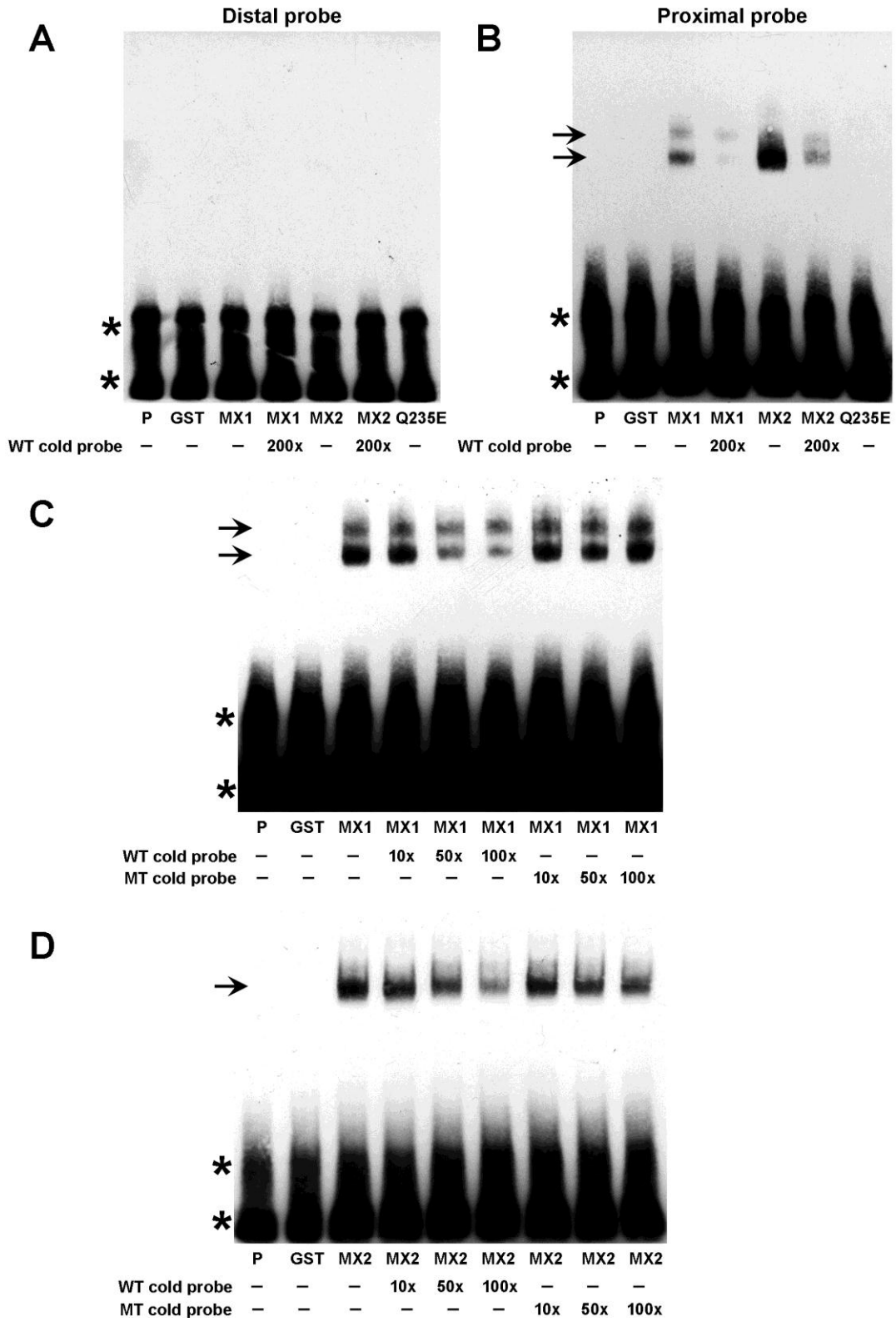


Figure 4-23: MEOX1 and MEOX2 bind to the proximal homeodomain binding site in the *p16^{INK4a}* promoter.

Figure 4-23: MEOX1 and MEOX2 bind to the proximal homeodomain binding site in the *p16^{INK4a}* promoter.

EMSA were used to assess the ability of the MEOX proteins to bind to the homeodomain binding sites within the *p16^{INK4a}* luciferase promoter. The DNA probes each contained one homeodomain binding site and correspond to -833 to -862 bp (Distal) and -538 to -567 bp (Proximal) upstream of the *p16^{INK4a}* translation start site. **(A)** Neither recombinant GST-tagged MEOX1 (MX1) nor MEOX2 (MX2) bound to the Distal probe. **(B)** Both MEOX1 and MEOX2 bound to the Proximal probe (arrow), while MEOX2^{Q235E} (Q235E) and GST alone did not. **(C-D)** Binding of MEOX1 **(C)** and MEOX2 **(D)** to the Proximal probe could be competed with excess wild type (WT), but not mutant (MT) cold probe, in which the homeodomain binding site was abolished. In all EMSAs, the first lane only contains the biotinylated probe (P) and the unbound probe is indicated by asterisks (*).

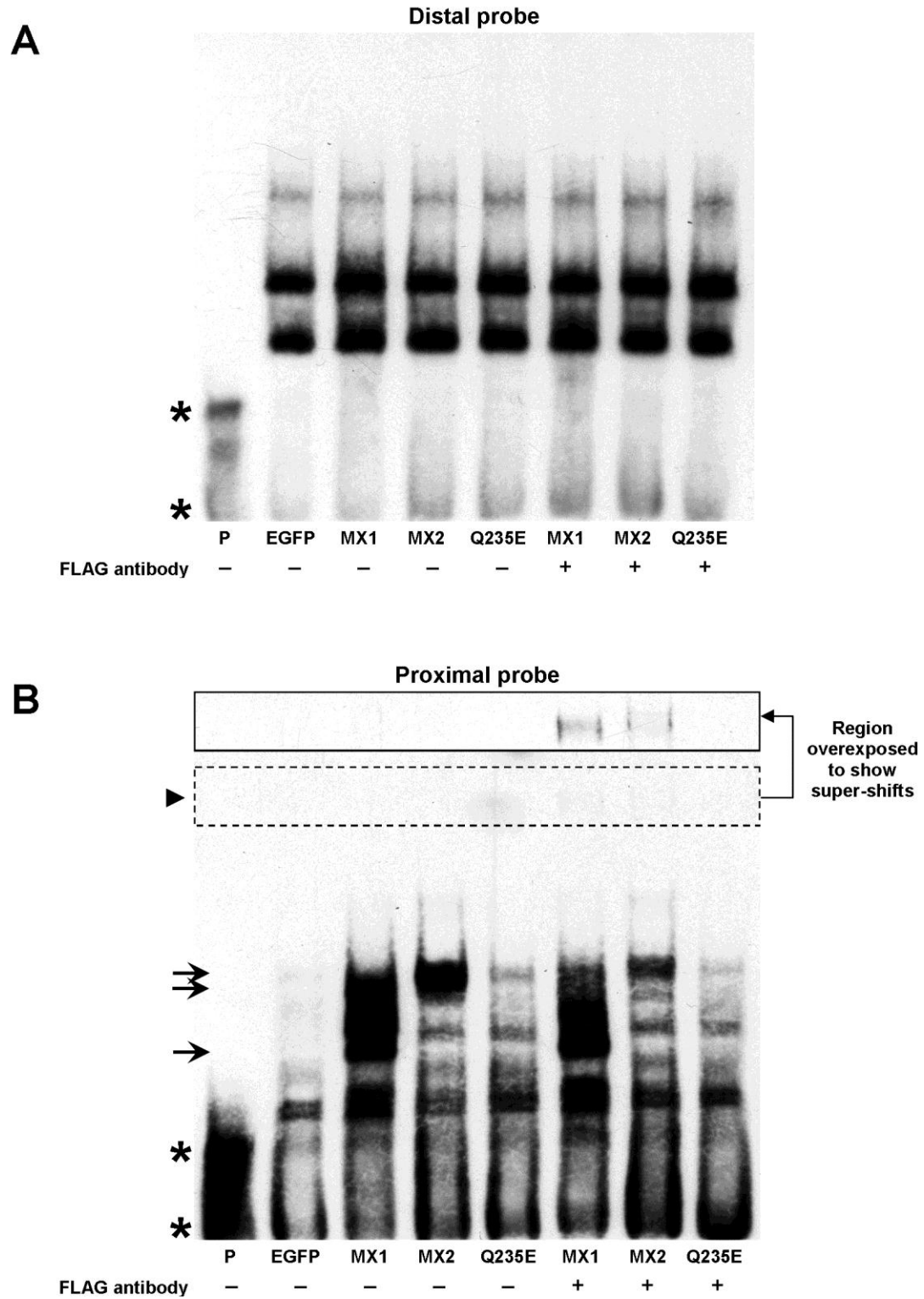


Figure 4-24: The proximal homeodomain binding site from the *p16^{INK4a}* promoter is bound by wild-type MEOX proteins in HUVEC nuclear extracts.

Figure 4-24: The proximal homeodomain binding site from the $p16^{INK4a}$ promoter is bound by wild-type MEOX proteins in HUVEC nuclear extracts.

(A) Nuclear extracts from HUVECs expressing N-terminally FLAG-tagged MEOX1 (MX1) or MEOX2 (MX2) were not able to shift the Distal probe since no unique complexes were seen upon their expression or addition of the FLAG antibody. (B) Incubation of nuclear extracts from HUVECs infected with MEOX1 or MEOX2 with the Proximal probe resulted in the formation of distinct complexes (arrows), indicating that both MEOX proteins can bind to this sequence. Addition of FLAG antibody caused this protein-probe complex to super-shift (arrowhead), confirming that the observed shift is a MEOX protein-probe complex. Incubation of nuclear extracts from HUVECs expressing MEOX2^{Q235E} (Q235E) were unable to cause a specific shift of the DNA probes and a super-shift was not observed in the presence of FLAG antibody. The lower exposure was carried out for 10 seconds, while the overexposure was carried out for 3.5 minutes. Nuclear extracts from HUVECs expressing enhanced green fluorescent protein (EGFP) were used as a negative control. In all EMSAs, the first lane only contains the biotinylated probe (P) and the unbound probe is indicated by asterisks (*).

the same bands are seen when the Proximal probe was incubated with HUVEC nuclear extracts from cells transduced with EGFP (Figure 4-24, panel B). To ensure that the shifts seen when the nuclear extracts from HUVECs expressing FLAG-tagged MEOX1 or MEOX2 were due to MEOX protein/Proximal probe interaction, we added an anti-FLAG antibody to the binding reaction mixture. Binding of the anti-FLAG antibody to the specific MEOX protein/Proximal probe complexes caused these complexes to super-shift (arrowhead), resulting from the formation of a larger complex (Figure 4-24, panel B). Furthermore, a corresponding reduction in the intensity of the smaller complex was observed (Figure 4-24, panel B). This super-shift did not occur when non-immune IgG was added in place of the anti-FLAG antibody (data not shown), confirming that it is due to its interaction with the MEOX proteins.

Thus, our findings show that the ability of MEOX1 and MEOX2 to bind DNA is necessary for activation of $p16^{INK4a}$ expression and that both MEOX1 and MEOX2 bind to the proximal, but not distal, homeodomain binding site from the 546 bp $p16^{INK4A}$ promoter. These results suggest that activation of transcription from the $p16^{INK4a}$ upstream promoter region by MEOX1 and MEOX2 is dependent upon their binding to the proximal homeodomain binding site.

4.4.3.4. *MEOX1 activates transcription of both CDKN2A isoforms in endothelial cells.*

The *CDKN2A* gene encodes two mRNA isoforms, $p16^{INK4a}$ and $p14^{ARF}$, and the transcription of each isoform is regulated by its own unique promoter [240]. These mRNA isoforms have unique first exons, but share common second and third exons [240] (Figure 4-25, panel A). However, the proteins encoded by these isoforms share no

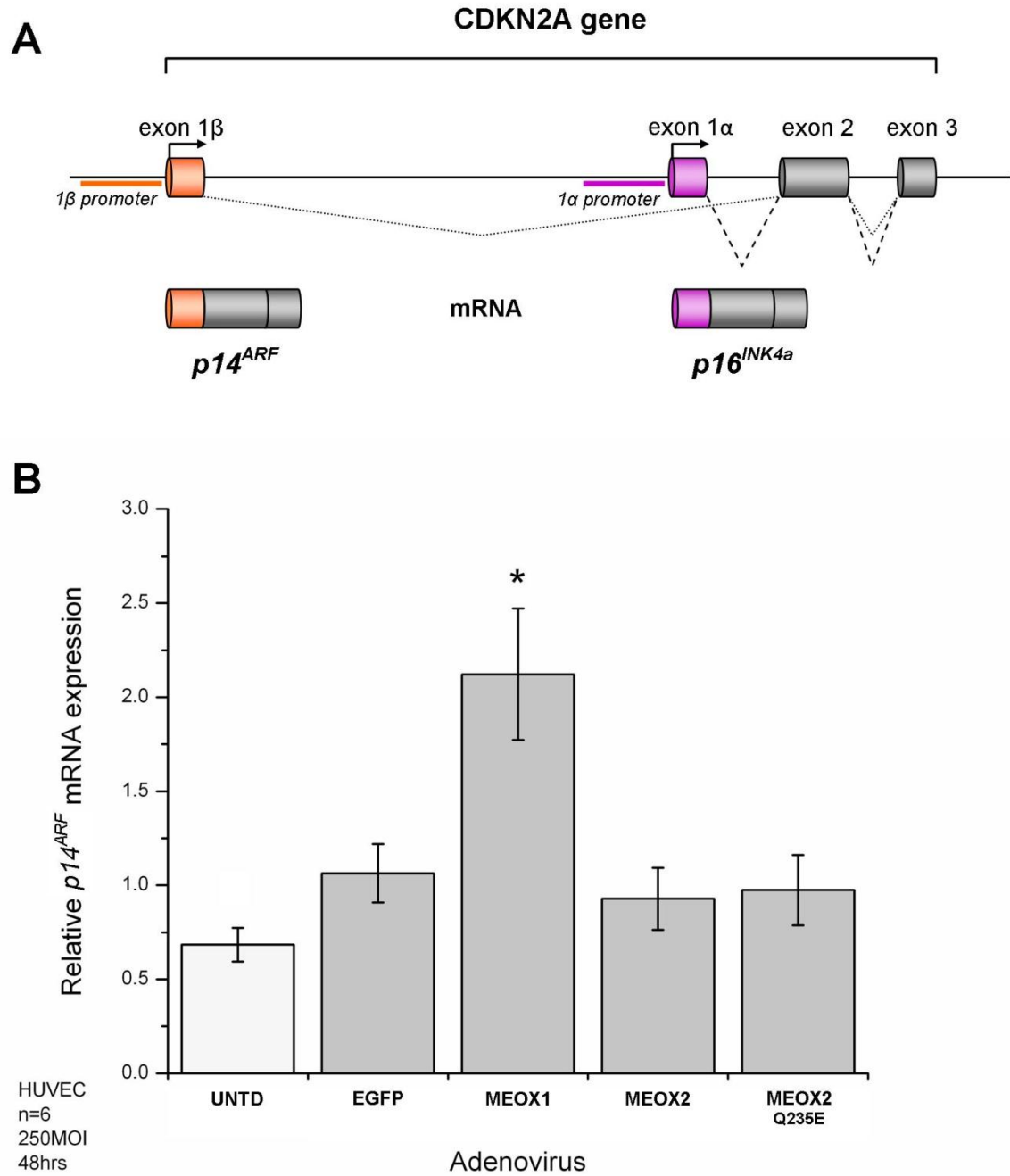


Figure 4-25: MEOX1, but not MEOX2, activates *p14^{ARF}* mRNA expression in HUVECs.

Figure 4-25: MEOX1, but not MEOX2, activates $p14^{ARF}$ mRNA expression in HUVECs.

(A) Schematic diagram of the *CDKN2A* gene and the alternative mRNA products, $p14^{ARF}$ and $p16^{INK4a}$. Transcription start sites are indicated by arrows and splicing events are shown as dotted ($p14^{ARF}$) or dashed ($p16^{INK4a}$) lines. (B) Relative level of $p14^{ARF}$ mRNA compared to EGFP transduced HUVECs. Total RNA was isolated from HUVECs 48 hours after adenoviral transduction at 250 MOI and the relative amount of mRNA was measured by quantitative real-time PCR. β -actin mRNA expression was used for inter-sample normalisation. UNTD signifies untransduced HUVECs. * Indicates a statistically significant change ($p < 0.05$) when compared to the EGFP control. Error bars represent the standard error of the mean (n=6).

sequence similarity, since the sequence from the second and third exons is translated in alternate reading frames [240]. While $p16^{INK4a}$ directly regulates the cell cycle by inhibiting cyclin/CDK interactions, $p14^{ARF}$ inhibits the negative regulation of p53 by MDM2 and thereby indirectly promotes the up-regulation of the CDK inhibitor $p21^{CIP1/WAF1}$ [240].

Given that $p21^{CIP1/WAF1}$ and $p16^{INK4a}$ are transcriptional targets of the MEOX proteins and that both MEOX1 and MEOX2 increase the levels of p53 protein in HUVECs, we were interested in investigating whether $p14^{ARF}$ is also a transcriptional target of the MEOX proteins in endothelial cells. We transduced HUVECs using adenoviral vectors, following which we performed quantitative real-time PCR to measure the changes in $p14^{ARF}$ mRNA expression. Viral transduction significantly increased $p14^{ARF}$ mRNA expression (Figure 4-25, panel B). However, compared to the EGFP control, we saw that MEOX1, but not MEOX2 or the DNA-binding domain mutated MEOX2^{Q235E}, significantly increased $p14^{ARF}$ mRNA expression 48 hours post-transduction (Figure 4-25, panel B). Thus, $p14^{ARF}$ may be a transcriptional target gene that is unique to MEOX1. Increased $p14^{ARF}$ expression could explain the augmented levels of p53 protein seen in MEOX1 over-expressing cells; however, p53 protein levels were equally augmented in MEOX2 over-expressing cells in which there is no induction of $p14^{ARF}$ expression. Additional experiments are needed to elucidate the potential cross-talk that may occur between the MEOX proteins and p53 mediated regulation of the cell cycle.

4.4.4. MEOX2 is sufficient, but may not be required for $p21^{CIP1/WAF1}$ and $p16^{INK4a}$ expression in ECs

Over-expression of MEOX1 and MEOX2 activates transcription of $p21^{CIP1/WAF1}$ and $p16^{INK4A}$ in endothelial cells. To test whether MEOX2 is essential for the expression of these targets, we attempted to knockdown MEOX2 in endothelial cells using small interfering RNA (siRNA). First using siGLO, a nuclear localized fluorescently labelled non-targeting siRNA, we verified that HUVECs could be efficiently transfected with siRNA. We detected the internalization of siGLO by HUVECs, which resulted in green fluorescence within the nucleus, 24 hours after transfection (Figure 4-26, panel A). Quantitative real-time PCR was used to measure the level of *MEOX2*, $p21^{CIP1/WAF1}$ and $p16^{INK4A}$ mRNA expression in HUVECs that were either mock transfected (no siRNA) or transfected with a pool of four non-targeting control siRNAs or *MEOX2*-targeting siRNAs. At 48 hours post-transfection, we surprisingly saw a reduction in *MEOX2* mRNA expression in cells treated with both the non-targeting siRNAs and the *MEOX2*-targeting siRNAs (Figure 4-26, panel B). As compared to mock transfected HUVECs, the down-regulation of *MEOX2* mRNA expression by the non-targeting siRNAs was half that of the knockdown by the *MEOX2*-targeting siRNAs (Figure 4-26, panel B). In contrast, there was no apparent reduction in $p21^{CIP1/WAF1}$ or $p16^{INK4a}$ mRNA expression by either siRNA treatment (Figure 4-26, panel B).

Due to the reduction in *MEOX2* mRNA expression by the non-targeting control siRNA pool, we repeated the siRNA knockdown experiment using a different type of endothelial cell: neonatal human dermal lymphatic microvascular endothelial cells (LECs). Compared to HUVECs, LECs have approximately 2.5-fold higher expression of

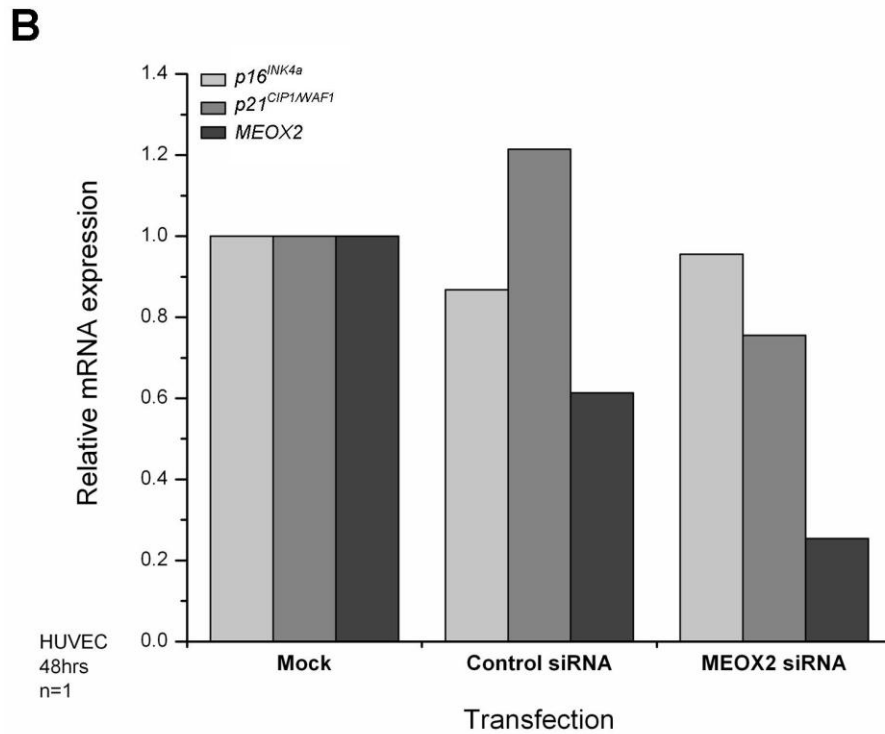
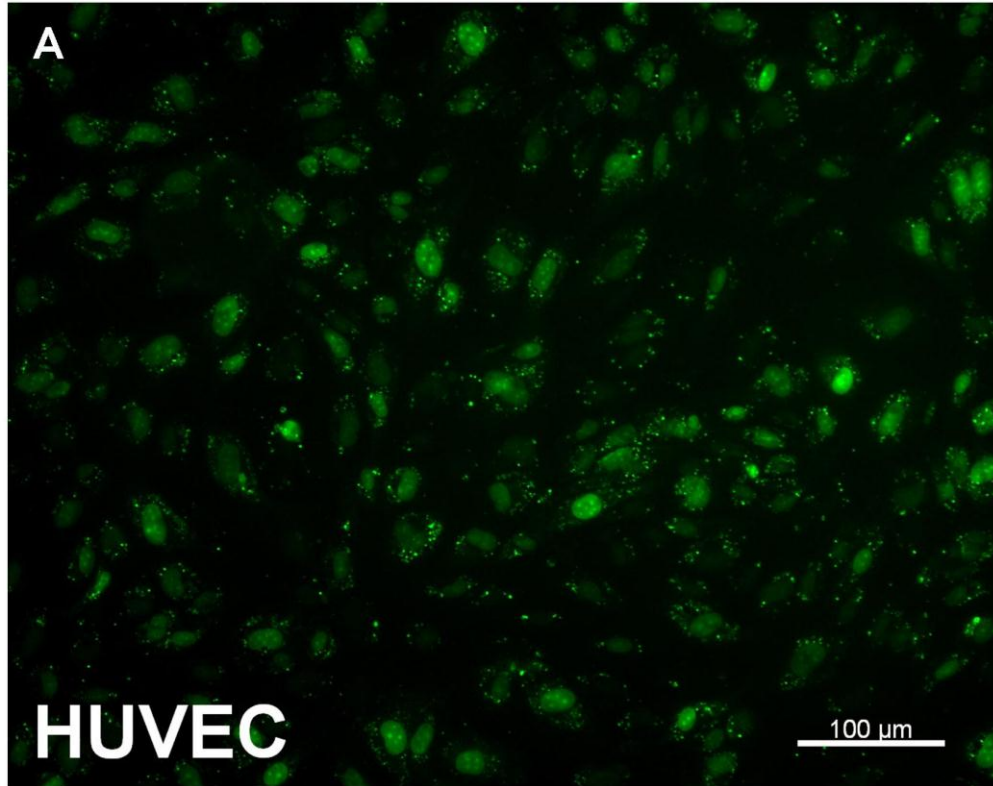


Figure 4-26: Control non-targeting siRNA pool decreased *MEOX2* mRNA expression in HUVECs.

Figure 4-26: Control non-targeting siRNA pool decreased *MEOX2* mRNA expression in HUVECs.

(A) HUVECs 24 hours after transfection with siGLO, a nuclear localized fluorescently labelled non-targeting siRNA. Scale bar is equal to 100 μm . (B) *MEOX2* specific siRNA pool decreased *MEOX2* mRNA expression in HUVECs by 74.6% at 48 hours post-transfection. A non-targeting siRNA pool decreased *MEOX2* mRNA expression by 38.7%. (n=1).

MEOX2 at the mRNA level, equivalent *p21^{CIP1/WAF1}* mRNA expression and 15-fold greater *p16^{INK4a}* mRNA expression (Figure 4-27, panel A). Prior to performing the siRNA knockdown experiments, we verified that the *MEOX1* and *MEOX2* induced changes in *p21^{CIP1/WAF1}* and *p16^{INK4a}* expression observed in HUVECs also occur in LECs. Similar to HUVECs (Figure 4-9; Figure 4-20.), western blot analysis of whole cell lysate from transduced LECs showed increased *p21^{CIP1/WAF1}* protein expression when wild-type *MEOX2* or DNA-binding domain mutated *MEOX2^{Q235E}* were over-expressed (Figure 4-27, panel B). Furthermore, over-expression of *MEOX1* in LECs resulted in increased *p16^{INK4a}* protein expression (Figure 4-27, panel B). Thus, the regulation of *p21^{CIP1/WAF1}* and *p16^{INK4a}* by *MEOX1* and *MEOX2* is common to endothelial cells from both the lymphatic and blood vasculature lineages.

Transfection of LECs with siGLO resulted in green fluorescence within the nucleus (arrows) (Figure 4-28, panel A), indicating that LECs are efficiently transfected with siRNA. LECs transfected with *MEOX2*-targeting siRNAs apparently decreased *MEOX2* mRNA expression by 74.4% at 24 hours and 82.1% at 48 hours post-transfection (Figure 4-28, panel B). Non-targeting siRNAs did not seemingly affect *MEOX2* mRNA expression 24 hours after transfection, but apparently decreased *MEOX2* mRNA expression by 16.4% after 48 hours (Figure 4-28, panel B). The expression of *p21^{CIP1/WAF1}* and *p16^{INK4a}* mRNA was seemingly unchanged in response to knockdown of *MEOX2* at 24 hours (Figure 4-28, panels C and D). Furthermore, their expression was apparently decreased to the same extent by both non-targeting and *MEOX2*-targeting siRNAs 48 hours after transfection (Figure 4-28, panels C and D).

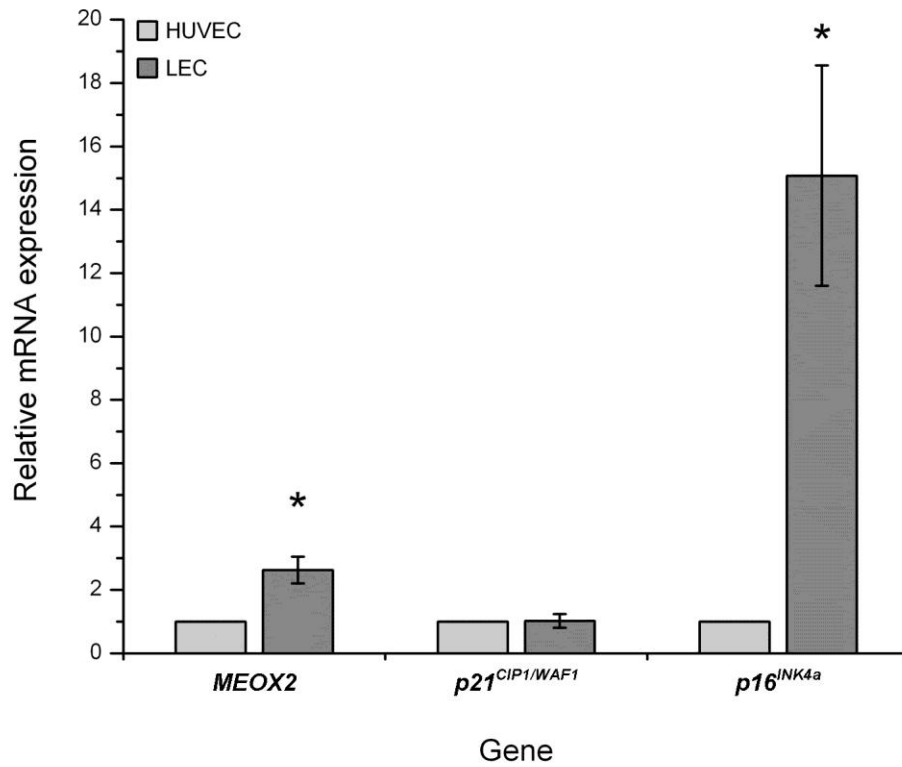
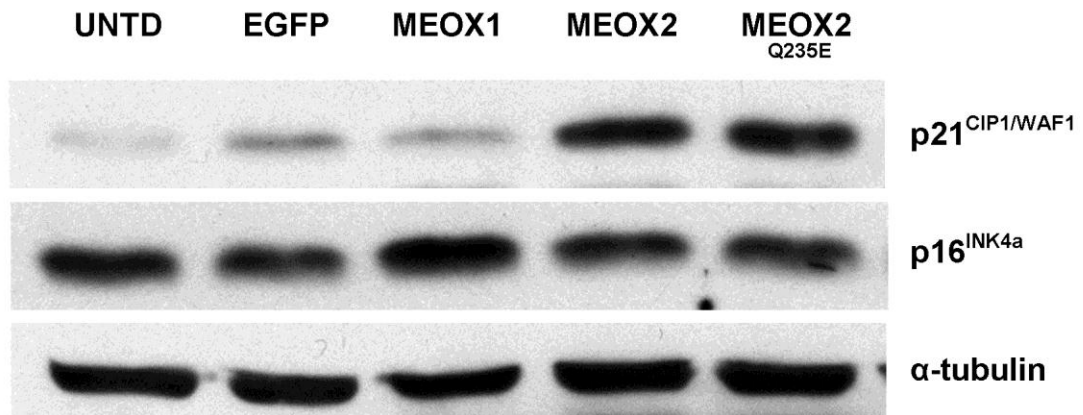
A**B**

Figure 4-27: MEOX1 and MEOX2 increase *p21^{CIP1/WAF1}* and *p16^{INK4a}* expression in LECs.

Figure 4-27: MEOX1 and MEOX2 increase $p21^{CIP1/WAF1}$ and $p16^{INK4a}$ expression in LECs.

(A) Relative *MEOX2*, $p21^{CIP1/WAF1}$ and $p16^{INK4a}$ mRNA expression in LECs compared to HUVECs. * Indicates a statistically significant change ($p < 0.05$) between LECs and HUVECs. Error bars represent the standard error of the mean ($n=4$). (B) A representative western blot showing increased $p16^{INK4a}$ protein in LECs over-expressing MEOX1 and increased $p21^{CIP1/WAF1}$ expression in LECs over-expressing MEOX2 and DNA-binding domain mutated MEOX2^{Q235E}. Proteins were isolated from LECs 48 hours after adenoviral transduction at 250 MOI. α -tubulin was used as a loading control. UNTD signifies untransduced LECs.

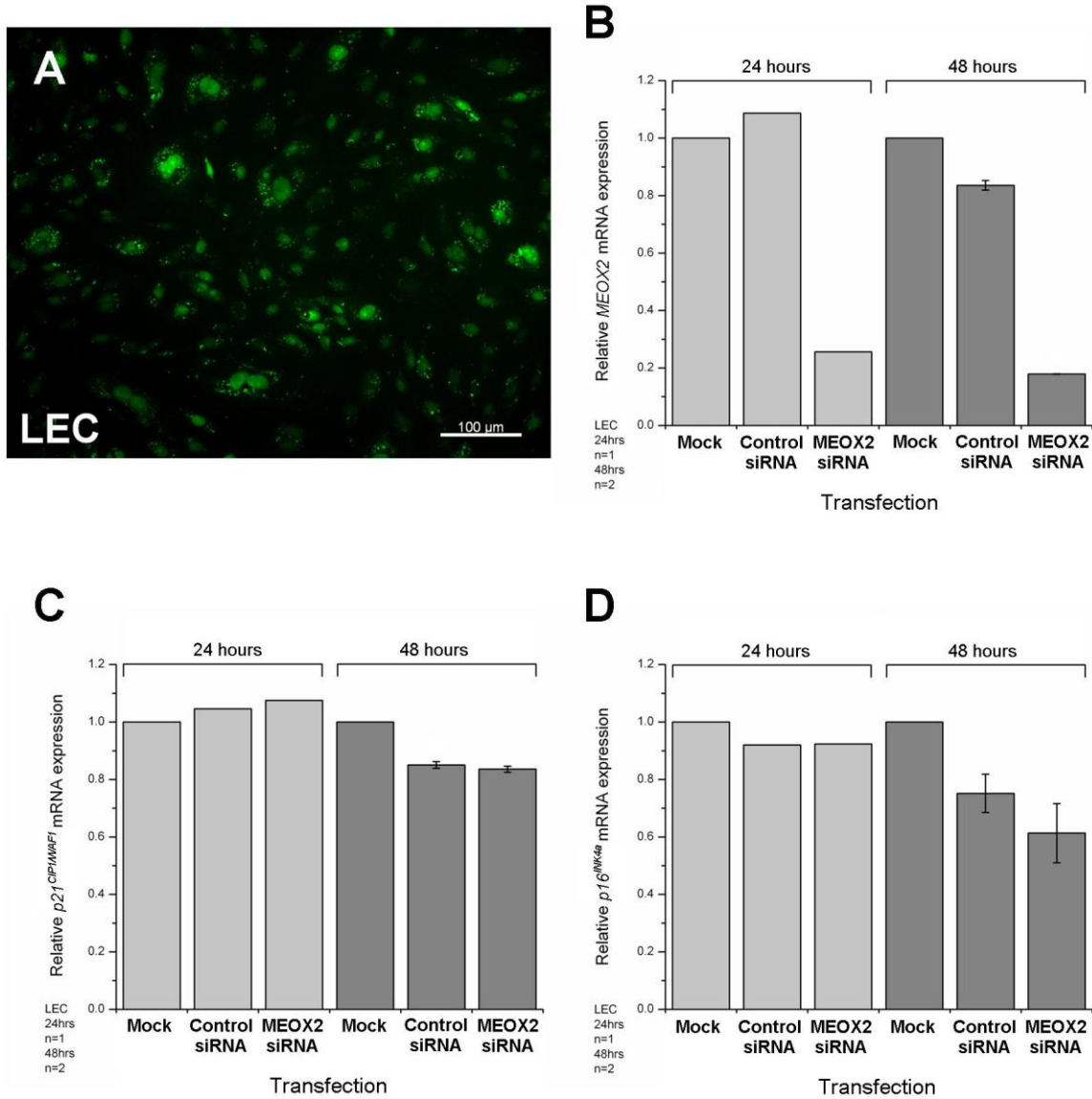


Figure 4-28: Knockdown of MEOX2 does not decrease $p21^{CIP1/WAF1}$ or $p16^{INK4a}$ mRNA expression in LECs.

Figure 4-28: Knockdown of MEOX2 does not decrease $p21^{CIP1/WAF1}$ or $p16^{INK4a}$ mRNA expression in LECs.

(A) LECs 24 hours after transfection with siGLO, a nuclear localized fluorescently labelled non-targeting siRNA. Scale bar is equal to 100 μm . (B) *MEOX2* targeted siRNA pool apparently decreased *MEOX2* mRNA expression in LECs by 74.4% and 82.1% at 24 and 48 hours post-transfection, respectively. A non-targeting siRNA pool only modestly decreased *MEOX2* mRNA expression by 16.4% after 48 hours, but did not seemingly decrease *MEOX2* expression at 24 hours post-transfection. (C) Knockdown of *MEOX2* in LECs did not seemingly affect $p21^{CIP1/WAF1}$ mRNA expression. (D) Knockdown of *MEOX2* in LECs did not seemingly affect $p16^{INK4a}$ mRNA expression. Error bars represent the standard error of the mean (n=1 (24 hours), n=2 (48 hours)).

This suggests that although MEOX2 is sufficient to increase the level of expression of $p21^{CIP1/WAF1}$ and $p16^{INK4a}$, MEOX2 may not be required for their basal transcription in endothelial cells. It is possible that the loss of MEOX2 may be compensated by MEOX1 or the many other transcription factors that activate the expression of these target genes [164,241,242]. In addition, as the half-life of the MEOX2 protein is not known and we do not possess an antibody to recognize endogenous MEOX2, we cannot be certain that the knockdown of *MEOX2* mRNA expression resulted in a comparable decrease in MEOX2 protein levels at the time points examined. We did not repeat the experiment at later time points due to the effects of the non-targeting control siRNA pool on *MEOX2* levels.

In contrast to our findings in endothelial cells, knockdown of MEOX2 in adventitial fibroblasts resulted in decreased $p21^{CIP1/WAF1}$ and $p16^{INK4a}$ expression at both the mRNA and protein level [168]. Thus, the transcription factors responsible for basal transcriptional regulation of these genes may vary between different cell types. MEOX2 plays a central role in the regulation of $p21^{CIP1/WAF1}$ and $p16^{INK4a}$ expression in adventitial fibroblasts, but our findings indicate that this is not the case in endothelial cells.

4.4.5. MEOX1 and MEOX2 prevent cellular proliferation and induce senescence

As p21^{CIP1/WAF1} and p16^{INK4a} regulate the cell-cycle, we tested whether MEOX1 and MEOX2 could induce changes in cellular proliferation. Using flow cytometry, we measured the incorporation of the thymidine analog 5-bromo-2-deoxyuridine (BrdU) into the DNA of cycling HUVECs. Differences in the amount of BrdU incorporation are representative of changes in the percentage of cells in the S phase of the cell cycle. As expected, expression of p53 in HUVECs (positive control) resulted in a significant decrease in the percentage of S phase cells as compared to the EGFP control (Figure 4-29). Likewise, we observed a decrease in the proportion of S phase cells when MEOX1 or MEOX2 were expressed in HUVECs (Figure 4-29). MEOX1 had the seemingly greatest effect on cellular proliferation and the DNA-binding domain mutated MEOX2^{Q235E} decreased the proportion of S phase cells to the same extent as wild-type MEOX2 (Figure 4-29). Furthermore, we saw that viral transduction significantly decreased the number of BrdU positive cells, indicating that viral transduction itself inhibits cell cycle progression in ECs. This was not unexpected as we saw that viral transduction trended towards inducing p21^{CIP1/WAF1} expression (Figure 4-9).

Next, propidium iodide staining was used to quantify the proportion of cells in all of the various stages of the cell cycle. Propidium iodide is a fluorescent dye that intercalates into DNA; thus within a cell, the fluorescent intensity of propidium iodide is proportional to the DNA content (Figure 4-30, panel A). We used flow cytometry to measure the fluorescence intensity of propidium iodide in HUVECs over-expressing MEOX proteins. Consistent with our findings using BrdU incorporation, we observed a decrease in the number of cells in S phase when p53, MEOX1, MEOX2 and DNA-

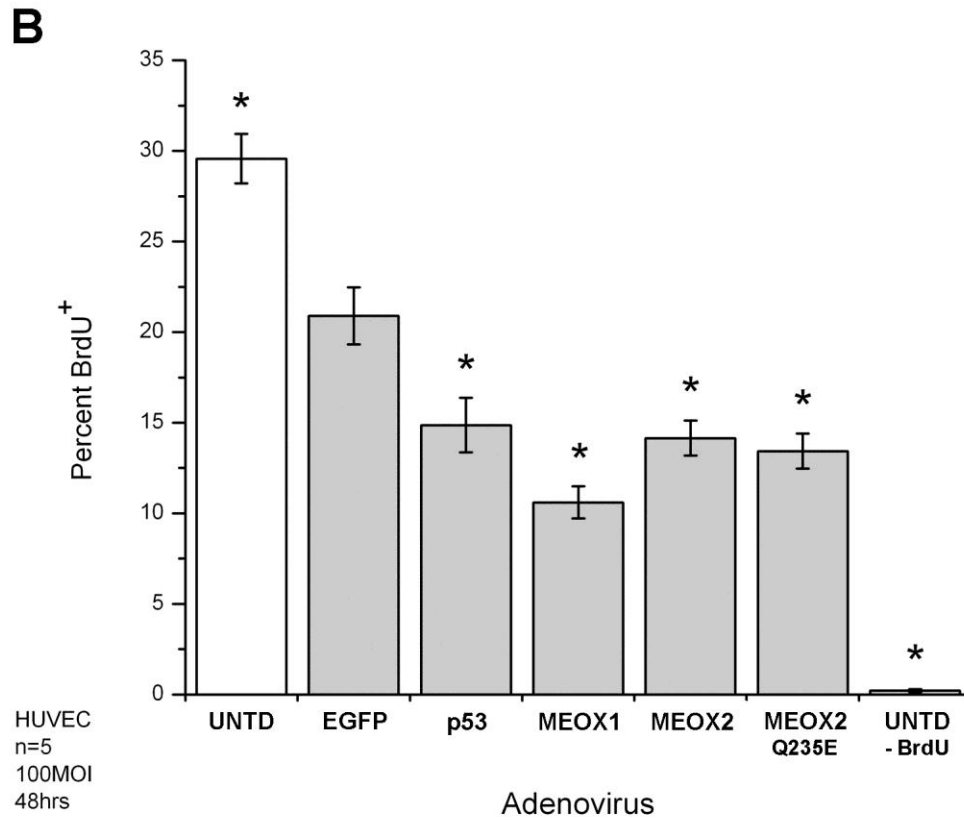
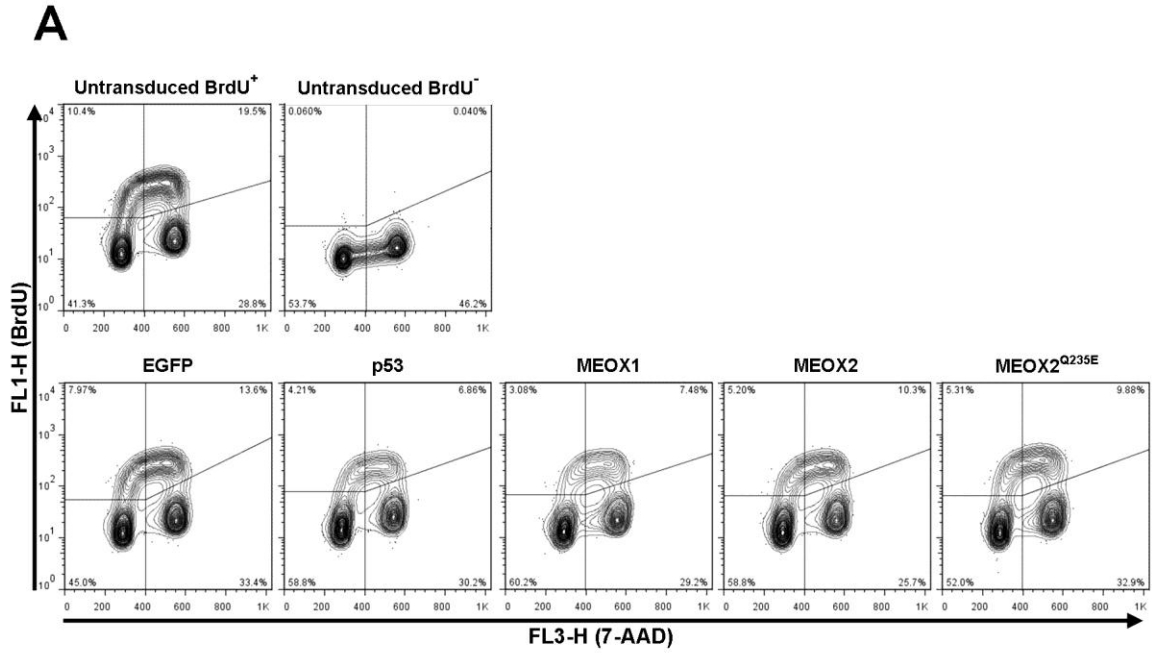


Figure 4-29: Regulation of HUVEC proliferation by MEOX1 and MEOX2.

Figure 4-29: Regulation of HUVEC proliferation by MEOX1 and MEOX2.

(A) Representative flow cytometry showing the density of BrdU⁺ endothelial cells (upper left and right quadrants). HUVECs were transduced at 100 MOI; 48 hours later, cells were labeled with BrdU for one hour prior to fixation. DNA was stained with 7-aminoactinomycin D (7-AAD). Untransduced cells (UNTD) that were not treated with BrdU (UNTD - BrdU) were used as a negative control. (B) Quantification of the flow cytometry data. As assessed by BrdU incorporation into cycling cells, over-expression of MEOX1, MEOX2 and DNA-binding domain mutated MEOX2^{Q235E} decreased cellular proliferation comparable to p53 (positive control). * Indicates a statistically significant change (p<0.05) compared to EGFP. Error bars represent the standard error of the mean (n=5).

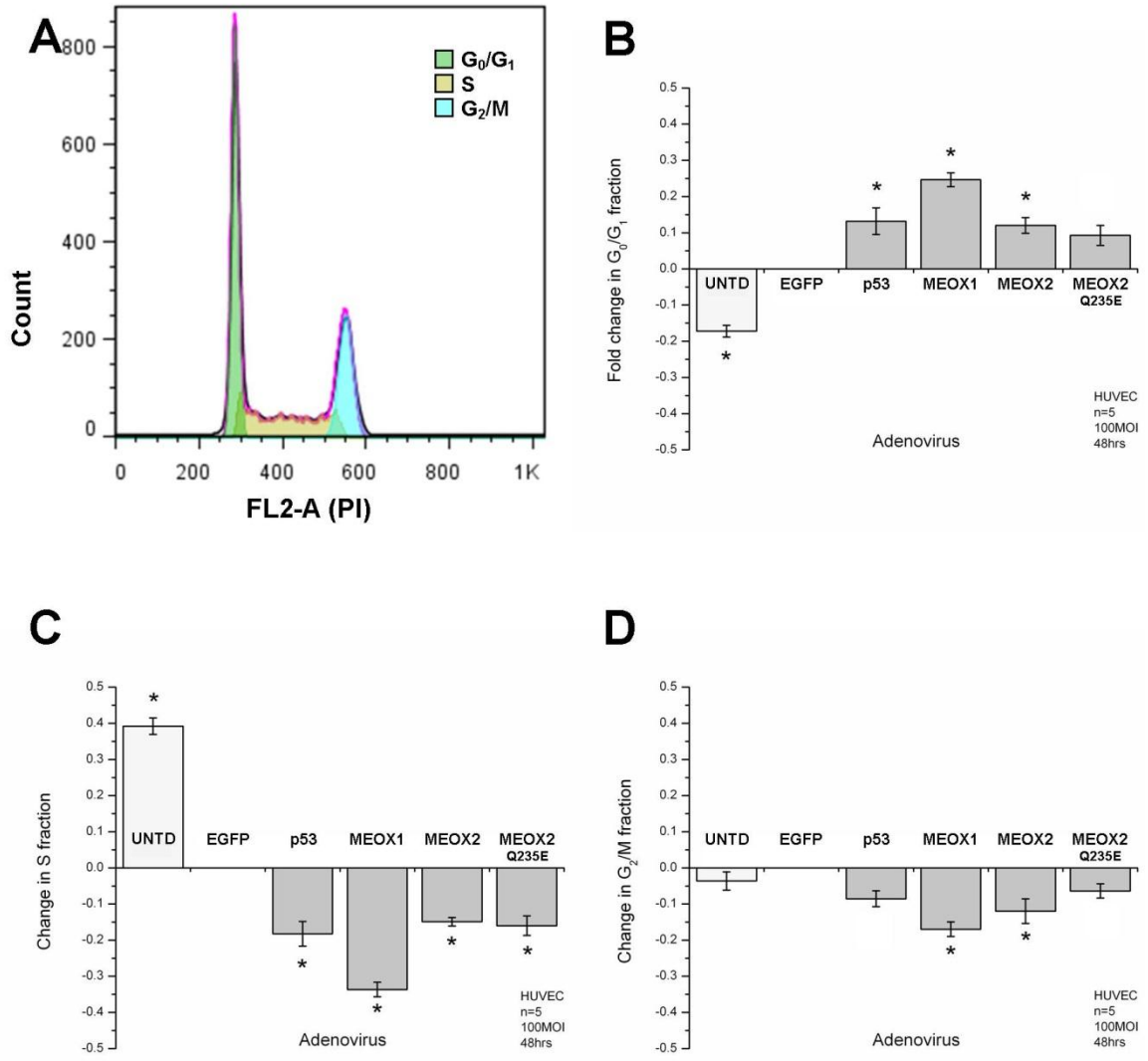


Figure 4-30: MEOX1 and MEOX2 increase the proportion of HUVECs in the G₀/G₁ phase of the cell cycle.

Figure 4-30: MEOX1 and MEOX2 increase the proportion of HUVECs in the G₀/G₁ phase of the cell cycle.

(A) Representative flow cytometry showing propidium iodide fluorescence intensity (a measure of DNA content) and its relation to the cell cycle phase. (B-D) Quantification of the flow cytometry data measuring the proportion of HUVECs in the various cell cycle phases 48 hours after adenoviral transduction at 100 MOI. MEOX1 and MEOX2 increase the proportion of G₀G₁ phase (B) cells and decreased the proportion of S phase (C) and G₂/M phase (D) cells. DNA-binding domain mutated MEOX2^{Q235E} decreases the proportion of S phase cells comparable to wild-type MEOX2. Over-expression of p53 was used as a positive control. * Indicates a statistically significant change (p<0.05) compared to EGFP. Error bars represent the standard error of the mean (n=5).

binding domain mutated MEOX2^{Q235E} were over-expressed in HUVECs (Figure 4-30, panel C). We also observed a decreased proportion of cells with G₂/M DNA content when MEOX1 or MEOX2 was over-expressed (Figure 4-30, panel D). Accordingly, in HUVECs over-expressing p53, MEOX1 or MEOX2, the number of cells in G₀/G₁ phase was significantly increased (Figure 4-30, panel B). These changes in cell cycle profile were expected since both p21^{CIP1/WAF1} and p16^{INK4a} inhibit CDKs that are active during the G₁ phase of the cell cycle. Interestingly, MEOX1 was seemingly the most potent cell cycle inhibitor (Figure 4-30). Presumably, this is due to its strong induction of p16^{INK4a} (Figure 4-20), and also perhaps due to its induction of p14^{ARF} (Figure 4-25, panel B), expression in HUVECs.

Unlike quiescence (reversible cell cycle arrest), senescence is a state of permanent cell cycle arrest and is associated with an increase in both p21^{CIP1/WAF1} and p16^{INK4a} protein expression. Thus, we ascertained whether the increased p21^{CIP1/WAF1} and p16^{INK4a} expression induced by MEOX1 and MEOX2 results in increased endothelial cell senescence. However, we first assessed replicative senescence as it occurs in our HUVEC culture system.

Examination of the change in proliferation rate of HUVECs over serial passage showed that the number of cell divisions per day that occur in passage 4 cells was decreased by half in passage 14 cell populations (Figure 4-31). This lower rate of cell division with increasing passage correlated with increased p21^{CIP1/WAF1} and p16^{INK4a} mRNA and protein expression (Figure 4-32). As assessed by SA-β-gal staining, the percentage of senescent cells also rose with increased passage (Figure 4-33). It is interesting to note that the expression of p21^{CIP1/WAF1} does not continue to rise with

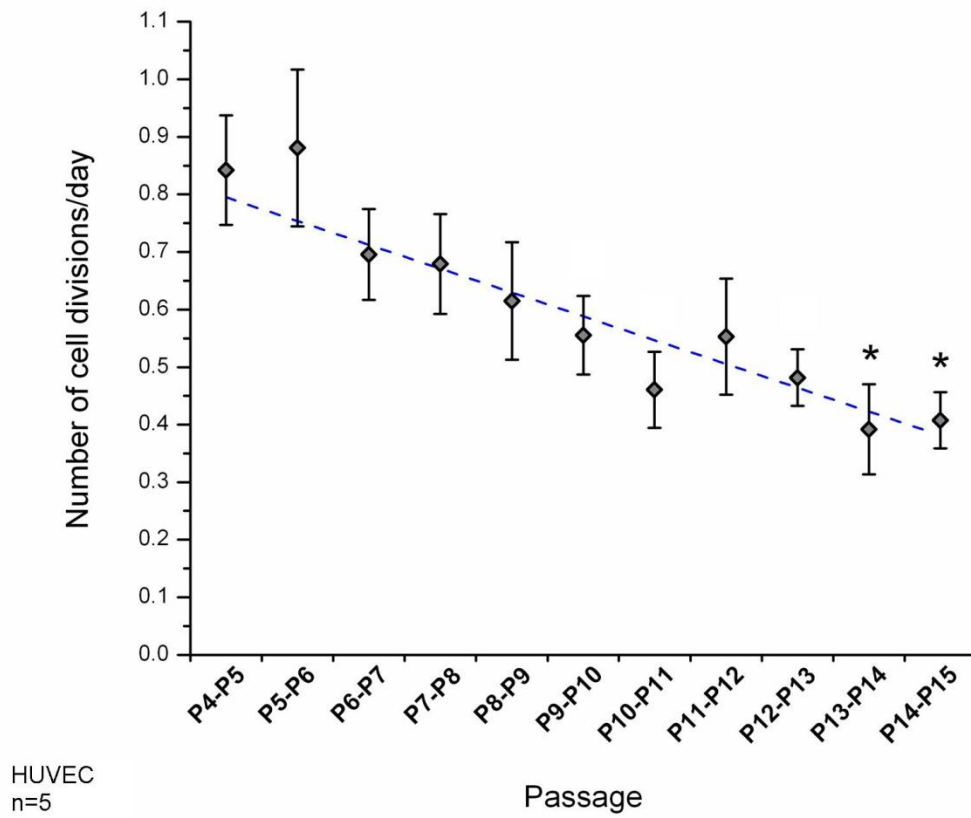


Figure 4-31: The proliferation rate of HUVECs decreases with increasing passage.

Figure 4-31: The proliferation rate of HUVECs decreases with increasing passage.

Cells at each passage were re-plated at 50% confluence (6.25×10^5 per 10 cm tissue culture plate) and then cultured to 95% confluence before the next passage. The number of passage 4 HUVECs which undergo mitosis within a 24 hour period is approximately double the number of passage 14 HUVECs that complete mitosis during the same period of time. The dashed blue line represents the line of best fit. The number of cell divisions per day was calculated using the equation: $([1.4427 \times \text{LN}(T)] - 19.253) / D$, where T represents the total number of cells and D represents the number of days since the last passage. The function $([1.4427 \times \text{LN}(X)] - 19.253)$ is the slope of the exponential growth curve of 625,000 cells. * Indicates a statistically significant change ($p < 0.05$) compared to P4-P5 cells. Error bars represent the standard error of the mean ($n=5$).

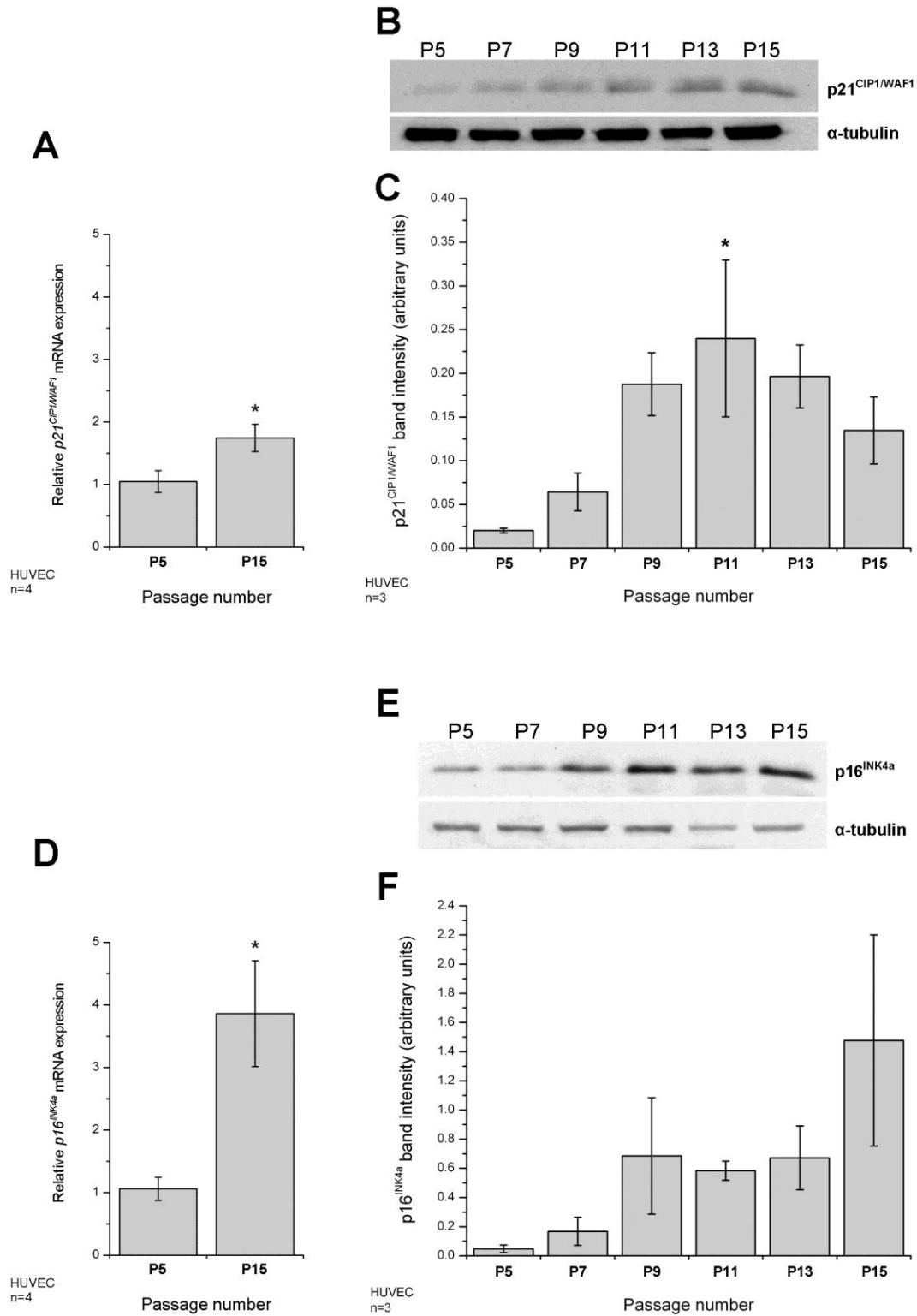


Figure 4-32: The mRNA and protein expression of $p21^{CIP1/WAF1}$ and $p16^{INK4a}$ increases with passage number in HUVECs.

Figure 4-32: The mRNA and protein expression of $p21^{CIP1/WAF1}$ and $p16^{INK4a}$ increases with passage number in HUVECs.

(A and D) Total RNA was isolated from passage 5 and passage 15 HUVECs 24 hours after being plated. The relative amount of $p21^{CIP1/WAF1}$ (A) and $p16^{INK4a}$ (D) mRNA was measured by quantitative real-time PCR. β -actin mRNA expression was used for inter-sample normalisation. (B and E) Representative western blots showing increased $p21^{CIP1/WAF1}$ (B) and $p16^{INK4a}$ (E) protein expression in HUVECs with increasing passage number. (C and F) Quantification of the relative amount of $p21^{CIP1/WAF1}$ (C) and $p16^{INK4a}$ (F) protein in HUVECs at passage 5, 7, 9, 11, 13 and 15. The intensity of the $p21^{CIP1/WAF1}$ and $p16^{INK4a}$ bands were normalized to the α -tubulin loading control. * Indicates a statistically significant change ($p < 0.05$) compared to P5 cells. Error bars represent the standard error of the mean (n=4 (A), n=3 (C), n=4 (D), n=3 (F)).

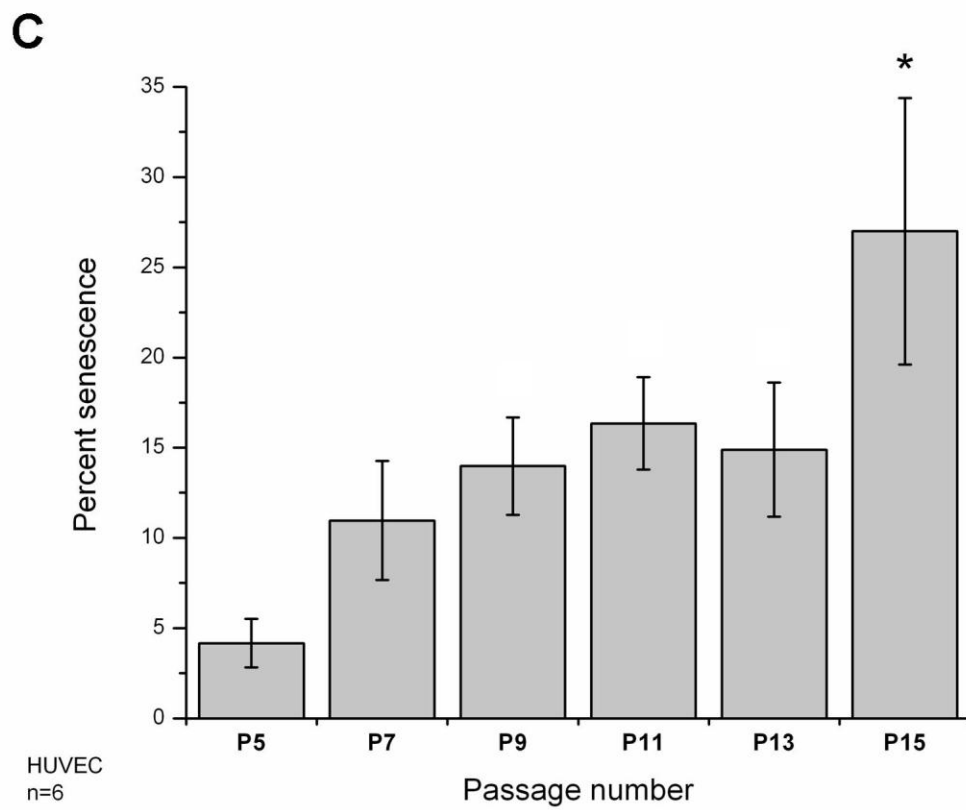
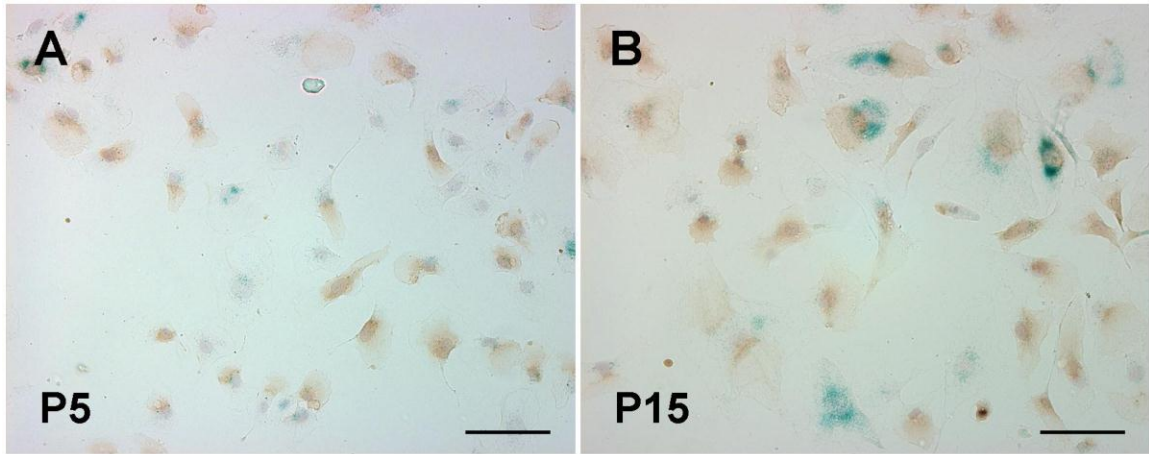


Figure 4-33: Senescence of HUVECs increases with passage number.

Figure 4-33: Senescence of HUVECs increases with passage number.

(A-B) Representative cytochemistry showing that the proportion of HUVECs that are positive for SA- β -gal staining (blue) increases with the age of the cell population. Nuclei were stained with hematoxylin (brown). Scale bars represent 100 μ m. (C) Quantification of the percent senescence in passage 5, 7, 9, 11, 13 and 15 HUVECs. The percent senescence was calculated by dividing the number of SA- β -gal positive cells by the total number of cells. * Indicates a statistically significant change ($p < 0.05$) compared to P5 cells. Error bars represent the standard error of the mean ($n=6$).

increasing passage (Figure 4-32). This may indicate that p21^{CIP1/WAF1} is necessary for senescence induction, but not required for the maintenance of senescence. As the levels of p21^{CIP1/WAF1}, p16^{INK4a} and senescence were lowest at passage 5, we performed all future senescence experiments using passage 5 cells.

Compared to EGFP, over-expression of MEOX2 in HUVECs resulted in increased senescence, as assessed by SA-β-gal staining (Figure 4-34). When MEOX1 was over-expressed in HUVECs, analogous to MEOX2, we observed a significant increase in the number of senescent cells (approximately 2-fold), as assessed by SA-β-gal staining (Figure 4-35). Specifically, this corresponded to an increase from 4.5% senescence to 9.8% and 10.9% senescence, when comparing untransduced cells to cells ectopically expressing MEOX1 and MEOX2, respectively. To our knowledge, the MEOX proteins are the second instance of homeodomain transcription factors capable of inducing senescence. Ectopic expression of VentX, a transactivator of p16^{INK4a} and p53, has recently been shown to cause senescence in cancer cells [164]. Corresponding to our results, these authors show that both p21^{CIP1/WAF1} and p16^{INK4a} are involved in permanent cell cycle arrest.

Interestingly, expression of DNA-binding domain mutated MEOX2^{Q235E} in HUVECs did not result in increased endothelial senescence (Figure 4-35). Thus, DNA-binding domain mutated MEOX2^{Q235E} over-expression decreased the proportion of S phase cells to the same extent as wild-type MEOX2 (Figure 4-29; Figure 4-30), but did not lead to increased endothelial senescence (Figure 4-35). This finding suggests that p21^{CIP1/WAF1} is the main inhibitor of cell cycle progression in response to MEOX2 expression; however both p21^{CIP1/WAF1} and p16^{INK4a} are required for the induction of the

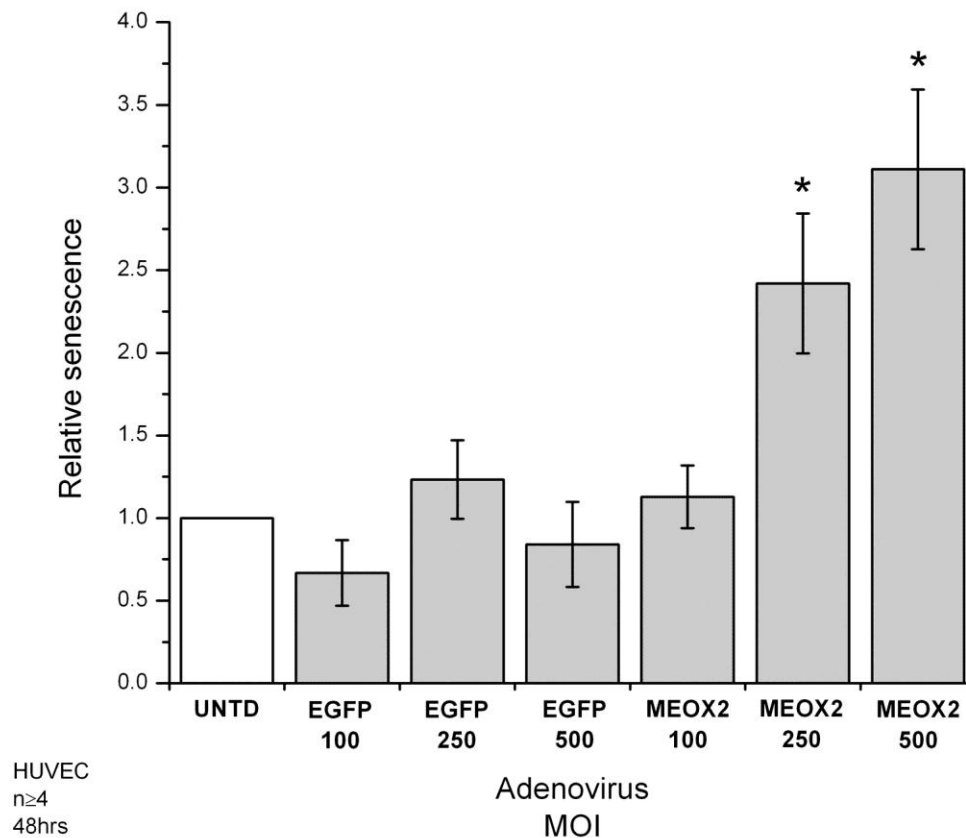


Figure 4-34: MEOX2 induces endothelial cell senescence.

Quantification of the percent senescence in HUVECs 48 hours after transduction with 100, 250 or 500 MOI of adenovirus encoding EGFP or N-terminal FLAG-tagged MEOX2. The number of SA- β -gal positive cells was divided by the total number of cells to obtain the percent senescence. * Indicates a statistically significant change ($p < 0.05$) between MEOX2 and EGFP over-expressing cells at the same viral dose. Error bars represent the standard error of the mean ($n \geq 4$).

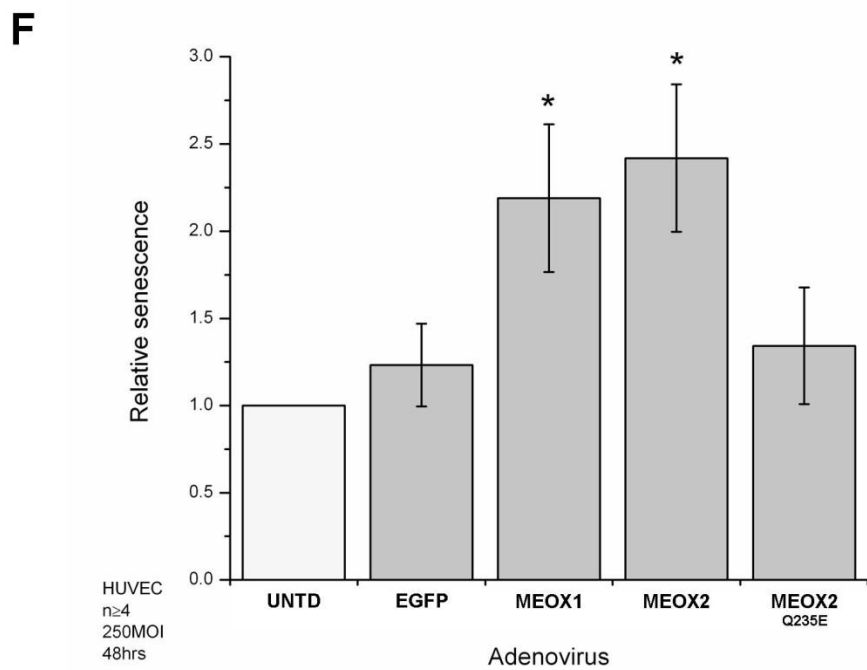
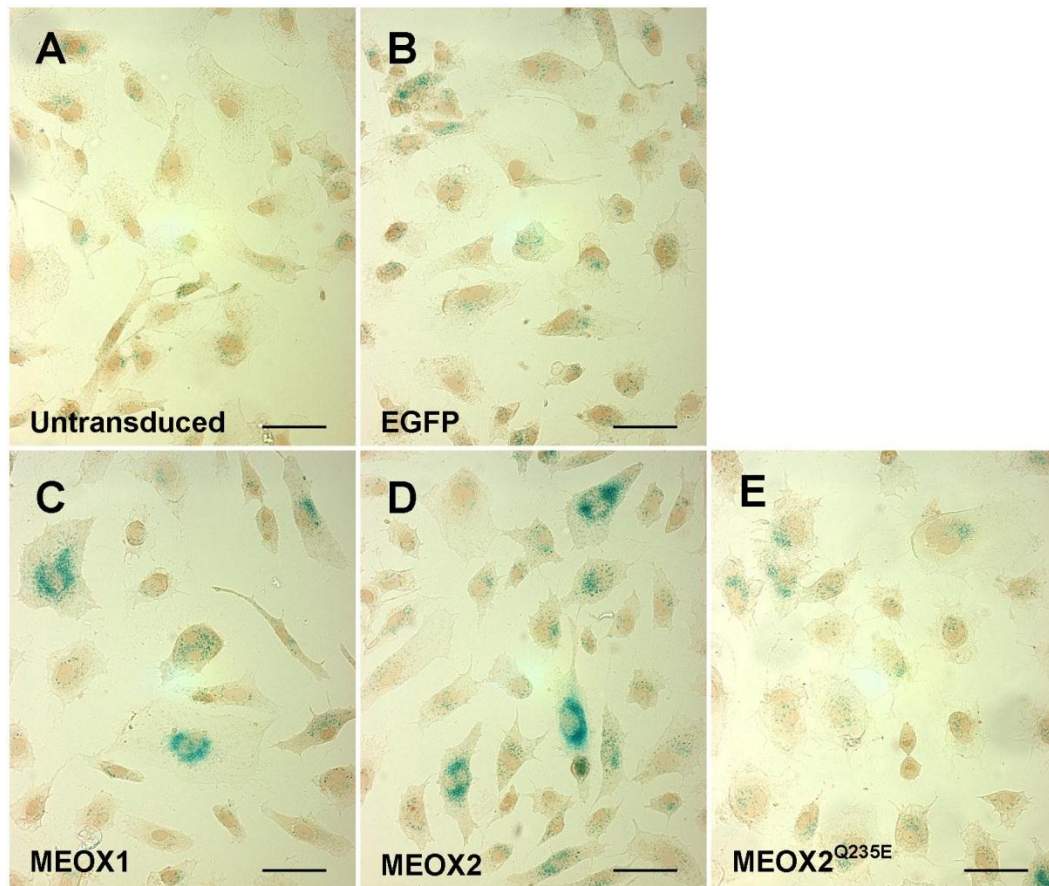


Figure 4-35: DNA-binding dependency of MEOX2 induced endothelial cell senescence.

Figure 4-35: DNA-binding dependency of MEOX2 induced endothelial cell senescence.

(A-E) Representative images showing SA- β -gal⁺ cells (blue). Nuclei were stained with hematoxylin (brown). Scale bars represent 50 μ m. (F) Quantification of SA- β -gal⁺ cells shows that both MEOX1 and MEOX2 expression increased the number of senescent HUVECs. In contrast, MEOX2^{Q235E} expression did not alter the level of endothelial cell senescence. HUVECs were transduced with N-terminal FLAG-tagged MEOX1 and MEOX2 adenoviral constructs at a MOI of 250; 48 hours later cells were fixed and stained. UNTD signifies untransduced HUVECs. * Indicates a statistically significant change ($p < 0.05$) when compared to the EGFP control. Error bars represent the standard error of the mean ($n \geq 4$).

cellular senescence program in HUVECs. Alternatively, MEOX2 may activate other genes that are required for senescence, in a DNA-binding dependent manner.

Since MEOX2 is sufficient to induce senescence, we hypothesized that its expression would also increase with cellular passage. When we compared the mRNA expression of MEOX2 in passage 5 and passage 15 cells, surprisingly we observed a significant (ten-fold) reduction in MEOX2 mRNA expression (Figure 4-36). This finding differs from a previous report that showed MEOX2 mRNA expression is increased in primary human keratinocytes that have undergone numerous population doublings [87]. However, MEOX2 may not be required to maintain senescence; rather it is possible that MEOX2 expression is increased at some point between passage 5 and passage 15 when it induces senescence but that its expression is not maintained. Alternatively, MEOX2 may not play a role in replicative senescence in endothelial cells. Due to the quick induction of senescence (48 hours post-transduction), we hypothesize that the MEOX proteins, similar to RAS over-expression, may induce premature senescence. However, we have not assessed changed in telomere length and thus, cannot exclude the possibility that MEOX induced senescence is related to telomere attrition.

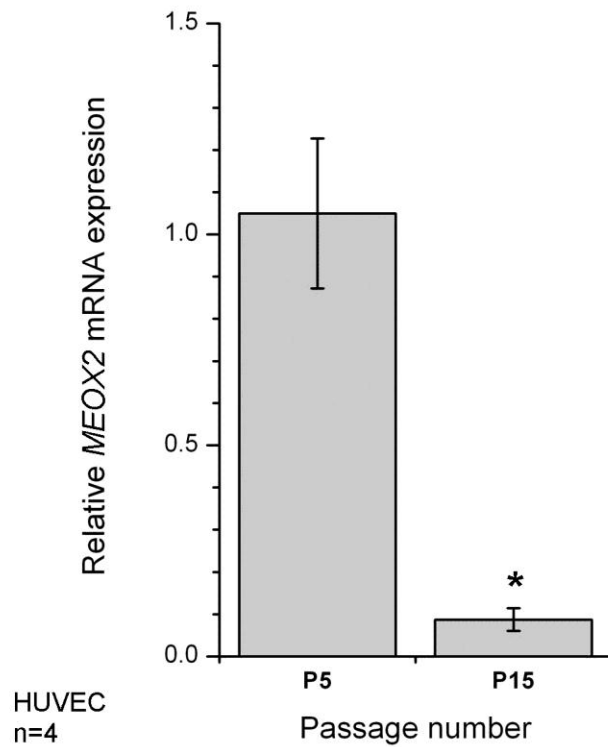


Figure 4-36: MEOX2 mRNA expression is decreased in aged HUVECs.

Total RNA was isolated from passage 5 and passage 15 HUVECs 24 hours after being plated. The relative amount of MEOX2 mRNA was measured by quantitative real-time PCR. *β-actin* mRNA expression was used for inter-sample normalisation. * Indicates a statistically significant change ($p < 0.05$) compared to P5 cells. Error bars represent the standard error of the mean ($n=4$).

4.5. Conclusions and future directions

In summary, we demonstrate for the first time that MEOX1 activates $p21^{CIP1/WAF1}$ and $p16^{INK4a}$ in primary endothelial cells. Our results revealed that the mechanism of transcriptional activation of these CDK inhibitor genes by MEOX1 and MEOX2 is distinct. The MEOX proteins activate $p16^{INK4a}$ in a DNA-binding dependent manner, whereas they induce $p21^{CIP1/WAF1}$ in a DNA-binding independent manner, which requires the SP1 transcription factor. In addition, we discovered that the regulation of the endothelial cell cycle by MEOX1 and MEOX2 may not be limited to transcriptional activation of $p21^{CIP1/WAF1}$ and $p16^{INK4a}$. MEOX1 activates transcription of $p14^{ARF}$. In addition, both MEOX1 and MEOX2 over-expression results in increased levels of p53 protein (Figure 4-37). Finally, we demonstrate that increased expression of the MEOX homeodomain transcription factors leads to cell cycle arrest in G₁ and endothelial cell senescence.

Future studies will focus on identifying the mechanism of MEOX1 induced $p14^{ARF}$ transcriptional activation in EC. In addition, we will determine the mechanism by which MEOX over-expression results in increased p53 expression (e.g. increased translation or protein stability) as well as the transcriptional status of the p53 protein (e.g. active or inactive). Furthermore, we will use *Meox* gene knockout mice (compared to wild-type mice) to study the effects of complete and partial loss of MEOX1 and MEOX2 expression on the angiogenic potential of the vasculature in response to ischemia and growth factor stimulation.

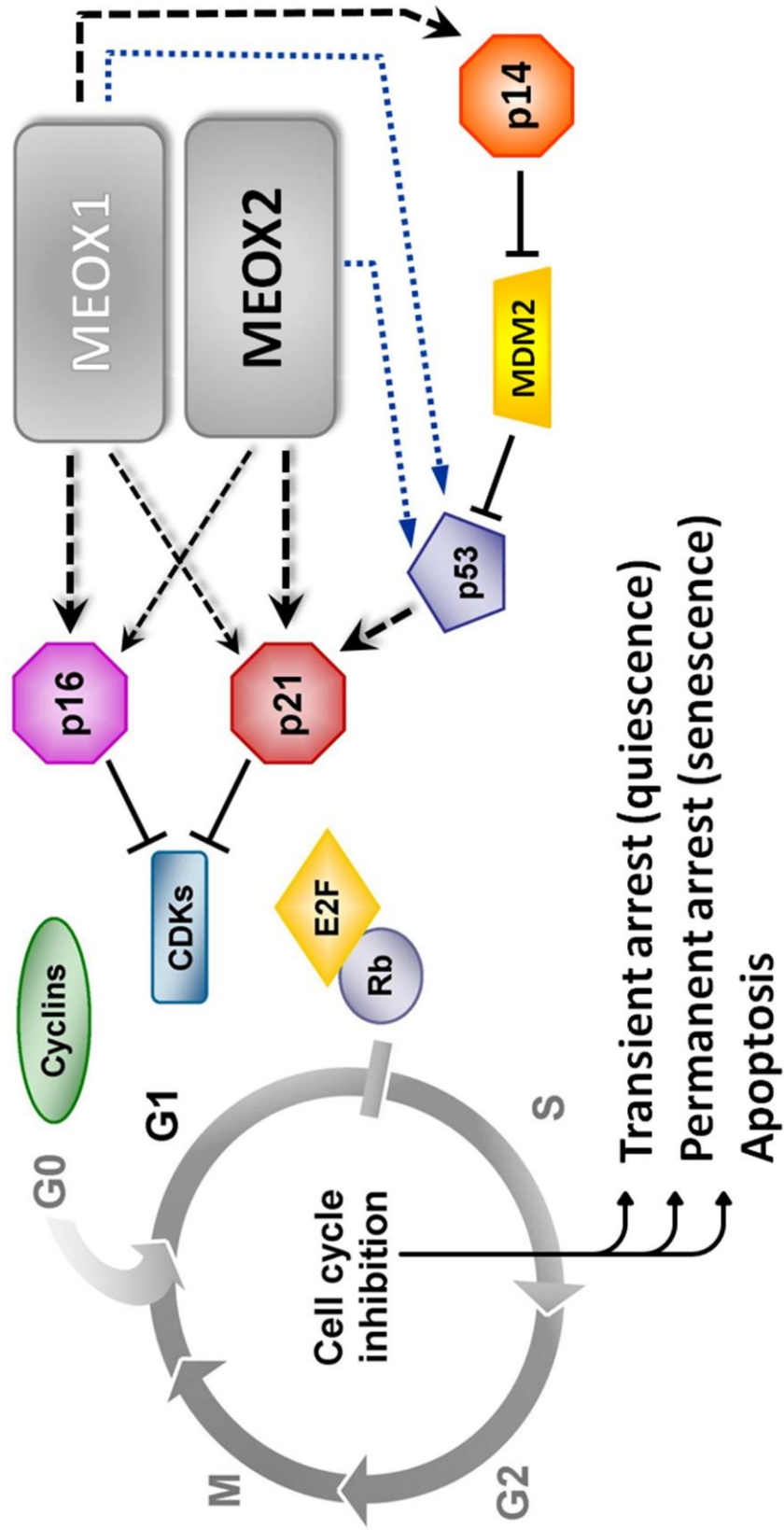


Figure 4-37: Regulation of the endothelial cell cycle by MEOX1 and MEOX2.

Figure 4-37: Regulation of the endothelial cell cycle by MEOX1 and MEOX2.

MEOX1 and MEOX2 increase the transcription of the CDK inhibitors $p21^{CIP1/WAF1}$ and $p16^{INK4a}$ and thereby inhibit cell cycle progression from G₁ to S phase. Activation of $p21^{CIP1/WAF1}$ transcription by MEOX1 and MEOX2 was previously shown to be independent of p53 [156]. However, MEOX1 and MEOX2 increase p53 protein expression. MEOX1 also increases $p14^{ARF}$ transcription, which may potentially increase p53 expression through inhibition of MDM2. Black dashed lines represent transcriptional up-regulation. Blue dotted lines represent post-translational up-regulation.

CHAPTER 5: IDENTIFICATION OF NOVEL MEOX TARGET GENES IN ENDOTHELIAL CELLS

5.1. Introduction

Identifying downstream target genes of the MEOX homeodomain proteins is key to understanding how these transcription factors elicit changes in the phenotype of vascular endothelial cells. The expression of several genes has been shown to be affected by MEOX protein over-expression or knockdown/knockout (Table 5-1). An understanding of how the MEOX homeodomain proteins regulate vascular EC functions has the potential to identify new treatment strategies for diseases that result from vascular dysfunction, such as atherosclerosis and AD. Two different approaches can be used to identify novel direct target genes: the candidate gene approach, which relies on previous observations of differential gene regulation in response to a factor of interest, or the *de novo* unbiased approach, which uses microarrays or direct sequencing to measure differential gene expression in response to a factor of interest.

Table 5-1: Genes that have altered expression levels in response to MEOX over-expression or knockout/knockdown.

	Expression changes	GENE / Alternate name (isoform)	Reference [#]
MEOX1	↑ mRNA	NKX3-2 / BAPX1	Rodrigo <i>et al.</i> 2004 [128]
	↑ mRNA	TBX18	Skuntz <i>et al.</i> 2009 [127]
	↑ mRNA	UNCX	Skuntz <i>et al.</i> 2009 [127]
	↑ mRNA, ↔ protein	CDKN1A / p21 ^{CIP1/WAF1}	Douville <i>et al.</i> 2011 [84]
	↑ mRNA, ↑ protein	CDKN2A (p16 ^{INK4a})	Douville <i>et al.</i> 2011 [84]
	↑ mRNA	CDKN2A (p14 ^{ARF})	Figure 4-26
MEOX2	↑ mRNA	NKX3-2 / BAPX1	Rodrigo <i>et al.</i> 2004 [128]
	↑ mRNA, ↑ protein	CDKN1A / p21 ^{CIP1/WAF1}	Smith <i>et al.</i> 1997 [156] Chen <i>et al.</i> 2007 [89] Douville <i>et al.</i> 2011 [84]
	↑ mRNA, ↑ protein	CDKN2A (p16 ^{INK4a})	Irelan <i>et al.</i> 2009 [87] Douville <i>et al.</i> 2011 [84]
	↓ mRNA, ↓ protein	FOXO4 / AFX	Wu <i>et al.</i> 2005 [171]
	↑ mRNA, ↑ protein	LRPAP1/RAP	Wu <i>et al.</i> 2005 [171]
	↓ mRNA	ITGA2	Markmann <i>et al.</i> 2003 [154]
	↓ protein	ITGB3	Witzenbichler <i>et al.</i> 1999 [158]
	↓ protein	ITGB5	Witzenbichler <i>et al.</i> 1999 [158]
	↓ mRNA	E-selectin	Patel <i>et al.</i> 2005 [170]
	↓ mRNA	VCAM-1	Patel <i>et al.</i> 2005 [170]
	↓ mRNA	ICAM-1	Patel <i>et al.</i> 2005 [170]
	↓ mRNA	CXCL1 / Gro-alpha	Patel <i>et al.</i> 2005 [170]

↑ denotes a significant increase
↔ denotes no significant change
↓ denotes a significant decrease

5.2. Rationale, hypothesis and aims

Wu *et al.* [171] demonstrated that MEOX2 expression is inversely proportional to the expression of the pro-apoptotic gene *FOXO4* in brain ECs. Increased *FOXO4* expression at the mRNA level was observed in brain ECs from individuals with AD (a pathological condition where MEOX2 expression is reduced) and at the protein level in *Meox2*^{+/-} mice [171]. Knockdown of MEOX2 expression in normal human brain ECs leads to increased *FOXO4* mRNA and protein expression [171]. Conversely, ectopic expression of MEOX2 in brain ECs from individuals with AD suppressed *FOXO4* expression at both the mRNA and protein level [171]. This finding suggests that the *FOXO4* gene is a direct target of MEOX2 in ECs and that MEOX2 represses *FOXO4* gene transcription.

FOXO4 is one of only a few genes that have been identified as potential direct transcriptional targets of MEOX2 (Table 5-1). Microarray analysis by Patel *et al.* [170] measured gene expression changes in HUVECs transduced with MEOX2 adenovirus (100 MOI) for 24 hours and identified 242 genes whose expression was changed by greater than two-fold (up- or down-regulated). However, just a subset of these genes (77) was listed and the differential expression of only three genes was verified at the mRNA and protein level by quantitative real-time PCR, western blot and flow cytometry [170]. To our knowledge, the effects of MEOX1 over-expression on gene expression in ECs have not yet been evaluated.

Due to the functional redundancy between MEOX1 and MEOX2 during development, we hypothesized that the majority of genes differentially expressed in ECs over-expressing MEOX1 or MEOX2 would be common to both MEOX transcription factors (e.g. the *FOXO4* gene). Furthermore, since MEOX1 and MEOX2 induce EC

senescence, we postulated that over-expression of the MEOX proteins would regulate genes that promote EC dysfunction.

To address these hypotheses, our aims were to:

- i) Compare the ability of MEOX1 and MEOX2 to repress *FOXO4* gene expression in ECs.
- ii) Identify novel candidate target genes of the MEOX transcription factors using expression microarrays.
- iii) Determine the cellular processes that are affected by MEOX protein over-expression in ECs using gene set enrichment analysis.
- iv) Validate the changes in gene expression observed by microarray.

5.3. Materials and methods

5.3.1. Cloning the *FOXO4* upstream promoter region

The putative *FOXO4* upstream promoter region was amplified by PCR from human genomic DNA that was isolated from HUVECs using the QIAamp DNA Mini Kit (Qiagen) according to the manufacturer's instructions. The primer sequences used were: forward (**MX105**) 5'-GCGGTACCCACACCTAAGGGAGACAGGGAAGGCTG-3' and reverse (**MX106**) 5'-GCGAGCTCGGATCCATACGTGGAGTTGGACCTCCC-3'. The *FOXO4* PCR product was digested with the *SacI* restriction enzyme and the pBluescript II SK + vector was digested with the *SmaI* and *SacI* restriction enzymes, following which they were ligated together. The putative *FOXO4* upstream promoter sequence was then verified by DNA sequencing at the University of Calgary. Subsequently, the *FOXO4* upstream promoter region was removed from the pBluescript II SK + vector by digestion with *EcoRI*, followed by filling of the 5' DNA overhang using the *DNA Polymerase I, Large (Klenow) Fragment*, and subsequent digestion with *SacI* and *BglI*. The pGL4.10[luc2] vector was digested with *KpnI*, followed by removal of the 3' DNA overhang using the *DNA Polymerase I, Large (Klenow) Fragment*, and then subsequently digested with *SacI*. The *FOXO4* upstream promoter region was ligated with the pGL4.10[luc2] vector to create a luciferase reporter construct that is driven by the *FOXO4* upstream promoter region.

5.3.2. Luciferase assays

Luciferase assays were performed as described in Chapter 4, section 4.3.5. The 1622 bp human *eNOS* upstream promoter region, pGL2 enhancer- F1 LUC [243], was obtained from Addgene (Plasmid # 22426).

5.3.3. Quantitative real-time PCR

Quantitative real-time PCR was performed as described in Chapter 4, section 4.3.6. Primer sequences are listed in Table 4-1.

5.3.4. Affymetrix expression arrays

HUVECs (7.5×10^5 /plate) were plated (untransduced) or transduced at 100 MOI with adenovirus encoding EGFP, MEOX1, MEOX2 or DNA-binding domain mutated MEOX2^{Q235} and then plated onto 10 cm tissue culture plates. RNA was isolated from the cells 48 hours after transduction using the RNeasy Plus kit (Qiagen), following the manufacturer's instructions. The RNA concentration, purity and integrity were analyzed using an Agilent 2100 Bioanalyzer. RNA from triplicate transductions/isolations were pooled and then the sample was labelled using the GeneChip 3' IVT Express Kit (Affymetrix). Samples were hybridized to GeneChip Human Genome U133 Plus 2.0 Arrays (Affymetrix) and scanned using a GeneChip Scanner 3000 (Affymetrix). HUVECs from three different lots were used; each array represents a sample of triplicate pooled RNA from the same lot of cells.

5.3.5. Data pre-processing and gene set enrichment analysis

Background-adjustment and inter-array normalization were performed using robust multi-array averaging (RMA) [244]. RMA and all other subsequent quality control and exploratory analyses (MAS5 present calls, hierarchical clustering and principal component analysis) were performed using the statistical software R. Gene set enrichment analysis (GSEA) [245,246] was performed using the following parameters: gene-set database = human gene ontology (GO) annotations, number of permutations = 2000, metric for ranking genes = t-test, maximum gene-set size = 500 and minimum

gene-set size = 10. These max/min gene-set size thresholds were chosen to omit large gene-sets with vague biological meanings and small gene-sets prone to false enrichment due to biological noise [247]. GSEA results were visualized in Cytoscape using the Enrichment Map plugin [247] with the following thresholds applied: p-value = 0.001, false discovery rate (FDR) = 0.2 and overlap coefficient = 0.5.

5.3.6. Western blot

HUVECs (2.5×10^5 cells/plate) were transduced with adenovirus and then plated onto 6 cm tissue culture plates. Cells were harvested and protein samples were prepared, separated by SDS-PAGE and transferred to nitrocellulose membranes as described in section 3.3.4.4. Primary antibodies used for western blot were: rabbit anti-Dyskerin [H-300] (Santa Cruz), rabbit anti-eNOS (Cell Signaling), rabbit anti-phospho eNOS (Thr495) (Cell Signaling), rabbit anti-actin (pan) (Sigma) and mouse anti- α -tubulin [DM1A] (AbCam). Primary antibody dilutions and incubation conditions are listed in Table 3-1. Horseradish peroxidase conjugated secondary antibodies were incubated and detected as described in section 3.3.4.4. Protein band intensities were quantified using the adjusted volume measurement (Adj.Vol.; CNT*mm²) in the Quantity One software (Bio-Rad).

5.3.7. Statistical analysis

Statistical analysis was performed as described in Chapter 4, section 4.3.14.

5.4. Results and discussion

5.4.1. MEOX2 does not regulate *FOXO4* gene expression in HUVECs

Wu *et al.* [171] identified the *FOXO4* gene as being transcriptionally repressed by MEOX2 in brain ECs. In order to determine whether MEOX2 regulates *FOXO4* transcription in ECs, we created a luciferase reporter construct that is controlled by a putative *FOXO4* promoter. This 2928 bp upstream promoter region contains the genomic DNA sequence between -2920 bp and +8 bp, relative to the translation start site of the *FOXO4* gene (Figure 5-1). We tested the ability of MEOX2 to regulate transcription from this upstream promoter region in HUVECs and found that transcription from this promoter was unchanged in the presence of MEOX2 (Figure 5-2, panel A). As the transfection efficiency of HUVECs is low, we decided to repeat these luciferase assays in HEK293 cells. Surprisingly, we demonstrated that MEOX2 activated instead of repressed transcription from the putative *FOXO4* promoter in HEK293 cells (Figure 5-2, panel A). This finding is contrary to our hypothesis (that MEOX2 would repress *FOXO4* transcription, rather than activate it), and thus we speculated that the regulation of *FOXO4* gene expression by MEOX2 may be cell type specific, or that this putative upstream promoter region is not involved in MEOX2 regulation of *FOXO4* expression in ECs.

To test the latter theory, we used quantitative real-time PCR to measure the level of endogenous *FOXO4* mRNA in HUVECs. We did not observe any changes in *FOXO4* mRNA expression when MEOX2 was over-expressed via adenoviral transduction of HUVECs (Figure 5-2, panel B). Therefore, we concluded that MEOX2 does not regulate *FOXO4* gene transcription in HUVECs. The difference between our results and the

CACACCTAAGGGGAGACAGGGGAAGGCTGAATAGGAGTTTTCCAAAAATAAGAGACGTGGAGAGGAAATGACAAG
AGGGATGATATCCCAGGATGCAGAGAGAAAAGGTATAAAAAGGGCATGGTATTTCCAGGAAATAGTGTGAAAC
TCTGCTTGTAACTTAGTGTGCAGGAAAAGGTGTGAAGTGGCCTGAATCTGAGGAGCCTGGCATGCCTTGCTA
GGGAATTTGAACTTTATCACACAGGCAATGGGGAAAAATCAGAGGAAGATTTAACCCAGGGAAATTAATCATGAT
CAAAAAAACAAAATTTATAGCCAGGCGCGGTGGCTCATGCCTGTAATCCCAGCACTTTTCCAGGCAAGGC
AGGTGGATCACTTGAAGTCAGGAGTTCAGACCAGCCTGAGCAACACGGTGAACCCCGTCTCTACAGAAA
ATACAAAAATTAAGCTGGGCGTGGTGGCACATGCCTGTAGTCCCAGCTACTCCCGAGGCTGAGATGGGAGGA
TTGCTTGAGTGCAGCAGGTCAAGGCTGCAGTGAAGCAAGATCACACCACTGCATTCAGTCTGAGTGCAG
AGCAAGACCCTGTCTCAAAAAAGAAGGAAAAGAAGGAAGGAAGGAAGGAAGGAAGGAAGGAAGGAAGGAAGGA
AAGGAGAAAAGAAAAGAAAAGAAAAGAAAAGAAAAGAAAAGAAAAGAAAAGAAAAGAAAAGAAAAGAAAAG
AGGAAGGAGAAAAGAAAAGAAAAGAAAAGAAAAGAAAAGAAAAGAAAAGAAAAGAAAAGAAAAGAAAAGAAA
ATTAATACGATCGCATGTAAGTTATATAATCCCAGTTCCTGCTCGTTGGGCAAGTCAATCTCTGAGCATTTGT
TAGTGTCTTCATCTATAAAAATGCGGATAATAGTGGTACCTACCTCATGGGGTTGAATTTGAGGAGTAAATGA
TTGAGGAGTAAATGAATTAATGTTTCGTAAGCAATTTTTCACAGAGACTGGCACATAATTAAGGGCTCCATAA
ATTTTAGCCATAATTAATCCAGACATGTTTCTTAGAACGGTAACCTTGCTGGCAGCTCTGAATATAAACTGTA
GTGAGGTAAGACTGATGGAAGGAGATCCAATTAAGATGATACTGCACCTTTTTTTTTTTTGTACAGGGGTG
TTATTCTGTCAACCAGGCTGGAGCACAGTGGCATGATCTTGGCTCACTGCAACCTCCACTCTTGGGTTCA
AGGACTCTCCACCTCAGCCTCCAAGTAGCTGGGACTACAGGTGCGTGCCCCACACCAGGCTAATTTTTT
CTATTTTTAGCAGAGATGGGTTTACCATGTTGGCCAGGCTGGTCTCAAACCTCTGACCTCAAGTGATCCG
CCTGCCTGCACCTCCCAAAGTGCTGATATTAAGGGCTCAGCCACTGCACCCGGCTGATCTCAATTAATTTAA
ATGCAGTTATAAATAGGTCTTGAACCTGGGATTTGGATGTAGAAAAGTTACGGAGATGAAGAAGTAATGGGTA
ATTAATCTAAGCTGTCTGCTTGGAGCTTGGGAGACTGGGTAGATCAGGACTACCATAAGTCAAATTCAGAG
ATAAGGGTAGCCAGAGGATAGGGGTGCGGGTGCAGGAACAGATAATGAGTTTTGGACCTGTTGAATGAGAA
TGAAGCCGTTGGAGATGTGAACCTGGAGAATATCGGTGTTGAAGGGAAAAGCCAGAAGAGCCAGTGGAGGAA
ACTGATTGGTAAGTGAACCTCACTGTCAAGTGGGAACTGCATATGGGGGGATGAAAGGCGGGTGGAGGGAGG
AGGAAGGGGGTGGAGGGAACACCACCGTGGGCTAACCATTTGTTTATGTTACACAAGCCCCCACCCAAC
TCTCCAACGTGCATACATCCTATTTTTCTAGTCAGTTCCTTGCTTCTTGCTTCTTGGTCTCCTGCATCTTTA
AGAGAAATATTTTTCCCTTTTGGCGTCTCCTAAATGAAGGAGGGAAAAGGGCTAGCACCTCTCAATCTGGT
CACCTACAGACTCTGAATCACAAAGGGAGACAATGGAAAAGGGGAAAAGGGCGAAAAACGATTCTTAAGAAA
AGAAAAGAGTCCGCGACGACTTCAATAATTAAGTTCACCTCGTTATATCCTGCCACGCGGCTCTCCTGC
CGCCGTATCGGGCTCCTGGCCGGAAGCAGGACGGGAGATGTAGTCTCAAGAGTGACCAGGGGTGGCACGA
CTGCAGAACTCGGTTTTCCGACTGGCTTTTCAGGGCGGTGCGCAGATGGCTGCCCGGCGAGTGGTAAACA
GAGCAGTCAGGAGGGGGCTGCTGCTTGGAGCAAAAACAAAAGGGGAAAACCCGGGGGGGGGGGGGGGGGGGG
TTGATAGGGGAATCGGTGCGGGAATAAGGGAGGCGCAGCCGCGGGGACCCGGACCCTAGTAAGAGTGGCG
AGAAGGGAAAGAGGGGGGGAAGGGGGAGTCAGGGGAGGGGCAAGTGACCGGGGGGAGCGGGGGCTGGGGGA
GGGCAGCAATCCGGGTGGAGGAAAATTTGGGAGGAGTGTCCGGGGGGCAGCAACTTAAGGGGGGAGGGGAA
TGCGGCTAAGGAGACGTTCCGGTGTGGGAGCGCAATATATGAGGGGATACAGTGCCTCAGGTTTTAAAAGAG
CAGGAAGCTGAGTGAGAGGTTGCAGAAAAAGTGTCTTCGCTCGGCAGAGGTTACAGGTGGCATCTCAGAAA
GAGCTTTGAGGCTACAGGCTGTAGTCCGGAAGGGGATCGGAGAACTGTGTGAAGGGACAGCTTAGGGACTA
GCGTCTTGGGACTAGGGGGGAAGTTCGCGACTTTCTGAAGACTGGCAGGAATGTGCCTCCTGGCCCTCGATG
CTTCCCCCTGAGGGGAGGCATCGTGAGGGACTGTGGCAGGCTTCACTGAACGCTGAGCCGGGGAGGTTCA
ACTCCACGTATGGATCC

ATGGATCC
 TLS

Figure 5-1: DNA sequence of the putative 2928 bp human *FOXO4* promoter.

Potential transcription factor binding sites are shown; homeodomain binding sites (red) and SP1 binding sites (green). The transcriptional start site (arrow) is indicated in orange and the translational start site (TLS) is indicated in blue.

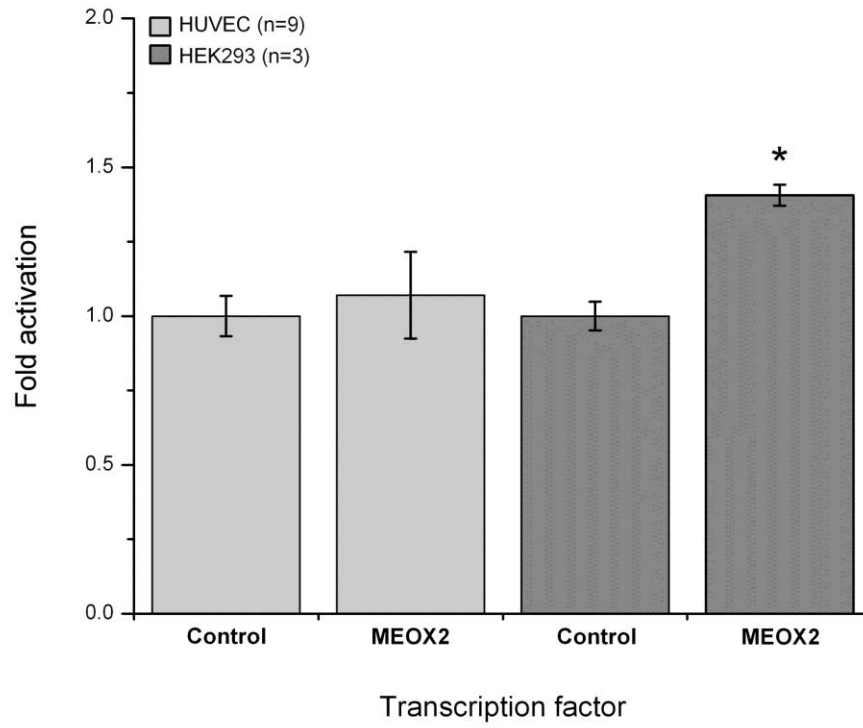
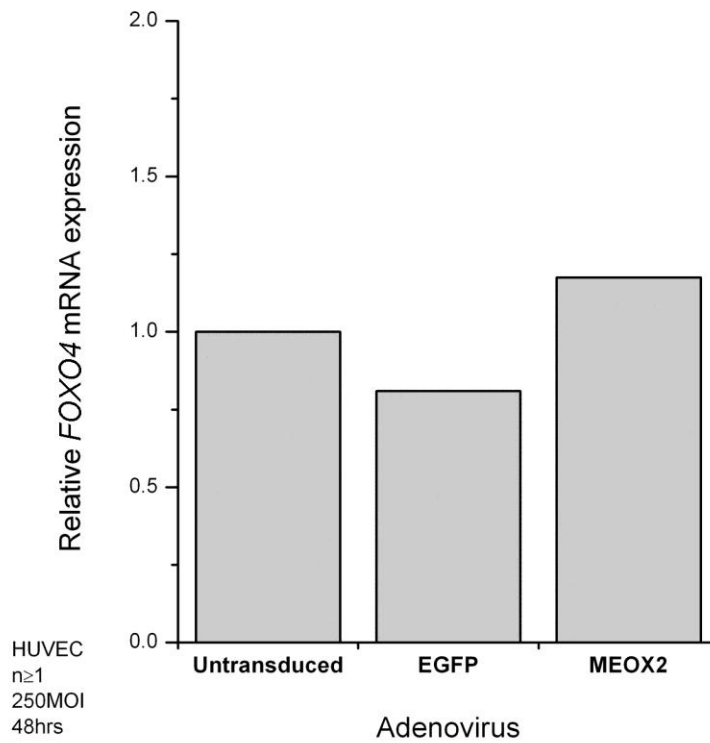
A**B**

Figure 5-2: MEOX2 does not regulate *FOXO4* transcription in HUVECs.

Figure 5 2: MEOX2 does not regulate *FOXO4* transcription in HUVECs.

(A) MEOX2 did not alter transcription from the 2928 bp *FOXO4* upstream promoter region in HUVECs. However, MEOX2 modestly activated transcription from the 2928 bp *FOXO4* upstream promoter region in HEK293 cells. * Indicates a statistically significant change ($p < 0.05$) compared to the empty vector control. Error bars represent the standard error of the mean (n=9 (HUVEC), n=3 (HEK293)). (B) Over-expression of MEOX2 in HUVECs had no effect on the level of *FOXO4* mRNA expression. HUVECs were transduced at 250 MOI for 48 hours, following which total RNA was isolated and the relative amount of *FOXO4* mRNA was measured by quantitative real-time PCR. β -*actin* mRNA expression was used for inter-sample normalisation. (n \geq 1).

previous study by Wu *et al.* [171] may be due to the type of ECs used: microvascular brain ECs versus macrovascular umbilical vein ECs. EC gene expression differs depending on the type (vein, artery or lymphatic), size (macrovascular or microvascular) and tissue origin of the vessel in which they reside [1,3]. It is possible that MEOX2 requires a transcriptional co-repressor in order to inhibit *FOXO4* gene expression and that this co-repressor is expressed in brain ECs but not in HUVECs.

5.4.2. Identification of novel endothelial MEOX target genes

Identification of MEOX target genes is key to determining the function of the MEOX proteins within the vasculature. Our microarray experiment was designed to answer the following question: what are the global gene expression changes in human ECs in response to MEOX protein over-expression? By using mRNA expression microarrays to identify genes that were directly and indirectly regulated by MEOX homeodomain protein over-expression in HUVECs, we would be able to discover cellular pathways, processes and functions that are regulated by the MEOX proteins in ECs. Over-expression of MEOX proteins in HUVECs was achieved using adenoviral transduction. As such, adenovirus encoding EGFP was used as a control for the effects of viral transduction. Furthermore, RNA from untransduced HUVECs was used as a baseline control. An overview of the microarray experiment is depicted in Figure 5-3.

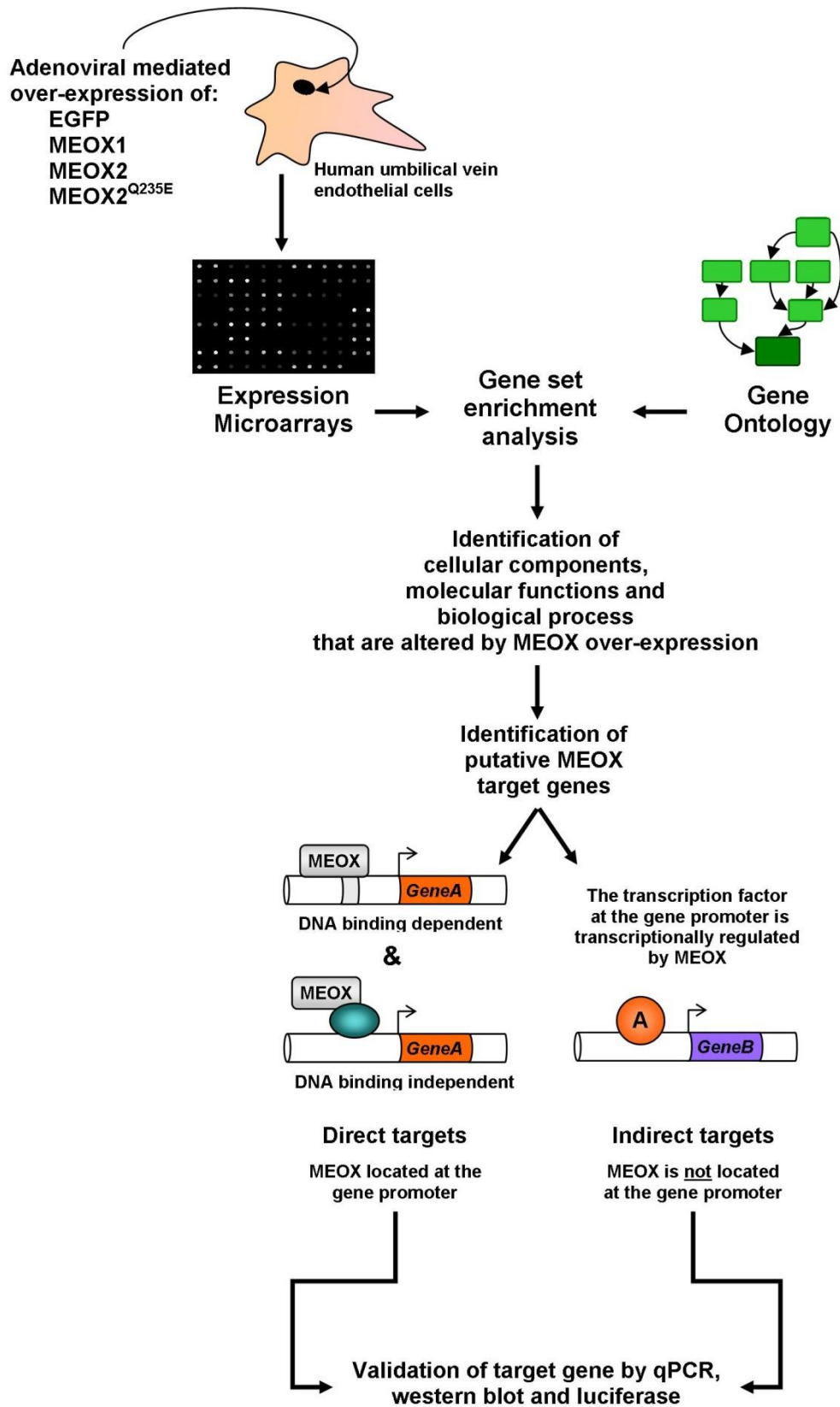


Figure 5-3: Diagrammatic overview of the microarray experiment.

Figure 5-3: Diagrammatic overview of the microarray experiment.

Expression microarrays were used to identify genes that are (directly or indirectly) affected by MEOX homeodomain protein over-expression in HUVECs. Gene-set enrichment analysis was used to identify cellular pathways, processes and functions that are influenced by the MEOX proteins in ECs. Candidate genes were validated by quantitative real-time PCR, western blot and luciferase analysis.

5.4.2.1. *Preliminary microarray data analysis; quality control and exploratory analysis*

The quality of the microarray data were analyzed by comparing the similarity of the robust multi-array average (RMA) signal distribution (Figure 5-4, panel A) and MAS5 present call ratios (Figure 5-4, panel B) for each sample. Disproportions in these parameters are an indicator of sample preparation or hybridization problems. The distribution of the RMA signals was nearly identical between all samples (Figure 5-4, panel A). This was not unexpected as RMA processing of the raw hybridization intensity values incorporates a normalization step to correct for signal distribution differences among samples. The percentage of MAS5 present calls was similar between all samples (Figure 5-4, panel B), indicating that approximately the same number of genes were expressed in the various samples. These measures indicated that the data were not biased by technical issues and that instead the gene expression differences are reflective of biological changes.

The samples were then analyzed using hierarchical clustering (Figure 5-4, panel C) and principal component analysis (PCA) (Figure 5-5). These explorative analyses were used to assess whether the obtained data reflected the experimental design. Hierarchical clustering of microarray samples (Figure 5-4, panel C) showed that the samples were not well separated according to class (Table 5-2 lists the experimental design classes). The dendrogram illustrates that the expression profiles of the transduced cells from the first microarray were more similar to the untransduced HUVECs than to the transduced cells from the second and third arrays. However, with the exception of the samples from the first microarray, the biological replicates clustered together, separated from the replicate

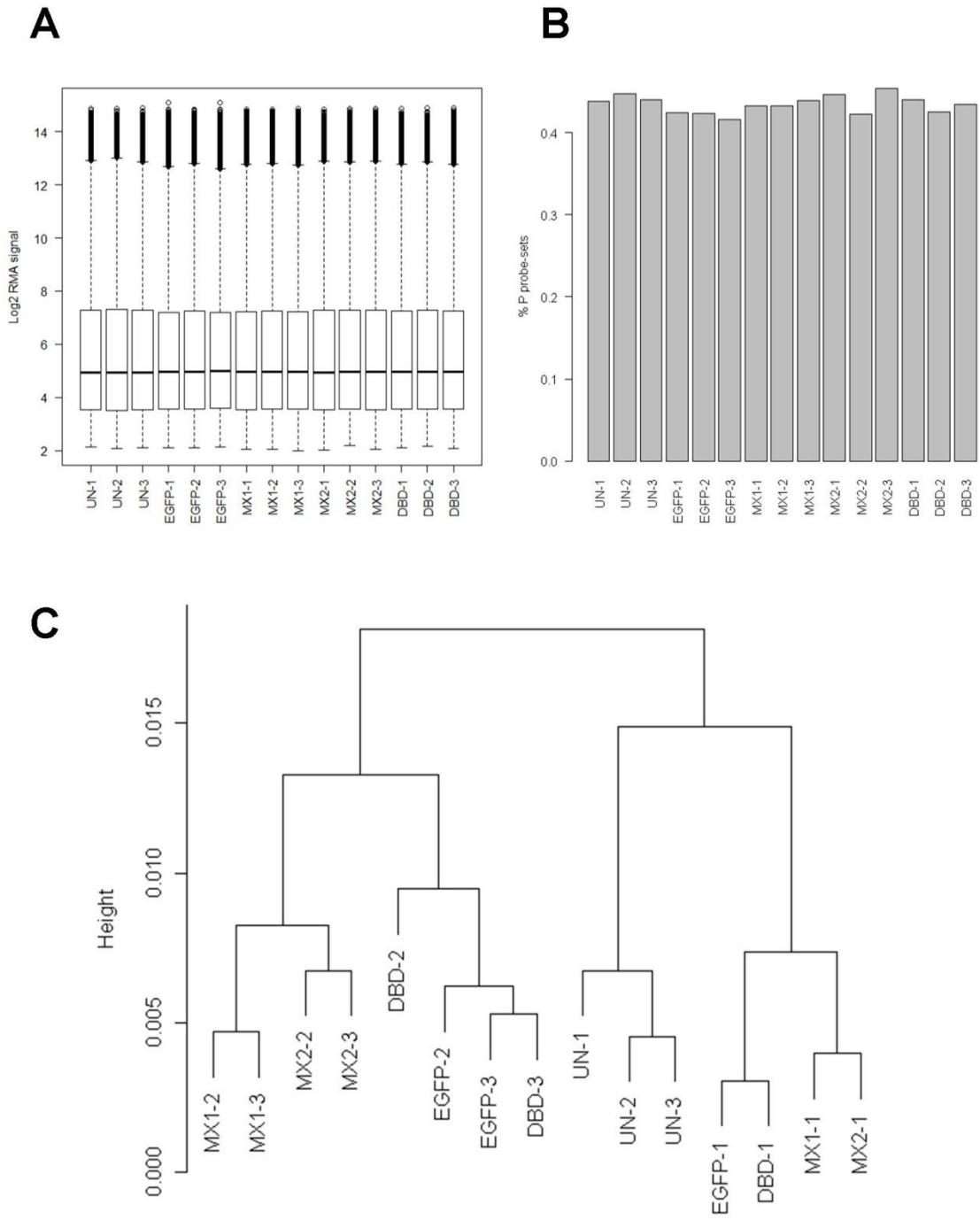


Figure 5-4: Microarray quality control.

Figure 5-4: Microarray quality control.

(A) Per-sample distribution of the RMA signals in log₂ scale. The distributions of the RMA signals were nearly identical between all samples. (B) The percentage of MAS5 detection present call (P) probe-sets is similar between all samples. (C) Hierarchical clustering of microarray samples. The dendrogram illustrates that the expression profiles of the transduced cells from the first microarray set (EGFP-1, MX1-1, MX2-1 and DBD-1) are more similar to the untransduced cells (UN) than to the transduced cells from the second and third set of arrays.

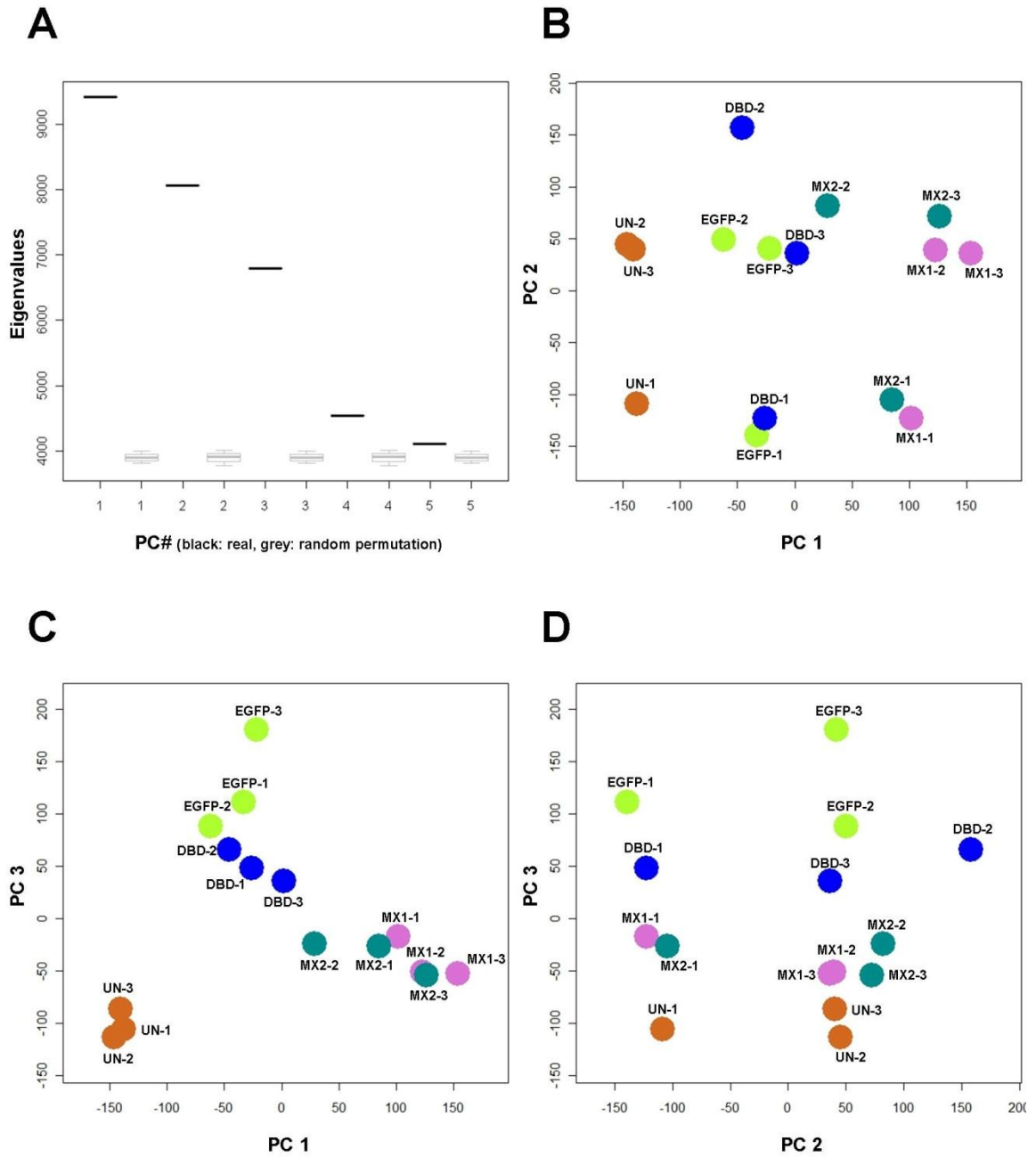


Figure 5-5: Principal component analysis of microarray samples.

Figure 5-5: Principal component analysis of microarray samples.

(A) Comparison of Eigenvalues from transduced HUVEC and randomized data as a means of identifying significant principal components. The Eigenvalue diagram, demonstrates that three principal components (PC) explain an amount of variability within the HUVEC samples that is larger than the randomized control. (B) PC 1 versus PC 2. (C) PC 1 versus PC 3. (D) PC 2 versus PC 3. PC 2 explains the variability caused by lot specific differences in HUVECs, while PC 1 and PC 3 explain the variability caused by adenoviral transduction and specific protein over-expression, although it is not clear which PC represents each factor.

Table 5-2: Overview of the experimental design classes.

	Sample classes	Number of technical replicates per biological sample	Number of biological replicates
UN	Untransduced HUVECs	3	3
EGFP	Enhanced green fluorescent protein	3	3
MX1	Wild type MEOX1	3	3
MX2	Wild type MEOX2	3	3
DBD	DNA-binding domain mutated MEOX2 ^{Q235E}	3	3

samples in the other classes. It is interesting to note that the expression profiles of HUVECs over-expressing DNA-binding domain mutated MEOX2^{Q235E} were more similar to the EGFP transduced control cells than to HUVECs over-expressing wild-type MEOX2. Furthermore, the expression profile of samples from HUVECs over-expressing MEOX1 or MEOX2 were segregated from the EGFP expressing cells.

PCA revealed similar findings to the hierarchical clustering dendrogram, where sample classes were loosely formed into groups and biological replicates were not always clustered. As demonstrated by the Eigenvalue diagram (Figure 5-5, panel A), three principal components (PC) explained an amount of variability within the HUVEC samples that was larger than the variability within the randomized control. By plotting these PCs versus each other, we clearly saw that PC 2 explained the variability caused by the different lot of HUVECs used for each biological replicate (Figure 5-5, panels B and D). Specifically, the lot of HUVECs used for the first set of microarrays was intrinsically very different from the two lots of HUVECs used for the second and third sets of arrays. When PC1 and PC3 were plotted versus each other (Figure 5-5, panel C), the transduced samples clustered together, segregated from the untransduced samples. Furthermore, the triplicate samples from each of the transduced sample classes were grouped together, with MEOX1 and MEOX2 transduced HUVEC samples showing little inter-class variability. Thus, PC 1 and PC 3 explain the variability caused by adenoviral transduction and specific protein over-expression, although it is not clear which PC represents each factor. Taken together, it can be inferred that the lot of cells, viral transduction and protein over-expression were all experimental factors that exerted a major influence on gene expression. The results of PCA did not fit well with the design

expectations as multiple factors influenced the observed gene expression changes in our experiment. Consequently, we anticipated difficulty in distinguishing which genes are truly affected by MEOX protein over-expression and which are due to other factors such as viral transduction. Furthermore, as multiple factors can influence the expression of the same gene, we surmise that some effects of MEOX protein over-expression may have been masked.

As a further measure of microarray reliability, we compared the relative expression of the known target genes *CDKN1A* (encodes $p21^{CIP1/WAF1}$) and *CDKN2A* (encodes $p16^{INK4a}$ and $p14^{ARF}$) by both microarray hybridization and quantitative real-time PCR from the same triplicate pooled RNA samples. Both methods yielded similar results (Figure 5-6), supporting the accuracy of the microarray sample preparation and hybridization. Relative to the EGFP control, we observed a trend for MEOX1, MEOX2 and DNA-binding domain mutated MEOX2^{Q235E} to induce $p21^{CIP1/WAF1}$ expression (Figure 5-6, panels A and C). However, with the exception of MEOX2 induced $p21^{CIP1/WAF1}$ expression as assessed by microarray hybridization, these apparent increases were not statistically significant, (Figure 5-6, panels A and C). This lower activation of $p21^{CIP1/WAF1}$ transcription is likely due to the smaller viral dose used for the microarray experiments (100 MOI versus 250 MOI used in Chapter 4, section 2). We chose to use 100 MOI for the microarray experiments to minimize the effects of viral transduction on EC gene expression. Nevertheless, viral transduction had a significant effect on the expression of $p21^{CIP1/WAF1}$ (Figure 5-6, panels A and C). The expression of $p16^{INK4a}$ was only affected by MEOX1 over-expression in HUVECs (Figure 5-6, panels B and D). It should be noted that the 207039_at probe set detects both the $p14^{ARF}$ and $p16^{INK4a}$

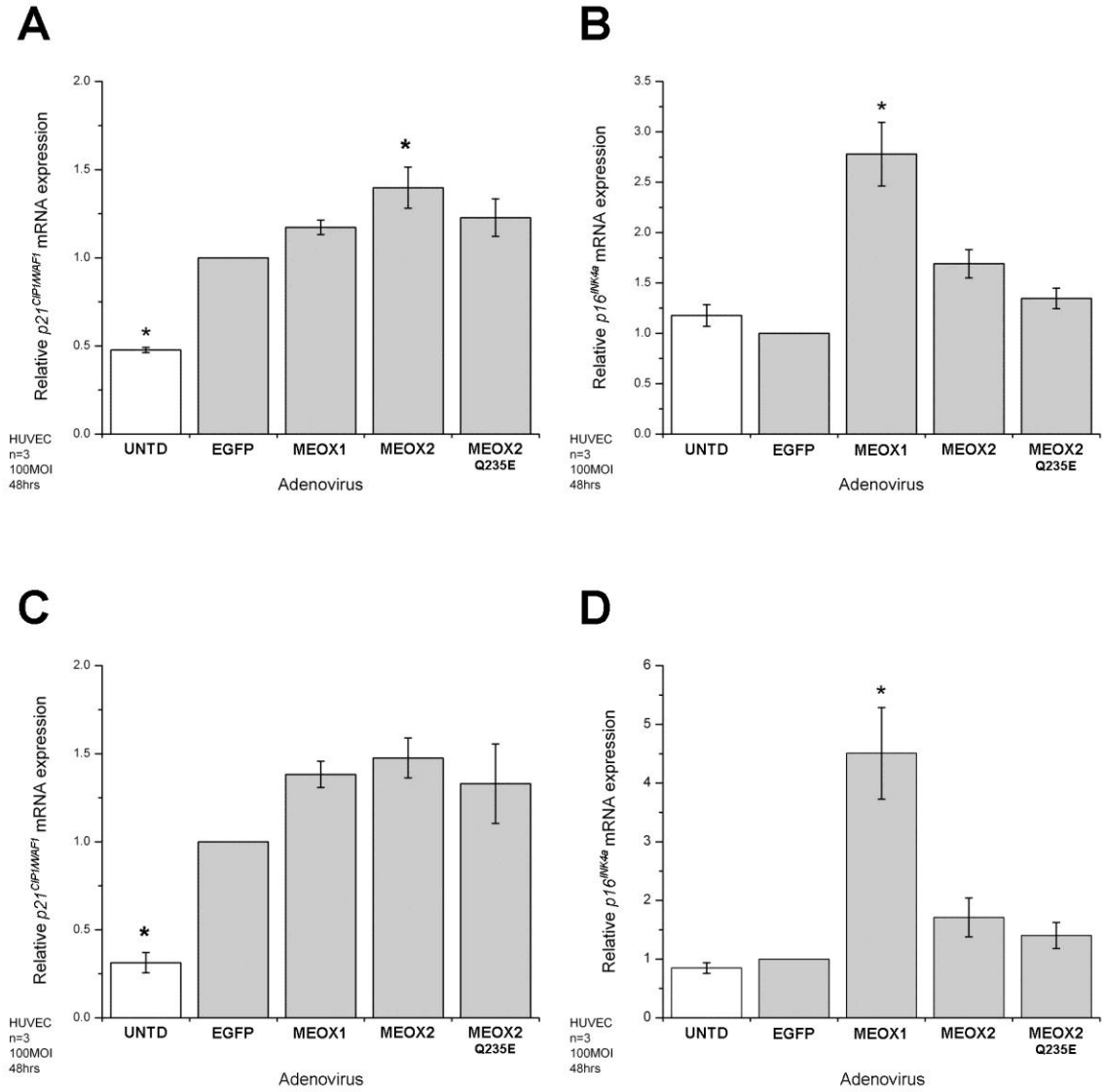


Figure 5-6: Relative expression of $p21^{CIP1/WAF1}$ and $p16^{INK4a}$ mRNA as measured by microarray hybridization and quantitative real-time PCR.

Figure 5-6: Relative expression of $p21^{CIP1/WAF1}$ and $p16^{INK4a}$ mRNA as measured by microarray hybridization and quantitative real-time PCR.

The same RNA samples were used for quantitative real-time PCR and microarray hybridization. (A and B) The relative level of $CDKN1A/p21^{CIP1/WAF1}$ (A) and $CDKN2A/p16^{INK4a}/p14^{ARF}$ (B) mRNA expression as measured by microarray. The linear expression values were normalized to EGFP for each array. Data are representative of the fluorescence values for the Affymetrix probe sets 202284_s_at ($CDKN1A/p21^{CIP1/WAF1}$) and 207039_at ($CDKN2a/p16^{INK4a}/p14^{ARF}$). (C and D) The relative $p21^{CIP1/WAF1}$ (C) and $p16^{INK4a}$ (D) mRNA expression was measured by quantitative real-time PCR. β -actin mRNA expression was used for inter-sample normalisation. * Indicates a statistically significant change ($p < 0.05$) from the EGFP control. Error bars represent the standard error of the mean (n=3 (A), n=3 (B), n=3 (C), n=3 (D)).

transcripts, while the quantitative real-time PCR primers are specific to the *p16^{INK4a}* transcript. Regardless, we obtained similar results, likely owing to the fact that MEOX1 activates transcription of both transcripts at 48 hours post-transduction (Figure 4-19; Figure 4-25, panel B), while MEOX2 does not. Furthermore, unlike *CDKN1A/p21^{CIP1/WAF1}*, we did not detect an effect of viral transduction on *CDKN2A/p16^{INK4a}/p14^{ARF}* expression (Figure 5-6).

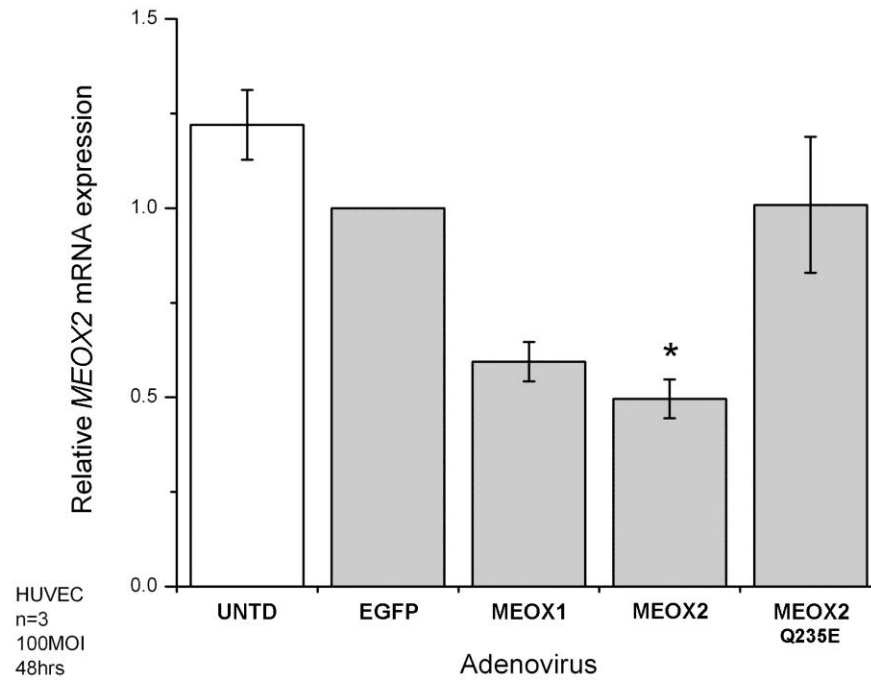
5.4.2.2. *Discovery of a MEOX2 negative feedback loop*

As viral transduction alone significantly impacted gene expression and endogenous *MEOX2* expression was decreased in response to cellular stress (such as siRNA transfection; Figure 4-26, panel B), we assessed whether adenoviral transduction of HUVECs affected endogenous *MEOX2* expression. Accordingly, we measured the levels of endogenous *MEOX2* mRNA expression in the different virally transduced HUVECs using PCR primers specific to the 5' UTR of *MEOX2* mRNA. Since the *MEOX2* adenoviral construct does not contain the 5' UTR, exogenous *MEOX2* mRNA expression is not detected using these primers.

As we surmised, viral transduction trended toward decreased endogenous *MEOX2* expression in HUVECs (Figure 5-7, panel A). However, surprisingly, we also saw that compared to EGFP over-expressing cells, *MEOX2* over-expression resulted in significantly decreased endogenous *MEOX2* mRNA expression (Figure 5-7, panel A). This negative feedback was dependent upon the ability of *MEOX2* to bind DNA, as over-expression of DNA-binding domain mutated *MEOX2*^{Q235E} did not alter endogenous *MEOX2* expression (Figure 5-7, panel A). When we compared the quantitative real-time PCR results to the microarrays, we observed a similar outcome (data not shown). We also determined from the microarrays that unlike *MEOX2*, the expression of *MEOX1* was unaffected by either viral transduction or by *MEOX* protein over-expression (Figure 5-7, panel B).

To confirm our results, we repeated the quantitative real-time PCR analysis with RNA isolated from transduced HUVECs. The expression of endogenous *MEOX2* was significantly decreased in *MEOX2* transduced HUVECs, as compared to EGFP, *MEOX1*

A



B

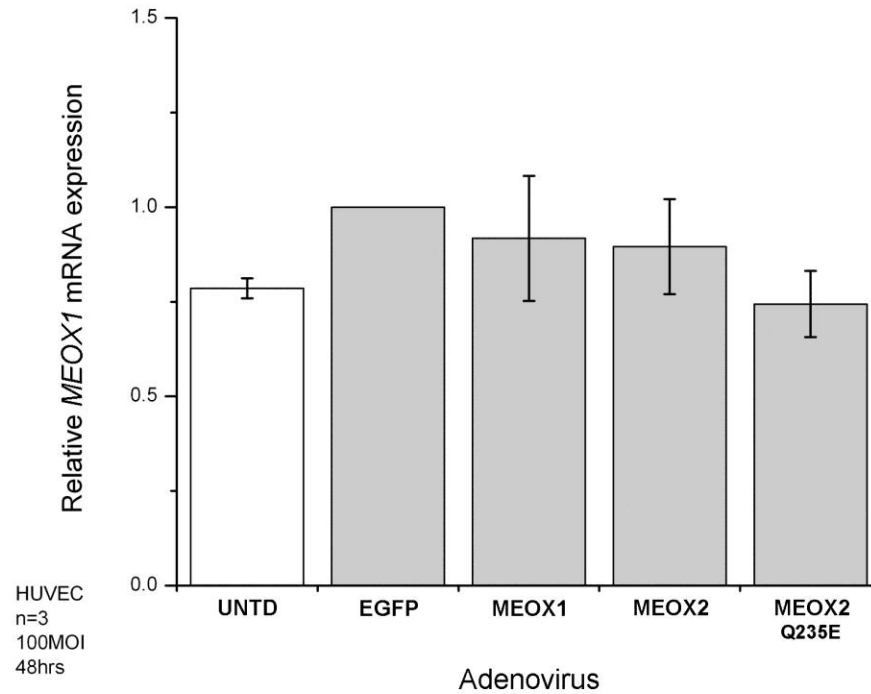


Figure 5-7: Endogenous *MEOX2* expression in HUVECs is decreased by ectopic *MEOX2* protein over-expression.

Figure 5-7: Endogenous *MEOX2* expression in HUVECs is decreased by ectopic *MEOX2* protein over-expression.

(A) Relative *MEOX2* mRNA expression was measured by quantitative real-time PCR. *β-actin* mRNA expression was used for inter-sample normalisation. The same RNA samples were used for quantitative real-time PCR and microarray analysis. (B) The relative level of endogenous *MEOX1* mRNA expression in transduced HUVECs, as measured by microarray. Endogenous *MEOX1* expression is unaffected *MEOX* protein over-expression. In contrast, endogenous *MEOX2* expression is affected by wild-type *MEOX2* protein over-expression. The microarray linear expression values were normalized to EGFP. Data are representative of the fluorescence values for the Affymetrix probe set 205619_s_at (*MEOX1*). * Indicates a statistically significant change ($p < 0.05$) from the EGFP control. Error bars represent the standard error of the mean (n=3 (A), n=3 (B)).

and DNA-binding domain mutated MEOX2^{Q235E} over-expressing cells (Figure 5-8, panel A). Furthermore, ectopic MEOX2 repressed endogenous *MEOX2* transcription in HUVECs in a time dependent manner (Figure 5-8, panel B). These findings suggest that the *MEOX2* gene is a transcriptional target of MEOX2 homeodomain protein repression and that this occurs via a DNA-binding dependent mechanism. ChIP experiments will be required to determine whether the *MEOX2* gene is a direct transcriptional target of its own gene product, or whether there are intermediate factors involved in this negative feedback loop.

It is interesting that MEOX1 does not affect its own transcription in ECs and that there may not be any reciprocal gene regulation between *MEOX1* and *MEOX2*. Similarly during development [127], the loss of one MEOX family member does not result in compensation though the increased transcription of the other family member in ECs. Furthermore, the discovery of a MEOX2 negative feedback loop suggests that maintaining the correct level of MEOX2 expression in vascular ECs is critical to the proper function of the vasculature. Indeed, there are diseases that are associated with increased (HGPS) or decreased (AD, hepatic portal hypertension) MEOX2 expression and are also characterized by impaired vascular function [171,181,185]. Positive and negative homeodomain transcription factor feedback loops have been described; however, positive autoregulation appears to be a much more common mechanism. Nevertheless, the CDX2 homeodomain protein (ANTP class) was shown to cell type specifically repress its own expression via a TAAT motif within the proximal upstream promoter region of the *CDX2* gene [248].

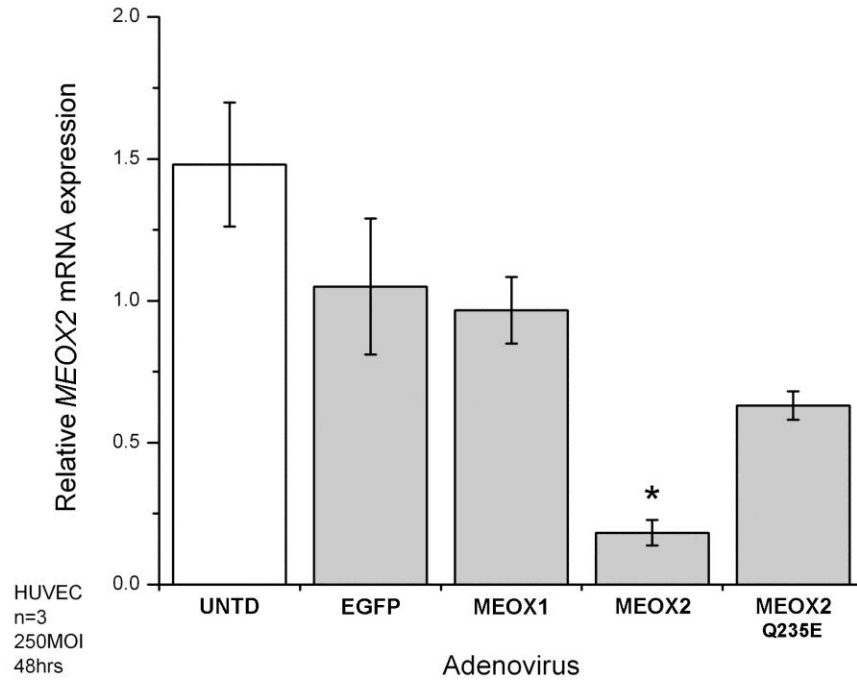
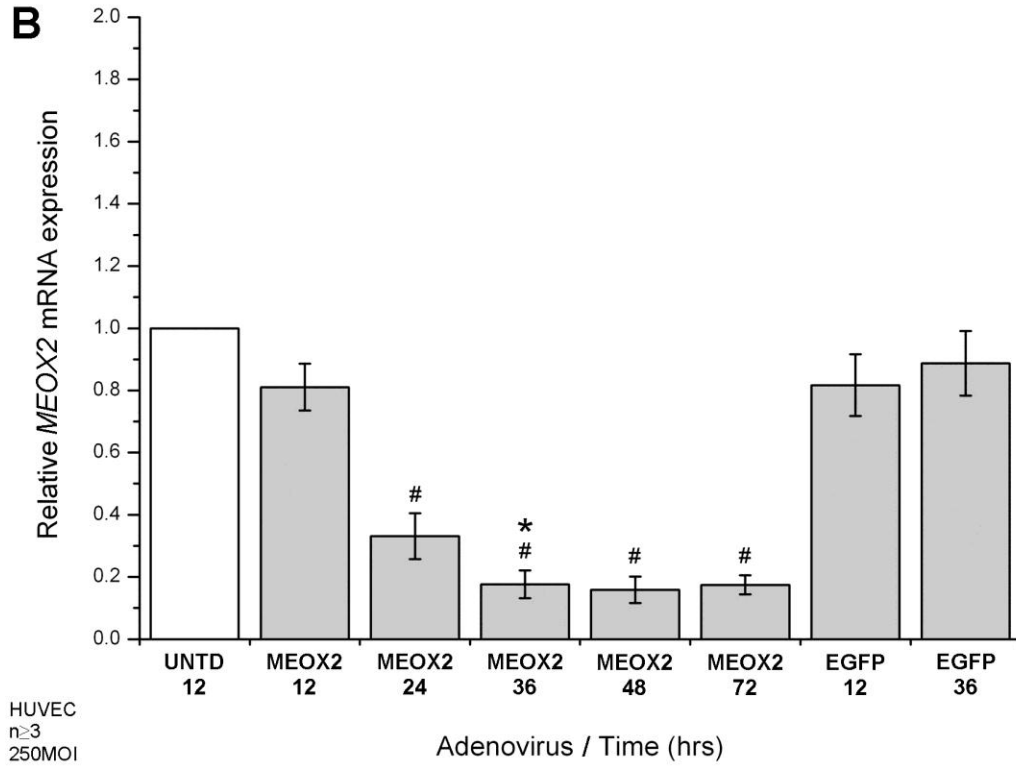
A**B**

Figure 5-8: MEOX2 time-dependently down-regulates its own mRNA expression in HUVECs.

Figure 5-8: MEOX2 time-dependently down-regulates its own mRNA expression in HUVECs.

(A) Relative level of endogenous *MEOX2* mRNA compared to EGFP transduced HUVECs. Total RNA was isolated from HUVECs 48 hours after adenoviral transduction at 250 MOI and the amount of mRNA was measured by quantitative real-time PCR. *β -actin* mRNA expression was used for inter-sample normalisation. (B) Level of *MEOX2* mRNA relative to untransduced HUVECs. Total RNA was isolated from HUVECs at 12, 24, 36, 48 and 72 hours after adenoviral transduction at 250 MOI and the relative amount of mRNA was measured by quantitative real-time PCR. *β -actin* mRNA expression was used for inter-sample normalisation. # Indicates a statistically significant change ($p < 0.05$) from untransduced HUVECs. * Indicates a statistically significant difference ($p < 0.05$) between MEOX2 and EGFP over-expressing cells. Error bars represent the standard error of the mean ($n=3$ (A), $n \geq 3$ (B)).

5.4.2.3. *Gene set enrichment analysis*

For the purpose of identifying novel target genes that are involved in biologically relevant EC processes, we performed gene set enrichment analysis (GSEA) on our microarray data. GSEA is a computational method used to identify sets of genes that best summarize the changes in gene expression between two biological states. We compared MEOX over-expressing EC gene expression profiles to control ECs over-expressing EGFP and ranked the genes according to the t-statistic of the differential expression. This ranked gene list was then compared to human gene ontology (GO) gene-sets (gene products that are grouped based on their biological function, cellular component or molecular function) using GSEA.

GSEA identified many GO gene-sets whose constituent genes were over or under represented in MEOX over-expressing ECs (Figure 5-9); that is to say that these GO gene-sets contained more genes whose expression was either increased or decreased than would be expected by random chance. Amongst these GO gene-sets, we saw that there was an increase in genes involved in lysosomal function (Figure 5-9). This result may be related to the induction of senescence by MEOX1 and MEOX2, as increased lysosomal content was shown to result in increased β -galactosidase activity in senescent HUVECs [249]. In addition, we observed that the expression of genes involved in angiogenesis, pseudouridine synthesis and regulation of the cell cycle were greatly decreased in response to both MEOX1 and MEOX2 over-expression in ECs (Figure 5-9; Figure 5-10). We chose to subsequently validate the expression of a few selected candidate genes from these GO gene-sets (shown in bold in Figure 5-9, coloured arrows in Figure 5-10).

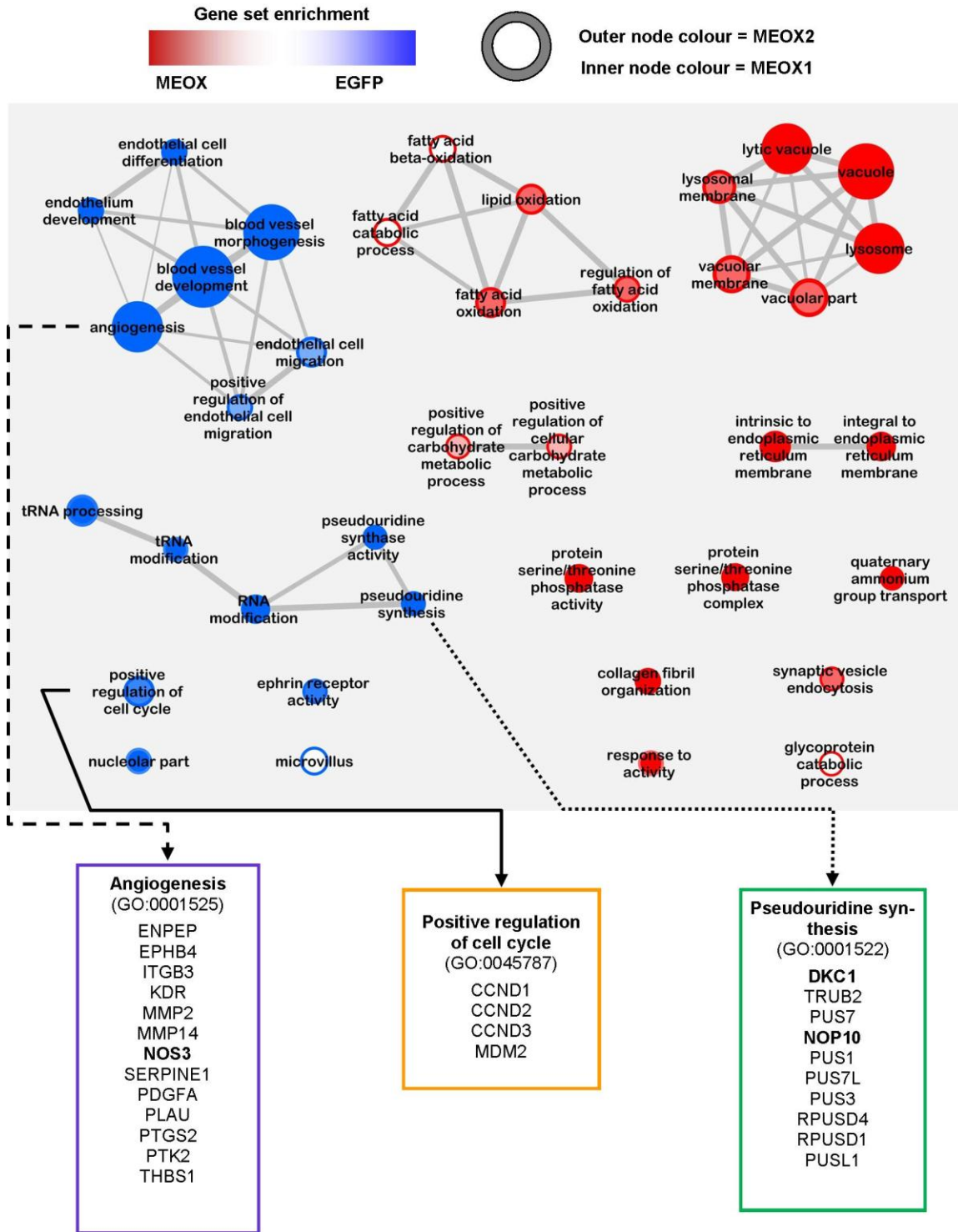


Figure 5-9: MEOX1 and MEOX2 decrease the expression of genes involved in angiogenesis, pseudouridine synthesis and cell cycle regulation.

Figure 5-9: MEOX1 and MEOX2 decrease the expression of genes involved in angiogenesis, pseudouridine synthesis and cell cycle regulation.

Enrichment map showing the gene ontology gene-sets whose constituent genes are over (red) and under (blue) represented in HUVECs over-expressing MEOX proteins, when compared to EGFP expressing control cells. Over-expression of MEOX1 and MEOX2 resulted in decreased expression of genes involved in angiogenesis (GO:0001525), pseudouridine synthesis (GO:0001522) and positive regulation of cell cycle (GO:0045787). The outer and inner node colours represent the enrichment value in MEOX2 or MEOX1 over-expressing cells compared to EGFP, respectively. The node size reflects the number of genes contained in each gene-set.

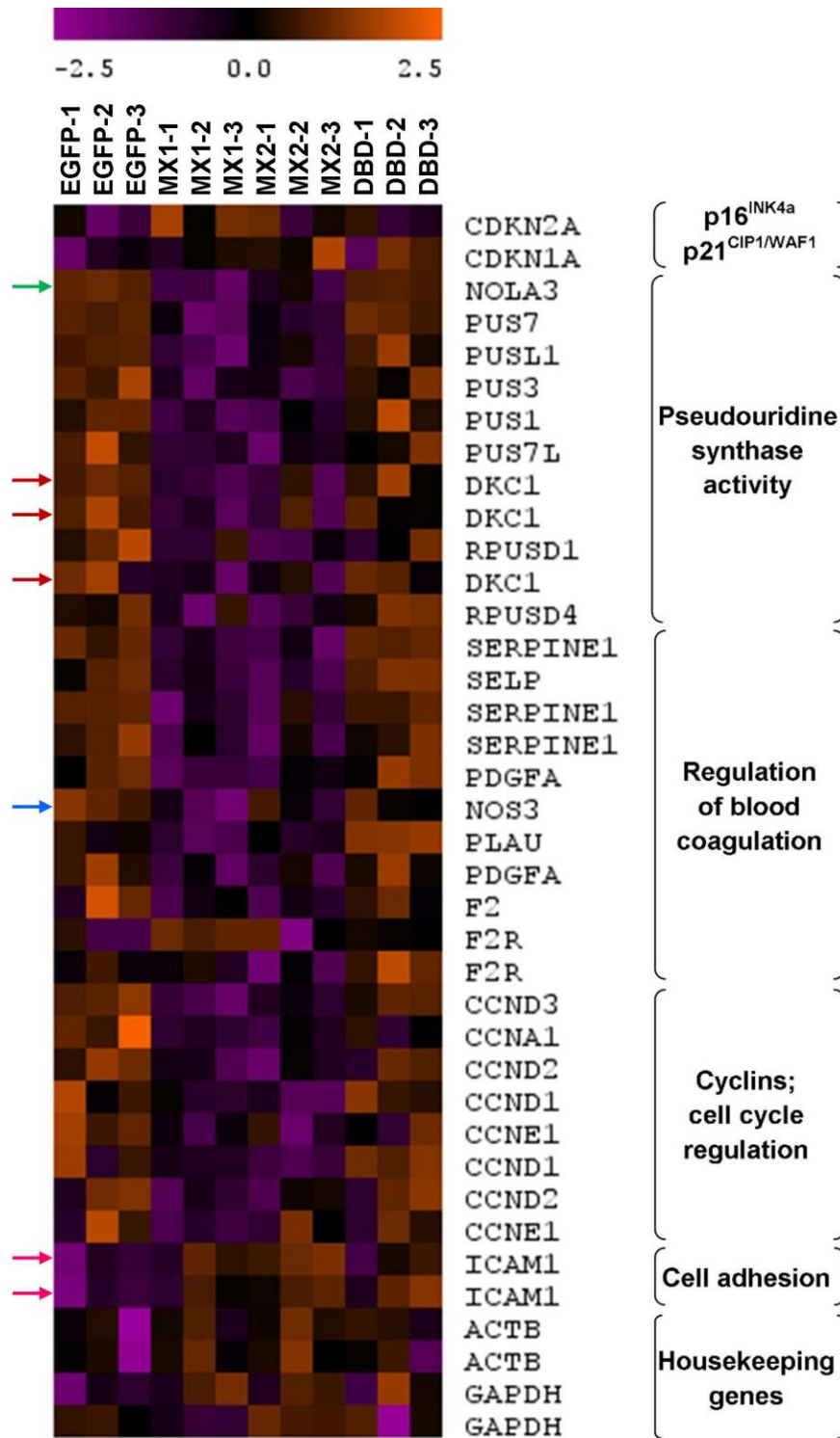


Figure 5-10: Heatmap demonstrating selected probe-set expression values from HUVECs over-expressing EGFP, MEOX1, MEOX2 or DNA-binding domain mutated MEOX2^{Q235E}.

Figure 5-10: Heatmap demonstrating selected probe-set expression values from HUVECs over-expressing EGFP, MEOX1, MEOX2 or DNA-binding domain mutated MEOX2^{Q235E}.

The expression values for each probe-set have been normalized by row. The expression of genes whose representative probe-set(s) are identified by an arrow were subsequently validated by quantitative real-time PCR. These include NOP10/NOLA3 (green), DKC1/Dyskerin (red), NOS3/eNOS (blue) and ICAM1 (pink).

5.4.2.4. *Validation of putative target genes*

We first chose to validate the expression of the pseudouridine synthase genes dyskerin (*DKC1*) and NOP10 ribonucleoprotein homolog (*NOP10*). Pseudouridine synthases catalyze the modification of uridine in RNA to pseudouridine [250]. This modification is required for the proper folding, stability, and ability of non-protein coding RNAs (such as rRNAs, tRNAs, snRNAs and snoRNAs) to efficiently interact with their protein binding partners [250]. Inhibition of RNA pseudouridylation can decrease ribosome biogenesis, mRNA splicing and telomerase activity, leading to cell cycle arrest and premature senescence [251]. Dyskerin is the pseudouridine synthase component of the H/ACA small nucleolar ribonucleoprotein (snoRNP) RNA modification complex [252]. NOP10 is another component of this complex and is essential for the pseudouridine synthase activity of the H/ACA snoRNP complex [252]. The H/ACA snoRNPs are required for rRNA modification and are a component of the telomerase complex [253,254]. Mutations in *DKC1*, *NOP10*, telomerase reverse transcriptase (*TERT*) and telomerase RNA component (*TERC*) cause Dyskeratosis Congenita, a rare disorder with features of premature aging such as reticulate skin pigmentation, nail dystrophy and bone marrow failure [255]. Individuals with Dyskeratosis Congenita or HGPS have both been shown to have shorter telomeres than controls [256,257].

In HUVECs over-expressing MEOX1 and MEOX2, we observed a trend towards decreased *NOP10* mRNA expression compared to the EGFP control (Figure 5-11, panel A). Interestingly, it appears as though *NOP10* mRNA expression was increased by adenoviral transduction and that MEOX over-expression has a repressive effect on *NOP10* gene expression. In support of this notion, the level of *NOP10* mRNA expression

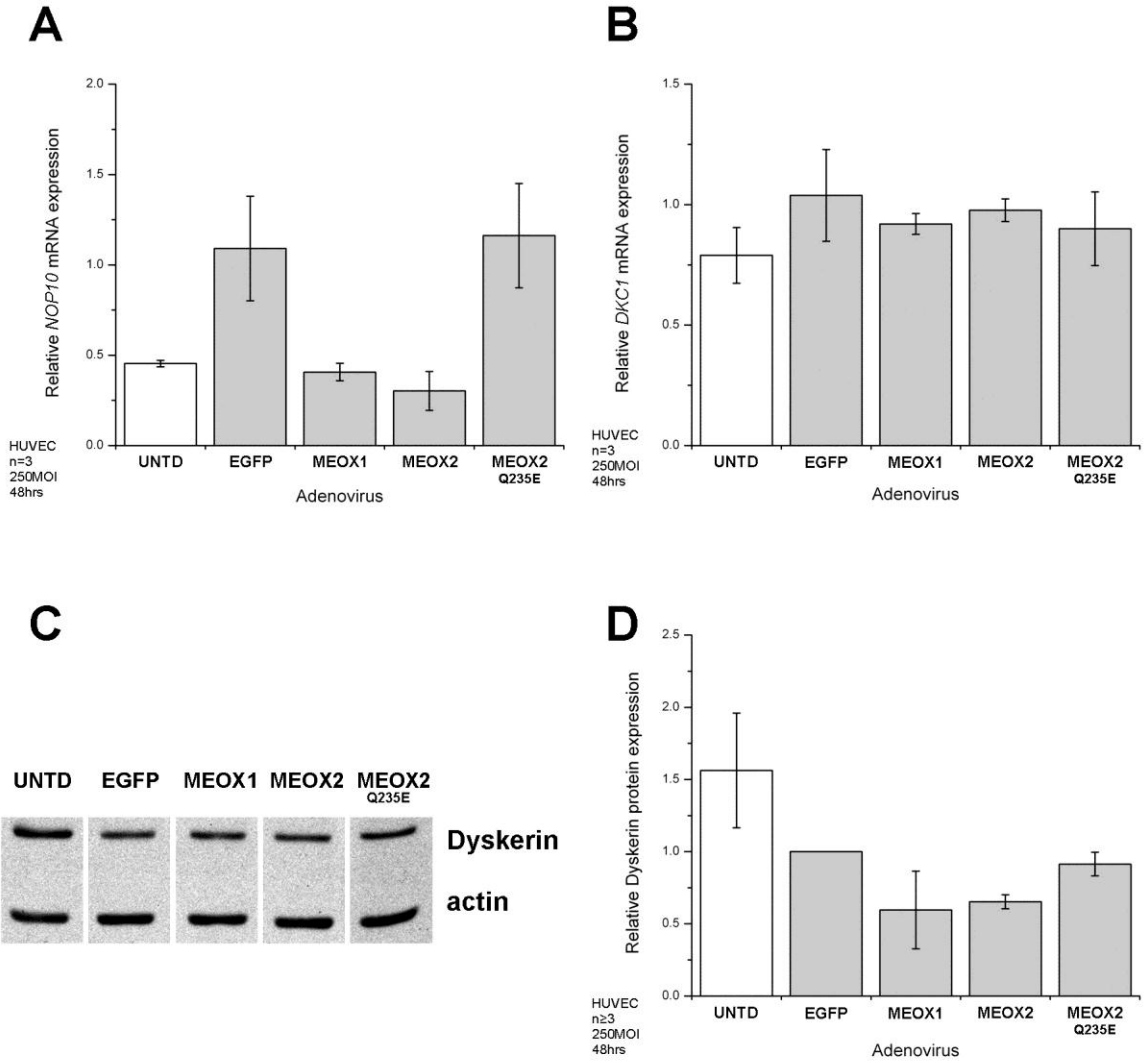


Figure 5-11: MEOX protein over-expression does not significantly affect the expression of pseudouridine synthase complex components.

Figure 5-11: MEOX protein over-expression does not significantly affect the expression of pseudouridine synthase complex components.

(A-B) Levels of *NOPI0* (A) and *DKCI* (B) mRNA relative to EGFP over-expressing HUVECs. Total RNA was isolated from HUVECs 48 hours post-transduction with 250 MOI of the indicated adenoviral constructs. The relative amounts of mRNA were measured by quantitative real-time PCR. *β-actin* mRNA expression was used for inter-sample normalisation. (C) Representative western blot showing the levels of Dyskerin protein in HUVECs over-expressing MEOX proteins. (D) Quantification of the relative amount of Dyskerin protein 48 hours after transduction with 250 MOI of adenovirus encoding EGFP or N-terminal FLAG-tagged MEOX proteins. The intensity of the Dyskerin band was normalized to the actin loading control. Error bars represent the standard error of the mean (n=3 (A), n=3 (B), n≥3 (D)).

in HUVECs over-expressing DNA-binding domain mutated MEOX^{Q235E} was comparable to the EGFP control (Figure 5-11, panel A). This suggests that the effect of MEOX2 on *NOP10* gene expression is dependent upon DNA-binding. However, as none of the observed differences reached statistical significance, more biological replicate experiments will have to be conducted in order to validate *NOP10* as a target of MEOX protein regulation. In contrast, we did not detect any consistent changes in the levels of *DKC1* mRNA or Dyskerin protein expression when any of the MEOX proteins were over-expressed in HUVECs (Figure 5-11, panels B-D). We therefore conclude that the *DKC1* gene is not a target of MEOX protein regulation.

ICAM-1 on the EC surface promotes inflammation by enabling leukocyte adhesion to the endothelium and thereby facilitates trans-endothelial migration from the blood into the surrounding tissue. Expression of ICAM-1 has been shown to be increased in senescent EC [31,258]. Concordant with this observation, we detected significantly increased *ICAM-1* mRNA expression in HUVECs over-expressing MEOX1 and MEOX2 by microarray. The microarray analysis by Patel *et al.* [170] also identified *ICAM-1* as a candidate of MEOX2 protein regulation. However, in contrast to our microarray results these authors showed that MEOX2 decreased the expression of ICAM-1 in ECs [170]. Thus, we wanted to validate the changes in *ICAM-1* mRNA expression which we observed by microarray.

Using quantitative real-time PCR we show that both MEOX1 and MEOX2 significantly increased the expression of *ICAM-1* mRNA in HUVECs (Figure 5-12). Surprisingly, we observed an even greater increase in *ICAM-1* mRNA expression in ECs over-expressing DNA-binding domain mutated MEOX2^{Q235E} (data not shown). In

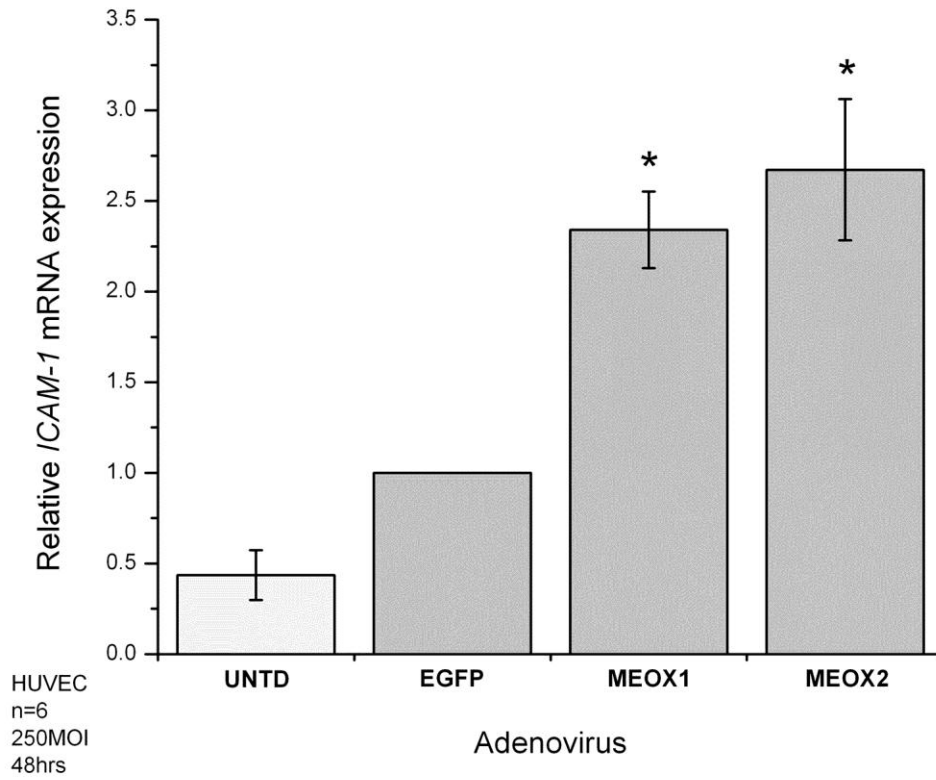


Figure 5-12: MEOX1 and MEOX2 up-regulate *ICAM-1* mRNA expression in HUVECs.

Level of *ICAM-1* mRNA relative to EGFP over-expressing HUVECs. Total RNA was isolated from HUVECs 48 hours post-transduction with 250 MOI of adenovirus. The relative amounts of mRNA were measured by quantitative real-time PCR. *β-actin* mRNA expression was used for inter-sample normalisation. * Indicates a statistically significant change ($p < 0.05$) when compared to the EGFP control. Error bars represent the standard error of the mean (n=6).

contrast to the study by Patel *et al.* [170], our data support a pro-inflammatory role for MEOX proteins in ECs. Of the 77 genes listed in their publication, we observed approximately 52% concordance with their findings (40 of the 77 genes were significantly changed in the same direction in our dataset). Thus, in future we will check for increased ICAM-1 protein expression in MEOX expressing HUVECs.

Constitutive production of NO by the endothelium is essential for mediating vasorelaxation (prevents VSMC contraction) and controlling blood coagulation (inhibits platelet aggregation). NO in the endothelium is produced by the eNOS enzyme [2,26]. Furthermore, decreased NO production by ECs is a key feature of EC dysfunction, which is characteristic of EC senescence [218].

The eNOS enzyme is encoded by the *NOS3* gene. Real-time PCR confirmed our microarray results that showed that MEOX1 and MEOX2 over-expression in HUVECs significantly decreased *eNOS* mRNA expression compared to the EGFP control (Figure 5-10; Figure 5-13, panel A). Correspondingly, we observed a decrease in total eNOS protein expression (Figure 5-13, panels B and C). As the enzymatic activity of eNOS is regulated by phosphorylation, we used phosphorylation site-specific antibodies to detect different phosphorylated forms of eNOS in HUVEC lysates. Consistent with the levels of total eNOS, we observed decreased Thr495 phosphorylated eNOS in response to MEOX1 and MEOX2 over-expression in HUVECs (Figure 5-13, panel B). Decreased Thr495 phosphorylated eNOS likely reflects the overall reduction in total eNOS protein. We did not however, detect any change in Ser1177 phosphorylated eNOS (data not shown). As Thr495 marks inactive eNOS and Ser1177 marks active eNOS, we speculate that in order to maintain NO production, proportionately more eNOS is being

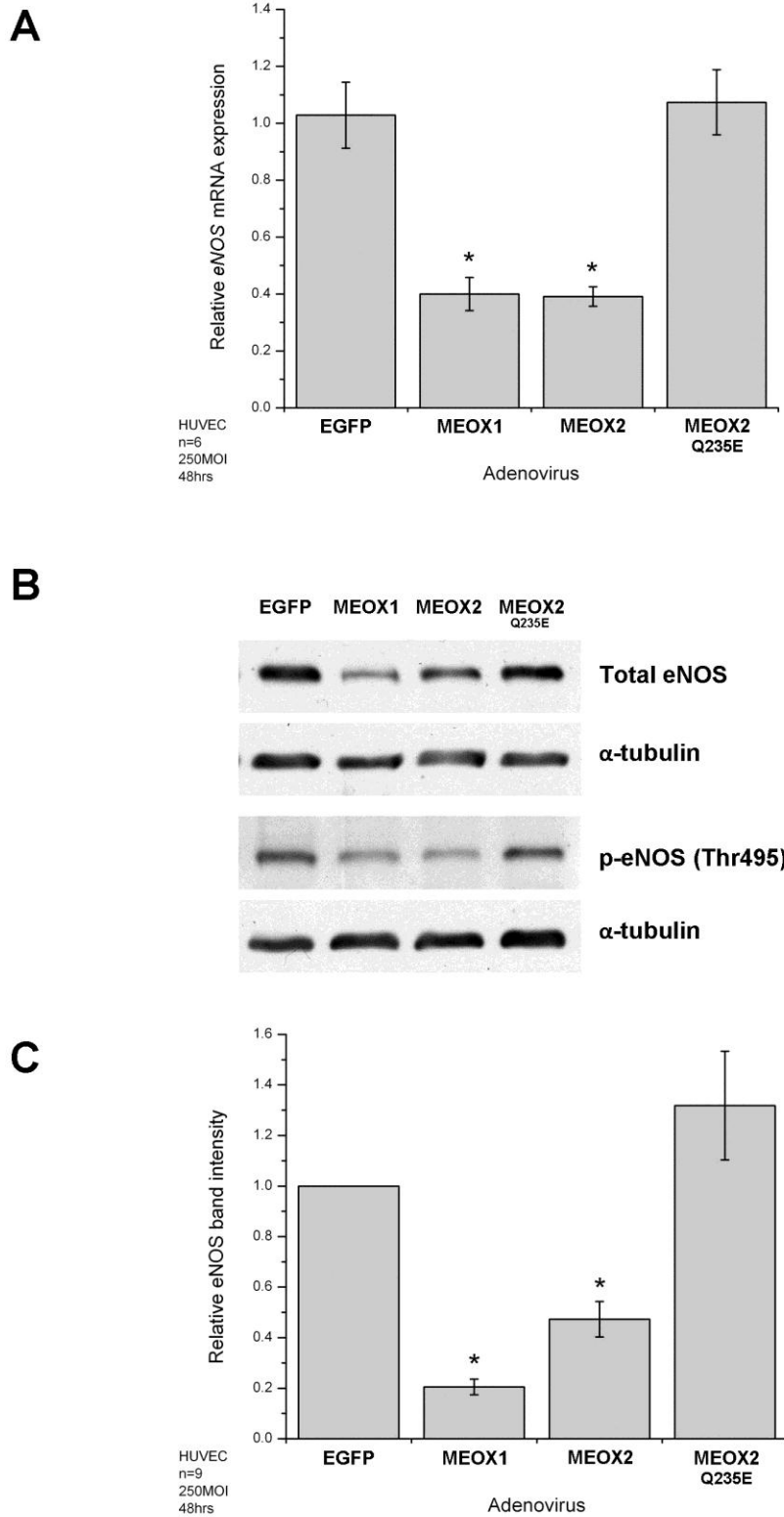


Figure 5-13: MEOX1 and MEOX2 reduce *eNOS* mRNA and protein expression in HUVECs.

Figure 5-13: MEOX1 and MEOX2 reduce *eNOS* mRNA and protein expression in HUVECs.

(A) Level of *eNOS* mRNA relative to EGFP over-expressing HUVECs. Total RNA was isolated from HUVECs 48 hours post-transduction with 250 MOI of adenovirus. The relative amounts of mRNA were measured by quantitative real-time PCR. *β-actin* mRNA expression was used for inter-sample normalisation. (B) Representative western blot showing the levels of total and Thr495 phosphorylated eNOS protein in HUVECs over-expressing MEOX proteins. (C) Quantification of the relative amount of total eNOS protein 48 hours after transduction with 250 MOI of adenovirus encoding EGFP or N-terminal FLAG-tagged MEOX proteins. The intensity of the eNOS band was normalized to the α -tubulin loading control. * Indicates a statistically significant change ($p < 0.05$) when compared to the EGFP control. Error bars represent the standard error of the mean (n=6 (A), n=9 (C)).

phosphorylated at Ser1177 in MEOX1 and MEOX2 over-expressing cells in an attempt to compensate for the reduction in the total eNOS protein.

Unlike wild-type MEOX2, over-expression of DNA-binding domain mutated MEOX2^{Q235E} did not decrease *eNOS* mRNA or protein expression in HUVECs (Figure 5-13), indicating that MEOX2 must bind to DNA in order to repress eNOS expression. This suggests that eNOS may be a direct transcriptional target of MEOX protein regulation. To test this hypothesis, we assessed the ability of MEOX1 and MEOX2 to decrease transcription from a 1622 bp human *eNOS* upstream promoter region (-1600 to +22 bp relative to the TSS) [243], which contains three putative homeodomain binding sites (Figure 5-14, panel A). Luciferase assay results show that both MEOX1 and MEOX2 decreased reporter gene transcription from the 1622 bp human *eNOS* promoter in HEK293 cells (Figure 5-14, panel B). This finding is exciting, as it suggests for the first time that MEOX1 and MEOX2 may be capable of repressing gene transcription. Alternatively, it is possible that the MEOX proteins activate a repressor of *eNOS* transcription.

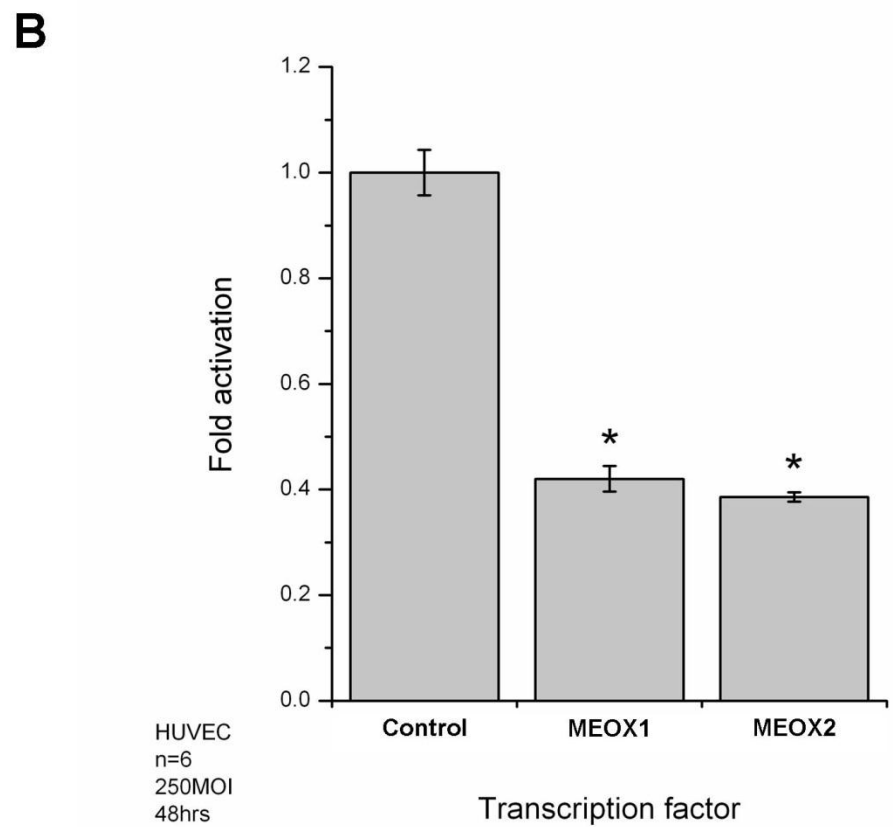
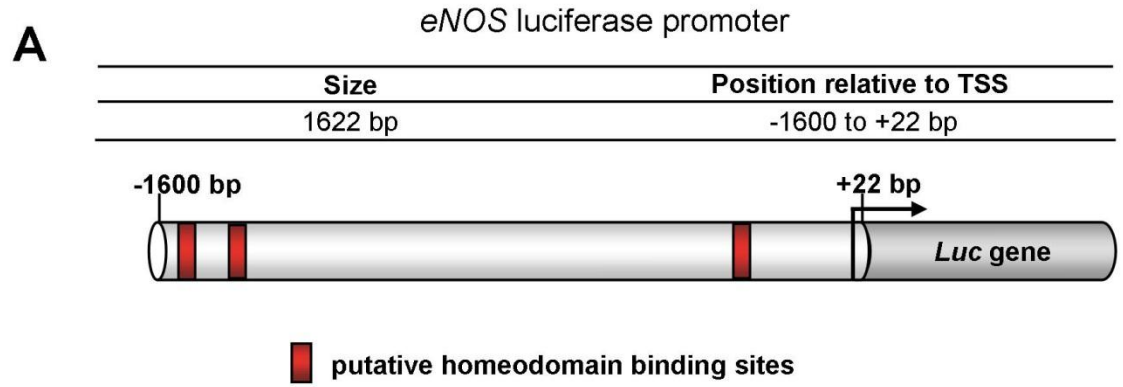


Figure 5-14: MEOX1 and MEOX2 repress transcription from the human *eNOS* promoter.

Figure 5-14: MEOX1 and MEOX2 repress transcription from the human *eNOS* promoter.

(A) Schematic diagram of the human 1622 bp *eNOS* upstream promoter region luciferase construct. The 5' terminus is indicated relative to the transcriptional start site (TSS) (arrow). Putative homeodomain binding sites are also shown. (B) Activation of the 1622 bp *eNOS* promoter driven luciferase reporter gene by MEOX1 and MEOX2 in HEK293 cells. * Indicates a statistically significant change ($p < 0.05$) when compared to the empty vector. Error bars represent the standard error of the mean ($n=6$).

5.5. Conclusions and future directions

Our findings indicate that the transcriptional roles of MEOX1 and MEOX2 are potentially largely redundant in ECs as the majority of genes which are modulated by MEOX2 are similarly regulated by MEOX1. Upon over-expression of MEOX1 or MEOX2 in HUVECs, we observed changes in EC gene expression that promote EC dysfunction; decreased *eNOS* expression and increased *ICAM-1* expression (Table 5-3) are expected to result in the loss of endothelial-dependent vasorelaxation and increased vascular inflammation. Furthermore, we show that *eNOS* is a putative transcriptional target gene of the MEOX homeodomain transcription factors and that MEOX1 and MEOX2 repress *eNOS* expression.

Future directions of this work will focus on identifying the molecular mechanism by which MEOX proteins regulate the *eNOS* upstream promoter region. To do so, we will use ChIP to verify MEOX binding to the *eNOS* upstream promoter region in HUVECs and mutate the putative homeodomain binding sites within the *eNOS* upstream promoter region in order to determine if the MEOX proteins regulate *eNOS* expression via homeodomain-DNA-binding. We will also measure the levels of NO and ROS production in MEOX over-expressing HUVECs. In addition, we will compare wild-type to *Meox* gene knockout mice to evaluate the *in vivo* effects of complete and partial loss of *Meox1* and *Meox2* expression on endothelial-dependent vasorelaxation.

Furthermore, we will confirm that increased *ICAM-1* mRNA expression in response to MEOX protein over-expression results in increased ICAM-1 protein on the EC surface and that this correlates with increased leukocyte adhesion to ECs *in vitro* and *in vivo*. To test whether decreased MEOX1 and MEOX2 expression prevents the

progression of atherosclerosis, we will cross *Meox* gene knockout mice with mouse models of atherosclerosis (apolipoprotein E (ApoE)^{-/-} or low-density lipoprotein receptor (LDLR)^{-/-}) and then study the time course of vascular disease progression.

Table 5-3: Novel genes that have altered expression levels in response to MEOX over-expression.

	Expression changes	GENE / Alternate name
MEOX1	↓ mRNA, ↓ protein	NOS3 / eNOS
	↑ mRNA	ICAM-1
MEOX2	↓ mRNA	MEOX2
	↓ mRNA, ↓ protein	NOS3 / eNOS
	↑ mRNA	ICAM-1

↑ denotes a significant increase

↓ denotes a significant decrease

CHAPTER 6:DISCUSSION, CONCLUSIONS AND FUTURE DIRECTIONS

6.1. Discussion and conclusions

EC dysfunction is a hallmark of vascular disease and is characterised by decreased angiogenic potential and reduced NO bioavailability [218]. In contrast, production of ROS and inflammatory mediators is increased in EC dysfunction [218]. Age is a major risk factor for the development of vascular diseases, such as atherosclerosis. As blood vessels age, they accumulate increasing numbers of senescent cells and have impaired angiogenic capabilities [212], which suggests that EC senescence causes endothelial dysfunction and promotes vascular disease [28,29]. Indeed, human atherosclerotic tissue has been shown to contain a higher proportion of senescent cells than disease-free tissue [30-32]. Furthermore, populations of senescent ECs were shown to have impaired angiogenic capabilities *in vitro* [36] and reduced nitric oxide synthase expression [33-35].

The MEOX homeodomain transcription factors, MEOX1 and MEOX2, are partially redundant during development [126] and share a highly conserved homeodomain (95% amino acid identity between the MEOX paralogs within this domain [84]), suggesting that they regulate the transcription of many common target genes. Currently, the only confirmed direct transcriptional target genes of MEOX2 are the cell cycle inhibitors *p21^{CIP1/WAF1}* and *p16^{INK4a}* that together mediate transient (quiescent) and permanent (senescent) cell cycle arrest [87,89].

Children affected by Hutchinson-Gilford Progeria Syndrome, a disease of premature aging, often die from accelerated atherosclerosis [29,181]. Microarray analysis has shown that *MEOX2* expression is significantly increased in cells from HGPS

patients [181,182]. Taken together, we questioned whether MEOX2 and MEOX1 play an active role in promoting endothelial senescence and atherosclerosis via target gene transcription.

In order to address the role of the MEOX transcription factors in ECs, we focused on their regulation of known target genes, identification of novel target genes and the possible cellular consequences of target gene regulation. Our results are summarized in Figure 6-1. We demonstrate for the first time that MEOX1 regulates the MEOX2 target genes *p21^{CIP1/WAF1}* and *p16^{INK4a}* in ECs. Consistent with this finding, we observed that increased expression of the MEOX transcription factors led to both G₁ phase cell cycle arrest and EC senescence.

Due to the rapid induction of senescence by the MEOX proteins (within 48 hours), we believe that MEOX induced senescence is a form of stress-induced premature senescence. However, as we have not assessed changes in telomere length or uncapping, we cannot discount the possibility that MEOX induced senescence may be a form of replicative senescence. Furthermore, albeit not statistically significant by quantitative real-time PCR, we observed an apparent decrease in *NOP10* expression when MEOX proteins were over-expressed in HUVECs. As *NOP10* is a component of the telomerase holoenzyme and is required for H/ACA snoRNPs activity [252,254], down-regulation of *NOP10* would support a role for the MEOX proteins in telomere maintenance and perhaps replicative senescence.

Furthermore, we identified *ICAM-1* and *eNOS* as candidate transcriptional target genes of MEOX1 and MEOX2 in ECs. The MEOX proteins increase the expression of *ICAM-1* in HUVECs, which would result in increased leukocyte adhesion to the

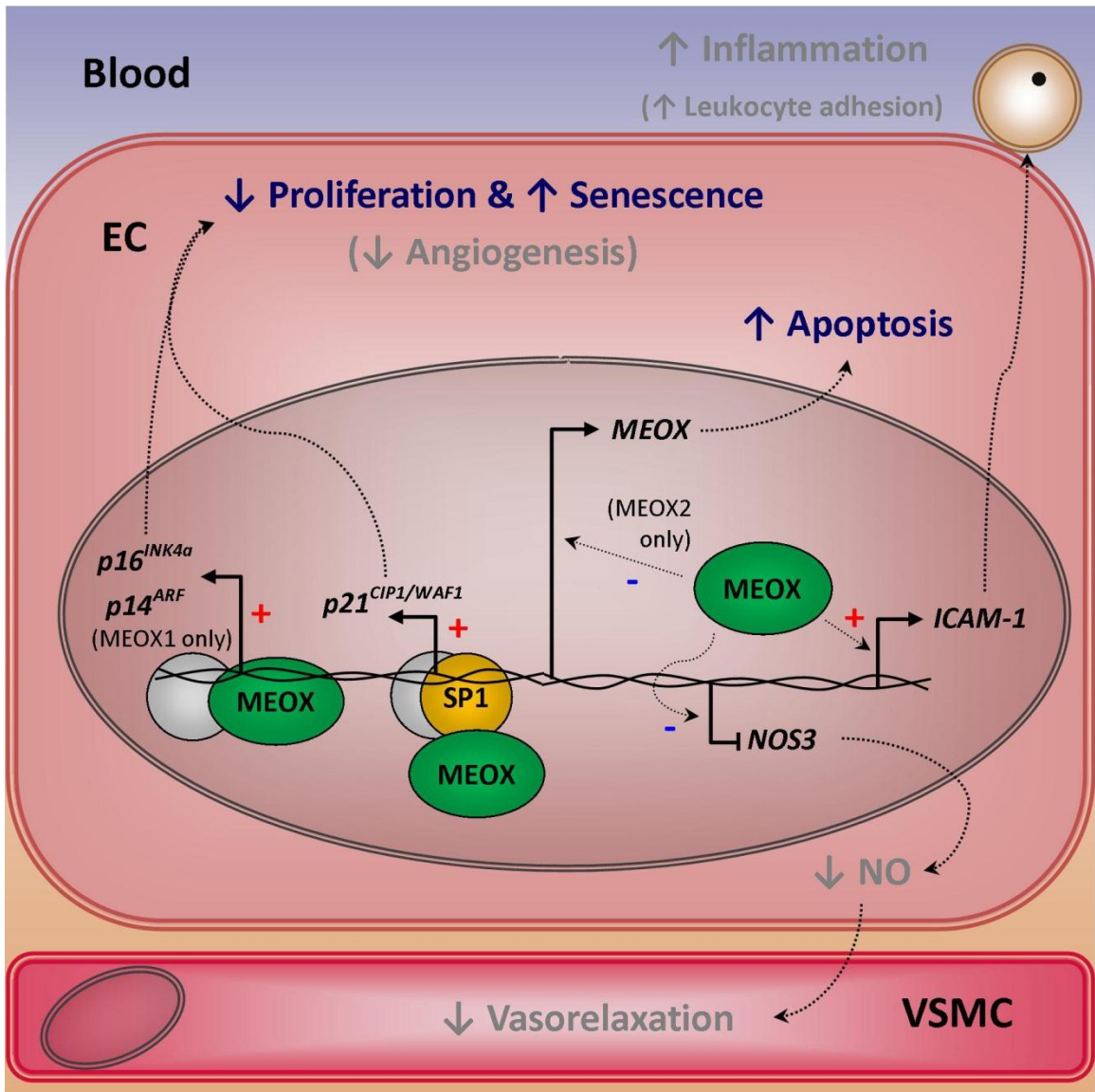


Figure 6-1: Diagrammatic summary of research findings.

Figure 6-1: Diagrammatic summary of research findings. In endothelial cells, activation of *p16^{INK4a}* (*CDKN2A* gene) is DNA-binding dependent, while activation of *p21^{CIP1/WAF1}* (*CDKN1A* gene) is DNA-binding independent and requires SP1. MEOX1 is also capable of activating the mRNA expression of *p14^{ARF}*, the alternative transcript of the *CDKN2A* gene. Consistent with the finding that the expression of these cell cycle inhibitors is augmented, we observed a decrease in endothelial cell proliferation and an increase in endothelial cell senescence (permanent cell cycle arrest). Sustained high levels of MEOX1 or MEOX2 expression for prolonged periods of time lead to apoptotic cell death. Interestingly, we observed that exogenous MEOX2 over-expression caused a decrease in endogenous *MEOX2* expression, suggesting a negative feedback mechanism. Novel target genes of MEOX1 and MEOX2 include *ICAM-1* and *NOS3* (*eNOS*). MEOX over-expression increased *ICAM-1* expression, which could potentially result in greater leukocyte adhesion to EC and inflammation. MEOX over-expression decreased *NOS3* expression, which may result in reduced nitric oxide (NO) production and endothelial dysfunction characterized by decreased vasorelaxation. Green ovals represent the MEOX1 and MEOX2 proteins. White circles represent the basal transcription machinery. Blue minus signs indicate a negative effect on gene expression by MEOX proteins. Red plus signs indicate a positive effect on gene expression by MEOX proteins. Cellular outcomes demonstrated in this thesis are written in blue. Cellular functions to be assayed for in future are written in grey.

endothelium and promotion of vascular inflammation *in vivo*. In contrast, the expression of *eNOS* is repressed by MEOX1 and MEOX2, which is expected to reduce NO production and thereby result in vasoconstriction and increased thrombosis. In addition, reduced NO production may result in increased intracellular ROS, since less ROS will be converted to peroxynitrite through its reaction with NO. Increased intracellular ROS can also promote EC senescence and inflammation.

In addition to the induction of EC senescence, we show that both MEOX1 and MEOX2 can induce apoptosis of ECs. Within the vasculature, impaired angiogenesis in combination with increased cell death would be expected to result in decreased endothelial integrity and/or microvascular regression. Loss of the endothelium triggers VSMC proliferation and vessel stenosis due to loss of NO production.

Intriguingly, although the expression profile of HUVECs over-expressing DNA-binding domain mutated MEOX2^{Q235E} was more similar to EGFP than to wild-type MEOX2, this DNA-binding deficient version of MEOX2 was still capable of certain MEOX2 functions. MEOX2^{Q235E} activated *p21^{CIP1/WAF1}* expression and inhibited cell proliferation. Furthermore, MEOX2^{Q235E} increased *ICAM-1* mRNA expression to a greater extent than wild-type MEOX2 (data not shown). In contrast, MEOX2^{Q235E} was unable to activate *p16^{INK4a}* and *eNOS* expression or induce EC senescence. Thus, it appears that MEOX2 functions in ECs can occur via DNA-binding dependent and independent mechanisms. Moreover, these results suggest that inhibition of MEOX2-DNA interaction may not be sufficient to preclude MEOX-induced EC dysfunction.

Together, our findings support a role for the MEOX transcription factors in enhancing the pathogenesis of atherosclerosis by mediating gene expression changes

which result in EC dysfunction. Thus, increased *MEOX2* expression in vascular EC of children with HGPS is likely to be playing an active role in promoting the accelerated atherosclerosis that occurs in these individuals. As there are vascular diseases that are associated with both increased and decreased *MEOX2* expression, we believe that the expression of *MEOX2* must be tightly regulated for the maintenance of proper EC function. We observed that over-expression of exogenous *MEOX2* significantly decreases the expression of endogenous *MEOX2* expression, suggesting that *MEOX2* can negatively autoregulate its own expression. We are confident that this reduction in endogenous *MEOX2* expression did not affect our results (and therefore the conclusions drawn from these results) as adenoviral mediated over-expression of exogenous *MEOX2* is certain to have produced a net gain of *MEOX2* protein within transduced ECs.

Our work had several limitations. First, we were unable to measure endogenous *MEOX* protein expression due to the lack of specific antibodies. Thus, we plan to have custom antibodies made against *MEOX1* and *MEOX2* for future experiments. Secondly, the apparent effects of control siRNA transfection on *MEOX2* mRNA expression (Figure 4-26) precluded the utility of this strategy to study *MEOX2* loss-of-function. However, we have recently obtained an adenoviral construct that encodes a short hairpin RNA (shRNA) that targets *MEOX2* mRNA, which will enable us to study the effects of *MEOX2* knockdown on EC function. An antibody to *MEOX2* will be essential to these experiments in order to assure that knockdown of *MEOX2* mRNA results in decreased *MEOX2* protein expression.

Although adenovirus mediated over-expression is a useful method to study gain-of-function effects of wild-type and mutant proteins, the major drawbacks of this

technique are non-specific effects due to: i) virus induced cellular changes, ii) the absence of normal gene regulation, iii) altered protein stoichiometry and iv) abnormal protein-protein and/or protein-DNA interactions. Altered subcellular localization or protein aggregation of over-expressed proteins can induce cellular stresses that are not specific to the normal function of the protein, as exemplified potentially by the apoptosis induced by MEOX2^{K195_K245del} over-expression in primary VSMCs (Figure 3-7). Furthermore, both adenoviral transduction and lipid mediated DNA transfection are transient gene delivery systems that can result in high inter-cellular heterogeneity of transgene delivery and consequently, variable mRNA and protein expression over time. Moreover, fluctuations in transduction and transfection efficiency cause high inter-assay variability. To overcome the limitations of these techniques, we will use genetically manipulated models, including stably transduced/transfected cell lines and transgenic mice. Stably transduced/transfected cells are especially advantageous because clones with modest levels of transgene expression (dependent upon the site of DNA integration and promoter used) can be selected. Genetic gain and loss of MEOX expression can be achieved via knock-in and knock-out strategies in mice, respectively. These mouse models will be key to understanding the *in vivo* effects of MEOX proteins in the vasculature.

Taken together, we conclude that:

- MEOX1 and MEOX2 have redundant functions in ECs due to the regulation of many common target genes including *p21^{CIP1/WAF1}*, *p16^{INK4a}*, *ICAM-1* and *eNOS*.
- MEOX1 and MEOX2 induce EC apoptosis and senescence, thereby promoting endothelial dysfunction.

6.2. Future directions

Although expression microarrays are advantageous because they enable the identification of overall pathways and functions that are influenced by MEOX proteins in ECs, they cannot distinguish between direct and indirect target genes. Thus, to identify direct transcriptional target genes of MEOX1 and MEOX2, we will use the ChIP-seq method [259] to isolate DNA fragments that are bound by the MEOX proteins in HUVECs. Comparison of the expression array data to the ChIP-seq results will allow us to confirm our findings, since it is expected that the majority of direct transcriptional target genes identified by ChIP-seq will also be identified as differentially regulated genes in the expression arrays. While ChIP can confirm the presence of a protein at a specific DNA fragment, it cannot discern whether the protein is directly bound to DNA or is present due to its interaction with other proteins. To address this, we will also perform ChIP-seq experiments using HUVECs expressing DNA-binding domain mutated MEOX1^{Q219E} and MEOX2^{Q235E} which contain point mutations that abolish their ability to bind to DNA but are not predicted to affect the protein-protein interaction capabilities of MEOX1 and MEOX2, respectively.

Discovering the identity of MEOX interacting proteins will help to further elucidate the mechanism of MEOX regulated target gene transcription. To date, there are only a few confirmed binding partners of MEOX1 and MEOX2 (Table 6-1). However, it is notable that the majority of these known interacting proteins are transcription factors. We hypothesize that many of the MEOX interacting proteins will be zinc finger transcription factors as our yeast-two-hybrid experiments indicate that the middle domain of MEOX2 is sufficient for zinc finger protein binding (Appendix A). Furthermore, the

Table 6–1: MEOX interacting proteins.

	Interacting protein	Reference [#]
MEOX1	PAX1	Stamataki <i>et al.</i> 2001 [85]
	SOX10	Wissmuller <i>et al.</i> 2006 [86]
MEOX2	PBX1	Thiaville <i>et al.</i> 2012 [180]
	PAX3	Stamataki <i>et al.</i> 2001 [85]
	RING finger protein 10	Lin <i>et al.</i> 2005 [88]
	SMAD2 SMAD3 SMAD4	Valcourt <i>et al.</i> 2007 [146]
	p65 I κ B β	Chen <i>et al.</i> 2010 [174]

middle domain is the second most conserved protein domain when comparing MEOX1 to MEOX2 (Figure 1-2). Knowledge of MEOX interacting proteins will provide insight into the molecular pathways that modulate MEOX function in vasculature ECs.

In order to isolate MEOX interacting proteins from ECs, two approaches will be employed: co-immunoprecipitation and tandem affinity purification. Ultimately, MEOX bound proteins will be isolated from ECs, separated using SDS-PAGE for comparison to controls and then identified by mass spectrometry. We have already commenced preparations for the tandem affinity purification experiments (described in Appendix E).

REFERENCES

1. Aird WC (2007) Phenotypic heterogeneity of the endothelium: I. Structure, function, and mechanisms. *Circ Res* 100: 158-173.
2. Mas M (2009) A Close Look at the Endothelium: Its Role in the Regulation of Vasomotor Tone. *European Urology Supplements* 8: 48-57.
3. Chi JT, Chang HY, Haraldsen G, Jahnsen FL, Troyanskaya OG, et al. (2003) Endothelial cell diversity revealed by global expression profiling. *Proc Natl Acad Sci U S A* 100: 10623-10628.
4. Abbott NJ, Ronnback L, Hansson E (2006) Astrocyte-endothelial interactions at the blood-brain barrier. *Nat Rev Neurosci* 7: 41-53.
5. Daneman R, Zhou L, Agalliu D, Cahoy JD, Kaushal A, et al. (2010) The mouse blood-brain barrier transcriptome: a new resource for understanding the development and function of brain endothelial cells. *PLoS One* 5: e13741.
6. Rensen SS, Doevendans PA, van Eys GJ (2007) Regulation and characteristics of vascular smooth muscle cell phenotypic diversity. *Neth Heart J* 15: 100-108.
7. Dzau VJ, Braun-Dullaeus RC, Sedding DG (2002) Vascular proliferation and atherosclerosis: new perspectives and therapeutic strategies. *Nat Med* 8: 1249-1256.
8. Ema M, Rossant J (2003) Cell fate decisions in early blood vessel formation. *Trends Cardiovasc Med* 13: 254-259.
9. Tang DG, Conti CJ (2004) Endothelial cell development, vasculogenesis, angiogenesis, and tumor neovascularization: an update. *Semin Thromb Hemost* 30: 109-117.
10. Ferrara N, Alitalo K (1999) Clinical applications of angiogenic growth factors and their inhibitors. *Nat Med* 5: 1359-1364.
11. Takashima S, Kitakaze M, Asakura M, Asanuma H, Sanada S, et al. (2002) Targeting of both mouse neuropilin-1 and neuropilin-2 genes severely impairs developmental yolk sac and embryonic angiogenesis. *Proc Natl Acad Sci U S A* 99: 3657-3662.
12. Eichmann A, Yuan L, Moyon D, Lenoble F, Pardanaud L, et al. (2005) Vascular development: from precursor cells to branched arterial and venous networks. *Int J Dev Biol* 49: 259-267.
13. Carmeliet P (2003) Angiogenesis in health and disease. *Nat Med* 9: 653-660.

14. Suri C, Jones PF, Patan S, Bartunkova S, Maisonpierre PC, et al. (1996) Requisite role of angiopoietin-1, a ligand for the TIE2 receptor, during embryonic angiogenesis. *Cell* 87: 1171-1180.
15. Wigle JT, Oliver G (1999) Prox1 function is required for the development of the murine lymphatic system. *Cell* 98: 769-778.
16. Oliver G, Alitalo K (2005) The lymphatic vasculature: recent progress and paradigms. *Annu Rev Cell Dev Biol* 21: 457-483.
17. Douville JM, Wigle JT (2007) Regulation and function of homeodomain proteins in the embryonic and adult vascular systems. *Can J Physiol Pharmacol* 85: 55-65.
18. Li WW, Talcott KE, Zhai AW, Kruger EA, Li VW (2005) The role of therapeutic angiogenesis in tissue repair and regeneration. *Adv Skin Wound Care* 18: 491-500; quiz 501-492.
19. Smith SK (2001) Regulation of angiogenesis in the endometrium. *Trends Endocrinol Metab* 12: 147-151.
20. Bloor CM (2005) Angiogenesis during exercise and training. *Angiogenesis* 8: 263-271.
21. Cooke JP (2000) The endothelium: a new target for therapy. *Vasc Med* 5: 49-53.
22. Blann AD (2003) Assessment of endothelial dysfunction: focus on atherothrombotic disease. *Pathophysiol Haemost Thromb* 33: 256-261.
23. Thum T, Haverich A, Borlak J (2000) Cellular dedifferentiation of endothelium is linked to activation and silencing of certain nuclear transcription factors: implications for endothelial dysfunction and vascular biology. *Faseb J* 14: 740-751.
24. Davignon J, Ganz P (2004) Role of endothelial dysfunction in atherosclerosis. *Circulation* 109: III27-32.
25. Deanfield JE, Halcox JP, Rabelink TJ (2007) Endothelial function and dysfunction: testing and clinical relevance. *Circulation* 115: 1285-1295.
26. Creager MA, Luscher TF, Cosentino F, Beckman JA (2003) Diabetes and vascular disease: pathophysiology, clinical consequences, and medical therapy: Part I. *Circulation* 108: 1527-1532.
27. Lee AC, Fenster BE, Ito H, Takeda K, Bae NS, et al. (1999) Ras proteins induce senescence by altering the intracellular levels of reactive oxygen species. *J Biol Chem* 274: 7936-7940.

28. Foreman KE, Tang J (2003) Molecular mechanisms of replicative senescence in endothelial cells. *Exp Gerontol* 38: 1251-1257.
29. Erusalimsky JD, Kurz DJ (2005) Cellular senescence in vivo: its relevance in ageing and cardiovascular disease. *Exp Gerontol* 40: 634-642.
30. Vasile E, Tomita Y, Brown LF, Kocher O, Dvorak HF (2001) Differential expression of thymosin beta-10 by early passage and senescent vascular endothelium is modulated by VPF/VEGF: evidence for senescent endothelial cells in vivo at sites of atherosclerosis. *Faseb J* 15: 458-466.
31. Minamino T, Miyauchi H, Yoshida T, Ishida Y, Yoshida H, et al. (2002) Endothelial cell senescence in human atherosclerosis: role of telomere in endothelial dysfunction. *Circulation* 105: 1541-1544.
32. Minamino T, Yoshida T, Tateno K, Miyauchi H, Zou Y, et al. (2003) Ras induces vascular smooth muscle cell senescence and inflammation in human atherosclerosis. *Circulation* 108: 2264-2269.
33. Sato I, Morita I, Kaji K, Ikeda M, Nagao M, et al. (1993) Reduction of nitric oxide producing activity associated with in vitro aging in cultured human umbilical vein endothelial cell. *Biochem Biophys Res Commun* 195: 1070-1076.
34. Hoffmann J, Haendeler J, Aicher A, Rossig L, Vasa M, et al. (2001) Aging enhances the sensitivity of endothelial cells toward apoptotic stimuli: important role of nitric oxide. *Circ Res* 89: 709-715.
35. Matsushita H, Chang E, Glassford AJ, Cooke JP, Chiu CP, et al. (2001) eNOS activity is reduced in senescent human endothelial cells: Preservation by hTERT immortalization. *Circ Res* 89: 793-798.
36. Uraoka M, Ikeda K, Kurimoto-Nakano R, Nakagawa Y, Koide M, et al. (2011) Loss of bcl-2 during the senescence exacerbates the impaired angiogenic functions in endothelial cells by deteriorating the mitochondrial redox state. *Hypertension* 58: 254-263.
37. Papageorgiou S, Gehring W (2007) The Homeobox as a Key for Understanding the Principles of the Genetic Control of Development. In *HOX Gene Expression*. Springer New York. pp. 1-13.
38. Gehring WJ, Affolter M, Burglin T (1994) Homeodomain proteins. *Annu Rev Biochem* 63: 487-526.
39. Abate-Shen C (2002) Deregulated homeobox gene expression in cancer: cause or consequence? *Nat Rev Cancer* 2: 777-785.
40. Holland PW, Booth HA, Bruford EA (2007) Classification and nomenclature of all human homeobox genes. *BMC Biol* 5: 47.

41. Scott MP, Weiner AJ (1984) Structural relationships among genes that control development: sequence homology between the Antennapedia, Ultrabithorax, and fushi tarazu loci of *Drosophila*. *Proc Natl Acad Sci U S A* 81: 4115-4119.
42. McGinnis W, Levine MS, Hafen E, Kuroiwa A, Gehring WJ (1984) A conserved DNA sequence in homeotic genes of the *Drosophila* Antennapedia and bithorax complexes. *Nature* 308: 428-433.
43. Qian YQ, Billeter M, Otting G, Muller M, Gehring WJ, et al. (1989) The structure of the Antennapedia homeodomain determined by NMR spectroscopy in solution: comparison with prokaryotic repressors. *Cell* 59: 573-580.
44. Otting G, Qian YQ, Billeter M, Muller M, Affolter M, et al. (1990) Protein--DNA contacts in the structure of a homeodomain--DNA complex determined by nuclear magnetic resonance spectroscopy in solution. *Embo J* 9: 3085-3092.
45. Billeter M, Qian YQ, Otting G, Muller M, Gehring W, et al. (1993) Determination of the nuclear magnetic resonance solution structure of an Antennapedia homeodomain-DNA complex. *J Mol Biol* 234: 1084-1093.
46. Garcia-Fernandez J (2005) The genesis and evolution of homeobox gene clusters. *Nat Rev Genet* 6: 881-892.
47. Tischfield MA, Bosley TM, Salih MA, Alorainy IA, Sener EC, et al. (2005) Homozygous HOXA1 mutations disrupt human brainstem, inner ear, cardiovascular and cognitive development. *Nat Genet* 37: 1035-1037.
48. Kameda Y, Nishimaki T, Takeichi M, Chisaka O (2002) Homeobox gene *hoxa3* is essential for the formation of the carotid body in the mouse embryos. *Dev Biol* 247: 197-209.
49. Kameda Y, Watari-Goshima N, Nishimaki T, Chisaka O (2003) Disruption of the *Hoxa3* homeobox gene results in anomalies of the carotid artery system and the arterial baroreceptors. *Cell Tissue Res* 311: 343-352.
50. Stadler HS, Higgins KM, Capecchi MR (2001) Loss of Eph-receptor expression correlates with loss of cell adhesion and chondrogenic capacity in *Hoxa13* mutant limbs. *Development* 128: 4177-4188.
51. Shaut CA, Keene DR, Sorensen LK, Li DY, Stadler HS (2008) HOXA13 Is essential for placental vascular patterning and labyrinth endothelial specification. *PLoS Genet* 4: e1000073.
52. Bergwerff M, Gittenberger-de Groot AC, Wisse LJ, DeRuiter MC, Wessels A, et al. (2000) Loss of function of the *Prx1* and *Prx2* homeobox genes alters architecture of the great elastic arteries and ductus arteriosus. *Virchows Arch* 436: 12-19.

53. Hallaq H, Pinter E, Enciso J, McGrath J, Zeiss C, et al. (2004) A null mutation of Hhex results in abnormal cardiac development, defective vasculogenesis and elevated Vegfa levels. *Development* 131: 5197-5209.
54. Liu X, Zhang X (2002) Effect of anti-sense oligodeoxynucleotides homeobox B2 on the proliferation and expression of primary human umbilical vein endothelial cells. *Chin J Traumatol* 5: 12-15.
55. Myers C, Charboneau A, Boudreau N (2000) Homeobox B3 promotes capillary morphogenesis and angiogenesis. *J Cell Biol* 148: 343-351.
56. Wigle JT, Harvey N, Detmar M, Lagutina I, Grosveld G, et al. (2002) An essential role for Prox1 in the induction of the lymphatic endothelial cell phenotype. *Embo J* 21: 1505-1513.
57. Mace KA, Hansen SL, Myers C, Young DM, Boudreau N (2005) HOXA3 induces cell migration in endothelial and epithelial cells promoting angiogenesis and wound repair. *J Cell Sci* 118: 2567-2577.
58. Bruhl T, Urbich C, Aicher D, Acker-Palmer A, Zeiher AM, et al. (2004) Homeobox A9 transcriptionally regulates the EphB4 receptor to modulate endothelial cell migration and tube formation. *Circ Res* 94: 743-751.
59. Rossig L, Urbich C, Bruhl T, Dernbach E, Heeschen C, et al. (2005) Histone deacetylase activity is essential for the expression of HoxA9 and for endothelial commitment of progenitor cells. *J Exp Med* 201: 1825-1835.
60. Wu Y, Moser M, Bautch VL, Patterson C (2003) HoxB5 is an upstream transcriptional switch for differentiation of the vascular endothelium from precursor cells. *Mol Cell Biol* 23: 5680-5691.
61. Winnik S, Klinkert M, Kurz H, Zoeller C, Heinke J, et al. (2009) HoxB5 induces endothelial sprouting in vitro and modifies intussusceptive angiogenesis in vivo involving angiopoietin-2. *Cardiovasc Res* 83: 558-565.
62. Bostrom K, Tintut Y, Kao SC, Stanford WP, Demer LL (2000) HOXB7 overexpression promotes differentiation of C3H10T1/2 cells to smooth muscle cells. *J Cell Biochem* 78: 210-221.
63. Park H, Choi HJ, Kim J, Kim M, Rho SS, et al. (2011) Homeobox D1 regulates angiogenic functions of endothelial cells via integrin beta1 expression. *Biochem Biophys Res Commun* 408: 186-192.
64. Boudreau N, Andrews C, Srebrow A, Ravanpay A, Cheresch DA (1997) Induction of the angiogenic phenotype by Hox D3. *J Cell Biol* 139: 257-264.

65. Boudreau NJ, Varner JA (2004) The homeobox transcription factor Hox D3 promotes integrin alpha5beta1 expression and function during angiogenesis. *J Biol Chem* 279: 4862-4868.
66. Hansen SL, Myers CA, Charboneau A, Young DM, Boudreau N (2003) HoxD3 accelerates wound healing in diabetic mice. *Am J Pathol* 163: 2421-2431.
67. Uyeno LA, Newman-Keagle JA, Cheung I, Hunt TK, Young DM, et al. (2001) Hox D3 expression in normal and impaired wound healing. *J Surg Res* 100: 46-56.
68. Barzelay A, Ben-Shoshan J, Entin-Meer M, Maysel-Auslender S, Afek A, et al. (2010) A potential role for islet-1 in post-natal angiogenesis and vasculogenesis. *Thromb Haemost* 103: 188-197.
69. Kohler EE, Cowan CE, Chatterjee I, Malik AB, Wary KK (2011) NANOG induction of fetal liver kinase-1 (FLK1) transcription regulates endothelial cell proliferation and angiogenesis. *Blood* 117: 1761-1769.
70. Rhoads K, Arderiu G, Charboneau A, Hansen SL, Hoffman W, et al. (2005) A role for Hox A5 in regulating angiogenesis and vascular patterning. *Lymphat Res Biol* 3: 240-252.
71. Chen Y, Gorski DH (2008) Regulation of angiogenesis through a microRNA (miR-130a) that down-regulates antiangiogenic homeobox genes GAX and HOXA5. *Blood* 111: 1217-1226.
72. Myers C, Charboneau A, Cheung I, Hanks D, Boudreau N (2002) Sustained expression of homeobox D10 inhibits angiogenesis. *Am J Pathol* 161: 2099-2109.
73. Shen X, Fang J, Lv X, Pei Z, Wang Y, et al. (2011) Heparin impairs angiogenesis through inhibition of microRNA-10b. *J Biol Chem* 286: 26616-26627.
74. Hong YK, Harvey N, Noh YH, Schacht V, Hirakawa S, et al. (2002) Prox1 is a master control gene in the program specifying lymphatic endothelial cell fate. *Dev Dyn* 225: 351-357.
75. Petrova TV, Makinen T, Makela TP, Saarela J, Virtanen I, et al. (2002) Lymphatic endothelial reprogramming of vascular endothelial cells by the Prox-1 homeobox transcription factor. *Embo J* 21: 4593-4599.
76. Shin JW, Min M, Larrieu-Lahargue F, Canron X, Kunstfeld R, et al. (2006) Prox1 Promotes Lineage-specific Expression of FGF Receptor-3 in Lymphatic Endothelium: A Role for FGF Signaling in Lymphangiogenesis. *Mol Biol Cell*.
77. Baxter SA, Cheung DY, Bocangel P, Kim HK, Herbert K, et al. (2011) Regulation of the lymphatic endothelial cell cycle by the PROX1 homeodomain protein. *Biochim Biophys Acta* 1813: 201-212.

78. Pruett ND, Visconti RP, Jacobs DF, Scholz D, McQuinn T, et al. (2008) Evidence for Hox-specified positional identities in adult vasculature. *BMC Dev Biol* 8: 93.
79. Bahrami SB, Veisheh M, Dunn AA, Boudreau NJ (2011) Temporal changes in Hox gene expression accompany endothelial cell differentiation of embryonic stem cells. *Cell Adh Migr* 5: 133-141.
80. Chung N, Jee BK, Chae SW, Jeon YW, Lee KH, et al. (2009) HOX gene analysis of endothelial cell differentiation in human bone marrow-derived mesenchymal stem cells. *Mol Biol Rep* 36: 227-235.
81. Futreal PA, Cochran C, Rosenthal J, Miki Y, Swenson J, et al. (1994) Isolation of a diverged homeobox gene, MOX1, from the BRCA1 region on 17q21 by solution hybrid capture. *Hum Mol Genet* 3: 1359-1364.
82. LePage DF, Altomare DA, Testa JR, Walsh K (1994) Molecular cloning and localization of the human GAX gene to 7p21. *Genomics* 24: 535-540.
83. Grigoriou M, Kastrinaki MC, Modi WS, Theodorakis K, Mankoo B, et al. (1995) Isolation of the human MOX2 homeobox gene and localization to chromosome 7p22.1-p21.3. *Genomics* 26: 550-555.
84. Douville JM, Cheung DY, Herbert KL, Moffatt T, Wigle JT (2011) Mechanisms of MEOX1 and MEOX2 regulation of the cyclin dependent kinase inhibitors p21 and p16 in vascular endothelial cells. *PLoS One* 6: e29099.
85. Stamataki D, Kastrinaki M, Mankoo BS, Pachnis V, Karagogeos D (2001) Homeodomain proteins Mox1 and Mox2 associate with Pax1 and Pax3 transcription factors. *FEBS Lett* 499: 274-278.
86. Wissmuller S, Kosian T, Wolf M, Finzsch M, Wegner M (2006) The high-mobility-group domain of Sox proteins interacts with DNA-binding domains of many transcription factors. *Nucleic Acids Res* 34: 1735-1744.
87. Irelan JT, Gutierrez Del Arroyo A, Gutierrez A, Peters G, Quon KC, et al. (2009) A functional screen for regulators of CKDN2A reveals MEOX2 as a transcriptional activator of INK4a. *PLoS One* 4: e5067.
88. Lin J, Friesen MT, Bocangel P, Cheung D, Rawszer K, et al. (2005) Characterization of Mesenchyme Homeobox 2 (MEOX2) transcription factor binding to RING finger protein 10. *Mol Cell Biochem* 275: 75-84.
89. Chen Y, Leal AD, Patel S, Gorski DH (2007) The homeobox gene GAX activates p21WAF1/CIP1 expression in vascular endothelial cells through direct interaction with upstream AT-rich sequences. *J Biol Chem* 282: 507-517.

90. Oma Y, Kino Y, Sasagawa N, Ishiura S (2004) Intracellular localization of homopolymeric amino acid-containing proteins expressed in mammalian cells. *J Biol Chem* 279: 21217-21222.
91. Paraguison RC, Higaki K, Yamamoto K, Matsumoto H, Sasaki T, et al. (2007) Enhanced autophagic cell death in expanded polyhistidine variants of HOXA1 reduces PBX1-coupled transcriptional activity and inhibits neuronal differentiation. *J Neurosci Res* 85: 479-487.
92. Altschul SF, Madden TL, Schaffer AA, Zhang J, Zhang Z, et al. (1997) Gapped BLAST and PSI-BLAST: a new generation of protein database search programs. *Nucleic Acids Res* 25: 3389-3402.
93. Candia AF, Hu J, Crosby J, Lalley PA, Noden D, et al. (1992) Mox-1 and Mox-2 define a novel homeobox gene subfamily and are differentially expressed during early mesodermal patterning in mouse embryos. *Development* 116: 1123-1136.
94. Gorski DH, LePage DF, Patel CV, Copeland NG, Jenkins NA, et al. (1993) Molecular cloning of a diverged homeobox gene that is rapidly down-regulated during the G0/G1 transition in vascular smooth muscle cells. *Mol Cell Biol* 13: 3722-3733.
95. Rallis C, Stamataki D, Pontikakis S, Mankoo BS, Karagogeos D (2001) Isolation of the avian homologue of the homeobox gene Mox2 and analysis of its expression pattern in developing somites and limbs. *Mech Dev* 104: 121-124.
96. Candia AF, Kovalik JP, Wright CV (1993) Amino acid sequence of Mox-2 and comparison to its Xenopus and rat homologs. *Nucleic Acids Res* 21: 4982.
97. Minguillon C, Garcia-Fernandez J (2002) The single amphioxus Mox gene: insights into the functional evolution of Mox genes, somites, and the asymmetry of amphioxus somitogenesis. *Dev Biol* 246: 455-465.
98. Wada S, Tokuoka M, Shoguchi E, Kobayashi K, Di Gregorio A, et al. (2003) A genomewide survey of developmentally relevant genes in *Ciona intestinalis*. II. Genes for homeobox transcription factors. *Dev Genes Evol* 213: 222-234.
99. Lowe CJ, Terasaki M, Wu M, Freeman RM, Jr., Runft L, et al. (2006) Dorsoventral patterning in hemichordates: insights into early chordate evolution. *PLoS Biol* 4: e291.
100. Chiang C, Patel NH, Young KE, Beachy PA (1994) The novel homeodomain gene *buttonless* specifies differentiation and axonal guidance functions of *Drosophila* dorsal median cells. *Development* 120: 3581-3593.
101. Degan BM, Degan SM, Fentenany G, Morse DE (1997) A Mox homeobox gene in the gastropod mollusc *Haliotis rufescens* is differentially expressed during larval morphogenesis and metamorphosis. *FEBS Lett* 411: 119-122.

102. Hinman VF, Degan BM (2002) Mox homeobox expression in muscle lineage of the gastropod *Haliothis asinina*: evidence for a conserved role in bilaterian myogenesis. *Dev Genes Evol* 212: 141-144.
103. Tarabykin VS, Lukyanov KA, Potapov VK, Lukyanov SA (1995) Detection of planarian *Antennapedia*-like homeobox genes expressed during regeneration. *Gene* 158: 197-202.
104. Naito M, Ishiguro H, Fujisawa T, Kurosawa Y (1993) Presence of eight distinct homeobox-containing genes in cnidarians. *FEBS Lett* 333: 271-274.
105. Hill A, Wagner A, Hill M (2003) Hox and paraHox genes from the anthozoan *Parazoanthus parasiticus*. *Mol Phylogenet Evol* 28: 529-535.
106. Ruvkun G, Hobert O (1998) The taxonomy of developmental control in *Caenorhabditis elegans*. *Science* 282: 2033-2041.
107. Minguillon C, Garcia-Fernandez J (2003) Genesis and evolution of the *Evx* and *Mox* genes and the extended Hox and ParaHox gene clusters. *Genome Biol* 4: R12.
108. Gauchat D, Mazet F, Berney C, Schummer M, Kreger S, et al. (2000) Evolution of Antp-class genes and differential expression of Hydra Hox/paraHox genes in anterior patterning. *Proc Natl Acad Sci U S A* 97: 4493-4498.
109. Pollard SL, Holland PW (2000) Evidence for 14 homeobox gene clusters in human genome ancestry. *Curr Biol* 10: 1059-1062.
110. Stelnicki EJ, Komuves LG, Holmes D, Clavin W, Harrison MR, et al. (1997) The human homeobox genes *MSX-1*, *MSX-2*, and *MOX-1* are differentially expressed in the dermis and epidermis in fetal and adult skin. *Differentiation* 62: 33-41.
111. Quinn LM, Johnson BV, Nicholl J, Sutherland GR, Kalionis B (1997) Isolation and identification of homeobox genes from the human placenta including a novel member of the Distal-less family, *DLX4*. *Gene* 187: 55-61.
112. Quinn LM, Latham SE, Kalionis B (2000) The homeobox genes *MSX2* and *MOX2* are candidates for regulating epithelial-mesenchymal cell interactions in the human placenta. *Placenta* 21 Suppl A: S50-54.
113. Murthi P, So M, Gude NM, Doherty VL, Brennecke SP, et al. (2007) Homeobox Genes are Differentially Expressed in Macrovascular Human Umbilical Vein Endothelial Cells and Microvascular Placental Endothelial Cells. *Placenta*.
114. Tallquist MD, Soriano P (2000) Epiblast-restricted Cre expression in MORE mice: a tool to distinguish embryonic vs. extra-embryonic gene function. *Genesis* 26: 113-115.

115. Candia AF, Wright CV (1996) Differential localization of Mox-1 and Mox-2 proteins indicates distinct roles during development. *Int J Dev Biol* 40: 1179-1184.
116. Jukkola T, Trokovic R, Maj P, Lamberg A, Mankoo B, et al. (2005) Meox1Cre: a mouse line expressing Cre recombinase in somitic mesoderm. *Genesis* 43: 148-153.
117. Mankoo BS, Collins NS, Ashby P, Grigorieva E, Pevny LH, et al. (1999) Mox2 is a component of the genetic hierarchy controlling limb muscle development. *Nature* 400: 69-73.
118. Reijntjes S, Stricker S, Mankoo BS (2007) A comparative analysis of Meox1 and Meox2 in the developing somites and limbs of the chick embryo. *Int J Dev Biol* 51: 753-759.
119. Wasteson P, Johansson BR, Jukkola T, Breuer S, Akyurek LM, et al. (2008) Developmental origin of smooth muscle cells in the descending aorta in mice. *Development* 135: 1823-1832.
120. Schwab K, Hartman HA, Liang HC, Aronow BJ, Patterson LT, et al. (2006) Comprehensive microarray analysis of Hoxa11/Hoxd11 mutant kidney development. *Dev Biol* 293: 540-554.
121. Jin JZ, Ding J (2006) Analysis of Meox-2 mutant mice reveals a novel postfusion-based cleft palate. *Dev Dyn* 235: 539-546.
122. Skopicki HA, Lyons GE, Schatteman G, Smith RC, Andres V, et al. (1997) Embryonic expression of the Gax homeodomain protein in cardiac, smooth, and skeletal muscle. *Circ Res* 80: 452-462.
123. Fisher SA, Siwik E, Branellec D, Walsh K, Watanabe M (1997) Forced expression of the homeodomain protein Gax inhibits cardiomyocyte proliferation and perturbs heart morphogenesis. *Development* 124: 4405-4413.
124. Candia AF, Wright CV (1995) The expression pattern of *Xenopus* Mox-2 implies a role in initial mesodermal differentiation. *Mech Dev* 52: 27-36.
125. Ikuta T, Yoshida N, Satoh N, Saiga H (2004) *Ciona intestinalis* Hox gene cluster: Its dispersed structure and residual colinear expression in development. *Proc Natl Acad Sci U S A* 101: 15118-15123.
126. Mankoo BS, Skuntz S, Harrigan I, Grigorieva E, Candia A, et al. (2003) The concerted action of Meox homeobox genes is required upstream of genetic pathways essential for the formation, patterning and differentiation of somites. *Development* 130: 4655-4664.

127. Skuntz S, Mankoo B, Nguyen MT, Hustert E, Nakayama A, et al. (2009) Lack of the mesodermal homeodomain protein MEOX1 disrupts sclerotome polarity and leads to a remodeling of the cranio-cervical joints of the axial skeleton. *Dev Biol* 332: 383-395.
128. Rodrigo I, Bovolenta P, Mankoo BS, Imai K (2004) Meox homeodomain proteins are required for Bapx1 expression in the sclerotome and activate its transcription by direct binding to its promoter. *Mol Cell Biol* 24: 2757-2766.
129. Otto A, Macharia R, Matsakas A, Valasek P, Mankoo BS, et al. (2010) A hypoplastic model of skeletal muscle development displaying reduced foetal myoblast cell numbers, increased oxidative myofibres and improved specific tension capacity. *Dev Biol* 343: 51-62.
130. Buchberger A, Freitag D, Arnold HH (2007) A homeo-paired domain-binding motif directs Myf5 expression in progenitor cells of limb muscle. *Development* 134: 1171-1180.
131. Kennedy KA, Porter T, Mehta V, Ryan SD, Price F, et al. (2009) Retinoic acid enhances skeletal muscle progenitor formation and bypasses inhibition by bone morphogenetic protein 4 but not dominant negative beta-catenin. *BMC Biol* 7: 67.
132. Savage J, Conley AJ, Blais A, Skerjanc IS (2009) SOX15 and SOX7 differentially regulate the myogenic program in P19 cells. *Stem Cells* 27: 1231-1243.
133. Gianakopoulos PJ, Skerjanc IS (2005) Hedgehog signaling induces cardiomyogenesis in P19 cells. *J Biol Chem* 280: 21022-21028.
134. Reijntjes S, Francis-West P, Mankoo BS (2010) Retinoic acid is both necessary for and inhibits myogenic commitment and differentiation in the chick limb. *Int J Dev Biol* 54: 125-134.
135. Petropoulos H, Gianakopoulos PJ, Ridgeway AG, Skerjanc IS (2004) Disruption of Meox or Gli activity ablates skeletal myogenesis in P19 cells. *J Biol Chem* 279: 23874-23881.
136. Savage J, Voronova A, Mehta V, Sendi-Mukasa F, Skerjanc IS (2010) Canonical Wnt signaling regulates Foxc1/2 expression in P19 cells. *Differentiation* 79: 31-40.
137. Gianakopoulos PJ, Skerjanc IS (2009) Cross talk between hedgehog and bone morphogenetic proteins occurs during cardiomyogenesis in P19 cells. *In Vitro Cell Dev Biol Anim* 45: 566-572.
138. Gianakopoulos PJ, Mehta V, Voronova A, Cao Y, Yao Z, et al. (2011) MyoD directly up-regulates premyogenic mesoderm factors during induction of skeletal myogenesis in stem cells. *J Biol Chem* 286: 2517-2525.

139. Goljanek-Whysall K, Pais H, Rathjen T, Sweetman D, Dalmay T, et al. (2012) Regulation of multiple target genes by miR-1/miR-206 is pivotal for C2C12 myoblast differentiation. *J Cell Sci*.
140. Kirilenko P, He G, Mankoo BS, Mallo M, Jones R, et al. (2011) Transient activation of *meox1* is an early component of the gene regulatory network downstream of *hoxa2*. *Mol Cell Biol* 31: 1301-1308.
141. Lin J, Ozeki M, Javel E, Zhao Z, Pan W, et al. (2003) Identification of gene expression profiles in rat ears with cDNA microarrays. *Hear Res* 175: 2-13.
142. Santagati F, Minoux M, Ren SY, Rijli FM (2005) Temporal requirement of *Hoxa2* in cranial neural crest skeletal morphogenesis. *Development* 132: 4927-4936.
143. Li Q, Ding J (2007) Gene expression analysis reveals that formation of the mouse anterior secondary palate involves recruitment of cells from the posterior side. *Int J Dev Biol* 51: 167-172.
144. Pantalacci S, Prochazka J, Martin A, Rothova M, Lambert A, et al. (2008) Patterning of palatal rugae through sequential addition reveals an anterior/posterior boundary in palatal development. *BMC Dev Biol* 8: 116.
145. Weiss KM, Ruddle FH, Bollekens J (1995) *Dlx* and other homeobox genes in the morphological development of the dentition. *Connect Tissue Res* 32: 35-40.
146. Valcourt U, Thuault S, Pardali K, Heldin CH, Moustakas A (2007) Functional role of *Meox2* during the epithelial cyostatic response to TGF-beta. *Mol Oncol* 1: 55-71.
147. Pfaff N, Fiedler J, Holzmann A, Schambach A, Moritz T, et al. (2011) miRNA screening reveals a new miRNA family stimulating iPS cell generation via regulation of *Meox2*. *EMBO Rep* 12: 1153-1159.
148. Bard J (2007) Systems developmental biology: the use of ontologies in annotating models and in identifying gene function within and across species. *Mamm Genome* 18: 402-411.
149. Bard JB, Lam MS, Aitken S (2008) A bioinformatics approach for identifying candidate transcriptional regulators of mesenchyme-to-epithelium transitions in mouse embryos. *Dev Dyn* 237: 2748-2754.
150. Gorski DH, Leal AJ (2003) Inhibition of endothelial cell activation by the homeobox gene *Gax*. *J Surg Res* 111: 91-99.
151. Bostrom P, Mann N, Wu J, Quintero PA, Plovie ER, et al. (2010) *C/EBPbeta* controls exercise-induced cardiac growth and protects against pathological cardiac remodeling. *Cell* 143: 1072-1083.

152. Amatschek S, Kriehuber E, Bauer W, Reininger B, Meraner P, et al. (2007) Blood and lymphatic endothelial cell-specific differentiation programs are stringently controlled by the tissue environment. *Blood* 109: 4777-4785.
153. Weir L, Chen D, Pastore C, Isner JM, Walsh K (1995) Expression of *gax*, a growth arrest homeobox gene, is rapidly down-regulated in the rat carotid artery during the proliferative response to balloon injury. *J Biol Chem* 270: 5457-5461.
154. Markmann A, Rauterberg J, Vischer P, Robenek H, Echtermeyer F, et al. (2003) Expression of transcription factors and matrix genes in response to serum stimulus in vascular smooth muscle cells. *Eur J Cell Biol* 82: 119-129.
155. Maillard L, Van Belle E, Smith RC, Le Roux A, Deneffe P, et al. (1997) Percutaneous delivery of the *gax* gene inhibits vessel stenosis in a rabbit model of balloon angioplasty. *Cardiovasc Res* 35: 536-546.
156. Smith RC, Branellec D, Gorski DH, Guo K, Perlman H, et al. (1997) p21CIP1-mediated inhibition of cell proliferation by overexpression of the *gax* homeodomain gene. *Genes Dev* 11: 1674-1689.
157. Zheng H, Xue S, Lian F, Hu ZL, Wang YY (2012) [Effects on proliferation and apoptosis of serum-induced rabbit VSMCs by adenovirus-mediated transfer of the *Gax* gene]. *Xi Bao Yu Fen Zi Mian Yi Xue Za Zhi* 28: 33-36.
158. Witzensichler B, Kureishi Y, Luo Z, Le Roux A, Branellec D, et al. (1999) Regulation of smooth muscle cell migration and integrin expression by the *Gax* transcription factor. *J Clin Invest* 104: 1469-1480.
159. Perlman H, Sata M, Le Roux A, Sedlak TW, Branellec D, et al. (1998) Bax-mediated cell death by the *Gax* homeoprotein requires mitogen activation but is independent of cell cycle activity. *Embo J* 17: 3576-3586.
160. Perlman H, Luo Z, Krasinski K, Le Roux A, Mahfoudi A, et al. (1999) Adenovirus-mediated delivery of the *Gax* transcription factor to rat carotid arteries inhibits smooth muscle proliferation and induces apoptosis. *Gene Ther* 6: 758-763.
161. Maillard L, Van Belle E, Tio FO, Rivard A, Kearney M, et al. (2000) Effect of percutaneous adenovirus-mediated *Gax* gene delivery to the arterial wall in double-injured atheromatous stented rabbit iliac arteries. *Gene Ther* 7: 1353-1361.
162. Yamashita J, Itoh H, Ogawa Y, Tamura N, Takaya K, et al. (1997) Opposite regulation of *Gax* homeobox expression by angiotensin II and C-type natriuretic peptide. *Hypertension* 29: 381-387.
163. Saito T, Itoh H, Yamashita J, Doi K, Chun TH, et al. (2005) Angiotensin II suppresses growth arrest specific homeobox (*Gax*) expression via redox-sensitive mitogen-activated protein kinase (MAPK). *Regul Pept* 127: 159-167.

164. Wu WH, Hu CP, Chen XP, Zhang WF, Li XW, et al. (2011) MicroRNA-130a mediates proliferation of vascular smooth muscle cells in hypertension. *Am J Hypertens* 24: 1087-1093.
165. Xia S, Tai X, Wang Y, An X, Qian G, et al. (2011) Involvement of Gax gene in hypoxia-induced pulmonary hypertension, proliferation, and apoptosis of arterial smooth muscle cells. *Am J Respir Cell Mol Biol* 44: 66-73.
166. Xia SJ, Dong JC, Bai L, Hu MD, Qian GS, et al. (2007) [The effects of Ad-Gax transfection on apoptosis and related gene expression in pulmonary arterial smooth muscle cells in hypoxic rat model]. *Zhonghua Nei Ke Za Zhi* 46: 755-759.
167. Andres V, Fisher S, Wearsch P, Walsh K (1995) Regulation of Gax homeobox gene transcription by a combination of positive factors including myocyte-specific enhancer factor 2. *Mol Cell Biol* 15: 4272-4281.
168. Liu P, Zhang C, Feng JB, Zhao YX, Wang XP, et al. (2008) Cross talk among Smad, MAPK, and integrin signaling pathways enhances adventitial fibroblast functions activated by transforming growth factor-beta1 and inhibited by Gax. *Arterioscler Thromb Vasc Biol* 28: 725-731.
169. Liu P, Zhang C, Zhao YX, Feng JB, Liu CX, et al. (2010) Gax gene transfer inhibits vascular remodeling induced by adventitial inflammation in rabbits. *Atherosclerosis* 212: 398-405.
170. Patel S, Leal AD, Gorski DH (2005) The homeobox gene Gax inhibits angiogenesis through inhibition of nuclear factor-kappaB-dependent endothelial cell gene expression. *Cancer Res* 65: 1414-1424.
171. Wu Z, Guo H, Chow N, Sallstrom J, Bell RD, et al. (2005) Role of the MEOX2 homeobox gene in neurovascular dysfunction in Alzheimer disease. *Nat Med* 11: 959-965.
172. Chen Y, Banda M, Speyer CL, Smith JS, Rabson AB, et al. (2010) Regulation of the expression and activity of the antiangiogenic homeobox gene GAX/MEOX2 by ZEB2 and microRNA-221. *Mol Cell Biol* 30: 3902-3913.
173. Dembinska-Kiec A, Polus A, Kiec-Wilk B, Grzybowska J, Mikolajczyk M, et al. (2005) Proangiogenic activity of beta-carotene is coupled with the activation of endothelial cell chemotaxis. *Biochim Biophys Acta* 1740: 222-239.
174. Chen Y, Rabson AB, Gorski DH (2010) MEOX2 regulates nuclear factor-kappaB activity in vascular endothelial cells through interactions with p65 and IkappaBbeta. *Cardiovasc Res* 87: 723-731.
175. Whittock NV, Coleman CM, McLean WH, Ashton GH, Acland KM, et al. (2000) The gene for Naegeli-Franceschetti-Jadassohn syndrome maps to 17q21. *J Invest Dermatol* 115: 694-698.

176. Vatanavicharn N, Graham JM, Jr., Curry CJ, Pepkowitz S, Lachman RS, et al. (2007) Diaphanospondylodysostosis: six new cases and exclusion of the candidate genes, PAX1 and MEOX1. *Am J Med Genet A* 143A: 2292-2302.
177. Staehling-Hampton K, Proll S, Paeper BW, Zhao L, Charmley P, et al. (2002) A 52-kb deletion in the SOST-MEOX1 intergenic region on 17q12-q21 is associated with van Buchem disease in the Dutch population. *Am J Med Genet* 110: 144-152.
178. Loots GG, Kneissel M, Keller H, Baptist M, Chang J, et al. (2005) Genomic deletion of a long-range bone enhancer misregulates sclerostin in Van Buchem disease. *Genome Res* 15: 928-935.
179. Linn SC, West RB, Pollack JR, Zhu S, Hernandez-Boussard T, et al. (2003) Gene expression patterns and gene copy number changes in dermatofibrosarcoma protuberans. *Am J Pathol* 163: 2383-2395.
180. Thiaville MM, Stoeck A, Chen L, Wu RC, Magnani L, et al. (2012) Identification of PBX1 Target Genes in Cancer Cells by Global Mapping of PBX1 Binding Sites. *PLoS One* 7: e36054.
181. Csoka AB, English SB, Simkevich CP, Ginzinger DG, Butte AJ, et al. (2004) Genome-scale expression profiling of Hutchinson-Gilford progeria syndrome reveals widespread transcriptional misregulation leading to mesodermal/mesenchymal defects and accelerated atherosclerosis. *Aging Cell* 3: 235-243.
182. Plasilova M, Chattopadhyay C, Ghosh A, Wenzel F, Demougin P, et al. (2011) Discordant gene expression signatures and related phenotypic differences in lamin A- and A/C-related Hutchinson-Gilford progeria syndrome (HGPS). *PLoS One* 6: e21433.
183. Deane R, Zlokovic BV (2007) Role of the blood-brain barrier in the pathogenesis of Alzheimer's disease. *Curr Alzheimer Res* 4: 191-197.
184. Rovelet-Lecrux A, Legallic S, Wallon D, Flaman JM, Martinaud O, et al. (2011) A genome-wide study reveals rare CNVs exclusive to extreme phenotypes of Alzheimer disease. *Eur J Hum Genet* 20: 613-617.
185. Zeng JH, Yang Z, Xu J, Qiu ML, Lin KC (2006) Down-regulation of the gax gene in smooth muscle cells of the splenic vein of portal hypertension patients. *Hepatobiliary Pancreat Dis Int* 5: 242-245.
186. Frullanti E, Galvan A, Falvella FS, Manenti G, Colombo F, et al. (2011) Multiple genetic loci modulate lung adenocarcinoma clinical staging. *Clin Cancer Res* 17: 2410-2416.

187. Cortese R, Hartmann O, Berlin K, Eckhardt F (2008) Correlative gene expression and DNA methylation profiling in lung development nominate new biomarkers in lung cancer. *Int J Biochem Cell Biol* 40: 1494-1508.
188. Ohshima J, Haruta M, Arai Y, Kasai F, Fujiwara Y, et al. (2009) Two candidate tumor suppressor genes, MEOX2 and SOSTDC1, identified in a 7p21 homozygous deletion region in a Wilms tumor. *Genes Chromosomes Cancer* 48: 1037-1050.
189. Li CM, Kim CE, Margolin AA, Guo M, Zhu J, et al. (2004) CTNNB1 mutations and overexpression of Wnt/beta-catenin target genes in WT1-mutant Wilms' tumors. *Am J Pathol* 165: 1943-1953.
190. Wang XC, Tian LL, Wu HL, Jiang XY, Du LQ, et al. (2010) Expression of miRNA-130a in nonsmall cell lung cancer. *Am J Med Sci* 340: 385-388.
191. Zhou P, Jiang W, Wu L, Chang R, Wu K, et al. (2012) miR-301a is a candidate oncogene that targets the homeobox gene Gax in human hepatocellular carcinoma. *Dig Dis Sci* 57: 1171-1180.
192. Zhou P, Chen Z, Chang RM, Jiang W, Wu LL, et al. (2012) Growth arrest-specific homeobox is associated with poor survival in patients with hepatocellular carcinoma. *Med Oncol*.
193. Cao G, Huang B, Liu Z, Zhang J, Xu H, et al. (2010) Intronic miR-301 feedback regulates its host gene, ska2, in A549 cells by targeting MEOX2 to affect ERK/CREB pathways. *Biochem Biophys Res Commun* 396: 978-982.
194. Xia S, Qian G, Hu M, Huang Y, Tan Y (2006) [Effects of Gax gene transfection on proliferation and expression of proto-oncogenes in A549 cells.]. *Zhongguo Fei Ai Za Zhi* 9: 221-225.
195. Xia S, Tai X, Dong J, Qian G, Hu M (2007) [Effect of Ad-Gax transfection on apoptosis of human lung adenocarcinoma A549 cells and its mechanism.]. *Zhongguo Fei Ai Za Zhi* 10: 269-274.
196. Mackay J, Mensah G (2004) *The Atlas of Heart Disease and Stroke*: World Health Organization. 112 p.
197. Balakumar P, Kaur T, Singh M (2008) Potential target sites to modulate vascular endothelial dysfunction: current perspectives and future directions. *Toxicology* 245: 49-64.
198. Fink SL, Cookson BT (2005) Apoptosis, pyroptosis, and necrosis: mechanistic description of dead and dying eukaryotic cells. *Infect Immun* 73: 1907-1916.
199. Duprez L, Wirawan E, Vanden Berghe T, Vandenabeele P (2009) Major cell death pathways at a glance. *Microbes Infect* 11: 1050-1062.

200. Kerr JF, Wyllie AH, Currie AR (1972) Apoptosis: a basic biological phenomenon with wide-ranging implications in tissue kinetics. *Br J Cancer* 26: 239-257.
201. Wyllie AH (1980) Glucocorticoid-induced thymocyte apoptosis is associated with endogenous endonuclease activation. *Nature* 284: 555-556.
202. Lindsay J, Esposti MD, Gilmore AP (2011) Bcl-2 proteins and mitochondria--specificity in membrane targeting for death. *Biochim Biophys Acta* 1813: 532-539.
203. Tang TT, Dowbenko D, Jackson A, Toney L, Lewin DA, et al. (2002) The forkhead transcription factor AFX activates apoptosis by induction of the BCL-6 transcriptional repressor. *J Biol Chem* 277: 14255-14265.
204. Kimes BW, Brandt BL (1976) Characterization of two putative smooth muscle cell lines from rat thoracic aorta. *Exp Cell Res* 98: 349-366.
205. Saward L, Zahradka P (1997) Coronary artery smooth muscle in culture: migration of heterogeneous cell populations from vessel wall. *Mol Cell Biochem* 176: 53-59.
206. Ruegg UT, Burgess GM (1989) Staurosporine, K-252 and UCN-01: potent but nonspecific inhibitors of protein kinases. *Trends Pharmacol Sci* 10: 218-220.
207. Karaman MW, Herrgard S, Treiber DK, Gallant P, Atteridge CE, et al. (2008) A quantitative analysis of kinase inhibitor selectivity. *Nat Biotechnol* 26: 127-132.
208. Firulli AB, Han D, Kelly-Roloff L, Koteliansky VE, Schwartz SM, et al. (1998) A comparative molecular analysis of four rat smooth muscle cell lines. *In Vitro Cell Dev Biol Anim* 34: 217-226.
209. Francis G, Kerem Z, Makkar HP, Becker K (2002) The biological action of saponins in animal systems: a review. *Br J Nutr* 88: 587-605.
210. Dong Z, Zeitlin BD, Song W, Sun Q, Karl E, et al. (2007) Level of endothelial cell apoptosis required for a significant decrease in microvessel density. *Exp Cell Res* 313: 3645-3657.
211. Carmeliet P (2005) Angiogenesis in life, disease and medicine. *Nature* 438: 932-936.
212. Rivard A, Fabre JE, Silver M, Chen D, Murohara T, et al. (1999) Age-dependent impairment of angiogenesis. *Circulation* 99: 111-120.
213. Blomen VA, Boonstra J (2007) Cell fate determination during G1 phase progression. *Cell Mol Life Sci* 64: 3084-3104.

214. Ekholm SV, Reed SI (2000) Regulation of G(1) cyclin-dependent kinases in the mammalian cell cycle. *Curr Opin Cell Biol* 12: 676-684.
215. Stott FJ, Bates S, James MC, McConnell BB, Starborg M, et al. (1998) The alternative product from the human CDKN2A locus, p14(ARF), participates in a regulatory feedback loop with p53 and MDM2. *Embo J* 17: 5001-5014.
216. Hayflick L, Moorhead PS (1961) The serial cultivation of human diploid cell strains. *Exp Cell Res* 25: 585-621.
217. Hayflick L (1965) The Limited in Vitro Lifetime of Human Diploid Cell Strains. *Exp Cell Res* 37: 614-636.
218. Erusalimsky JD (2009) Vascular endothelial senescence: from mechanisms to pathophysiology. *J Appl Physiol* 106: 326-332.
219. Bodnar AG, Ouellette M, Frolkis M, Holt SE, Chiu CP, et al. (1998) Extension of life-span by introduction of telomerase into normal human cells. *Science* 279: 349-352.
220. Hastings R, Qureshi M, Verma R, Lacy PS, Williams B (2004) Telomere attrition and accumulation of senescent cells in cultured human endothelial cells. *Cell Prolif* 37: 317-324.
221. Moiseeva O, Mallette FA, Mukhopadhyay UK, Moores A, Ferbeyre G (2006) DNA damage signaling and p53-dependent senescence after prolonged beta-interferon stimulation. *Mol Biol Cell* 17: 1583-1592.
222. Serrano M, Lin AW, McCurrach ME, Beach D, Lowe SW (1997) Oncogenic ras provokes premature cell senescence associated with accumulation of p53 and p16INK4a. *Cell* 88: 593-602.
223. Campisi J, d'Adda di Fagagna F (2007) Cellular senescence: when bad things happen to good cells. *Nat Rev Mol Cell Biol* 8: 729-740.
224. Krishnamurthy J, Torrice C, Ramsey MR, Kovalev GI, Al-Regaiey K, et al. (2004) Ink4a/Arf expression is a biomarker of aging. *J Clin Invest* 114: 1299-1307.
225. Narita M, Nunez S, Heard E, Lin AW, Hearn SA, et al. (2003) Rb-mediated heterochromatin formation and silencing of E2F target genes during cellular senescence. *Cell* 113: 703-716.
226. Ferbeyre G, de Stanchina E, Querido E, Baptiste N, Prives C, et al. (2000) PML is induced by oncogenic ras and promotes premature senescence. *Genes Dev* 14: 2015-2027.

227. Dimri GP, Lee X, Basile G, Acosta M, Scott G, et al. (1995) A biomarker that identifies senescent human cells in culture and in aging skin in vivo. *Proc Natl Acad Sci U S A* 92: 9363-9367.
228. el-Deiry WS, Tokino T, Velculescu VE, Levy DB, Parsons R, et al. (1993) WAF1, a potential mediator of p53 tumor suppression. *Cell* 75: 817-825.
229. Koutsodontis G, Kardassis D (2004) Inhibition of p53-mediated transcriptional responses by mithramycin A. *Oncogene* 23: 9190-9200.
230. Mandal S, Davie JR (2010) Estrogen regulated expression of the p21 Waf1/Cip1 gene in estrogen receptor positive human breast cancer cells. *J Cell Physiol* 224: 28-32.
231. Kessler DS (1997) Siamois is required for formation of Spemann's organizer. *Proc Natl Acad Sci U S A* 94: 13017-13022.
232. Le TN, Du G, Fonseca M, Zhou QP, Wigle JT, et al. (2007) Dlx homeobox genes promote cortical interneuron migration from the basal forebrain by direct repression of the semaphorin receptor neuropilin-2. *J Biol Chem* 282: 19071-19081.
233. Salichs E, Ledda A, Mularoni L, Alba MM, de la Luna S (2009) Genome-wide analysis of histidine repeats reveals their role in the localization of human proteins to the nuclear speckles compartment. *PLoS Genet* 5: e1000397.
234. el-Deiry WS, Harper JW, O'Connor PM, Velculescu VE, Canman CE, et al. (1994) WAF1/CIP1 is induced in p53-mediated G1 arrest and apoptosis. *Cancer Res* 54: 1169-1174.
235. Boehme KA, Blattner C (2009) Regulation of p53--insights into a complex process. *Crit Rev Biochem Mol Biol* 44: 367-392.
236. Philipsen S, Suske G (1999) A tale of three fingers: the family of mammalian Sp/XKLF transcription factors. *Nucleic Acids Res* 27: 2991-3000.
237. Li L, Davie JR (2010) The role of Sp1 and Sp3 in normal and cancer cell biology. *Ann Anat* 192: 275-283.
238. Karpova TS, Kim MJ, Spriet C, Nalley K, Stasevich TJ, et al. (2008) Concurrent fast and slow cycling of a transcriptional activator at an endogenous promoter. *Science* 319: 466-469.
239. Lickwar CR, Mueller F, Hanlon SE, McNally JG, Lieb JD (2012) Genome-wide protein-DNA-binding dynamics suggest a molecular clutch for transcription factor function. *Nature* 484: 251-255.

240. Serrano M (2000) The INK4a/ARF locus in murine tumorigenesis. *Carcinogenesis* 21: 865-869.
241. Gartel AL, Tyner AL (1999) Transcriptional regulation of the p21((WAF1/CIP1)) gene. *Exp Cell Res* 246: 280-289.
242. Gil J, Peters G (2006) Regulation of the INK4b-ARF-INK4a tumour suppressor locus: all for one or one for all. *Nat Rev Mol Cell Biol* 7: 667-677.
243. Zhang R, Min W, Sessa WC (1995) Functional analysis of the human endothelial nitric oxide synthase promoter. Sp1 and GATA factors are necessary for basal transcription in endothelial cells. *J Biol Chem* 270: 15320-15326.
244. Irizarry RA, Hobbs B, Collin F, Beazer-Barclay YD, Antonellis KJ, et al. (2003) Exploration, normalization, and summaries of high density oligonucleotide array probe level data. *Biostatistics* 4: 249-264.
245. Subramanian A, Tamayo P, Mootha VK, Mukherjee S, Ebert BL, et al. (2005) Gene set enrichment analysis: a knowledge-based approach for interpreting genome-wide expression profiles. *Proc Natl Acad Sci U S A* 102: 15545-15550.
246. Mootha VK, Lindgren CM, Eriksson KF, Subramanian A, Sihag S, et al. (2003) PGC-1alpha-responsive genes involved in oxidative phosphorylation are coordinately downregulated in human diabetes. *Nat Genet* 34: 267-273.
247. Merico D, Isserlin R, Stueker O, Emili A, Bader GD (2010) Enrichment map: a network-based method for gene-set enrichment visualization and interpretation. *PLoS One* 5: e13984.
248. Xu F, Li H, Jin T (1999) Cell type-specific autoregulation of the Caudal-related homeobox gene Cdx-2/3. *J Biol Chem* 274: 34310-34316.
249. Kurz DJ, Decary S, Hong Y, Erusalimsky JD (2000) Senescence-associated (beta)-galactosidase reflects an increase in lysosomal mass during replicative ageing of human endothelial cells. *J Cell Sci* 113 (Pt 20): 3613-3622.
250. Charette M, Gray MW (2000) Pseudouridine in RNA: what, where, how, and why. *IUBMB Life* 49: 341-351.
251. Meier UT (2005) The many facets of H/ACA ribonucleoproteins. *Chromosoma* 114: 1-14.
252. Hamma T, Ferre-D'Amare AR (2006) Pseudouridine synthases. *Chem Biol* 13: 1125-1135.
253. Mitchell JR, Wood E, Collins K (1999) A telomerase component is defective in the human disease dyskeratosis congenita. *Nature* 402: 551-555.

254. Pogacic V, Dragon F, Filipowicz W (2000) Human H/ACA small nucleolar RNPs and telomerase share evolutionarily conserved proteins NHP2 and NOP10. *Mol Cell Biol* 20: 9028-9040.
255. Kirwan M, Dokal I (2009) Dyskeratosis congenita, stem cells and telomeres. *Biochim Biophys Acta* 1792: 371-379.
256. Alter BP, Baerlocher GM, Savage SA, Chanock SJ, Weksler BB, et al. (2007) Very short telomere length by flow fluorescence in situ hybridization identifies patients with dyskeratosis congenita. *Blood* 110: 1439-1447.
257. Decker ML, Chavez E, Vulto I, Lansdorp PM (2009) Telomere length in Hutchinson-Gilford progeria syndrome. *Mech Ageing Dev* 130: 377-383.
258. Shelton DN, Chang E, Whittier PS, Choi D, Funk WD (1999) Microarray analysis of replicative senescence. *Curr Biol* 9: 939-945.
259. Robertson G, Hirst M, Bainbridge M, Bilenky M, Zhao Y, et al. (2007) Genome-wide profiles of STAT1 DNA association using chromatin immunoprecipitation and massively parallel sequencing. *Nat Methods* 4: 651-657.
260. Ho SN, Hunt HD, Horton RM, Pullen JK, Pease LR (1989) Site-directed mutagenesis by overlap extension using the polymerase chain reaction. *Gene* 77: 51-59.
261. Barik S (1996) Site-directed mutagenesis in vitro by megaprimer PCR. *Methods Mol Biol* 57: 203-215.
262. Rigaut G, Shevchenko A, Rutz B, Wilm M, Mann M, et al. (1999) A generic protein purification method for protein complex characterization and proteome exploration. *Nat Biotechnol* 17: 1030-1032.
263. McKinnell IW, Ishibashi J, Le Grand F, Punch VG, Addicks GC, et al. (2008) Pax7 activates myogenic genes by recruitment of a histone methyltransferase complex. *Nat Cell Biol* 10: 77-84.

APPENDICES

Appendix A: MEOX2 middle region is sufficient for zinc finger binding

- Referred to in Chapter 1 (section 1.3.1.2), Chapter 3 (section 3.2), Chapter 4 (section 4.4.2.3) and Chapter 6 (section 6.2).

We conducted a GAL4 yeast-two-hybrid screen of a mouse 11-day embryo cDNA library using human MEOX2 as bait and identified zinc finger protein 672 (ZFP672) as being a potential binding partner of MEOX2. The ability of yeast to grow in the absence of essential amino acids indicate an interaction between the bait and prey proteins – forming a transcription factor complex that is able to activate amino acid biosynthesis genes.

Drop tests using different versions of MEOX2 show that homeodomain deleted MEOX2^{ΔHD} and the middle domain of MEOX2^{MID} interact with the *Zfp672* cDNA clone #194a (Figure A-1, panel A). We concluded that the middle domain of MEOX2 was sufficient for binding to ZFP672. As the cDNA clone #194a did not contain the entire *Zfp672* mRNA sequence, we were able to establish that ZFP672 interacts with the MEOX2 middle domain via its zinc finger domains (data not shown).

In order to verify that the MEOX2 middle domain was required for MEOX2 interaction with ZFP672, we created a version of MEOX2 in which the middle region was deleted. Drop tests showed that deletion of the middle domain of MEOX2 abolished its ability to interact with ZFP672 (Figure A-1, panel B).

Although the function of ZFP672 is unknown, it is predicted to be a nuclear transcription factor, thus making it a potential transcriptional co-factor of MEOX2.

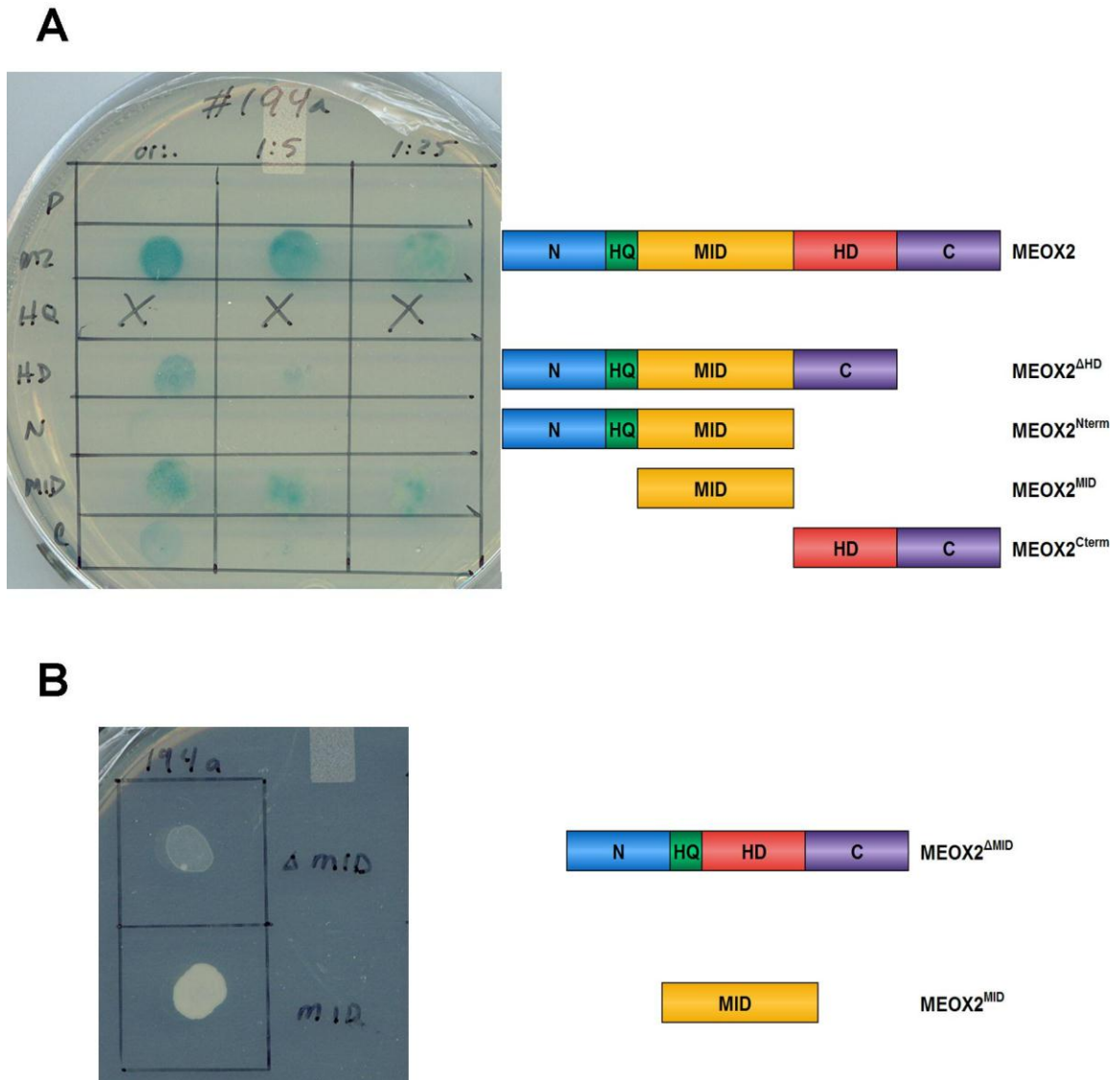


Figure A-1: The middle region of MEOX2 is sufficient for interaction with mouse zinc-finger protein 672.

Figure A-1: The middle region of MEOX2 is sufficient for interacting with mouse zinc-finger protein 672.

(A) GAL4 yeast-two-hybrid drop test demonstrating that wild-type MEOX2, homeodomain deleted MEOX2 (MEOX2^{ΔHD}) and the middle domain of MEOX2 (MEOX2^{MID}) interacted with ZFP672, enabling yeast to grow on media lacking essential amino acids. The image was taken 12 days after plating the yeast. P represents the empty vector control. (B) Yeast-two-hybrid drop test demonstrating that in contrast to MEOX2^{MID}, middle domain deleted MEOX2 (MEOX2^{ΔMID}) did not interact with ZFP672. The image was taken 6 days after plating the yeast.

Appendix B: Description of MEOX construct generation

- Referred to in Chapter 3 (sections 3.3.2 and 3.3.3) and Chapter 4 (sections 4.3.2 and 4.3.8).

B.1. MEOX-EGFP fusion protein constructs

The pp53-EGFP (Clontech) vector was a gift from Dr. N. Mesaeli (Weill Cornell Medical College in Qatar). The p53 coding sequence was excised from this vector using *EcoRI/BamHI* restriction enzyme digestion. Subsequently, full-length mouse *Meox1* was amplified by PCR from a cDNA clone (IMAGE ID 464899, Invitrogen) using the **MX003** and **MX004** primers, digested with *EcoRI/BamHI* and then ligated in-frame into the *EcoRI/BamHI* digested EGFP vector, creating a C-terminal EGFP-tagged construct. Full-length human *MEOX2* was amplified by PCR from a cDNA clone (IMAGE ID 3917118, Invitrogen) using the **MX001** and **MX002** primers, digested with *EcoRI/BamHI* and then similarly cloned into the EGFP vector. The homeodomain deleted *Meox1*^{K180_K230del} and *MEOX2*^{K195_K245del} constructs were amplified by PCR from the pCMV-Tag4A vector using the **MX003** and **MX004** primers or the **MX001** and **MX002** primers, respectively, digested with *EcoRI/BamHI* and then cloned into the EGFP vector. The middle domain deleted *MEOX2*^{T89_V182del} construct in pCMV-Tag4A was amplified by PCR using the **MX001** and **MX002** primers and then digested with *EcoRI/BamHI* prior to cloning into the EGFP vector.

B.2. *MEOX-FLAG fusion protein constructs*

Full-length mouse *Meox1* was amplified by PCR from a cDNA clone (IMAGE ID 464899, Invitrogen) using the **MX003** and **MX008** primers, digested with *EcoRI/XhoI* and then ligated in-frame into the pCMV-Tag4A vector (Stratagene), creating a C-terminal FLAG-tagged construct. Subsequently, the C-terminal FLAG-tagged *Meox1* construct was amplified from the pCMV-Tag4A vector using the **MX003** and **NOTI** primers, digested with *EcoRI/NotI* and cloned into the pcDNA3.1(+) vector. The **MX100** and **MX095** primers were used to amplify *Meox1* from the pCMV-Tag4A vector for cloning into the *EcoRI/XhoI* digested pCMV-Tag2B vector (Stratagene), to create an N-terminal FLAG-tagged construct.

Wild-type *Meox1* in the pCMV-Tag4A vector was used as a template to create two DNA-binding deficient versions of *Meox1*. The DNA-binding domain mutated *Meox1*^{Q219E} construct was created by splice overlap extension PCR [260] using the mutagenesis primers **MX022** and **MX023**, which changed CAA (Q) to GAA (E) at amino acid position 220. This mutant construct was then cloned into the pcDNA3.1(+) and pCMV-Tag2B vectors as described for wild-type *Meox1*. The homeodomain deleted construct *Meox1*^{K180_K230del} was created by using megaprimer PCR [261] using the **MX033** primer with the **MX003** and **MX008** primers. The *Meox1*^{K180_K230del} construct was subsequently cloned into the pCMV-Tag2B vector as described for wild-type *Meox1*.

Full-length human *MEOX2* was amplified by PCR from a cDNA clone (IMAGE ID 3917118, Invitrogen) using the **MX001** and **MX005** primers, digested with *EcoRI/XhoI* and then ligated into the *EcoRI/XhoI* digested pCMV-Tag4A vector, thereby generating a C-terminal FLAG-tagged *MEOX2* construct. Subsequently, the C-terminal

FLAG-tagged *MEOX2* construct was amplified from the pCVM-Tag4A vector using the **MX001** and **NOTI** primers, digested with *EcoRI/NotI* and cloned into the pcDNA3.1(+) vector. The **MX096** and **MX097** primers were used to amplify *MEOX2* from the pCMV-Tag4A vector for cloning into the *BamHI/XhoI* digested pCMV-Tag2B vector.

Wild-type *MEOX2* in the pCMV-Tag4A vector was used as a template to create several mutant versions of *MEOX2*. The DNA-binding domain mutated *MEOX2*^{Q235E} construct was created by splice overlap extension PCR using the mutagenesis primers **MX024** and **MX025**, which changed CAA (Q) to GAA (E) at amino acid position 235. This mutant construct was then cloned into the pcDNA3.1(+) and pCMV-Tag2B vectors as described for wild-type *MEOX2*. The homeodomain deleted constructs *MEOX2*^{K195_K245del} and *MEOX2*^{K188_K245del} were created by megaprimer PCR using the **MX032** primer or the **MX101** primer with the **MX001** and **MX005** primers, respectively. The *MEOX2*^{K195_K245del} construct was subsequently cloned into the pCMV-Tag2B vector as described for wild-type *MEOX2*. The middle domain deleted construct *MEOX2*^{T89_V182del} was created by complete *EcoRI* and partial *HincII* digestion of the pCMV-Tag4A-*MEOX2* construct. The 5' end of the *MEOX2* cDNA was amplified by PCR using the **MX001** and **MX085** primers and then ligated into the partially digested vector.

The histidine/glutamine rich domain deleted construct *MEOX2*^{H68_Q85del} in pCMV-Tag2B was created from the pCMV-Tag2B-*MEOX2* vector by splice overlap extension PCR using the **MX096**, **MX109**, **MX108** and **MX097** primers, while *MEOX2*^{H68_Q85del} in pcDNA3.1(+) was created from the pcDNA3.1-*MEOX2* vector by splice overlap extension PCR using the **MX001**, **MX109**, **MX108** and **NOTI** primers.

The untagged version of *MEOX2* in the pCMV-Tag4A vector (pCMV-Tag4A-*MEOX2*-STOP) was created from the pCMV-Tag4A-*MEOX2* vector by PCR amplification using the **MX001** and **MX097** primers, digestion with *EcoRI/XhoI* and then ligation with the empty *EcoRI/XhoI* digested pCMV-Tag4A vector. This construct has one stop codon inserted between the *MEOX2* coding region and the FLAG-tag, thereby preventing fusion of the FLAG-tag to *MEOX2*.

Primer sequences are listed in Table B-1. All of the aforementioned expression constructs were sequence verified at the University of Calgary and are listed in Table B-2.

B.3. *MEOX* adenovirus constructs

Adenovirus encoding C-terminal FLAG-tagged *Meox1*, *MEOX2* and *MEOX2*^{K195_K245del} adenoviral constructs were created by excising the *MEOX* cDNA from the pCMV-Tag4A by restriction enzyme digestion. The plasmid pCMV-Tag4A constructs were digested with *EcoRI*, following which the 5' DNA overhangs were filled using the *Large (Klenow) Fragment of DNA Polymerase I* as per the manufacturer's instructions (New England Biolabs). The construct was then digested using *KpnI*. Subsequently, the *MEOX* cDNA was ligated to the pShuttle-CMV vector which had been digested with *BglIII*, 5' DNA overhangs filled using *Large (Klenow) Fragment of DNA Polymerase I*, and then digested using *KpnI*.

Adenovirus encoding N-terminal FLAG-tagged *Meox1*, *MEOX2*, *MEOX2*^{Q235E} and *MEOX2*^{K195_K245del} adenoviral constructs were created by excising the *MEOX* cDNA from the pCMV-Tag2B vector by *NotI/XhoI* digestion, followed by ligation into the

Table B-1: List of PCR primers used to create MEOX1 and MEOX2 expression constructs.

Primer	Direction	Sequence	Restriction site
MX001	Forward	5'-GGGAATTC <u>CCGGG</u> ATTATCCGAGCTCTG-3'	<i>EcoRI</i>
MX002	Reverse	5'-GCCGATCCTAAGTGCGCATGCTCTGAG-3'	<i>BamHI</i>
MX003	Forward	5'-GCGAATTCGCAGTGGACAGCAGATGGACC-3'	<i>EcoRI</i>
MX004	Reverse	5'-GCCGATCCCTCTGAACTTGGAGAAAGC-3'	<i>BamHI</i>
MX005	Reverse	5'-GGGCTCGAGTAAGTGCGCATGCTCTGAG-3'	<i>XhoI</i>
MX008	Reverse	5'-GGCTCGAGCTCTGAACTTGGAGAAAGCTGC-3'	<i>XhoI</i>
MX022	Forward	5'-CCTTTCTGAGCGGCAGGTCAAAGTCTGGTTCGAAAACCCGGAGGATG-3'	
MX023	Reverse	5'-CATCCTCCGGTTTTCGAACCCAGACTTTGACCTGCCGCTCAGAAAAGG-3'	
MX024	Forward	5'-GACAGGTGAAAGTCTGGTTCGAAACAGGGGGATGAAAGTGGAAAGAGGG-3'	
MX025	Reverse	5'-CCCTCTCCACTTCATCCGCCTGTTTTCCGAACCCAGACTTTACCTGTC-3'	
MX032	Forward	5'-CCCAGGAAAGAAAGGACAGCATTTACCGTGGACAGCAAGGAGCTGCCGGC-3'	
MX033	Forward	5'-GGAAAGGAGAGGACAGCCTTACCAGGGGTGTCAGCCTGTGTCCCCACAGGAG-3'	
MX085	Reverse	5'-TTGCAGAGCCTGGTGTCTGCTGC-3'	<i>partial HincII</i>
MX095	Reverse	5'-GCCTCGAGTCACTCTGAACCTGGAGAAAGC-3'	<i>XhoI</i>
MX096	Forward	5'-GGGGATCCATGGAACACCCCGCTCTTTGG-3'	<i>BamHI</i>
MX097	Reverse	5'-GCCCTCGAGTCAATAAGTGGCATGCTCTG-3'	<i>XhoI</i>
MX100	Forward	5'-GGGAATTCATGGATCCAGTGGCCAAC-3'	<i>EcoRI</i>
MX101	Forward	5'-GTCAGAAAGTCAACAGCAACCCAGGGTGGACAGCAAGGAGCTGCCGGC-3'	
MX108	Forward	5'-GTTTGCCAGCCAGCATCACAGGGGGCTCTGCAACCAACTGGCACCTCC-3'	
MX109	Reverse	5'-GGAGGTGCCAGTTGGTTTGCAGACCCCTGTGATGCTGGCTGGCAAAC-3'	
NOTI	Reverse	5'-GGGGCGGCCCTACTTATCGTCGTCATCCTTGTA-3'	<i>NotI</i>

Underlines indicate the restriction enzyme sequences.

Shading indicates the primers that were designed by other lab members.

Table B-2: List of expression vectors and the MEOX1 and MEOX2 proteins that they encode.

Vector	Fusion protein	Description
pMEOX1-EGFP	MEOX1-EGFP	C-terminal EGFP-tag wild-type MEOX1
pMEOX1ΔHD-EGFP	MEOX1 ^{K180_K230del} -EGFP	C-terminal EGFP-tag homeodomain deleted MEOX1
pMEOX2-EGFP	MEOX2-EGFP	C-terminal EGFP-tag wild-type MEOX2
pMEOX2ΔHD-EGFP	MEOX2 ^{K195_K245del} -EGFP	C-terminal EGFP-tag homeodomain deleted MEOX2
pMEOX2ΔMID-EGFP	MEOX2 ^{T89_V182del} -EGFP	C-terminal EGFP-tag middle domain deleted MEOX2
pCMV-Tag4A-MEOX1	MEOX1-FLAG	C-terminal FLAG-tag wild-type MEOX1
pCMV-Tag4A-MEOX1DDBDmt	MEOX1 ^{Q220E} -FLAG	C-terminal FLAG-tag DNA-binding domain mutated MEOX1
pCMV-Tag4A-MEOX1ΔHD	MEOX1 ^{K180_K230del} -FLAG	C-terminal FLAG-tag homeodomain deleted MEOX1
pCMV-Tag4A-MEOX2	MEOX2-FLAG	C-terminal FLAG-tag wild-type MEOX2
pCMV-Tag4A-MEOX2DDBDmt	MEOX2 ^{Q235E} -FLAG	C-terminal FLAG-tag DNA-binding domain mutated MEOX2
pCMV-Tag4A-MEOX2ΔHD	MEOX2 ^{K195_K245del} -FLAG	C-terminal FLAG-tag homeodomain deleted MEOX2
pCMV-Tag4A-GAXΔHD	MEOX2 ^{K188_K245del} -FLAG	C-terminal FLAG-tag homeodomain deleted MEOX2
pCMV-Tag4A-MEOX2ΔMID	MEOX2 ^{T89_V182del} -FLAG	C-terminal FLAG-tag middle domain deleted MEOX2
pCMV-Tag4A-MEOX2-STOP	MEOX2	Untagged wild-type MEOX2
pCMV-Tag2B-MEOX1	FLAG-MEOX1	N-terminal FLAG-tag wild-type MEOX1
pCMV-Tag2B-MEOX1DDBDmt	FLAG-MEOX1 ^{Q220E}	N-terminal FLAG-tag DNA-binding domain mutated MEOX1
pCMV-Tag2B-MEOX2	FLAG-MEOX2	N-terminal FLAG-tag wild-type MEOX2
pCMV-Tag2B-MEOX2DDBDmt	FLAG-MEOX2 ^{Q235E}	N-terminal FLAG-tag DNA-binding domain mutated MEOX2
pCMV-Tag2B-MEOX2ΔHD	FLAG-MEOX2 ^{K195_K245del}	N-terminal FLAG-tag homeodomain deleted MEOX2
pCMV-Tag2B-MEOX2ΔCAX	FLAG-MEOX2 ^{H68_Q85del}	N-terminal FLAG-tag histidine/glutamine rich domain deleted MEOX2
pcDNA3-MEOX1	MEOX1-FLAG	C-terminal FLAG-tag wild-type MEOX1
pcDNA3-MEOX1DDBDmt	MEOX1 ^{Q220E} -FLAG	C-terminal FLAG-tag DNA-binding domain mutated MEOX1
pcDNA3-MEOX2	MEOX2-FLAG	C-terminal FLAG-tag wild-type MEOX2
pcDNA3-MEOX2DDBDmt	MEOX2 ^{Q235E} -FLAG	C-terminal FLAG-tag DNA-binding domain mutated MEOX2
pcDNA3-MEOX2ΔCAX	MEOX2 ^{H68_Q85del} -FLAG	C-terminal FLAG-tag histidine/glutamine rich domain deleted MEOX2

Shading indicates the vectors that were conceived and cloned by other lab members.

NotI/XhoI digested pShuttle-CMV vector. All adenovirus constructs are listed in Table B-3.

B.4. *MEOX-GST fusion proteins*

Meox1, *MEOX2*, *MEOX2*^{Q235E} and *MEOX2*^{K195_K245del} coding sequences were excised from the pCMV-Tag2B vector with *EcoRI/XhoI* (*Meox1*) or *BamHI/XhoI* (*MEOX2*), and cloned into the pET-41a(+) vector (Novagen), creating C-terminal GST-tagged constructs.

Table B-3: List of adenoviruses and the MEOX1 and MEOX2 proteins that they encode.

Adenovirus	Fusion protein	Description
Ad-MEOX1-C	MEOX1-FLAG	C-terminal FLAG-tag wild-type MEOX1
Ad-MEOX2-C	MEOX2-FLAG	C-terminal FLAG-tag wild-type MEOX2
Ad-MEOX2ΔHHD-C	MEOX2 ^{K195_K245del} -FLAG	C-terminal FLAG-tag homeodomain deleted MEOX2
Ad-N-MEOX1	FLAG-MEOX1	N-terminal FLAG-tag wild-type MEOX1
Ad-N-MEOX2	FLAG-MEOX2	N-terminal FLAG-tag wild-type MEOX2
Ad-N-MEOX2DBDmt	FLAG-MEOX2 ^{Q235E}	N-terminal FLAG-tag DNA-binding domain mutated MEOX2
Ad-N-MEOX2ΔHHD	FLAG-MEOX2 ^{K195_K245del}	N-terminal FLAG-tag homeodomain deleted MEOX2

No shading indicates the adenoviruses that were cloned by other lab members.

Shading indicates the adenoviruses that were cloned, amplified and titered by other lab members.

Appendix C: The location of the FLAG epitope does not affect MEOX expression or function

- Referred to in Chapters 3 (section 3.4) and Chapter 4 (section 4.4.2.1).

To ensure that addition of the FLAG epitope to MEOX1 and MEOX2 did not affect the expression, localization or function of the MEOX proteins, we created both N-terminal and C-terminal FLAG-tagged constructs and performed direct comparative studies. In addition, we created an untagged MEOX2 construct: MEOX2-STOP. A detailed description of the constructs and their generation is discussed in Appendix B.

Transfection of HEK293 cells with N-terminal and C-terminal FLAG-tagged versions of MEOX1 and MEOX2 showed no difference in the expression or localization of the MEOX proteins, as assessed by western blot (Figure C-1) and fluorescent immunocytochemistry (Figure C-2) using an anti-FLAG antibody. Similarly, the pattern of expression and localization of MEOX1, MEOX2 and homeodomain deleted MEOX2^{K195_K245del} was identical between HUVECs transduced with adenovirus encoding N-terminal or C-terminal FLAG-tagged proteins (compare Figure 3-8 and Figure 3-12).

To test for differences in the transcriptional capabilities of differentially FLAG-tagged MEOX2, we performed luciferase assays with N-terminal, C-terminal and untagged versions of MEOX2. All three versions of MEOX2 were equally capable of activating transcription from a 2272 bp *p21^{CIP1/WAF1}* promoter (Figure C-3), indicating that the FLAG epitope does not alter the ability of MEOX2 to induce transcription in this system. Finally, we compared the ability of N-terminal and C-terminal FLAG-tagged MEOX1 and MEOX2 to increase endogenous *p21^{CIP1/WAF1}* protein expression in

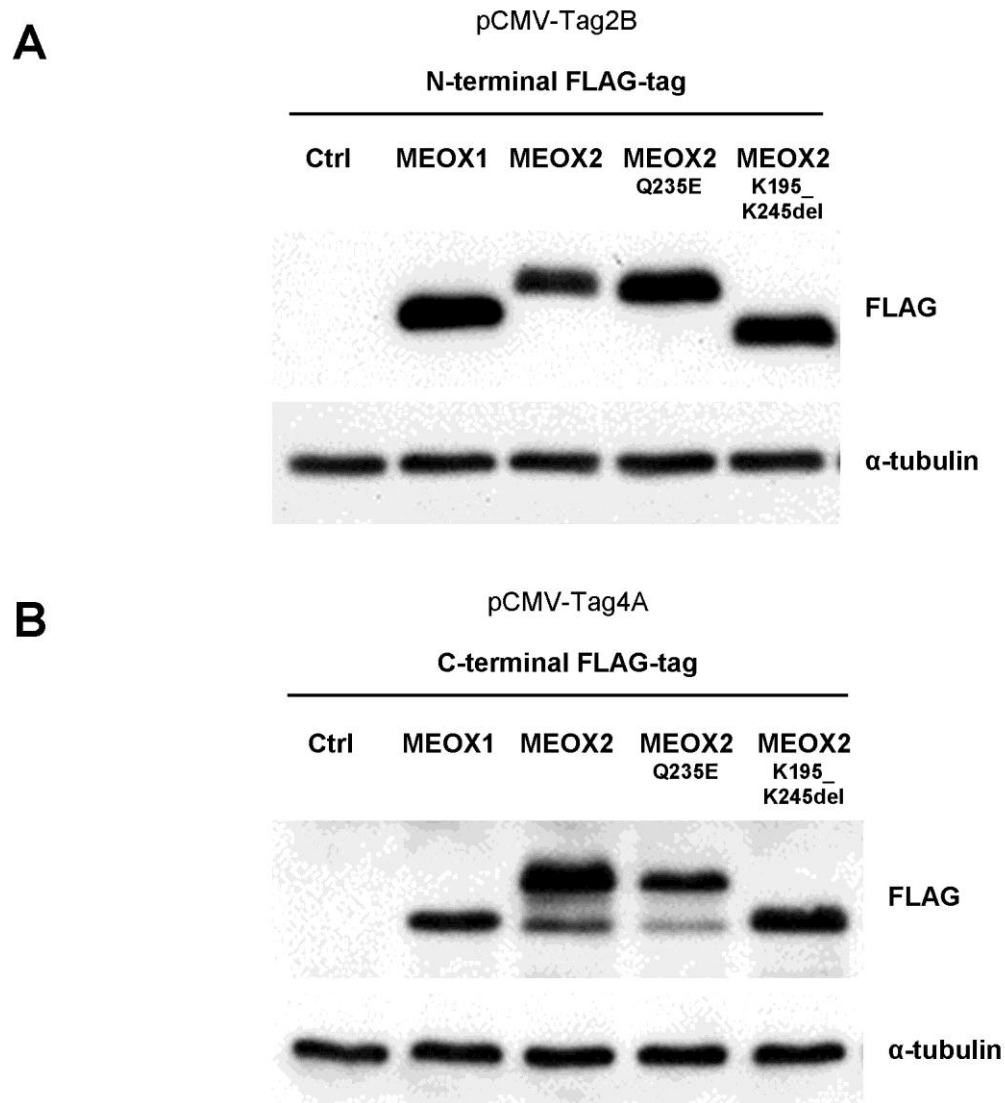


Figure C-1: Expression of N-terminal and C-terminal FLAG-tagged MEOX proteins in HEK293 cells.

Western blots showing that the location of the FLAG epitope at the N-terminal (A) or C-terminal (B) does not alter MEOX protein expression in HEK293 cells. Whole cell lysate was collected for SDS-PAGE 24 hours after transfection. MEOX proteins were detected using an anti-FLAG antibody. α -tubulin was used as a loading control.

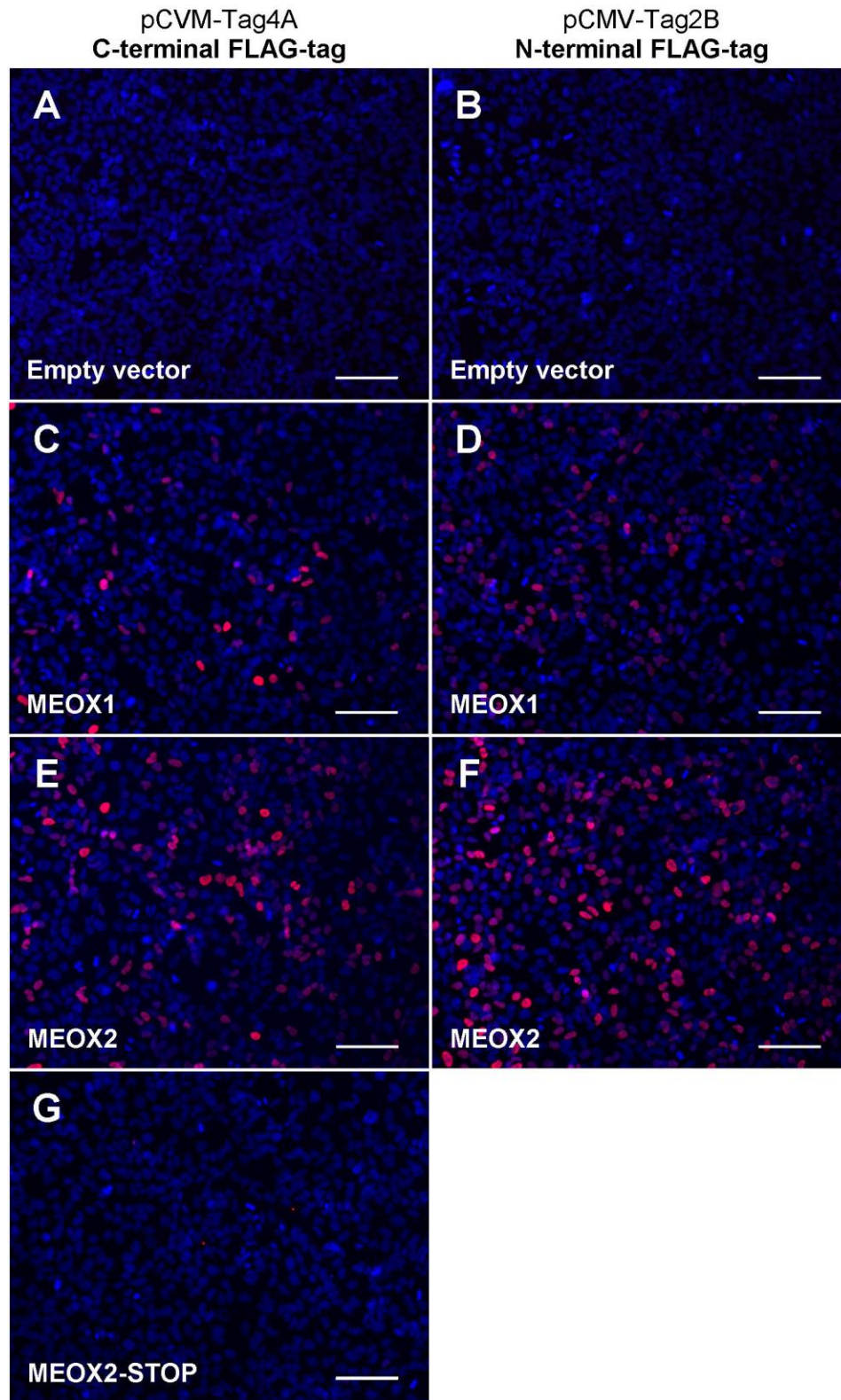


Figure C-2: Nuclear localization of N-terminal and C-terminal FLAG-tagged MEOX proteins in HEK293 cells.

Figure C-2: Nuclear localization of N-terminal and C-terminal FLAG-tagged MEOX proteins in HEK293 cells.

Fluorescent immunocytochemistry demonstrating that the location of the FLAG epitope does not affect the nuclear localization of MEOX1 or MEOX2 in HEK293 cells. Insertion of a stop codon between the MEOX2 and FLAG coding sequences in the pCMV-Tag4A vector successfully created an untagged version of MEOX2 (G). Cells were fixed and stained 24 hours post-transfection. MEOX proteins were detected using an anti-FLAG antibody. Nuclei were stained with DAPI. Scale bars represent 20 μm .

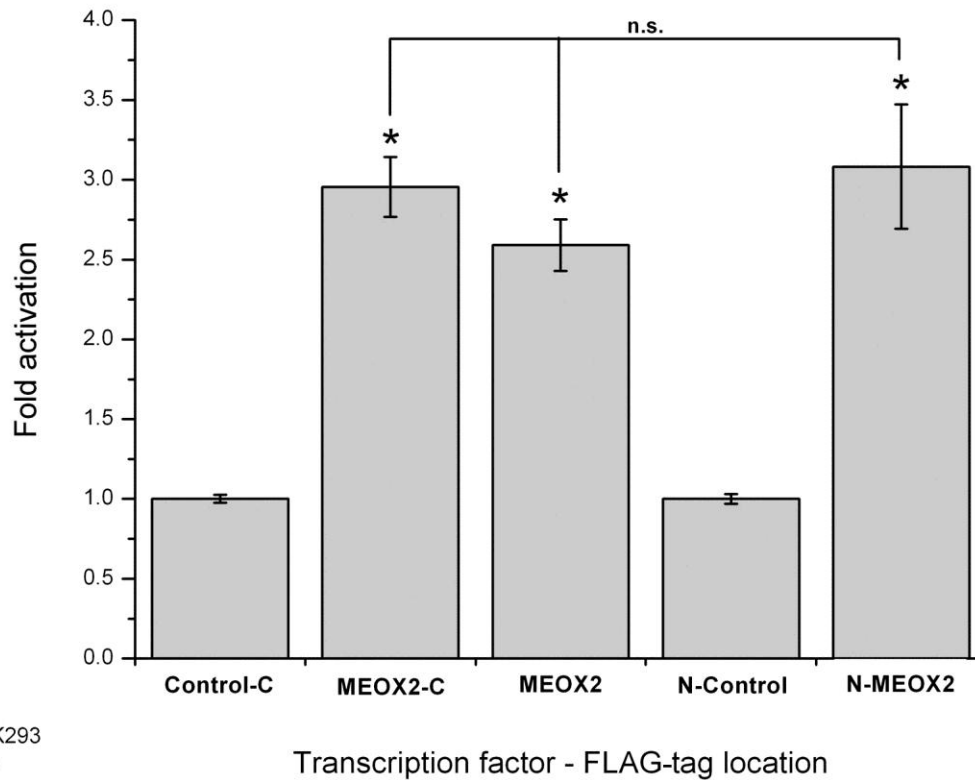


Figure C-3: The position or inclusion of the FLAG epitope does not affect MEOX2 transcriptional activation from the 2272 bp $p21^{CIP1/WAF1}$ promoter.

Luciferase assay demonstrating the ability of C-terminal FLAG-tagged MEOX2 (MEOX2-C), un-tagged MEOX2 (MEOX2) and N-terminal FLAG-tagged MEOX2 (N-MEOX2) proteins to activate a 2272 bp $p21^{CIP1/WAF1}$ promoter as compared to their respective empty vector controls (Control-C or Control-N). * Indicates a statistically significant change ($p < 0.05$) when compared to the empty vector controls. n.s. denotes no statistically significant difference ($p < 0.05$) in promoter activation is observed between the various MEOX2 proteins. Error bars represent the standard error of the mean ($n=6$).

HUVECs. We observed equivalent results with both tagged versions of the MEOX proteins; Meox1 and homeodomain deleted MEOX2^{K195_K245del} do not significantly increase p21^{CIP1/WAF1} protein expression, while MEOX2 increases p21^{CIP1/WAF1} expression comparable to p53 (Figure C-4).

Taken together, we conclude that addition of the FLAG epitope, to either terminus of the MEOX proteins, does not measurably affect their localization, expression or function *in vitro*.

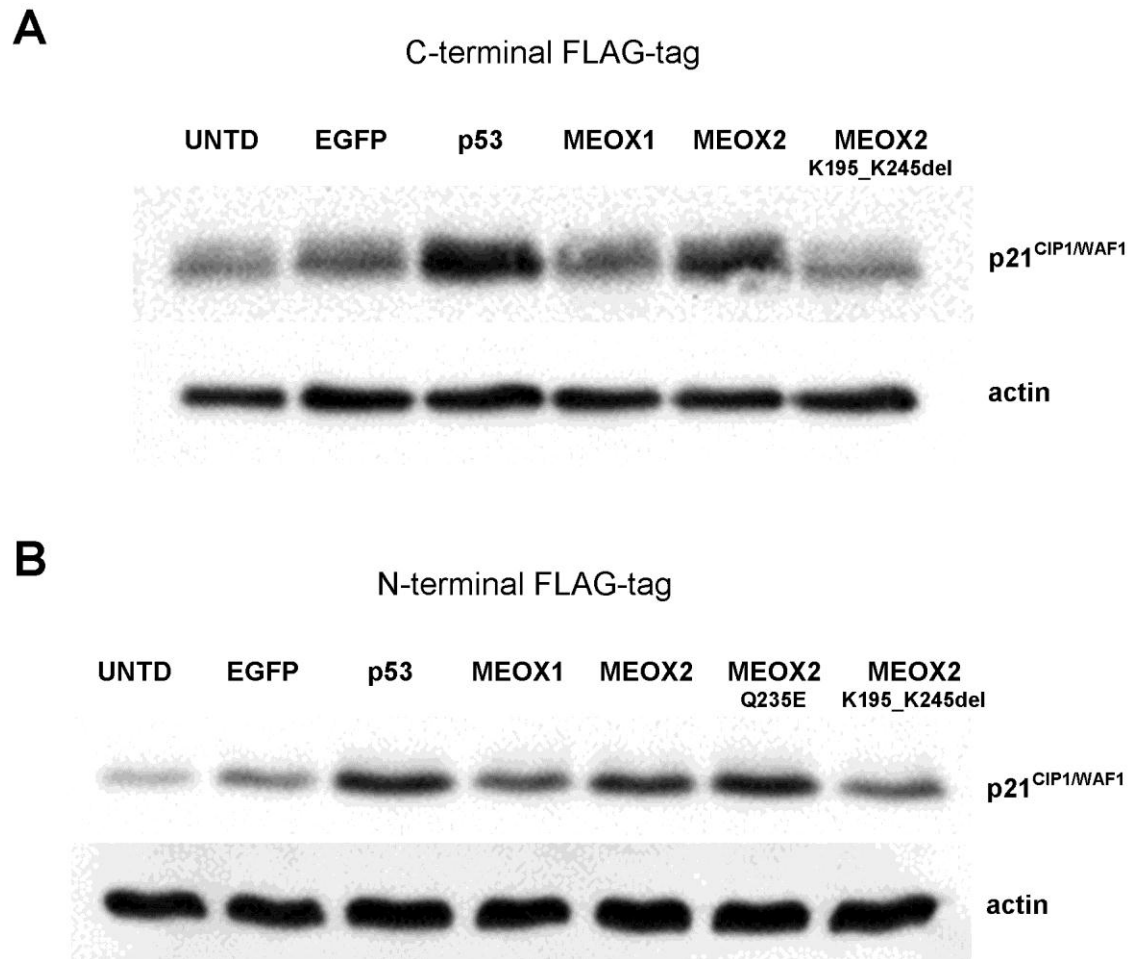


Figure C-4: The position of the FLAG-tag does not affect MEOX2 activation of *p21^{CIP1/WAF1}* expression in endothelial cells.

Representative western blots showing increased p21^{CIP1/WAF1} protein in HUVECs over-expressing p53, MEOX2 and DNA-binding domain mutated MEOX2^{Q235E} but not Meox1 or homeodomain deleted MEOX2^{K195_K245del}. Increased p21^{CIP1/WAF1} expression due to adenoviral transduction is evident when comparing EGFP and untransduced (UNT) cells. Total protein was isolated from HUVECs 48 hours after adenoviral transduction at 250 MOI with C-terminal FLAG-tagged MEOX constructs (A) or N-terminal FLAG-tagged MEOX constructs (B). Actin was used as a loading control.

Appendix D: Chromatin immunoprecipitation optimization and troubleshooting

- Referred to in Chapter 4 (section 4.3.10).

The resolution of ChIP is dependent upon the consistent size of the input chromatin DNA fragments. In other words, to be confident that a protein is bound adjacent to the PCR amplicon, the DNA fragments must be relatively small. We tested various sonication routines for the purpose of identifying which one would consistently produce DNA fragments that are between 200 and 800 bp, predominantly. Formaldehyde cross-linked cells were suspended in SDS Lysis Buffer (Millipore) and then sonicated 4, 6, 8, and 10 times for 10 seconds each using a Misonix XL-2000 series sonicator (Qsonica) set to “2”. The sonicated cell lysate was reverse cross-linked and the nucleic acids were purified by phenol:chloroform extraction followed by ethanol precipitation. RNA was degraded by incubation with 10 µg RNase A (Invitrogen) for 15 minutes at 37°C. The size of the DNA fragments was visualized by agarose gel electrophoresis (Figure D-1). We concluded that 10 seconds of sonication followed by 30 seconds of rest, repeated 10 times, was the optimal sonication routine as it produced the DNA fragments within the desired size range.

Next, we wanted to verify that we could efficiently immunoprecipitate (IP) proteins using antibody and magnetic (Dynabeads Protein G, Invitrogen) or polyacrylamide (Protein A/G UltraLink Resin, Pierce) beads. To this end, we lysed cells in RIPA buffer (50 mM Tris pH 7.4, 150 mM NaCl, 1 mM EDTA, 1 mM EGTA, 0.5% Na-deoxycholate, 1% Triton-X 100 and 0.1% SDS), following which we performed overnight IPs at 4°C. The following day, beads were added to the IPs and incubated for 1

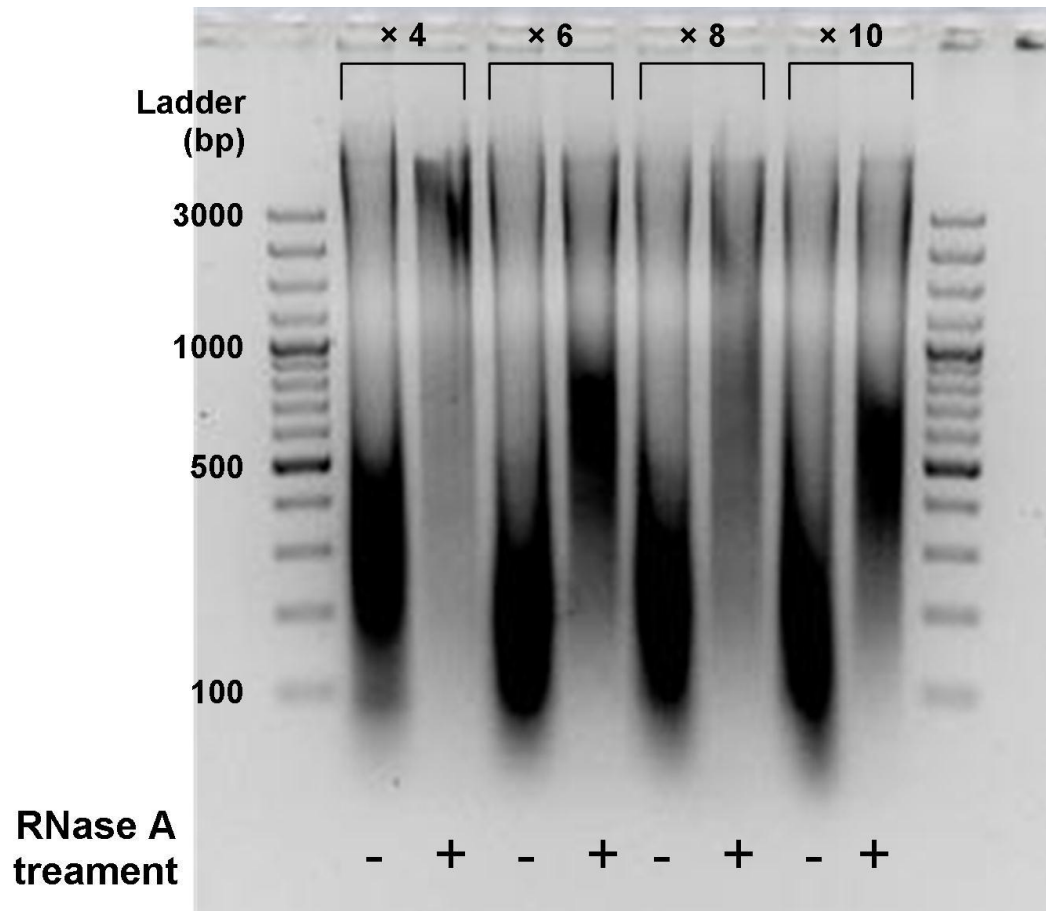


Figure D-1: Test for optimal DNA fragmentation using sonication.

(A) Formaldehyde cross-linked cells were sonicated 4, 6, 8, and 10 times for 10 seconds each. Samples were treated with or without RNaseA to degrade RNA. DNA fragments were separated by agarose gel electrophoresis.

hour at 4°C to collect the antibody. The beads were removed from the supernatant, washed, and then the protein was eluted from the beads by boiling them in 1× loading buffer (55.5 mM Tris pH 7.4, 11.1% glycerol, 2.2% SDS, 0.1% bromophenol blue and 33.3 mM DTT) for 5 minutes. Equal ratios of protein from the supernatant and beads were separated by SDS-PAGE and then immunoblotted.

To begin, we immunoprecipitated the RNA polymerase II enzyme from untreated HUVEC lysates using an anti-RNAP antibody (Millipore) and magnetic beads (Figure D-2, panel A). As shown by immunoblot with the anti-RNAP antibody, we were successfully able to IP RNA polymerase II using the anti-RNAP antibody, but not the anti-MEOX2 antibody (Figure D-2, panel A). Next, we repeated the experiment using anti-FLAG or anti-MEOX2 antibodies and magnetic beads to IP the MEOX2 protein from transduced HUVEC lysate (Figure D-2, panel B). Immunoblotting with the anti-FLAG antibody revealed that exogenously expressed MEOX2 was bound to the magnetic beads, even in the absence of antibody (Figure D-2, panel B). When polyacrylamide beads were used to collect the anti-FLAG antibody from IPs of transduced HUVEC lysates, we observed by immunoblot that exogenous MEOX2 was not bound to the beads in the absence of antibody (Figure D-2, panel C).

Thus, we performed all subsequent ChIP assays using polyacrylamide or agarose beads, as MEOX2 does not non-specifically bind to these types of beads (Figure D-2, panel C and data not shown).

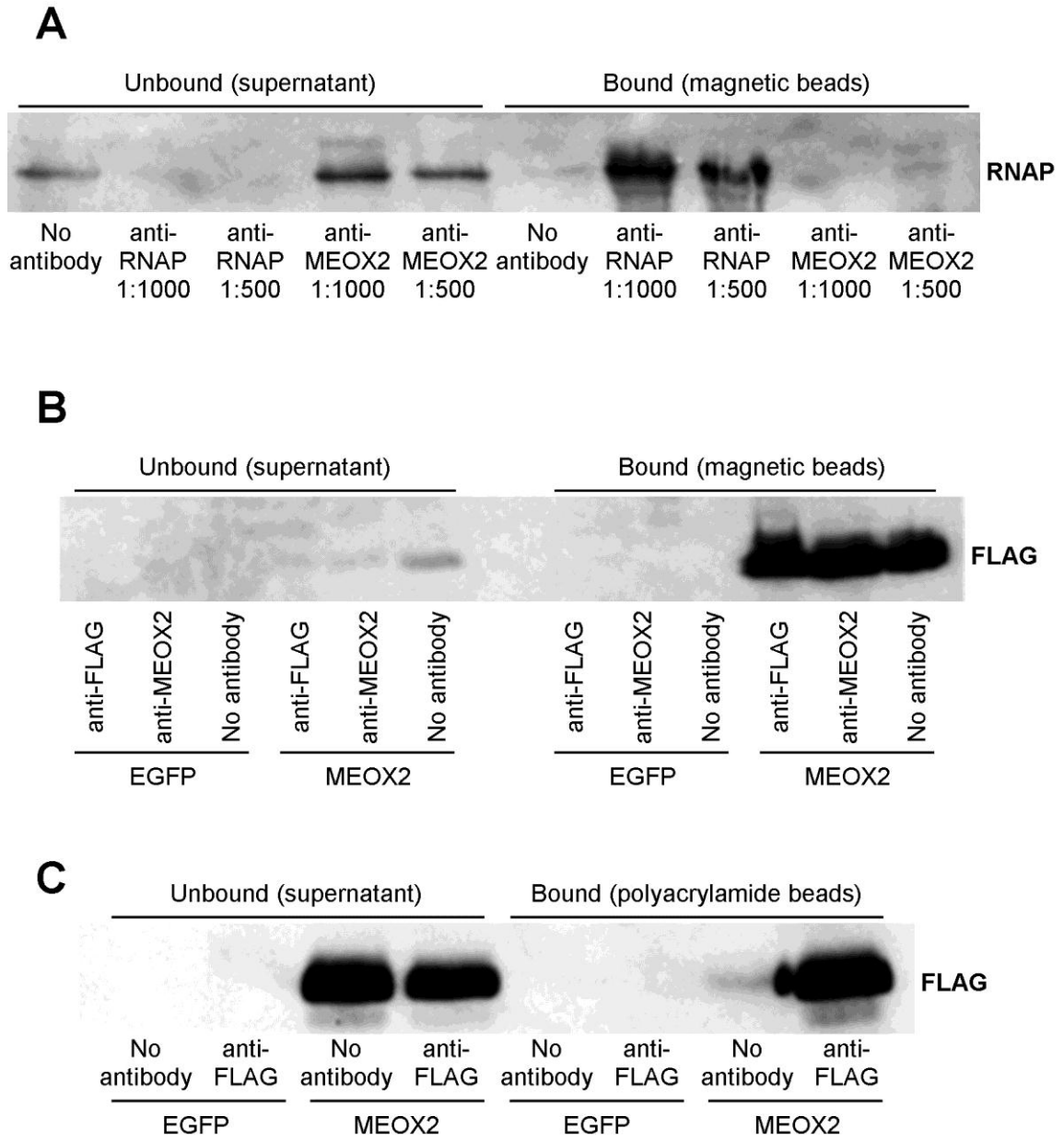


Figure D-2: MEOX2 binds to magnetic beads, but not to polyacrylamide beads.

Figure D-2: MEOX2 binds to magnetic beads, but not to polyacrylamide beads.

(A) RNA polymerase II was immunoprecipitated from untreated HUVEC lysates using anti-RNAP. Anti-MEOX2 antibodies were used as a negative control. The antibodies were collected using magnetic beads (Dynabeads, Invitrogen). RNA polymerase II was detected by western blot using anti-RNAP antibody. (B) N-terminal FLAG-tagged MEOX2 was immunoprecipitated from transduced HUVEC lysates (Ad-EGFP or Ad-MEOX2) using anti-FLAG or anti-MEOX2 antibodies. The antibodies were collected using magnetic beads (Dynabeads, Invitrogen). Exogenous MEOX2 expression was detected by western blot using anti-FLAG antibody. (C) N-terminal FLAG-tagged MEOX2 was immunoprecipitated from transduced HUVEC lysates (Ad-EGFP or Ad-MEOX2) using an anti-FLAG antibody. The antibody was collected using polyacrylamide beads (Ultralink resin, Pierce). Exogenous MEOX2 expression was detected by western blot using an anti-FLAG antibody.

Appendix E: Identification of MEOX binding partners

- Referred to in Chapter 6 (section 6.2).

In order to isolate MEOX interacting proteins from ECs, we plan to use the tandem affinity purification tag (TAP-TAG) method [262,263]. Ultimately, MEOX bound proteins will be isolated from EC nuclear extracts by column purification (Figure E-1, panel B), separated using SDS-PAGE and visualized using silver stain for comparison to controls. Proteins will be in gel trypsin digested, and then sent for identification by matrix-assisted laser desorption/ionization, time-of-flight (MALDI-TOF) mass spectrometry.

To this end, we cloned MEOX1, MEOX2, MEOX2^{Q235E} and MEOX2^{K195_K245del} into the pBRIT-TAP retroviral vector, creating MEOX proteins that are fused to a C-terminal 6×HIS-3×FLAG-tag (TAP-tag) (Figure E-1, panel A). The pBRIT-TAP retroviral vector was transfected into the Phoenix-Eco packaging cell line to produce ecotropic retrovirus. Owing to the hazards of creating and using retroviruses which can stably transduce human cells via transgene integration into the host genome, we chose to create ecotropic retrovirus that can only transduce murine cells.

To test the ability of the generated virus to transduce murine cells and to produce TAP-tagged proteins, we transduced NIH/3T3 cells (mouse fibroblasts) with the retrovirus and then used western blot to detect the expression of the TAP-tagged MEOX proteins in cell lysates (Figure E-2, panel A). C-terminal TAP-tagged MEOX proteins were robustly expressed in NIH/3T3 cells, indicating that we successfully produced ecotropic retrovirus encoding our proteins of interest. As we want to isolate MEOX

Figure E 1: Summary of MEOX2 bound protein purification using the TAP-TAG system.

(A) Tandem affinity purification tag (TAP-TAG) amino acid sequence. (B) TAP-TAG MEOX proteins will be used to co-purify interacting proteins from the mouse brain EC line (bEnd.3). The TAP-tag is composed of 6×HIS and 3×FLAG epitopes separated by a linker region that contains a Tobacco etch virus (TEV) protease cleavage site. Isolated proteins will be identified by mass spectroscopy and further characterized. Interacting protein purification using this TAP-TAG was previously performed by McKinnell *et al.* [263].

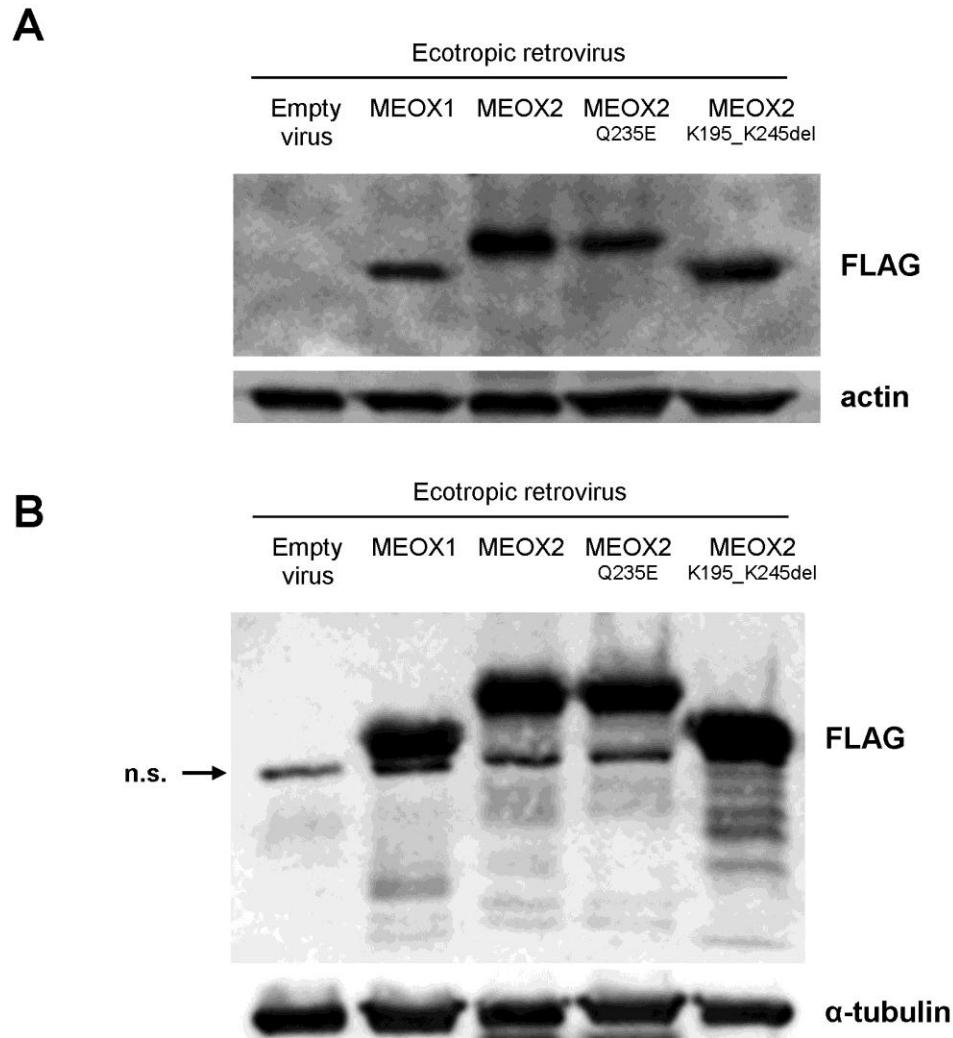


Figure E-2: Expression of TAP-tagged MEOX proteins in mouse cells transduced with ecotropic retrovirus.

Western blot showing the TAP-tagged MEOX1, MEOX2, DNA-binding domain mutated MEOX2^{Q235E} and homeodomain deleted MEOX2^{K195_K245del} are expressed in NIH/3T3 cells 24 hours post-transduction (**A**) and following (1 μg/mL) puromycin selection for stably transformed bEnd.3 cells (**B**). TAP-tagged proteins were detected using an anti-FLAG antibody. Actin or α-tubulin was used as loading control. n.s. denotes a non-specific band.

interacting proteins from ECs, we chose the bEnd.3 mouse brain EC line as a model system. We transduced bEnd.3 cells with the MEOX ecotropic retrovirus and then used puromycin treatment (1 $\mu\text{g}/\text{mL}$) to select cells which had stably integrated the retroviral DNA. Western blot and fluorescent immunocytochemistry confirmed the expression of stably integrated C-terminal TAP-tagged MEOX proteins in puromycin selected bEnd.3 whole cell extracts (Figure E-2, panel B and data not shown).

To ensure that the expression and subcellular localization of the MEOX proteins was not affected by the addition of the TAP-tag, we transfected HEK239 cells with the retroviral vectors and then performed fluorescent immunocytochemistry (Figure E-3). We observed no difference in the localization of the C-terminal TAP-tagged MEOX proteins as compared to N-terminal or C-terminal FLAG-tagged MEOX proteins (data not shown); expression of MEOX1, MEOX2 and MEOX2^{Q235E} was primarily nuclear and MEOX2^{K195_K245del} was expressed throughout the cell (Figure E-3). Therefore, the TAP-tag does not affect the localization of the MEOX proteins. Next, we assessed whether the TAP-tag affected the ability of the MEOX proteins to bind to DNA. When nuclear extracts from HEK293 cells transfected with the retroviral vector were used for EMSAs, we observed that both the wild-type MEOX1 and MEOX2 bound to the *p21^{CIP1/WAF1}* probe, but the DNA-binding domain mutated MEOX2^{Q235E} and homeodomain deleted MEOX2^{K195_K245del} could not (Figure E-4). Hence, the TAP-tag does not interfere with the ability of the MEOX proteins to bind DNA. Finally, to test the function of the TAP-tagged MEOX proteins, we transfected HEK293 cells with the retroviral vector and then performed luciferase assays and quantitative real-time PCR. We did not observe any change in the level of transcription from the *p21^{CIP1/WAF1}* upstream promoter region in the

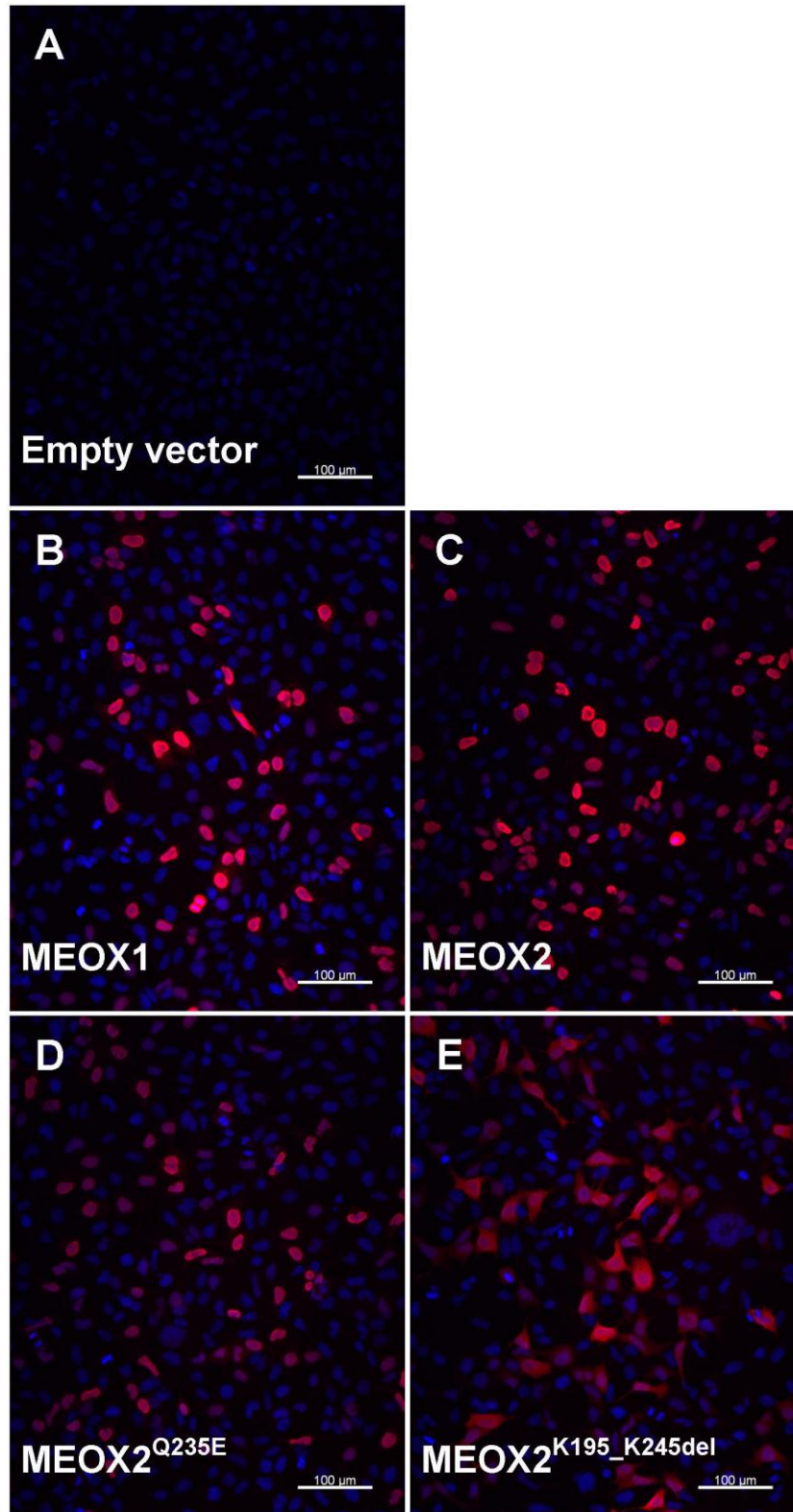


Figure E-3: Expression of C-terminal TAP-tagged MEOX proteins in HEK293 cells.

Figure E-3: Expression of C-terminal TAP-tagged MEOX proteins in HEK293 cells.

The localization of TAP-tagged MEOX1, MEOX2, DNA-binding domain mutated MEOX2^{Q235E} and homeodomain deleted MEOX2^{K195_K245del} proteins were detected using an anti-FLAG antibody (red). Nuclei were stained with DAPI (blue). The TAP-tag does not appear to alter the normal localization of the MEOX proteins as the localization of MEOX1, MEOX2 and DNA-binding domain mutated MEOX2^{Q235E} is nuclear, whereas the localization of the homeodomain deleted MEOX2^{K195_K245del} is found throughout the cell. Scale bars represent 100 μm .

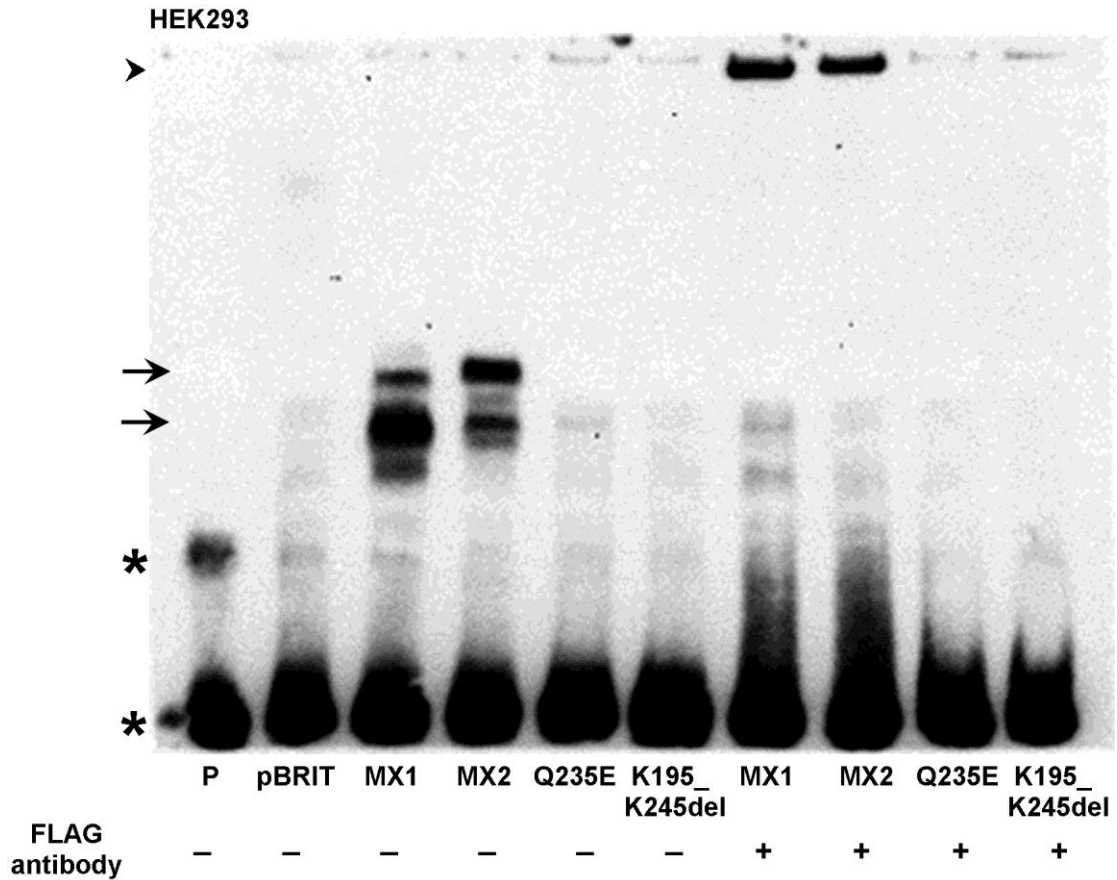


Figure E-4: TAP-tagged MEOX proteins bind to a DNA probe containing homeodomain binding sites from the $p21^{CIP1/WAF1}$ promoter.

Nuclear extracts from HEK293 cells transfected with TAP-tagged MEOX proteins were used to demonstrate the ability of these proteins to bind DNA. The DNA probe (P) contained a known MEOX2 binding site from the $p21^{CIP1/WAF1}$ upstream promoter region [89]. TAP-tagged MEOX1 (MX1) and MEOX2 (MX2) are capable of binding to DNA, as demonstrated by shifted biotinylated probe (arrows). DNA-binding domain mutated MEOX2^{Q235E} (Q235E) and homeodomain deleted MEOX2^{K195_K245del} (K195_K249del) did not bind DNA. The biotinylated MEOX1 or MEOX2 bound probe was supershifted (arrowhead) when nuclear extracts were pre-incubated with an anti-FLAG antibody.

presence of the TAP-tagged MEOX proteins, nor did we detect any change in the amount of endogenous *p21^{CIP1/WAF1}* mRNA expression (Figure E-5). Thus, although the localization and DNA-binding ability of the MEOX proteins is not affected by the C-terminal TAP-tag, it appears that this tag affects the ability of MEOX1 and MEOX2 to activate transcription of the *p21^{CIP1/WAF1}* target gene. As MEOX activation of *p21^{CIP1/WAF1}* transcription occurs in a DNA-binding independent manner, this suggests that the C-terminal TAP-tag may interfere with some MEOX protein-protein interactions. For this reason, we will compare the tandem affinity purification results to co-immunoprecipitation of MEOX interacting proteins from nuclear extracts of HUVECs over-expressing N-terminal FLAG-tagged MEOX proteins (using a FLAG antibody) or endogenous protein (using a MEOX2 antibody).

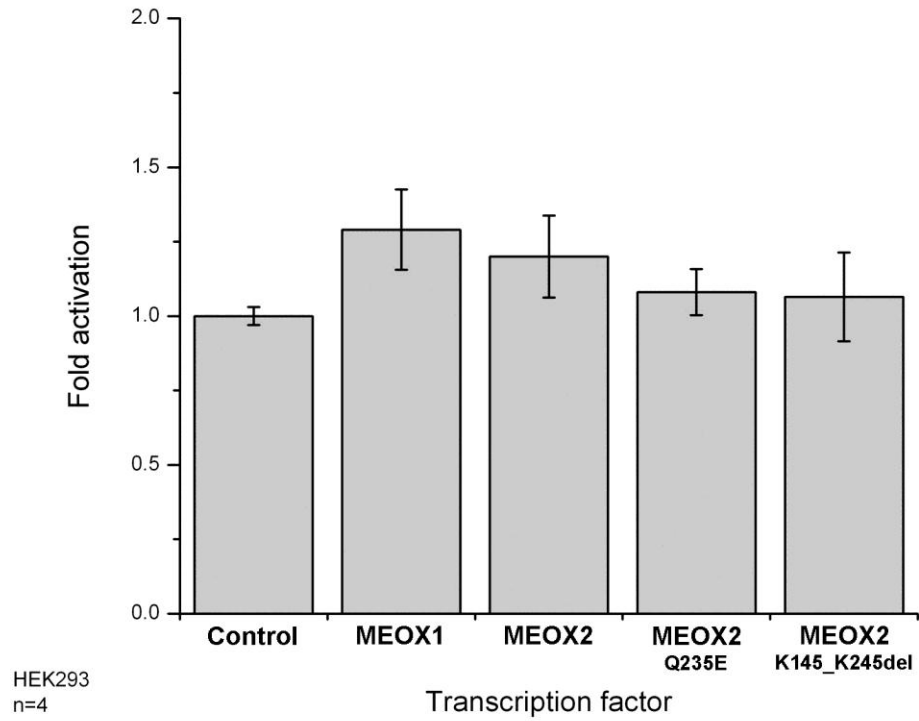
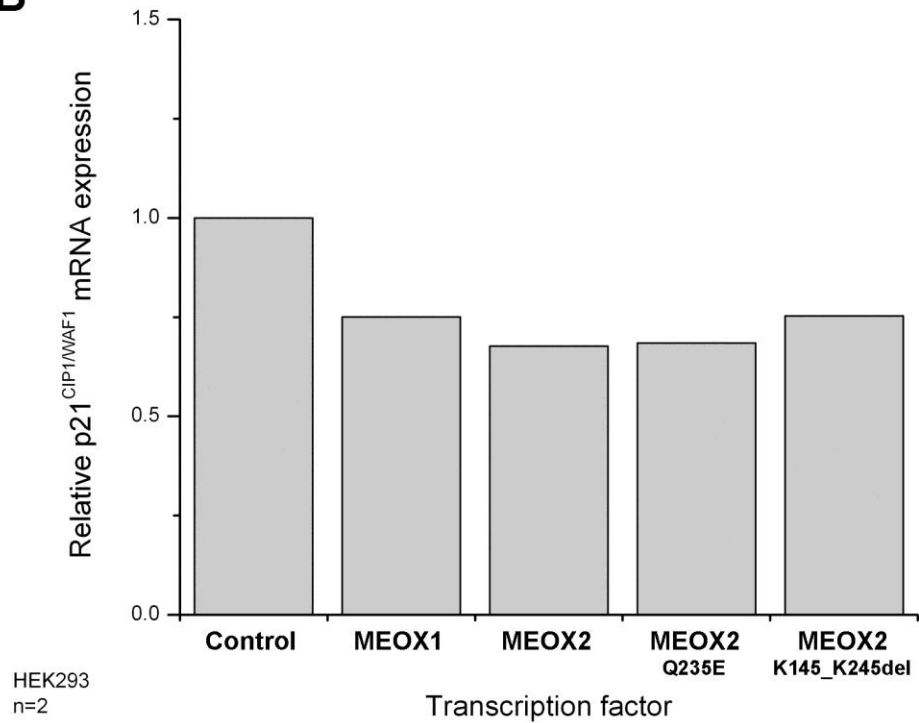
A**B**

Figure E-5: TAP-tagged MEOX proteins do not induce *p21*^{CIP1/WAF1} expression.

Figure E-5: TAP-tagged MEOX proteins do not induce $p21^{CIP1/WAF1}$ expression.

(A) Luciferase assays showing the lack of activation of the $p21^{CIP1/WAF1}$ upstream promoter region in HEK293 cells by C-terminal TAP-tagged MEOX proteins. (B) Quantitative real-time PCR showing the relative levels of $p21^{CIP1/WAF1}$ mRNA expression in HEK293 cells 24 hours after transfection with C-terminal TAP-tagged MEOX proteins.

